THE UNIVERSITY OF TASMANIA LIBRARY

PETROGENESIS OF GARNET AND SPINEL PERIDOTITES

A study with particular reference to the role of chromium in geothermometry and geobarometry.

by

Klaus Georg Nickel (Dipl.-Geol.)

Submitted in fulfilment of the requirements for the degree of Doctor of Philosophy.

University of Tasmania

HOBART

1983

This thesis contains no material which has been accepted for the award of any other degree or diploma in any university, and to the best of my knowledge and belief, contains no copy or paraphrase of material previously published or written by another person, except where due reference is made in the text of this thesis.

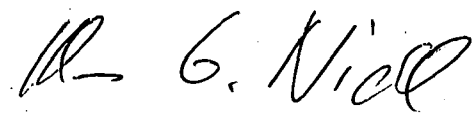

K. G. Nickel

University of Tasmania
May, 1983.

You delight in laying down laws,
Yet you delight more in breaking them.
Like children playing by the ocean who build sand-towers
With constancy and then destroy them with laughter.
But while you build your sand-towers the ocean
Brings more sand to the shore, And when you destroy them
The ocean laughs with you.

Kahlil Gibran

CONTENTS

LIST OF FIGURES

List of figures cont. page

List of Figures cont. page

List of figures cont. page

LIST OF TABLES

ABSTRACT

Spinel and garnet peridotites are the dominant rock types of the upper mantle. Petrography, mineralogy, bulk rock and mineral chemistry of spinel lherzolites from inclusions in basanites in Victoria, Australia were studied to provide evidence for their petrogenesis and relation to host rocks and to other xenolithic rock types occurring within these host rocks. Experimental studies in ultramafic systems were carried out to infer P,T conditions of the origin of garnet peridotites, particularly those of xenolithic occurrence in kimberlites reported in the literature, to investigate the relation between garnet and spinel peridotites and to give clues to the relation between host rocks, garnet peridotites and simultaneously occurring xenoliths, megacrysts and minerals.

Ultramafic inclusions from two neighbouring localities in Victoria, Australia (Lake Bullenmerri and Mt Leura) include spinel lherzolites with and without hydrous phases, wehrlites, pyroxenites and hornblendites. Mineral chemistry provides evidence for equilibrium crystallization for individual nodules at a depth near 45 km but over a range of temperatures. Temperature estimates yield systematic differences between anhydrous assemblages > phlogopite-bearing assemblages > amphibole-bearing assemblages. Bulk rock variation of MgO, CaO, Al_2O_3 and compatible element contents in lherzolite and harzburgite has been modelled as an early partial melting event, giving rise to various degrees of depletion. The extracted liquid was of picritic composition.

Amphiboles in spinel lherzolites are developed independently of the early partial melting event and postdate it. They crystallized as a response to near-isochemical metamorphic reaction, consequent on addition of water. The hydration events predate but are not precursor conditions for production of basanite. Hydration-metasomatism occurs in the uppermost mantle above the LVZ, but this is most probably not the region of formation

of the alkaline magams. The emplacement and passage of alkaline magmas through the lithosphere/upper mantle may be the cause of local metasomatism and hydration.

Wehrlites, pyroxenites, some lherzolites, and hornblendites are precipitates from magmas fractionating and/or crystallizing at mantle depths. Observable wallrock reaction is extremely restricted (about 1 cm) as evidenced by composite xenoliths.

Experiments in the systems $CaO-MgO-Al_2O_3-SiO_2$ (CMAS) and $SiO_2-MgO-Al_2O_3-CaO-Cr_2O_3$ (SMACCR) show that spinel and garnet in peridotitic assemblages are related by an univariant reaction in the CMAS system, but coexist with each other over a range of P,T conditions in the SMACCR system. Both the width and location of this field in P,T space is dependent on the Cr/Cr+Al ratio of the bulk composition.

Temperature estimates for assemblages containing two pyroxenes by the method of Wells (1977) give satisfactory results for the range of 1000-1400°C and 15-40 kb in all systems studied (CMAS, SMACCR and multicomponent "natural" systems). Doubts on the accuracy of this thermometer exist particularly at low temperatures (<900°C), but for most xenolithic occurrences of natural garnet lherzolites, temperatures may be estimated by this method with considerable confidence.

Cr-Al distributions between ortho- and clinopyroxene as well as between pyroxenes and spinel show a regular behaviour in the SMACCR system, independent of pressure and temperature. The Cr-Al exchange between garnet and spinel is sensitive to temperature in the SMACCR system above 1200°C and a thermometer based on this reaction has been calibrated for the simple system. Experiments in multicomponent systems show however strong compositional dependencies of this reaction, rendering it as of no use for practical geothermometry.

The solubility of both Al_2O_3 and Cr_2O_3 in orthopyroxene coexisting with garnet and clinopyroxene is dependent on pressure, temperature and

composition of the coexisting phases. By both thermodynamic reasoning and empirical curve-fitting these dependencies have been modelled in the CMAS and SMACCR systems, resulting in barometric expressions for these systems. The results have been combined with recent experimental investigations in Fe-bearing systems and two independent empirical geobarometers were calibrated, giving satisfactory and consistent results when applied to experiments in multicomponent systems and natural garnet lherzolites.

P,T estimates for various suites of garnet lherzolite xenoliths show differing distributions of P and T comditions of equilibration for different provinces and host rocks. Low temperature xenoliths (<1100°C) from South Africa and Russia outline a geotherm comparable to steady-state geotherms for continental shields. High-temperature xenoliths (>1100°C) from South Africa are derived from a narrow pressure interval around 48-51 kb, covering a range of temperatures from 1100-1400°C. Russian samples with transitional temperatures (1050-1200°C) indicate a parallel trend to South African xenoliths. Garnet lherzolites from lamprophyre (Four-Corners area, southwestern U.S.A.) equilibrated over a range of ≃1000-1200°C at a narrow pressure range around 36-39 kb. Samples from oceanic environments (Solomon Islands), young continental areas (N.S.W., Australia) and the Ile Bizard locality (Canada) show P,T conditions of equilibration in agreement for estimates of P,T conditions for oceanic upper mantle based on heat-flow data or convecting mantle models.

The data on P,T estimates for garnet lherzolites from South Africa have been combined with melting studies on peridotitic systems and lquidus studies on kimberlite to infer conditions of 160-180 km depths and 1400-1500°C for the origin of South African kimberlites. Megacrysts and cumulates found in those kimberlites are precipitates from pre-dating magmas fractionating and/or crystallizing at mantle depths. Diamonds crystallized from pre-dating magmas at conditions close to the graphite-

diamond boundary (900-1300°C, 40-55 kb). Megacrysts, cumulates and diamonds are probably related to kimberlitic magmas, but are xenolithic/xenocrystic to the host kimberlite.

ACKNOWLEDGEMENTS

Firstly and above all, I wish to express my gratitude to my supervisor, Professor D.H. Green, whose friendship, guidance, advice and encouragment were of greatest benefit throughout the course of this study.

Of great value were discussions with and comments by Dr D. Ellis, Dr S. Harley, Mr K. Harris, Dr C. Hatton, Dr G. Jenner, Mr S. Kuehner, Dr H.St. O'Neill, Mr N. Ortez, Mr E. Reid, Mr W. Taylor, Dr R. Varne and Mr G. Wheller.

I am grateful to Mr Keith Harris for his instruction and assistance in the high pressure laboratory and Dr R. Berry and Mr R. Allen for their help in computer modelling. For help and assistance in the use of the microprobe I am indebted to Mr W. Jablonski and Mr R. Lincolne.

During the collection of the samples from Victoria, Australia, I was accompanied and helped by Mr A. Day, Dr I. Nicholls and Dr R. Varne, for which I thank them all. The help with XRF and XRD analyses from Dr D. Ellis, Mr R. Ford, Mr K. Harris and Mr P. Robinson is gratefully acknowledged.

This project was financed by a scholarship from the University of Tasmania. I thank Mrs J. Pongratz for the efficient typing of this thesis.

Many of my fellow students and members of the staff of the Geology Department of the University of Tasmania made this place an enjoyable one to work in and in this respect I wish to thank Dr A. Bush, Mr J. Hajitaheri and Mr W. Naschwitz in particular for their friendship and good sense of humour.

My special thanks I wish to express to Dr C. Eastoe not only for continued friendship, but also for his fine taste in music and the many ways to enjoy Tasmanian fruits, and his delightful way of introducing me to the habits and peculiarities of the culture, language and nature of this unique island.

Finally, I have to thank my wife, Regina, for her love, patience and understanding, which provided an important basis for the continuity of the work. Last, but not least, I thank my daughter, Melanie, for convincing me that there are good reasons to work for and to do the job as rapidly and efficiently as I could.

GLOSSARY OF SYMBOLS AND ABBREIVATIONS USED IN THE TEXT

I. Abbreviations of mineral names

amph	amphibole
ap	apatite
CaCrTs	calcium-chromium-tschermaks molecule ($CaCrAlSiO_6$) in clinopyroxene
CaTs	calcium-aluminium-tschermaks molecule ($CaAl_2SiO_6$)
cpx	clinopyroxene
di	diopside
en	enstatite
fo	forsterite
gr	grossular
gt	garnet
ilm	ilmenite
kn	knorringite
MgCrTs	magnesium-chromium-tschermaks molecule ($MgCrAlSiO_6$)
MgTs	magnesium-aluminium-tschermaks molecule ($MgAl_2SiO_6$)
ol	olivine
opx	orthopyroxene
pi	picotite
py	pyrope
phlo	phlogopite
sp	spinel
uv	uvarovite

II. General expressions

Ca'	molar Ca/Ca+Mg (x 100)
CFMAS	chemical system $CaO-FeO-MgO-Al_2O_3-SiO_2$
CMAS	chemical system $CaO-MgO-Al_2O_3-SiO_2$
Cr'	molar Cr/Cr+Al (x 100)
FMAS	chemical system $FeO-MgO-Al_2O_3-SiO_2$
MAS	chemical system $MgO-Al_2O_3-SiO_2$
Mg'	molar Mg/Mg+Fe (x 100)
P	pressure
SGL	seeded glass-type starting material
SMACCR	chemical system $SiO_2-MgO-Al_2O_3-CaO-Cr_2O_3$
SOGP	starting material made from sintered oxides + pure pyrope (garnet) + pure picotite (spinel).
SSO	seeded sintered oxide starting material

III. Reactions

A $MgAl_2O_4 + 2(Ca,Mg)MgSi_2O_6 = (Ca,Mg)_3Al_2Si_3O_{12} + Mg_2SiO_4$

spinel; ortho, clinopyroxene; garnet; forsterite

B $Mg_2Si_2O_6 + MgAl_2SiO_6 = Mg_3Al_2Si_3O_{12}$

enstatite; MgTs; pyrope

C $MgCrAlSiO_6 + CaAl_2SiO_6 = CaCrAlSiO_6 + MgAl_2SiO_6$

MgCrTs (opx); CaTs (cpx); CaCrTs (cpx); MgTs (opx)

D $Mg_3Al_2Si_3O_{12} + MgCr_2O_4 = Mg_3Cr_2Si_3O_{12} + MgAl_2O_4$

pyrope; picotite; knorringite; spinel

E $Mg_3Al_2Si_3O_{12} + Ca_3Cr_2Si_3O_{12} = Ca_3Al_2Si_3O_{12} + Mg_3Cr_2Si_3O_{12}$

pyrope; uvarovite; grossular; knorringite

F $2Mg_2Si_2O_6 + 2MgCrAlSiO_6 = Mg_3Al_2Si_3O_{12} + Mg_3Cr_2Si_3O_{12}$

enstatite; MgCrTs; pyrope; knorringite

G $Ca_3Cr_2Si_3O_{12} + Fe_3Al_2Si_3O_{12} = Ca_3Al_2Si_3O_{12} + Fe_3Cr_2Si_3O_{12}$

uvarovite; almandine; grossular; Fe-Cr garnet

IV. Symbols used in thermodynamic expressions

a_i^j	activity of component i in phase j
$dG_{1,T}(I)$	standard state free energy change of reaction (I) at 1 bar and temperature of interest (cal/mol)
$dG_{P,T}(I)$	standard state free energy change of reaction (I) at pressure and temperature of interest (cal/mol)
$dG_{rec}(I)$	standard state free energy change of cross-site (reciprocal) reaction (I) at 1 bar and temperature of interest (cal/mol)
$dH(I)$	standard state enthalpy change of reaction (I) at 1 bar and temperature of interest (cal/mol)
$dH_{rec}(I)$	standard state enthalpy of cross-site (reciprocal) reaction (I) at 1 bar and temperature of interest (cal/mol)
$dS(I)$	entropy change of reaction (I) at temperature of interest (cal/mol K = e.u.)
$dS_{rec}(I)$	entropy change of cross-site (reciprocal) reaction (I) at temperature of interest (cal/mol K = e.u.)
dV_r	standard molar volume change of reaction
γ	activity coefficient
$H^i_{f,298}$	enthalpy of formation from the elements of phase i at 298.15 K

$K(I)$	equilibrium constant of reaction (I)
$K_D(I)$	distribution coefficient for reaction (I)
R	universal gas constant 1.987
S^i_{298}	entropy of formation of phase i from the elements at 298.15 K
V^o_i	standard molar volume of phase i at 298.15 K
W_{i-j}	interaction parameter for non-ideal interactions between elements i and j
X^j_i	mole fraction of component/element i in phase/site j.

INTRODUCTION

Although ultramafic xenoliths had long been known and studied, the suggestion that they may represent samples of the Earth's mantle (Wagner, 1928) gave them additional interest and possible significance. Based on the petrography, mineralogy, bulk rock chemistry and mineral chemistry of ultramafic xenoliths, models have been proposed on the vertical and lateral characteristics of the upper mantle.

Within the last two decades an increasing recognition of the complexity of this stratum has developed from studies on lherzolite inclusions in both kimberlites and basaltic rocks. The first part of this thesis is such a study of upper mantle samples from Victoria, Australia.

The study of xenoliths can document phase relationships and provide some information on relationships between rock types. However, the xenolithic character of the lherzolites and their transport within host magmas or intrusive breccias means that we do not have any *a priori* information on the depths of origin. Without this information the xenoliths cannot be used to establish the detailed nature of the Earth's upper mantle. The logical and historical way of achieving this is to study phase relations and their sensitivity to pressure and temperature, using the methods of experimental petrology and thermodynamics.

The Al_2O_3 content of orthopyroxene coexisting with garnet is known to be sensitive to both temperature and pressure. Early experimental studies in both simple and complex systems nearly two decades ago (Boyd & England, 1964; Green & Ringwood, 1967) have been followed by many studies in order to experimentally calibrate a geobarometer.

There are two principal ways to calibrate such a geobarometer: (a) calibrate the Al_2O_3 content of orthopyroxene in simple systems with few chemical components, or (b) to experiment with natural systems. Experimental studies on multicomponent systems such as "pyrolite" (Green & Ringwood, 1967,

1970) have the advantage of being closest to assemblages found in garnet lherzolite xenoliths, but do have significant disadvantages:
(1) due to the complexity it is very difficult to resolve the effects of any single chemical component on the solubility of Al_2O_3 in orthopyroxene;
(2) in order to gain enough analyzable grains of pyroxenes and garnet, natural chemical systems are aften removed from estimates of actual mantle compositions (e.g. "pyrolite - 40% olivine", Green & Ringwood, 1967, 1970);
(3) as evidenced by the chemical variability of garnet lherzolite nodules from kimberlites and spinel lherzolites from basaltic rocks (cf. Proceedings of the International Kimberlite Conferences 1-3, 1975, 1979, in prep.), the upper mantle is not chemically homogeneous and thus there is no unique chemical composition appropriate for experiments.

The method of calibration of a barometer from simple systems allows the experimenter to investigate the effect of a given chemical component on the solubility of Al_2O_3 in orthopyroxene and treat this data thermodynamically. On the other hand, this approach has the disadvantage of using chemical compositions which are removed from those of natural rocks. Extrapolations of data from simple systems always have the inherent danger of being misinterpretations because of the possible effects of chemical components which are not present in the simple systems, but which are components of the natural rock.

In consequence it is necessary to increase the complexity of simple systems in a stepwise manner to understand the effects of chemical components and to cross-check the results with those from natural systems. The past two decades have thus seen numerous experimental studies in simple systems of differing complexity, namely MgO-Al_2O_3-SiO_2 (MAS) (Arima & Onuma, 1977; Boyd & England, 1964; Danckwerth & Newton, 1979; Hensen & Essene, 1971; Howells & O'Hara, 1975, 1978; Lane & Ganguly, 1980; McGregor, 1974; Perkins *et al.*, 1981), CaO-MgO-Al_2O_3-SiO_2 (CMAS) (Akella, 1976; Howells & O'Hara, 1978; Perkins & Newton, 1980), FeO-MgO-Al_2O_3-SiO_2 (FMAS) (Harley, 1981;

Harley & Green, 1982; Holdaway, 1976; Wood, 1974), and CaO-FeO-MgO-Al_2O_3-SiO_2 (CFMAS) (Akella & Boyd, 1973, 1974; Ellis & Green, 1979; Harley, 1981; Harley & Green, 1982; Hensen, 1973; Wood, 1974).

The present study follows this method of increasing the complexity of simple systems by the addition of Cr_2O_3 to CMAS; the system is thus SiO_2-MgO-Al_2O_3-CaO-Cr_2O_3 (SMACCR). The addition of Cr_2O_3 to the system is a further necessary step towards natural mantle compositions, because most spinels and garnets in lherzolites contain Cr as a major component. The system SMACCR also provides the means to investigate possible effects of Cr on the Ca-Mg exchange between pyroxenes and to put constraints on the accuracy of thermometers based on this reaction (Wells, 1977; Wood & Banno, 1973; Lindsley *et al.*, 1981). Furthermore Cr-Al exchange reactions are investigated with reference to their potential as independent thermometers or barometers.

Uncertainties of Al_2O_3 contents of orthopyroxenes in the system CMAS (Howells & O'Hara, 1978) necessitated some additional experiments in this system.

The data from CMAS and SMACCR were then combined with a recent study on FMAS and CFMAS to obtain an empirical expression for geobarometry and geothermometry in the CFMASCR system. Finally, this expression was subject to testing by an experimental study in two complex model mantle compositions with different Cr/Al ratios.

The study then returns to natural peridotites, particularly the garnet peridotites occurring as xenoliths in kimberlites and other basaltic rocks, applying the experimental results and the thermodynamic analysis of these results to deduce the conditions of crystallization of these samples and thus to infer the P,T conditions existing in the upper mantle. On the basis of these inferred P,T conditions the relations between lherzolites and host rocks are discussed and a model for the genesis of kimberlites and diamonds is presented.

PART I

ULTRAMAFIC XENOLITHS FROM LAKE BULLENMERRI AND MT LEURA (VICTORIA, AUSTRALIA) AND THEIR BEARING ON THE EVOLUTION OF THE CONTINENTAL UPPER MANTLE.

1. INTRODUCTION

The xenoliths and megacrysts found in the Pliocene-recent Victorian Newer Volcanics have attracted much attention in recent years because of their abundance and great variety. Work has been carried out concentrating on various aspects including isotope studies (Cooper & Green, 1969; Dasch & Green, 1975), uranium distribution (Kleeman *et al.*, 1969), and on various types - e.g. megacrysts (Irving,1974a), pyroxene-rich xenoliths (Irving, 1974b; Ellis, 1976), lherzolites (Frey & Green, 1974), composite xenoliths (Irving, 1980), as well as their host basalts (Frey *et al.*, 1978; Green, 1973a; Irving & Green, 1976).

These papers have shown that the lherzolites represent accidental xenoliths brought up from the mantle and that the pyroxene-rich xenoliths are high pressure precipitates from either the host magma or preceding magmas.

In a series of papers, Green (e.g. 1973a,b) emphasized the role of water in the genesis of undersaturated basaltic magmas and the implications of the high pressure limit of amphibole stability (Green & Ringwood, 1967b; Lambert & Wyllie, 1968; Green, 1970) to the presence of the low velocity zone, the migration of a water-rich fluid phase in the mantle and the crystallization of amphibole within the lithosphere and particularly at its base. Recent papers on hydrous phases and on metasomatism in the upper mantle (e.g. Best, 1975; Boettcher & O'Neil, 1980; Carswell, 1975; Embey-Isztin, 1976; Francis, 1976a,b; Kesson & Price, 1972; Lloyd & Bailey, 1975; Dawson & Smith, 1982; Mengel *et al.*, 1982; Menzies & Murthy, 1980; Roden *et al.*, 1982; Varne, 1970; Wass, 1980; Wass *et al.*, 1980; Wass & Rogers, 1980; Wilshire *et al.*, 1980; Wilshire & Trask, 1971) have studied and interpreted the role of amphibole and phlogopite in upper mantle xenoliths and there are differing views on the relationship of such hydrous phases to magma genesis and on the pervasive or local character of amphibole-producing metasomatism.

Amphibole and phlogopite have been reported as rare or minor phases in xenoliths from the Newer Volcanics (Ellis, 1976; Frey & Green, 1974; Wass & Irving, 1976), but recently Hollis (1981) and Sutherland & Hollis (1982) reported localities at the maar-type volcanoes Lake Bullenmerri and Lake Gnotuk, at which amphibole-bearing xenoliths are dominant. The present work describes xenoliths from Lake Bullenmerri and nearby Mt Leura, concentrating on petrography, mineral and bulk rock chemistry and the use of these data to deduce a model of mantle evolution beneath the eruption centres.

The location of the two volcanoes is shown in fig. 1 and the geologic setting has been described by Grayson & Mahoney (1910) and Singleton & Joyce (1969).

2. PETROGRAPHY AND MINERALOGY

2.1 HOST ROCKS

The Newer Volcanics province shows a large range of magma types, including quartz tholeiite, olivine tholeiite, olivine basalt, alkali olivine basalt, hawaiite, K-rich hawaiite, nepheline basanite, transitional olivine analcimite, olivine hawaiite and nepheline mugearite. The rocks were described and data on their chemistry were given by Irving & Green (1976), and earlier papers quoted therein.

At both Lake Bullenmerri and Mt Leura the host rocks to the xenoliths are vesicular basanites (table 1) containing small zoned olivine and uncommon clinopyroxene phenocrysts in a groundmass of clinopyroxene, olivine, plagioclase, ilmenite, nepheline, apatite and glass. Unusually large, discrete crystals (termed megacrysts) of amphibole, clinopyroxene and anorthoclase have reaction rims against groundmass. Amphibole is relatively common in Lake Bullenmerri samples.

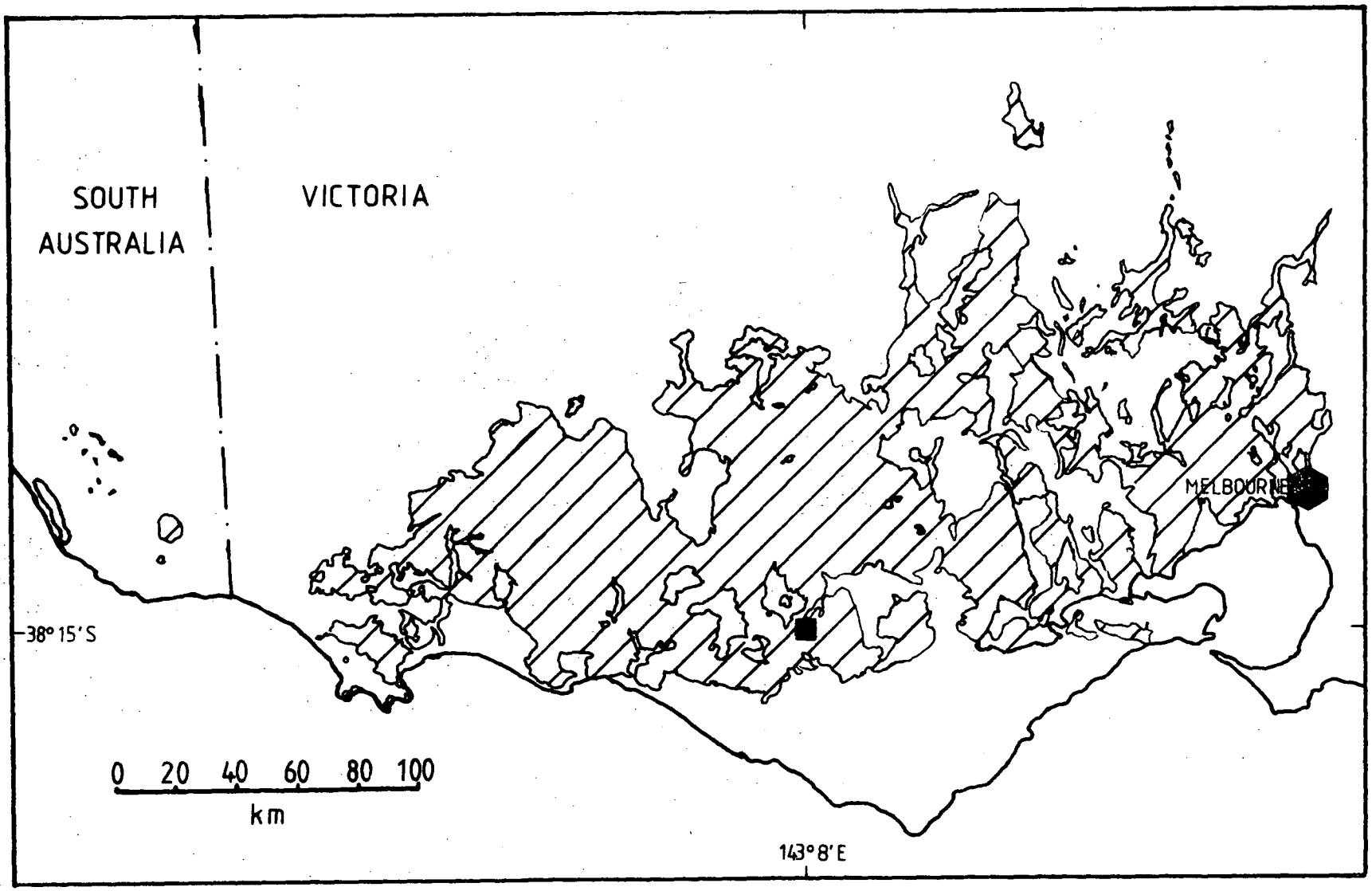

Figure 1: Sample location. The hatched area is the outline of the Newer Volcanics according to Singleton & Joyce (1969). The black square marks the position of both Lake Bullenmerri (a maar) and Mt Leura (a composite cinder cone).

Table 1: Chemical analyses of host rocks, normalised to 100%, volatile-free.

	Mt Leura	Lake Bullenmerri
	no.2650*	BMH-9
SiO_2	45.0	44.87
TiO_2	3.2	2.99
Al_2O_3	13.0	13.01
FeO*	13.0	12.25
MnO	0.2	0.17
MgO	9.9	13.01
CaO	8.5	6.74
Na_2O	4.1	3.67
K_2O	2.2	2.31
P_2O_5	1.1	0.84
Cr_2O_3	0.05	0.08
NiO	0.05	0.06
or	13.0	13.65
ab	14.5	13.77
an	10.6	12.21
ne	11.0	9.36
di	19.6	12.63
ol	17.8	26.94
ilm	6.1	5.68
mt	4.8	3.95
ap	2.6	1.98
Mg*	65.5	69.0

Mg* = 100 x (Mg/Mg+Fe), based on Fe^{++}/Fe^{+++} = 0.8.

FeO* = Fe_{tot} as FeO.

2650* is sample 2650 of Irving & Green (1976), Green (1973a).

2.2 XENOLITHS

On the basis of mineralogical, textural and chemical differences, the xenoliths have been grouped into several types:

A - lherzolites (ol > opx > cpx > sp ± amph ± mica)
  1 - without hydrous phases or remnants thereof ("anhydrous")
  2 - amphibole-bearing
  3 - phlogopite-bearing
  4 - with sites of former hydrous phases, now present only as secondary assemblages
  5 - amphibole- and phlogopite-bearing
  6 - Fe-rich (amphibole-bearing)
  7 - layered or banded

B - wehrlites (ol > cpx ± amph ± sp ± opx ± mica ± ap)

C - harzburgites (ol > opx > sp ± amph)

D - hornblendites (amph > mica > ilm ± cpx ± opx ± titanomag ± ol)

E - composite xenoliths (two or more different types of rock in one specimen)

F - pyroxenites (gt, cpx, opx ± sp ± amph)

G - cumulate texture wehrlite (ol > cpx, amph, phlo).

Summary rock descriptions are listed in table 2, more detailed descriptions of the nodules, including the composite xenoliths, are given in appendix 1.

The textures of the peridotitic rocks are classified following Mercier & Nicolas (1975) into protogranular, porphyroclastic and recrystallized (equigranular or tabular), but it must be noted that most samples represent transitional types.

The optical characteristics of the minerals are as described by previous authors (Brown *et al.*, 1980; Frey & Green, 1974; Frey & Prinz, 1978; Harte, 1977; Kleeman *et al.*, 1969; Mercier & Nicolas, 1975; Pike *et al.*, 1980; Toxopeus, 1977; White, 1966). Only some of the more specific features of the minerals found in the xenoliths are described below.

Table 2: Rock description in form of summary table.

Crosses under two categories for any criterion denote transitional types, e.g. crosses under both medium and fine grainsize mean medium to fine grainsize.

Abbreviations used:

Grainsize* = dominant grainsize; PG = protogranular; PO = porphyroclastic; RE = recrystallized-equigranular or tabular; c = coarse; m = medium; f = fine; n = nil; w = weak; s = strong; fr = fresh; bk = breakdown products of hydrous phases present; ol = olivine; opx = orthopyroxene; cpx = clinopyroxene; sp = spinel; gt = garnet; amph = amphibole; phlo = phlogopite; ap = apatite; ilm = ilmenite; titanom = titano-magnetite; intergr = intergrowth texture.

Table 2: Rock description in form of summary table.

Group/Sample		Phases	Texture			Grainsize*			Foliation			Exsolutions in pyroxenes	Amphibole			Special features
			PG	PO	RE	c	m	f	n	w	s		n	fr	bk	
A-1	BM-54	ol,opx,cpx,sp		+	+		+	+		+			+			Few veinlets of brownish glass.
	BM-69	ol,opx,cpx,sp		+		+	+			+	+		+			Sp concentrated in layers.
	BM-99	ol,opx,cpx,sp		+		+	+		+				+			
	BM-160	ol,opx,cpx,sp	+	+		+			+				+			Few veinlets of brownish glass.
	LE-00	ol,opx,cpx,sp		+	+		+	+		+	+		+			Is part of composite xenoliths.
	LE-50	ol,opx,cpx,sp		+			+		+				+			Ol shows small strain features (kink bands).
	LE-532	ol,opx,cpx,sp		+			+			+			+			
	LE-539	ol,opx,cpx,sp	+	+		+	+				+		+			Sp as patches paralleling foliation.
	LE-2664	ol,opx,cpx,sp	+			+			+			+	+			
A-2	BM-9	ol,opx,cpx, amph		+		+					+	+		+	+	Cpx with marginal breakdown.
	BM-15	ol,opx,cpx, sp,amph		+	+			+	+					+		Sp patches larger than dominant grainsize (2 mm).
	BM-27	ol,opx,cpx, sp,amph	+	+		+				+		+		+		Large sp with rounded ol,opx inclusions.
	BM-58	ol,opx,cpx, sp,amph		+	+			+	+			+		+	+	Cpx with marginal breakdown.
	BM-62	ol,opx,cpx, sp,amph	+	+		+			+			+		+	+	Sp with rounded ol,opx inclusions.
	BM-74	ol,opx,cpx, sp,amph	+	+		+			+			+		+	+	
	BM-134	ol,opx,cpx, sp,amph		+		+	+				+	+		+	+	
	BM-139	ol,opx,cpx, sp,amph	+	+			+				+			+	+	Cpx with marginal breakdown.
	BM-147	ol,opx,cpx, sp,amph		+		+	+			+		+		+	+	
	BM-161	ol,opx,cpx, sp,amph	+	+		+			+			+		+	+	
	BM-166	ol,opx,cpx, sp,amph	+	+		+			+			+		+	+	
	BM-167	ol,opx,cpx, sp,amph		+		+					+	+		+	+	
	LE-2641	ol,opx,cpx, sp,amph	+			+			+			+		+	+	Rare amphibole.
A-3	LE-67	ol,opx,cpx, sp,amph	+	+		+				+		+	+			
	LE-68	ol,opx,cpx, sp,amph		+		+			+	+			+			
A-4	BM-48	ol,opx,cpx,sp		+		+	+			+		+			+	Some veinlets of brownish glass.
	BM-144	ol,opx,cpx,sp	+			+			+			+			+	Some patches with darker brown glass (from phlogopite?)
	BM-162	ol,opx,cpx,sp	+	+		+				+		+			+	
	LE-4	ol,opx,cpx,sp		+			+	+		+					+	Cpx with marginal breakdown.
	LE-19	ol,opx,cpx,sp	+	+		+			+			+			+	
	LE-544	ol,opx,cpx,sp	+	+		+			+			+			+	
	LE-2662	ol,opx,cpx,sp		+			+		+	+		+			+	Cpx with frequent breakdown halo.
A-5	BM-143	ol,opx,cpx, sp,amph,phlo		+	+		+	+	+					+		Clusters of small cpx with outline of large (1 cm) euhedral cpx.
A-6	BM-47	ol,opx,cpx, amph		+		+	+		+	+		+		+	+	Opx small, large and abundant amph.
	BM-154	ol,opx,cpx, sp,amph	+	+		+				+				+	+	Opx small, large and abundant amph.
B	BM-18	ol,opx,sp, cpx,amph,ap	+	+		+			+			+		+	+	Rare opx, large cpx are poikilitic.
	BM-51	ol,cpx,amph, sp,ap			+		+	+			+			+		Some large amph (up to 1 cm).
	BM-135	ol,cpx,amph		+	+			+		+				+	+	
	BM-142	ol,cpx		+	+		+	+		+					+	Cpx occasionally poikilitic, abundant amph breakdown patches.
	BM-152	ol,cpx,amph, opx,sp	cumulus			variable						+		+		Larger grains rounded, pockets of dunitic material (+sp), rare opx.
	LE-27	ol,cpx,phlo, opx,sp	+	+			+				+		+			Phlo common parallel to foliation oriented patches.
C	BM-163	ol,opx,amph, sp	+			+			+			+		+	+	
D	BM-117	amph,phlo, ilm,titanom, ol	intergr.			+			+					+		Ilm- exsolution from amph, some brownish glass.
	BM-156	amph,phlo, ilm	intergr.			+			+					+		Contains fine grained pyroxenite (opx,cpx,ilm,phlo,amph matrix).
G	BM-168	ol,cpx, amph,phlo, opx	cumulus			+			+					+	+	Rare opx,cpx with marginal breakdown, partly poikilitic, some dark brown glass.

Exsolution lamellae of orthopyroxene in clinopyroxene and *vice versa* are present in some but not all samples and it is noteworthy that exsolution of orthopyroxene and spinel from clinopyroxene is more commonly developed in amphibole-bearing lherzolites than in other lherzolites.

In some samples, clinopyroxene develops a rim containing small glass inclusions within a clinopyroxene of lower Na_2O content (Kleeman *et al.*, 1969, fig.1; Frey & Green, 1974), which may be interpreted as breakdown of primary clinopyroxene under low pressure, high temperature conditions. In addition, primary clinopyroxene commonly occurs adjacent to patches of glass containing euhedral spinel + olivine + clinopyroxene (the latter commonly growing on the neighbouring primary clinopyroxene, fig. 2 of Kleeman *et al.*, 1969). These patches are interpreted as products of breakdown and incongruent melting of former hydrous phases, commonly amphibole but also occasionally phlogopite (Frey & Green, 1974) and are not melting products of the primary clinopyroxene + spinel + orthopyroxene + olivine assemblage (appendix 2).

Primary spinel is variable in composition and colour (from yellow-brown to deep red-brown) and in those xenoliths where amphibole is present (or was originally present) the amphibole or its breakdown products almost always occurs in contact with spinel.

Amphibole varies in modal abundance (up to 15%) in groups A to C and is a very pale brown, pleochroic pargasite. It commonly mantles spinel but also occurs as a dispersed euhedral to anhedral phase included in or between any of the major minerals. Many examples of partial breakdown to olivine + clinopyroxene + spinel + glass have been observed and the petrographic and analytical data from such examples provides evidence for interpretation of all such (ol + cpx + sp + glass) patches as products of amphibole (and/or phlogopite) breakdown (see appendix 2).

In the hornblendites the amphibole is darker brown pleochroic Ti-rich pargasite to kaersutite, forming large grains in intergrowth with phlogopite and ilmenite. Exsolution of ilmenite from kaersutite occurs and Ellis

(1976) describes an example with large euhedral amphibole and intercumulus ilmenite and phlogopite. In one sample (BM-156) the hornblendite contains an included pyroxenite (opx, cpx, minor ol and interstitial brown hornblende).

Phlogopite is rare in the lherzolites but where it occurs it is subhedral to euhedral and may be entirely included within olivine or at grain boundaries. Except for occasional occurrences as a minor phase localized within thin mylonite zones (Frey & Green, 1974), there is no textural evidence that phlogopite is an introduced (metasomatic or replacement) phase in the lherzolites. One wehrlite (LE-27) has unusually abundant phlogopite occurring in lenticular patches parallel to the foliation.

Garnet has only been observed in pyroxenites, forming large subhedral to euhedral neoblasts with kelphytic rims. Apatite has previously been reported as a rare primary accessory phase in lherzolites from Mt Noorat (west of Mt Leura) (Cooper & Green, 1969; Kleeman *et al.*, 1969; Frey & Green, 1974) and wehrlite from Mt Leura (Kleeman *et al.*, 1969). Apatite was not observed in lherzolites examined in this study, but was found as a turbid interstitial phase within two wehrlites (BM-18, BM-51).

3. BULK ROCK CHEMISTRY

Discussions of bulk rock chemistry (table 3) must bear in mind three constraining difficulties: (i) the coarse grain size and small sample size (most are < 20 cm) make representative sampling difficult; (ii) mineral banding enhances the problems of representative sampling; and (iii) concentrations of Na, K, Ti, P are very low and detection limits of XRF analyses are similar to abundance levels, so that large relative errors can result.

To overcome problems with the Na_2O analyses at levels which are near the detection limit of XRF analyses for lherzolites, harzburgites and wehrlites, a different approach has been used. Since the composition of all phases is known from microprobe analyses, modal abundances can be calculated by a least-squares fit to the analysed bulk rock composition. This has been done on the basis of nine elements, excluding Na. The quality of fitting can be demonstrated by a low sum of least-squares. Given the modal abundances, the Na-content of the bulk rock has been calculated from the analysed minerals.

On the basis of bulk rock chemistry, subsets can be distinguished. The AFM diagram (fig. 2) shows a single linear trend for hydrous and anhydrous lherzolites and the harzburgite, clearly separated from the data points of wehrlites, Fe-rich lherzolites and the cumulate BM-168. The wehrlites and Fe-rich lherzolites may be interpreted as following a different cumulate trend. Lherzolites of group A-5 and A-7 however fall off both trends, indicating different histories.

A similar result is obtained by the plot Mg/Mg+Fe vs. Cr/Cr+Al (fig. 3), Lherzolites, again regardless of their mineralogy, form a linear trend at a high angle to that for the cumulates (except BM-142). In this plot, not only the harzburgite is in line with the lherzolites, but also the lherzolites of group A-5 and A-7.

Table 3: Chemical analyses of bulk rocks, normalised to 100% on volatile-free basis.

	Group A-1			Group A-2						A-4
	BM-69	BM-99	BM-160	BM-9	BM-134	BM-162	BM-167	BM-139	BM-15	BM-144
Na_2O	0.14	0.12	0.14	0.19	0.32	0.19	0.19	0.72	0.40	0.16
MgO	44.12	44.25	40.26	45.95	44.41	42.26	40.65	38.35	37.99	40.36
Al_2O_3	1.65	1.69	2.91	0.72	1.25	2.12	2.75	3.59	3.86	2.62
SiO_2	43.72	44.36	45.19	43.87	43.15	44.64	44.30	44.51	44.95	44.80
K_2O	nd	nd	nd	0.03	0.03	nd	nd	0.17	0.03	nd
CaO	1.47	1.72	2.60	0.67	1.22	2.20	2.64	3.49	3.54	2.54
TiO_2	0.04	0.05	0.10	0.02	0.04	0.06	0.11	0.17	0.17	0.08
FeO*	8.10	7.98	8.01	7.70	8.80	7.67	8.58	8.26	8.27	8.62
Cr_2O_3	0.33	0.42	0.39	0.39	0.35	0.46	0.37	0.41	0.41	0.41
MnO	0.14	0.13	0.14	0.12	0.15	0.13	0.14	0.14	0.14	0.13
NiO	0.30	0.29	0.28	0.32	0.32	0.28	0.27	0.23	0.24	0.27
Mg'	90.7	90.6	90.0	91.4	90.0	90.8	89.4	89.2	89.1	89.3
Cr'	11.5	14.4	8.25	26.7	16.2	12.7	8.3	7.0	6.7	9.6
Zr	2	9	4	2	5	3	5	32	16	10
Sc	10	8	9.4	6	7	11	12	16	15	11
V	49	42	55	30	36	56	63	89	86	58
Sr	-	21	10	21	33	4	11	75	32	13
Ba	3	6	10	9	16	6	6	40	11	14

	A-5	Group A-6		A-7	Group B					C
	BM-143	BM-154	BM-47	BM-137	BM-18	BM-135	BM-142	BM-51	BM-152	BM-163
Na_2O	0.64	0.30	0.55	0.81	0.51	0.46	0.25	0.82	0.40	0.24
MgO	36.09	41.68	38.37	30.96	44.01	42.58	42.39	41.77	38.12	46.90
Al_2O_3	4.30	1.54	2.45	7.64	1.04	1.04	0.70	1.71	1.73	0.68
SiO_2	45.67	43.34	44.40	44.15	42.30	42.13	41.60	42.36	42.02	43.39
K_2O	0.08	0.04	0.14	0.09	0.07	0.06	0.10	0.11	0.04	0.02
CaO	4.74	1.60	2.88	6.24	2.50	2.98	1.83	3.96	3.65	0.63
TiO_2	0.45	0.14	0.07	0.44	0.10	0.11	0.10	0.07	0.31	0.02
FeO*	7.02	10.44	10.33	6.24	8.32	9.85	12.17	8.00	13.19	7.27
Cr_2O_3	0.67	0.40	0.44	0.84	0.39	0.34	0.33	0.51	0.20	0.38
MnO	0.12	0.15	0.18	0.11	0.15	0.15	0.23	0.14	0.13	0.13
NiO	0.22	0.29	0.24	0.21	0.28	0.27	0.29	0.26	0.22	0.31
P_2O_5		0.01	0.04	0.05	0.35	nd	nd	0.35	nd	0.04
Mg'	90.2	87.7	86.9	89.9	90.4	88.5	86.1	90.3	83.3	92.0
Cr'	9.4	14.7	10.8	6.8	19.8	18.1	24.0	16.8	7.2	27.3
Zr	19	21	29	42	2	36	72	24	13	5
Sc	19	7	13	30	8	7	5	12	9	7
V	121	43	72	180	39	37	23	54	71	24
Sr	83	18	80	100	294	80	69	242	34	76
Ba	36	11	19	70	42	21	12	41	35	33

	Group D		Groups E/F			G
	BM-117	BM-156	BM-114	BM-116G	BM-116C	BM-168
Na_2O	2.11	1.53	1.11	1.11	1.36	0.51
MgO	12.35	13.27	16.96	17.27	19.52	31.09
Al_2O_3	14.14	12.42	13.94	14.72	11.75	4.14
SiO_2	38.12	43.40	48.06	47.37	47.84	43.60
K_2O	1.77	0.93	0.07	0.04	0.13	0.23
CaO	9.90	12.38	12.83	12.94	13.95	6.12
TiO_2	7.48	4.10	0.14	0.19	0.33	0.71
FeO*	8.83	11.73	6.49	5.95	3.90	13.71
Cr_2O_3	0.01	0.05	0.15	0.15	1.01	0.07
MnO	0.11	0.13	0.19	0.19	0.08	0.17
NiO	0.02	0.02	0.04	0.04	0.07	0.15
P_2O_5	nd	0.01	0.02	0.01	nd	0.03
Mg'	63.4	66.8	82.3	83.8	89.9	80.8
Zr	55	46	26	11	10	42
Sc	22	27	53	47	39	13
V	549	449	219	221	218	133
Sr	572	337	123	102	186	111
Ba	311	171	31	21	125	81

FeO* = Fe total as FeO
Mg' = Mg/(Mg+Fe)
Cr' = Cr/(Cr+Al)
Major elements in wt.%.
Trace elements in ppm.

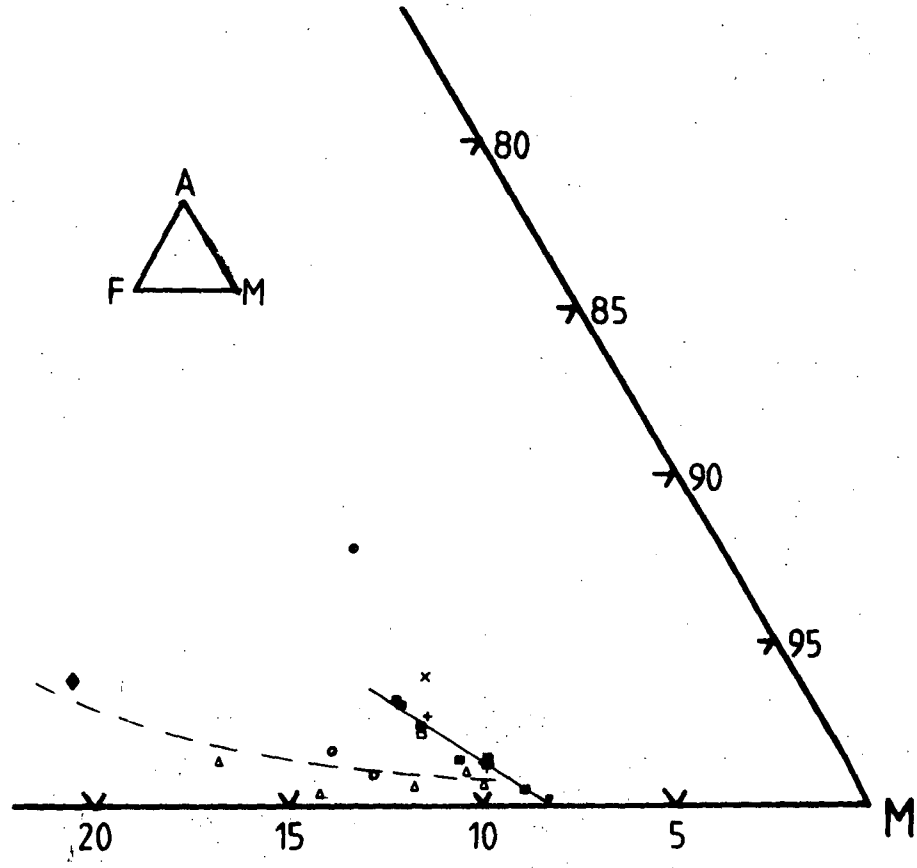

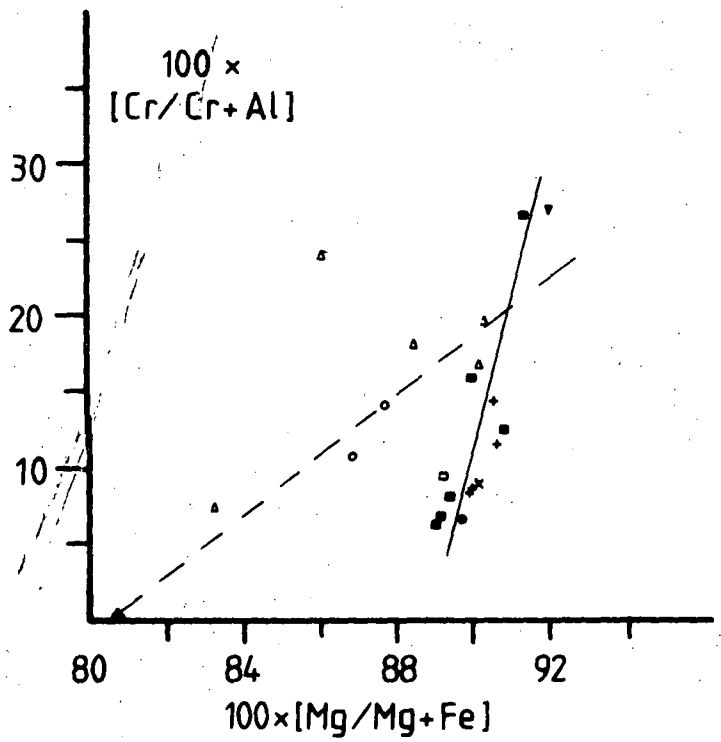

Symbols

Lherzolites
- anhydrous (A 1)
- amphibole bearing (A 2)
- with secondary ass. after hydrous phases (A 4)
- amphibole + phlogopite bearing (A 5)
- Fe-rich (A 6)
- layered or banded (A 7)

- Wehrlites (B)
- Harzburgites (C)
- cum. text. wehrlite (G)

Figures 2 and 3: Bulk rock compositions of ultramafic xenoliths from Lake Bullenmerri in mole %.
Top - plots of $A(Al_2O_3)$-F(FeO)-M(MgO).
Bottom - Cr/Cr+Al vs. Mg/Mg+Fe.
Solid and dashed lines are visually plotted trends for residual lherzolites and cumulates respectively. Note that FeO is total Fe as FeO.

In chemical variation diagrams of the type MgO (wt.%) vs. oxides or trace elements the wehrlites, Fe-rich lherzolites and other cumulates do not form clear trends, but tend to scatter. This may be seen as evidence that those do not belong to one single group. They may originate in different events and represent cumulates from different sources (e.g. picrite, basanite).

The lherzolites (except groups A-5 and A-7) on the other hand exhibit regular variations with MgO for a number of oxides and trace elements (fig. 4). The best correlations are given with Al_2O_3 and CaO, showing a very well defined linear trend. Variations with SiO_2, TiO_2, Sc, and V may be interpreted as having a slight curvature, but their trends are still reasonably approximated by a straight line. FeO and Cr_2O_3 do not correlate with MgO, but remain approximately constant at 8.25 $\pm$ 1% and 0.40 $\pm$ 0.1% respectively. A straight line chemical variation in oxides or oxide ratios is suggestive of having the character of a mixing line for those elements.

Na_2O, Ba, Sr and Zr show only a very weak or no correlation with MgO. However, the variations of these elements in most of the amphibole-bearing lherzolites are within the compositional spectrum of the anhydrous lherzolites.

Efforts have been made to analyse for K_2O, P_2O_5, Rb, Y, and Nb. The detected range ($K_2O \leq 0.03\% \leq P_2O_5 \leq 0.04\%$, Rb $\leq$ 3 ppm, Y $\leq$ 3 ppm, Nb $\leq$ 2 ppm) was in each case close to the detection limit of XRF analyses, hence their variation cannot provide significant trends. Nonetheless the low concentrations of K_2O, P_2O_5, Rb, Y and Nb in both hydrous and anhydrous lherzolites argues that these elements have not been added in large, significant amounts to the hydrous lherzolites. However, sample BM-139 shows unusual high values for K_2O, Nb as well as Na_2O, Sr, Ba and Zr. This sample has an exceptionally high modal abundance of amphibole (approx. 15%) and thus may provide evidence for metasomatic chemical change. It should be noted that the sample is small, and thus the exceptional values may also be due to non-representative sampling.

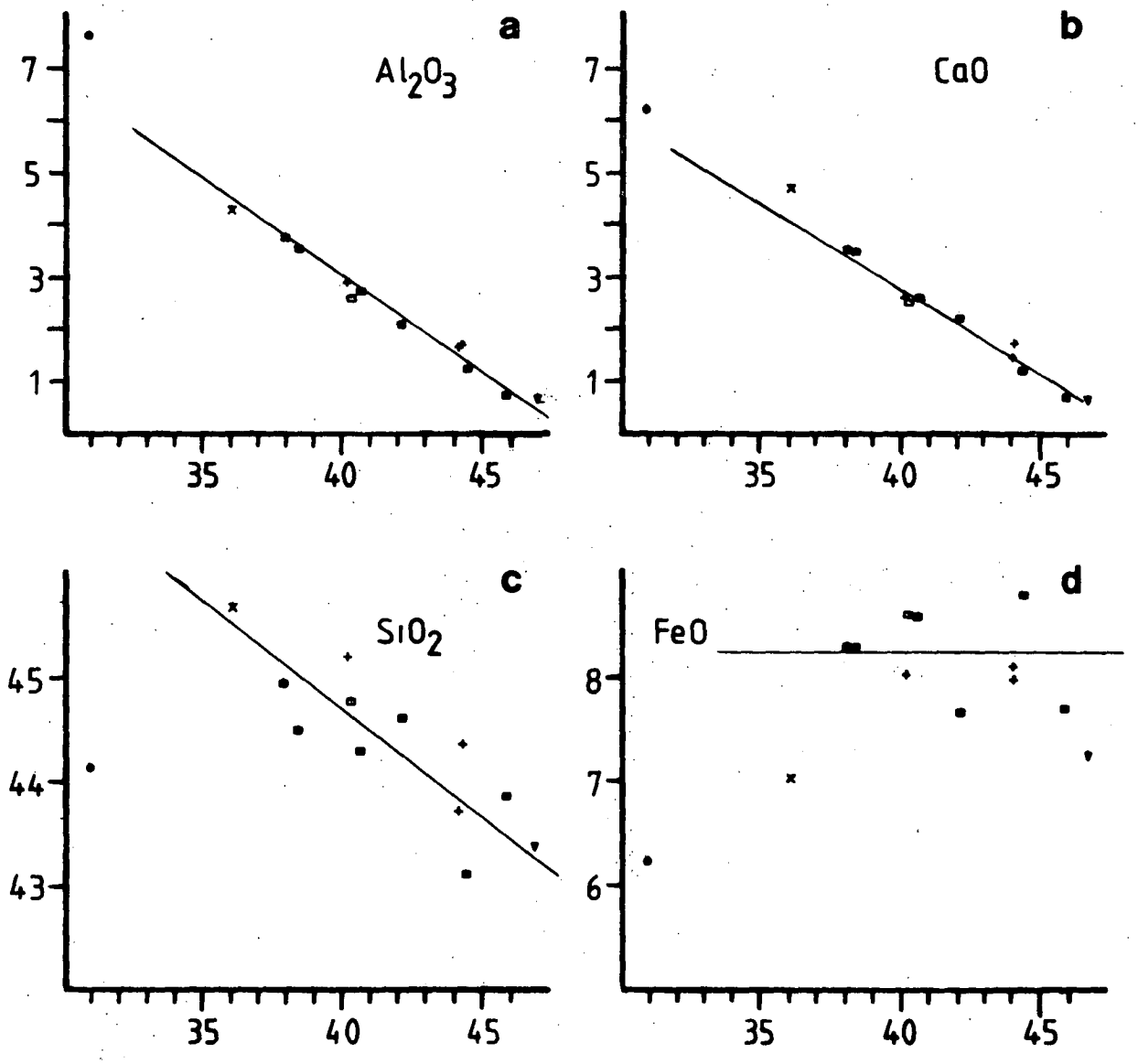

re 4a-m: Bulk rock concentrations of major and trace elements of lherzolite and harzburgite nodules (groups A1-A5, A7, C) from Lake Bullenmerri plotted against wt.% MgO. Major elements (4a-h) in wt.%, trace elements (4i-m) in ppm. Solid lines are visually plotted trends for oxides/elements with clear linear correlations. Note that lherzolites of groups A5 and A7 were excluded from the fit and that FeO is total Fe as FeO. Symbols as for figure 2.

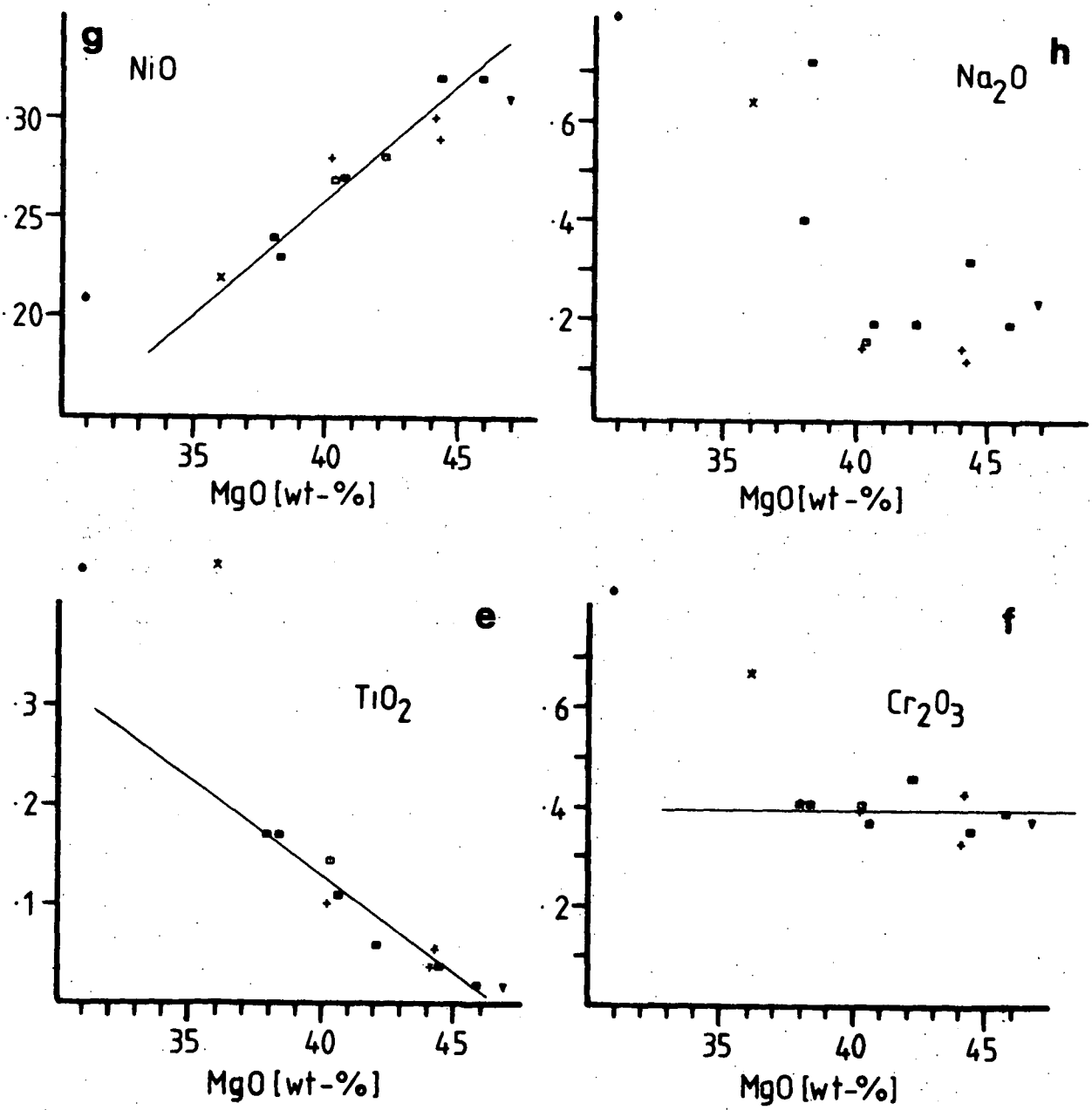
g
NiO
.30
.25
.20
35
40
45
MgO [wt-%]
h
Na_2O
.6
.4
.2
35
40
45
MgO [wt-%]
e
TiO_2
.3
.2
.1
35
40
45
MgO [wt-%]
f
Cr_2O_3
.6
.4
.2
35
40
45
MgO [wt-%]

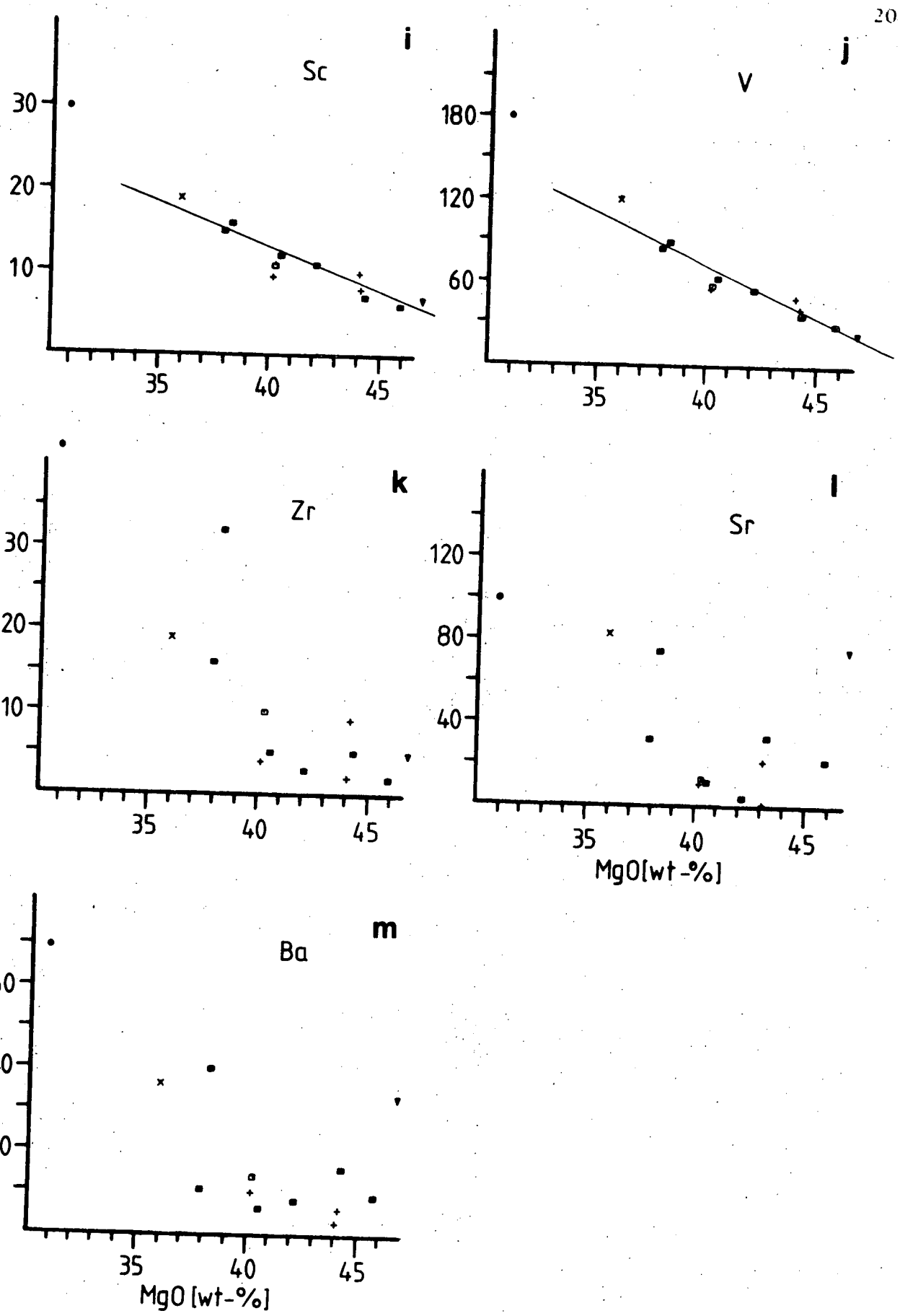
i
Sc
30
20
10
35
40
45
j
V
180
120
60
35
40
45
k
Zr
30
20
10
35
40
45
l
Sr
120
80
40
35
40
45
MgO[wt-%]
m
Ba
60
40
20
35
40
45
MgO [wt-%]

The group A-5 sample is not only unusual in containing both amphibole and phlogopite, but also in being Mg-poor. It is in line with the trends for the lherzolites for most elements, but shows strong deviation in Ti and Cr and minor deviation in Fe and Ca.

Group A-7 sample differs from the trends for the other lherzolites for every element, especially TiO_2, Cr_2O_3, FeO and SiO_2. Although it is relatively Mg-poor, its Mg value is still high (89.8) and although it is very rich in Cr_2O_3 its Cr/Cr+Al ratio remains low (6.8). It is also unusual in MgO vs. NiO, where all other groups show identical behaviour.

4. MINERAL CHEMISTRY

Analyses of the constituent phases are listed in appendix 3. The spinel lherzolites show the typical range of compositions observed in many localities (e.g. Basaltic Volcanism Study Project, 1981; Frey & Green, 1974; Frey & Prinz, 1978; Kuno, 1969; Kuno & Aoki, 1970; Maaløe & Aoki, 1977; Ross *et al.*, 1954; White, 1966) with olivine in the range Fo_{88-92} and principal variations being in the Al_2O_3 content of pyroxenes and the Cr/Cr+Al ratio of spinel.

The wehrlites and lherzolites of groups A-5 to A-7 and group B have olivine in the range Fo_{90-82}, compatible with the interpretation that they are of cumulate or recrystallized cumulate origin, their parent magma being picrite, olivine tholeiite or undersaturated olivine basalt, basanite etc. One of the wehrlites (BM-152) which on textural grounds has been classified as a cumulate or intrusion breccia with early cumulate fragments enclosed in intercumulus phases, shows supporting mineralogical evidence for this in that the olivine and clinopyroxene of the dunitic (amphibole-free) cumulate have slightly higher Mg values than olivine and clinopyroxene of the intercumulus matrix.

The group C harzburgite shows affinities with the group A lherzolites and is very refractory in terms of Mg values of olivine and orthopyroxene and in the high Cr/Al of spinel. The amphibole is similarly Mg-rich and high in Cr_2O_3, but is the most Na-rich of all amphiboles analysed and contains moderately high K_2O.

The group D hornblendites are markedly more Fe-rich than all other assemblages and this pattern continues in the composite xenoliths in which amphibole-phlogopite veinlets occur. By contrast the pyroxenites examined do not include examples of Fe-rich pyroxenite described by Ellis (1976) (including samples from Mt Leura), but are Mg-rich and highly aluminous, with compositions resembling those of the lherzolite suite. Consistent with the highly magnesian clinopyroxenes (Mg_{89-91}), the garnets are also highly magnesian (Mg_{79-82}) but with low Cr_2O_3 contents (lower than co-existing clinopyroxene).

The distinctive cumulate textured wehrlite (group G) has mineral compositions closest to those of group B wehrlites and group D hornblendites.

5. CONDITIONS OF CRYSTALLIZATION OF LHERZOLITE XENOLITHS

Chemical equilibrium between coexisting mineral phases may be inferred if there is regular, systematic partitioning of elements among phases. It is possible to use some element partitioning relationships to deduce P,T conditions of equilibration, while other relationships may be used qualitatively to infer similarities or differences in conditions of crystallization.

5.1 Fe/Mg PARTITIONING

Plots of Fe/Mg ratios of the phases olivine, orthopyroxene, clinopyroxene and amphibole all reveal linear relationships with varying degrees of scatter (fig. 5). The problem of uncertainty of Fe^{+++}/Fe^{++} from microprobe analyses limits the extent to which element partitioning can be used to infer temperatures of crystallization, but the covariance among all four phases argues that all are equilibrated phases and that amphibole in particular is not a late, independent metasomatic-introduced phase (i.e. all components associated with amphibole growth were present prior to or during the crystallization of the olivine-pyroxene-amphibole assemblages).

The $(Fe/Mg)_{ol}$ vs. $(Fe/Mg)_{cpx}$ plot (fig. 5C) reveals some scatter of points but a systematically lower value of $K_D = (Fe/Mg)_{cpx}/(Fe/Mg)_{ol}$ for amphibole - bearing assemblages than for anhydrous or phlogopite-bearing lherzolites. Uncertainty in Fe^{++}/Fe^{+++} of clinopyroxene prevents meaningful temperature estimates, but lower temperatures of crystallization of the amphibole-bearing lherzolites are inferred using an empirical experimental calibration (Mori & Green, 1978).

The Fe/Mg partitioning between spinel and olivine shows a strong compositional dependence on Cr/Cr+Al of spinel (fig. 6). Ambiguity in the calibration of the potential olivine-spinel geothermometer (Evans & Frost, 1975; Engi & Evans, 1980; Roeder *et al.*, 1979) prevents any comparative temperature determination from these data.

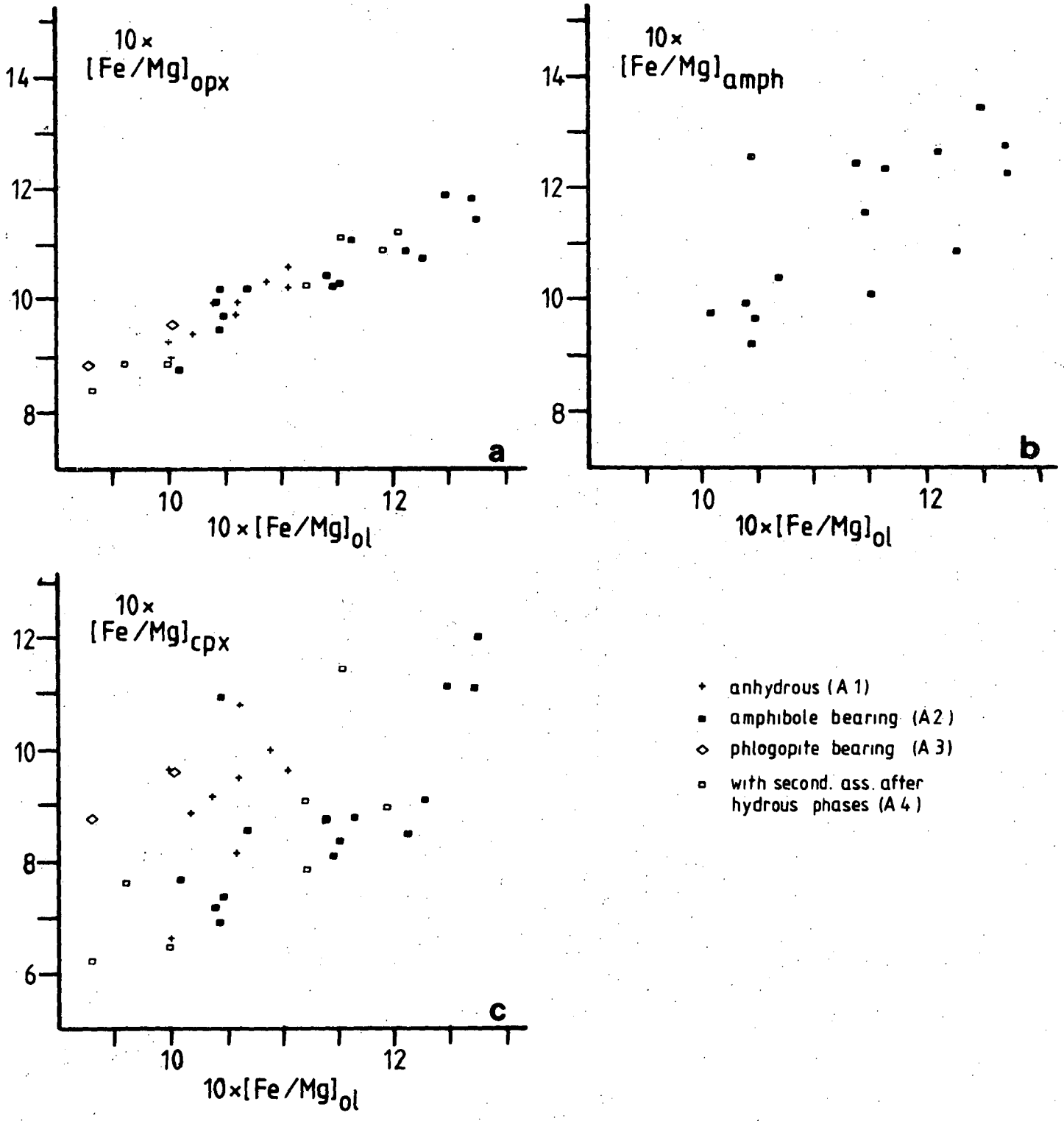

Figure 5a-c: Molar Fe/Mg of olivine vs. Fe/Mg of coexisting orthopyroxene (a), amphibole (b), and clinopyroxene (c). Fe is total Fe. Plotted are values for lherzolites of groups A1-A4.

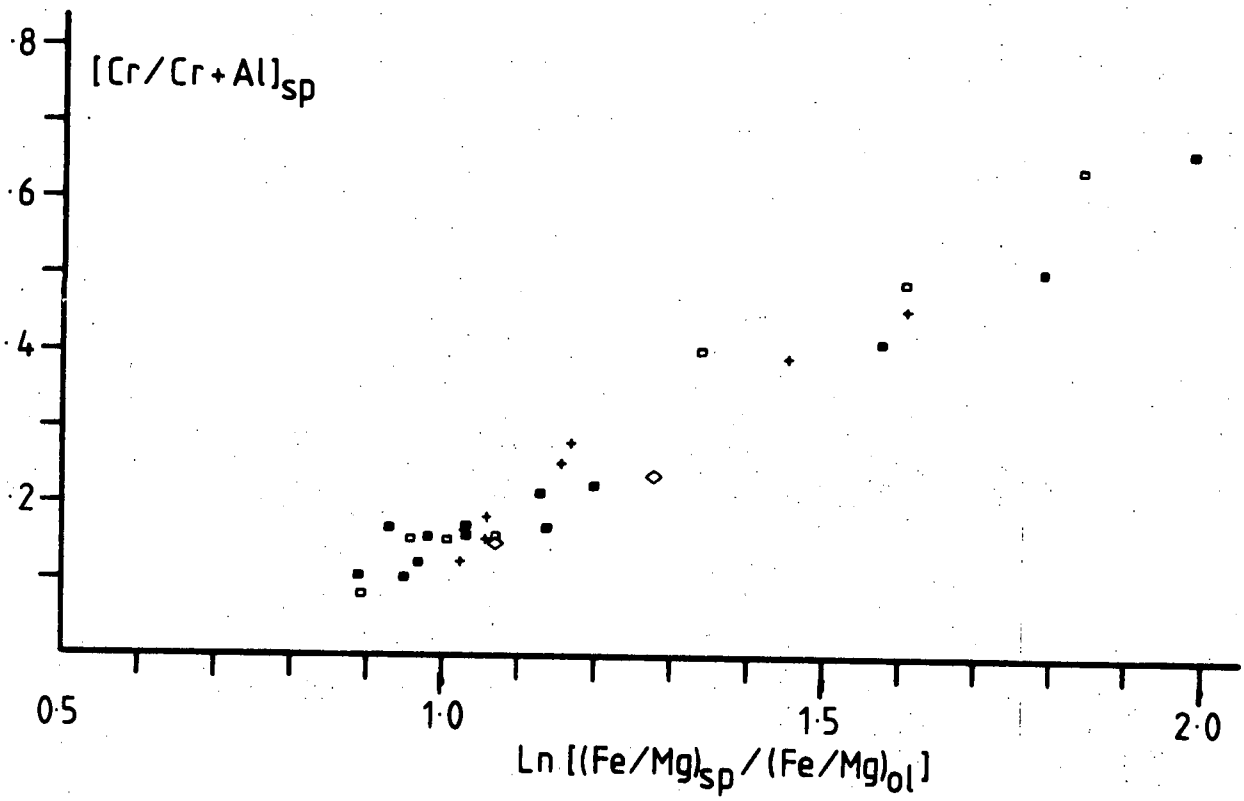

re 6: Cr/Cr+Al of spinel vs. the *ln* K_D[(Fe/Mg) spinel/(Fe/Mg) olivine] for lherzolites of groups A1-A4. Symbols as for figure 5.

5.2 Cr/Al PARTITIONING AND Al^{IV}/Si PARTITIONING

The data in table 2 show positive correlation of Cr/Al between spinel, opx, cpx, and amphibole (fig. 7). The plots of $(Cr/Al)_{opx}$ vs. $(Cr/Al)_{sp}$ and $(Cr/Al)_{cpx}$ both show weak systematic grouping of the amphibole-bearing and amphibole-free data. This relationship and its potential as a geothermometer (McGregor, 1982) is discussed later.

The substitution of Al for Si provides further evidence for equilibrium between phases. Plots of $(Al^{IV}/Si)_{cpx}$ vs. both $(Al^{IV}/Si)_{opx}$ and $(Al^{IV}/Si)_{amph}$ (fig. 8) show strong correlation and linear relationships.

To summarize the element partitioning data for coexisting minerals, the regularity of compositional relationships shows that olivine - two pyroxenes - spinel and amphibole (where present) crystallized together in equilibrium at varying P,T conditions (cf. Section 5.3) in a limited range of bulk compositions. In particular, amphibole is an equilibrium phase within the assemblage in which it occurs and does not reflect disequilibrium or arrested replacement process by superimposed metasomatic events.

The limited number of samples containing phlogopite does not permit a similar analysis of the element partitioning relations between phlogopite and other phases, but it may be noted that phlogopite, apart from occurrences in mylonite zones (Frey & Green, 1974) is in textural equilibrium and consistently shows Mg values lower than coexisting pyroxenes and higher than coexisting amphibole. (Note that the Mg-value referred to is based on total Fe and low values for amphibole and phlogopite are in part at least attributable to Fe^{+++} contents - cf. Frey & Green, 1974.)

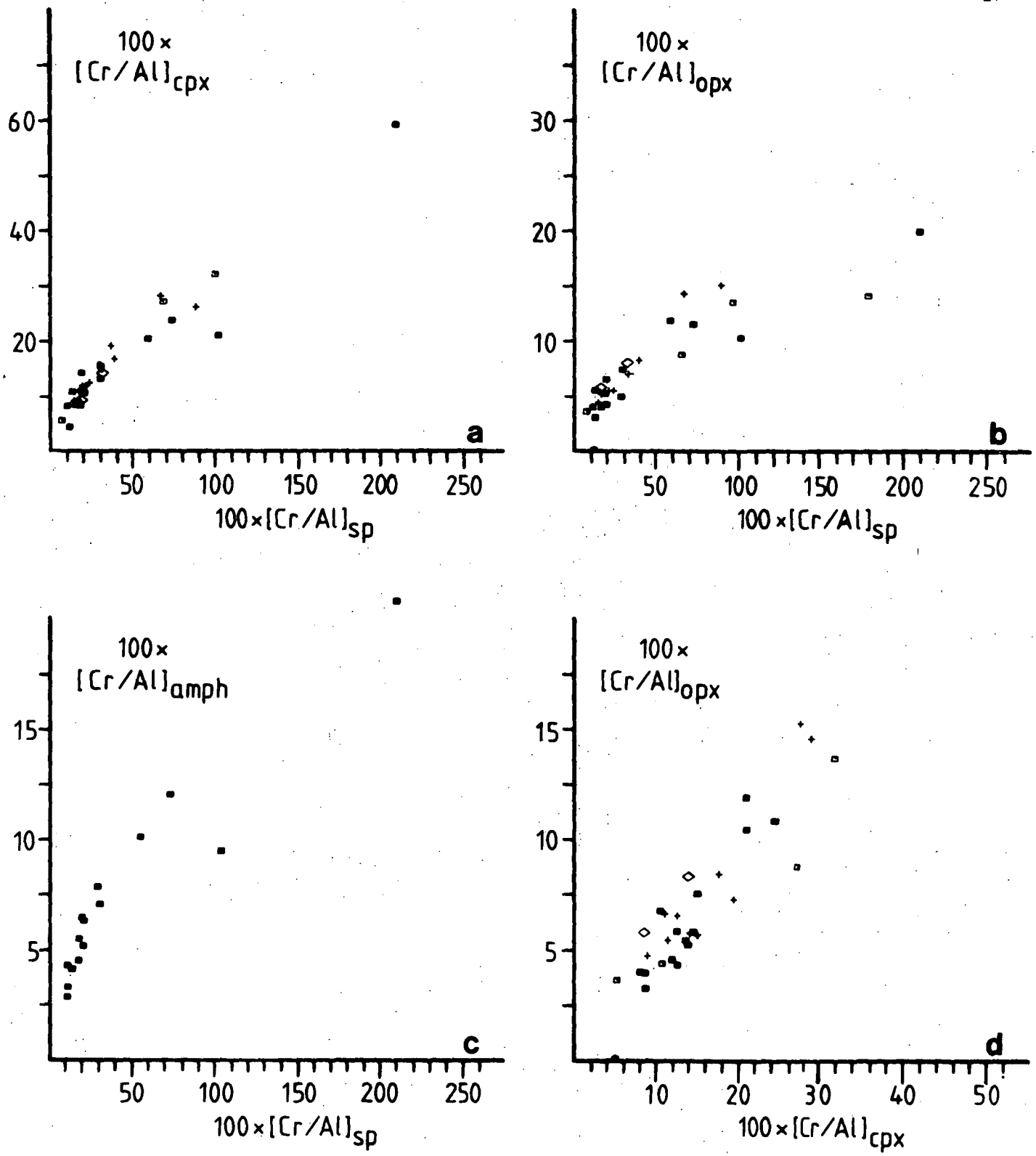

Figure 7a-d: Plots of molar Cr/Al ratio of spinel vs. Cr/Al of clinopyroxene (a), orthopyroxene (b) and amphibole (c), and Cr/Al orthopyroxene vs. Cr/Al clinopyroxene (d) for coexisting minerals in lherzolites of groups A1-A4. Symbols as for figure 5.

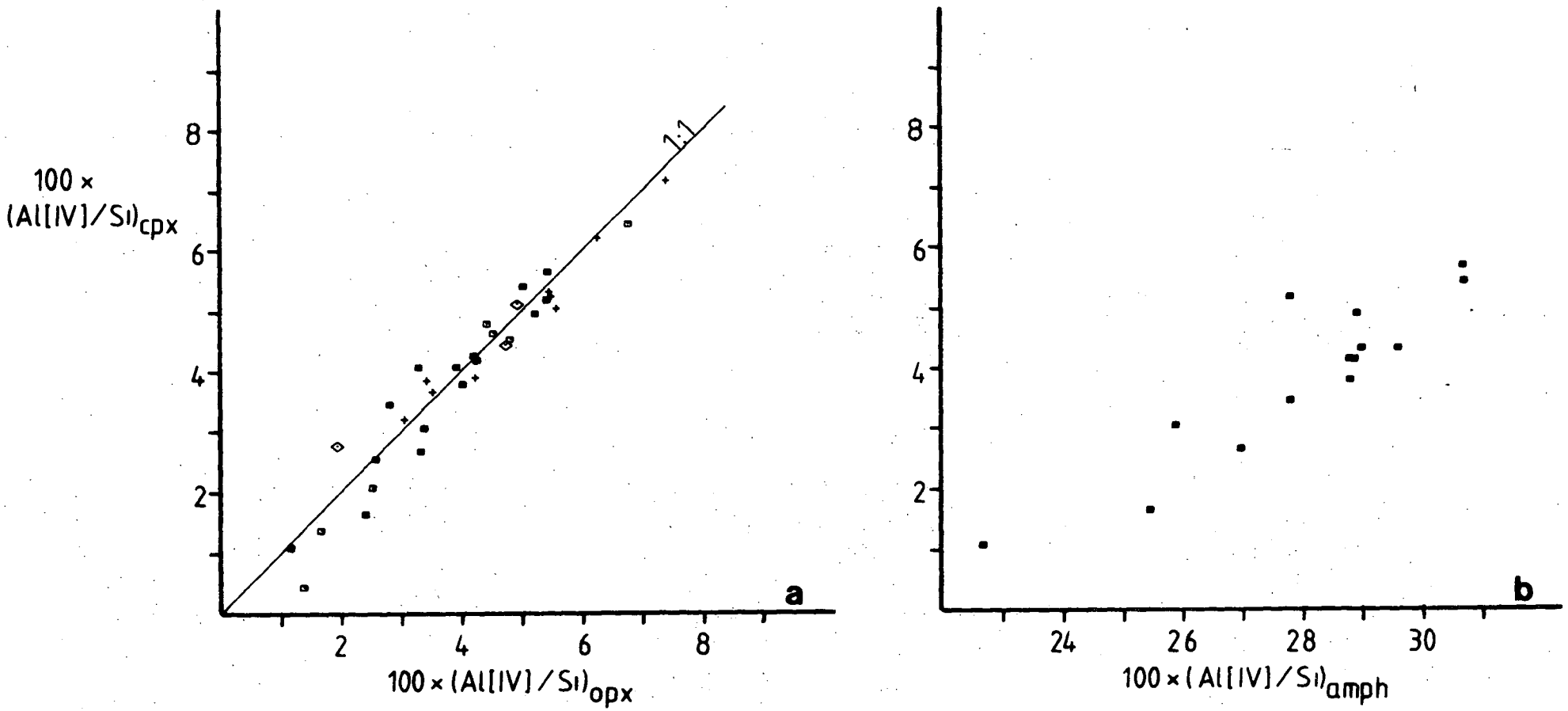

Figure 8a,b: Ratio Al^{IV}/Si of orthopyroxene (a) and amphibole (b) vs. Al^{IV}/Si of clinopyroxene of coexisting minerals in lherzolites of groups A1-A4. Al^{IV} of pyroxenes were calculated from the structural formula based on 6 oxygen as 2-Si and Al^{IV} of amphibole as 8-Si (based on 23 oxygen). Symbols as for figure 5.

5.3 GEOTHERMOMETRY/BAROMETRY FROM MINERAL EQUILIBRIA

The currently available geothermometers and geobarometers all show considerable uncertainties and deviations from each other (Carswell & Gibb, 1980), so that the determination of numerical values for P,T is likely to include large uncertainties. However, internal consistency has been demonstrated for some models and the indications for relative temperature distributions are regarded as meaningful.

The lherzolites and their pyroxenes are highly magnesian. In this compositional range the geothermometer of Wells (1977) yields better agreement with experimental data (Carswell & Gibb, 1980; Mitchell *et al.*, 1980; Mori & Green, 1978; also chapter 23 of this study) compared with Wood & Banno's (1973) formulation. The thermometer of Wells (1977) has therefore been applied.

The range of calculated temperatures is from 810°C to 1070°C for all rocks containing two pyroxenes. The distribution of temperature estimates for lherzolites is not random, but shows correlation with mineralogy (fig. 9), the lowest recorded temperatures occurring in amphibole-bearing types, intermediate temperatures in phlogopite-bearing types and higher temperature in anhydrous types. The anhydrous lherzolites do not (with one exception, for which the calculated temperature is much lower than all others) show exsolutions in the pyroxenes.

Thus they do not retain textural evidence of their cooling history but rather record only one relatively high temperature of equilibration. Dasch & Green (1975) obtained evidence from Sr-isotopes and Rb/Sr systematics for an "age" of approx. 700 Ma which they suggested was related to late Precambrian/Cambrian magmatic activity, the lherzolites representing residual mantle from such magma segregation and thus recording a high temperature event or events within the mantle. The isotopic age may record events when the region was part of an oceanic regime (Crawford & Keays, 1978; Crawford, 1983) with a high geothermal gradient.

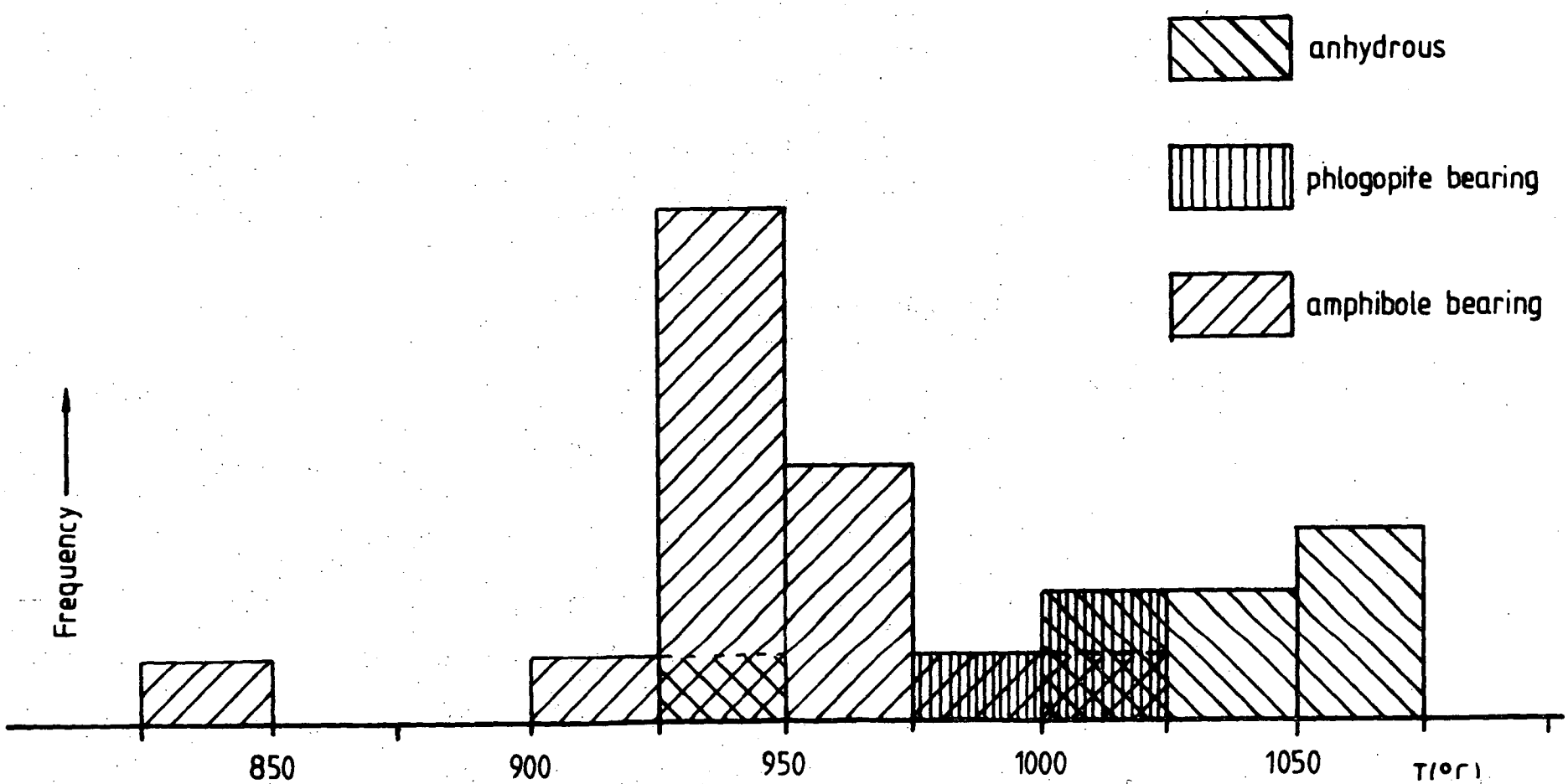

Figure 9: Temperature estimates for lherzolites (groups A1-A3) in relation to their mineralogy. Temperatures were estimated by the method of Wells (1977).

The hydrous lherzolites on the other hand commonly show exsolutions in pyroxenes and thus record a cooling history. The water may have helped in the process of annealing recrystallization in adjustment to later lower geothermal gradients.

The P-conditions for the lherzolites cannot be determined with any reliability, because no generally accepted experimental data exist for a geobarometer for spinel lherzolites. A possible exception is the olivine-clinopyroxene barometer of Adams & Bishop (1982). The application of the barometer requires high-quality data for Ca in olivine. The microprobe in this study was used in energy-dispersive mode and the resolution for the low levels of Ca in olivine is too low to allow application of this barometer at this stage. Only the stability field for spinel in peridotitic systems can this be used here, giving the range of approximately 8-20 kb.

The two pyroxenites, from which garnet has grown and which are assumed to be from similar depths, have been used for the calculation of P. The barometer of Harley (1981) was used, based on the reaction enstatite + Mg-tschermak's molecule = garnet. Since the reaction is temperature-dependent, absolute numbers of T become important, so that a second thermometer, which involves garnet (Fe/Mg exchange gt-cpx, Ellis & Green, 1979) has been utilized. This thermometer gives generally somewhat higher T estimates (Carswell & Gibb, 1980), so that a range of likely P results. The values obtained are in the region of 12-16 kb (table 4).

A second approach towards a P estimation utilizes the experimental data obtained in a liquidus phase study on the basanite of Mt Leura (no.2650 + 10% ol; Green, 1973a). A summary diagram of the liquidus phases for this composition containing 6.5% H_2O is given in fig. 10.

The mineralogy of cumulate textured wehrlite BM-168 (group G) has been compared with the experimentally produced phases and the bracketing conditions for the phases of BM-168 are listed in table 5, again pointing towards pressures around 15 kb.

Table 4: Pressure-temperature estimates for garnet-pyroxenites from Lake Bullenmerri.

Sample	P_a(kb)	T_E(°C)	T_W(°C)	T_a(°C)	P_c(kb)
BM-114	13	1034	978	978	13.0
	15	1042	978	1034	14.9
				1042	15.1
BM-116	13	1009	986	986	12.9
	15	1019	986	1009	13.6
				1019	14.0

P_a = pressure assumed for calculation of T by the method of Ellis & Green (1979)
T_E = temperature estimated by the method of Ellis & Green (1979)
T_W = temperature estimated by the method of Wells (1977)
T_a = temperature assumed for calculation of pressure
P_c = pressure calculated by the method of Harley (1981).

Table 5: Comparison of phase compositions from experimental studies on basanite and a cumulate from Lake Bullenmerri.

P (kb)	15	15	BM-168
T (°C)	1120	1080	
Mg' (ol)	79-80	73-75	80.8
Mg' (cpx)	81-83	76-78	82.6
Mg' (mica)	81-82	79	80.6
Mg' (amph)	absent	74-78	78.8

P, T are experimental conditions
Mg' = Mg/(Mg+Fe)

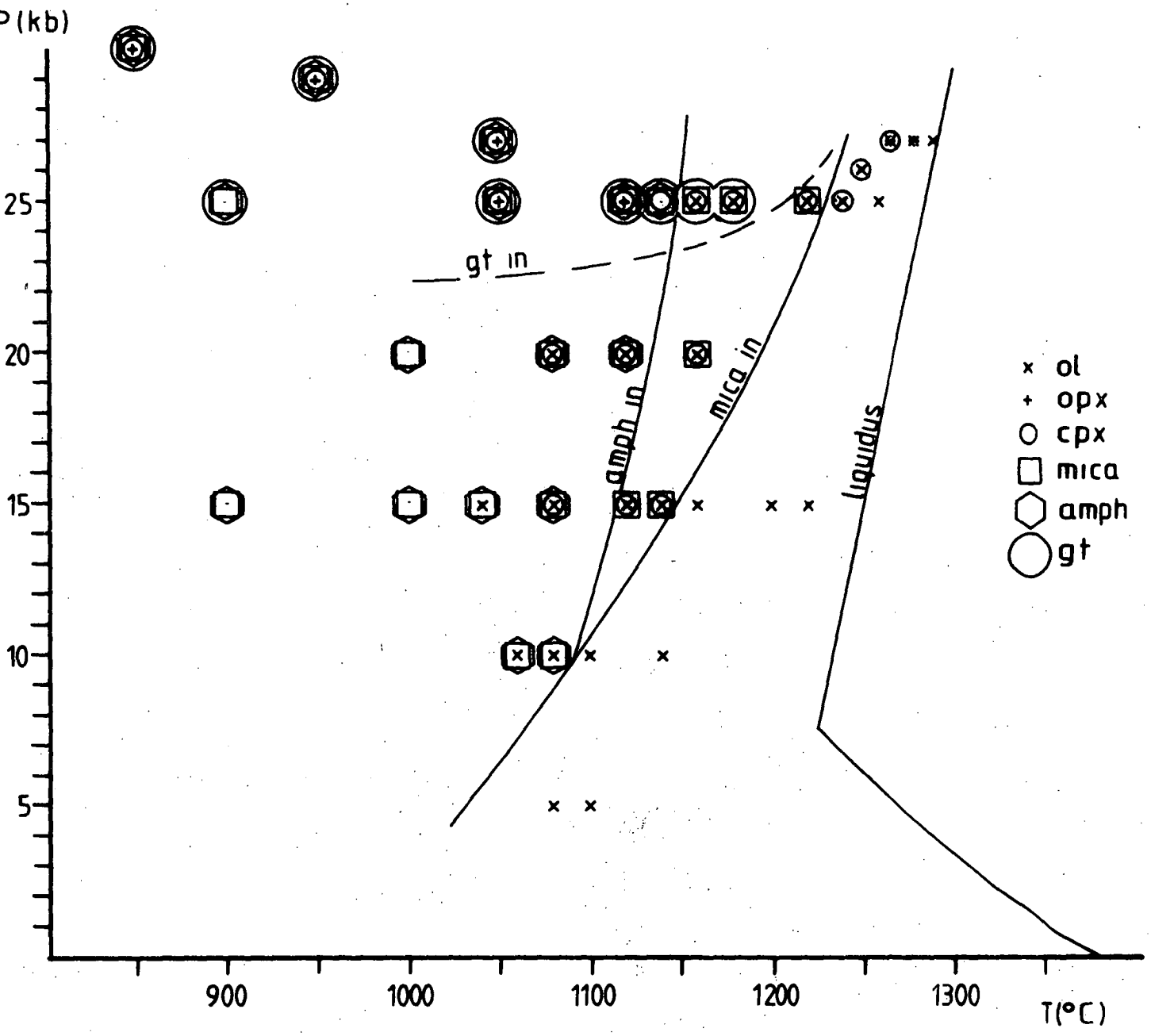

Figure 10: Phases crystallizing in equilibrium with liquid generated from sample 2650 of basanite from Mt Leura + 10% olivine + 6.5% H_2O (Green, 1973a).

Assuming a selective sampling process, all or most of the other xenoliths are inferred to come from similar depths.

6. INTERACTION BETWEEN MAGMAS AND LHERZOLITE WALLROCK

Wallrock relationhsips between magma and lherzolites can be observed in the case of composite xenoliths.

The composite xenolith BM-109 consists of amphibole-bearing lherzolite and a vein of hornblendite. The amphibole of the vein has high TiO_2 and low Cr_2O_3 contrasting with the high Cr_2O_3, low TiO_2 pargasite of the lherzolite. Exactly on the border between the two rock types a transitional amphibole, having both high Cr_2O_3 and TiO_2 has been found (Tr-amph of BM-109, appendix 3), which is slightly zoned in Cr towards a core of spinel. Thus it is possible to form intermediate amphiboles by reaction of veining magma and wallrock, but this type is restricted to a thin contact zone (<1 cm in this case). Because of the limited nature of this reaction it is concluded that the existence of pargasitic amphibole as a disseminated phase, particularly in large nodules (up to 20 cm diameter), in which no veins are present, is evidence for an origin by a process other than direct reaction between wallrock and veining magma.

Similarly the composite xenolith BM-116, consisting of lherzolite + pyroxenite, can be used to assess the effect of wallrock reaction. Pyroxenites are interpreted as high pressure precipitates from magmas (Irving, 1980; Wilshire *et al.*, 1980). The garnet within the pyroxenites from Lake Bullenmerri is not a magmatic precipitate, but a consequence of metamorphic reaction between aluminous pyroxene and spinel on cooling at high pressures (Irving, 1974b; Ellis, 1976; Hollis, 1981). At the contact of the two rock types (width approximately 1 cm) a garnet-free zone exists with wormy intergrowth of green spinel and clinopyroxene, followed by a thin shell of clinopyroxenite and a sharp contact with the lherzolite.

Whichever petrogenetic model for this succession is applied (diffusion interaction between lherzolite and pyroxenite, or development of a chemical gradient within the crystallizing/fractionating magma), the affected zone is very small. This very limited wallrock reaction again makes it unlikely that far-reaching or large-scale alterations of the wallrock take place.

It should be noted that because there is some wallrock reaction within the first centimetre of the contact, the chemistry of thin veins is likely to be slightly altered, e.g. towards higher Mg-values or lower Ti. This applies to the 1.3 cm thick vein of hornblendite in sample BM-109 and particularly to the few millimetre thick phlogopite vein in sample LE-00. Therefore, the original chemistry of veining materials may be better represented by discrete xenoliths (such as the hornblendites BM-117 and BM-156, each of which has a diameter of about 20 cm), and which are likely to stem from thicker veins and dykes. Thus these samples have been used to infer the nature of the hornblende-precipitating magma.

Sample BM-156 contains a patch consisting mainly of Cr-free, Ti-rich, low-Mg pyroxenes (Mg values ≈75) within a matrix of poikilitic amphibole. The matrix amphibole of the pyroxenite has a higher Mg-value (Mg_{72}) than that of the enclosing hornblendite (Mg_{68}) (amphibole b and a of BM-156, appendix 3). From the chemical character of the patch in relation to its host and the textural evidence I prefer to interpret the pyroxenite as a precipitate from a magma, which later precipitated the intergrown amphibole and mica. I thus interpret the hornblendite as a precipitate from a magma rather than vapour-phase fluid on the basis of this sample and on the similarity of hornblende compositions to near-liquidus phases of basanite and nepheline mugearite (cf. Irving, 1971). Also, cumulate textures have been reported for amphibole-bearing nodules elsewhere in the Newer Volcanics (Ellis, 1976).

The inference that the brown kaersutitic hornblende is a magmatic precipitate is a further constraint on possible wallrock reactions, because the permeability of anhydrous lherzolites to basaltic magmas is extremely low, but permeability to a fluid is probably much higher (Rovetta, 1981). The conclusion that kaersutitic hornblendites are precipitates from a magma and that the magma has very limited capabilities of wallrock reaction does not exclude a relationship between disseminated amphiboles in lherzolites and pyroxenite/hornblendite veining system. The amphibole-precipitating magmas are hydrous (cf. Green, 1973a) and so may release excess H_2O during crystallization. This water may then enter the lherzolite wall-rock and cause widespread hydration reactions such as cpx + sp+ $H_2O \rightarrow$ amph. Thus amphibole produced in this way is uniformly distributed through the lherzolite, nucleation sites being determined by local chemical composition (e.g. cpx-sp contact). This contrasts with the expectation of a zonal arrangement or gradient in amphibole abundance, if the H_2O-rich fluid is also a source of major components of the amphibole (i.e. a strongly metasomatising fluid).

7. PETROGENESIS OF THE UPPERMOST MANTLE BENEATH VICTORIA

The linear character of the chemical variations in the lherzolite nodules makes it possible to model the composition of the nodules as residual mantle compositions for varying degrees of extraction of partial melts. As a source composition one of the most fertile lherzolite nodules (BM-15) has been chosen. This nodule is closely comparable with model mantle compositions in both major elements and trace element concentrations (cf. Green *et al.*, 1979; Ringwood, 1966; Frey *et al.*, 1978) (table 6A), and is similar in composition to the most "fertile" nodules of similar world-wide occurrences (Jagoutz *et al.*, 1979).

If we apply a batch melting model to this source composition then the oxide composition of the extracted partial melt must lie on the extended trendlines for the oxide variations within the nodules themselves. Matching of MgO, Al_2O_3 and CaO can be achieved using olivine melilitites or basanites as the extracted melts, but this matching produces source compositions with extremely high TiO_2 and Na_2O (i.e. > 1%) and requires 5-30% melt extraction to produce the observed lherzolite range. High degrees of melting for olivine melilitites or basanites are inconsistent with four-phase residual mineralogy (olivine, orthopyroxene, clinopyroxene, garnet) for these liquids as deduced from experimental studies which suggest degrees of partial melting around 5% (Green, 1973a; Frey *et al.*, 1978). These models are also inconsistent with experimental studies suggesting depths of 80-100 km rather than 40-60 km for magma segregation for these magmas (Green, 1973a, Brey & Green, 1977).

It has previously been suggested that the lherzolite mineralogy of the Victorian lherzolites may reflect early magmatic events associated with oceanic lithosphere in the late Precambrian (Crawford & Keays, 1978; Crawford, 1983). Experimental results on model mantle and natural lherzolites (Green *et al.*, 1979) argue that picritic liquids are extracted

from a mantle under oceanic conditions. Therefore a liquid composition has been chosen resembling closely a possible parental picrite (DSDP 3-18 + 17% ol) for MORB (Green *et al.*, 1979; table 6A) but also constrained to fit the lherzolite trend lines passing through the model source (BM-15). The results of the mixing calculations are listed in table 6B. The fit is generally very good for all major oxides including TiO_2. The least satisfactory fit is with FeO. It should be noted that even though Na_2O shows only a weak correlation with the MgO in the nodules and hence some scatter in the source estimations is expected, the calculated values for Na_2O are consistent with or only slightly higher than those for model mantles and fertile nodules. The misfit of sample BM-139 has previously been related to the exceptionally high pargasite content of this nodule.

The chemical variations within the lherzolites, including both hydrous and anhydrous examples, can thus be satisfactorily explained by early partial melting events. Comparison with lherzolite nodules from other localities shows that similar relations exist for a number of locations. However, garnet lherzolites from kimberlite cannot be modelled this way (appendix 4).

The presence of hydrous phases and their textural relationships to clinopyroxene and spinel suggests that a fluid phase, composed mainly of water, entered the rocks and changed their mineralogy in a near-isochemical way. The water entering the lherzolites may however contain elements in in the order of ppm concentrations. The changes in chemistry for major oxides would then be undetectable, but may be significant for some trace elements. The quantitative effect on trace element concentrations such as REE cannot be assessed at this stage. While Stosch & Seck (1980) record systematic differences in REE patterns for anhydrous and hydrous lherzolites from West Germany, Frey & Green (1974), working on Victorian lherzolites, did not.

The close matching obtained in table 6B suggests that the batch melting model is probably a close approximation, but it is envisaged that

Table 6a

	Pyrolite a	Pyrolite b	BM-15	DSDP3-18 + 17% ol	Picrite used	Pyrolite*
Na_2O	0.40	0.57	0.40	1.65	1.65	
MgO	38.80	37.50	37.99	16.70	17.70	
Al_2O_3	4.40	3.50	3.86	13.70	12.80	
SiO	45.00	45.20	44.95	48.30	48.10	
K_2O	0.003	0.13	0.03	0.01	0.01	
CaO	3.40	3.10	3.54	10.90	10.80	
TiO_2	0.17	0.71	0.17	0.60	0.62	
FeO	7.60	8.60	8.27	7.90	7.90	
Cr_2O_3	0.45	0.43	0.41	0.06	0.06	
MnO	0.11	0.14	0.14	0.12	0.12	
NiO	0.26	0.20	0.24	0.08	0.08	
Zr			16			15.5
Sc			15			20
V			86			75

Pyrolite a from Green *et al.*, 1979; pyrolite b from Ringwood, 1966;
* pyrolite from Frey *et al.*, 1978.

Table 6b: Mantle compositions calculated as composition of residual nodule + X% picrite = source.

	BM-139 +2.6%	BM-144 +10.6%	BM-167 +11.8%	BM-162 +16.5%	BM-160 +16.9%	BM-99 +21.8%
Na_2O	0.72	0.32	0.36	0.43	0.40	0.45
MgO	38.05	37.86	38.03	38.02	38.07	38.13
Al_2O_3	3.85	3.69	3.95	3.87	4.04	4.10
SiO_2	44.88	45.03	44.86	45.02	44.88	44.86
K_2O	0.17	0.00	0.00	0.00	0.01	0.00
CaO	3.70	3.41	3.61	3.61	3.58	3.69
TiO_2	0.18	0.14	0.17	0.15	0.20	0.17
FeO	8.30	8.52	8.52	7.67	8.15	7.90
Cr_2O_3	0.40	0.37	0.33	0.39	0.38	0.34
MnO	0.14	0.13	0.14	0.13	0.14	0.13
NiO	0.23	0.25	0.25	0.25	0.23	0.24

	BM-69 +22.9%	BM-134 +25.0%	BM-9 +27.7%	BM-163 +29.9%	BM-15 nodule
Na_2O	0.49	0.65	0.59	0.66	0.40
MgO	38.15	38.11	38.06	38.20	37.99
Al_2O_3	4.21	4.14	4.06	4.31	3.86
SiO_2	44.81	44.74	44.97	44.84	44.95
K_2O	0.00	0.03	0.02	0.02	0.03
CaO	3.61	3.62	3.47	3.68	3.54
TiO_2	0.17	0.19	0.19	0.20	0.17
FeO	8.07	8.65	7.74	7.47	8.27
Cr_2O_3	0.27	0.28	0.30	0.28	0.41
MnO	0.14	0.14	0.12	0.13	0.14
NiO	0.25	0.26	0.25	0.24	0.24

processes transitional between fractional partial melting and batch melting occur. This may result in a slight curvature for some element variations.

In the model presented, the sampled area is envisaged as a source region, in which magma segregation took place. Local incomplete segregation is envisaged and would result in areas consisting of varying proportions of depleted source and trapped melt. Table 6B shows that the residue, melt and source are related as 70% residue (harzburgite) + 30% melt (picrite) = source lherzolite (BM-15). Any simple mixtures of residue and melt will fall on the variation lines defined by the depleted nodules.

The two unusual lherzolites (BM-143 and BM-137) noted previously do not fit the simple mixing model. More complex processes must be involved, but cannot be specified. The layered texture of BM-137 may be a consequence of pressure-solution creep, a process suggested for some alpine peridotites (Dick & Sinton, 1979). Alternatively it may be interpreted as being a part of a hornblende-ariegite dyke (Lensch, 1976).

The cumulates transported alongside the lherzolites are difficult to recognize and to model, because they may either stem from the period of the early partial melting event or may be derived from later magmatic events including the early eruptions of the host magma suite. Recrystallization of these cumulates occurs as evidenced by the metamorphic growth of garnet in the pyroxenites. Original textures are thus in many cases eliminated, though cumulate textured pyroxenites and wehrlites have been documented by Ellis (1976), distinct in both mineral chemistry and petrography from the now recrystallized cumulates.

Additional difficulties arise from a possible late-stage change in mineralogy: if the hydration events occurred at a late stage, early cumulates too may have suffered from this process. Amphiboles originally precipitated and those produced by hydration of cumulates will be hard to distinguish. Therefore, classification has to rely largely on bulk rock chemistry and to some extent on mineral chemistry.

In those cases where cumulus textures are well preserved it is possible to infer the character of a parental magma. This is the case for BM-168, which for this reason has been placed in a separate group (G). The preservation of excellent cumulate texture is consistent with an origin from basanites related to, but slightly preceding the eruption of the host basanite.

8. SUMMARY OF THE EVOLUTION OF THE UPPERMOST MANTLE BENEATH VICTORIA AND CONCLUSIONS (fig. 11)

1. Lherzolites are the major rock type of the uppermost mantle (lithosphere) of the region at a depth of less than 60 km, probably around 45 km.
2. This part of the subcontinental lithosphere records an early history of extraction of picrite basalt of oceanic type from a relatively homogeneous mantle comparable to the model mantle "pyrolite". This early history is likely to reflect the presence of a marginal sea basin in late Precambrian times.
3. The chemical variation of the lherzolites is due to varying degrees of extraction of such a liquid, thereby introducing heterogeneity into the mantle. The uppermost mantle is not simply zoned chemically from fertile to refractory, but at any depth all degrees of depletion (from 0-30%) may be present.
4. Pargasitic amphibole in the lherzolites is developed as a later and probably much later, event by a near-isochemical hydration reaction of the phases of the lherzolites, particularly involving spinel. Other than addition of water and in a few rare cases of small amounts of Na_2O and K_2O possibly, there is no evidence for addition of other components in other than trace (ppm) amounts.

5. Hydration metasomatism occurs within the lithosphere and predates or is contemporaneous with the development of the alkaline magmatism. However the lithosphere is not the source region of the alkaline magmas so that the presence of amphibole or phlogopite cannot be taken as evidence that mantle metasomatism is a precursor event to alkaline magmatism.
6. Hydration metasomatism changes the mineralogy of parts of the lithosphere into a five-phase assemblage. Thus it introduces a mineralogical heterogeneity which does not reflect a major chemical heterogeneity super-imposed on that produced by earlier partial melting event(s).
7. Within the lithosphere, segregated bodies of magma from the earliest magmatic event(s) and later batches of magma passing through the lithosphere may crystallize, either partially or completely, giving rise to cumulates such as pyroxenites, hornblendites, wehrlites and Fe-rich lherzolites. Cumulates are often reworked and recrystallized. The existence of pockets, lenses, dykes and veins of this nature adds further to the present heterogeneous character of the lithosphere.
8. Wallrock reaction of magmas fractionating under mantle pressure is very restricted and contributes only very locally to the chemistry and mineralogy of the lithosphere. However these magmas may release water upon crystallization and produce widely distributed hydration reactions in the lherzolites (and early cumulates). Thus it seems more likely that the development of alkaline magmatism is the precursor of the hydration metasomatism of the uppermost mantle rather than *vice versa*.

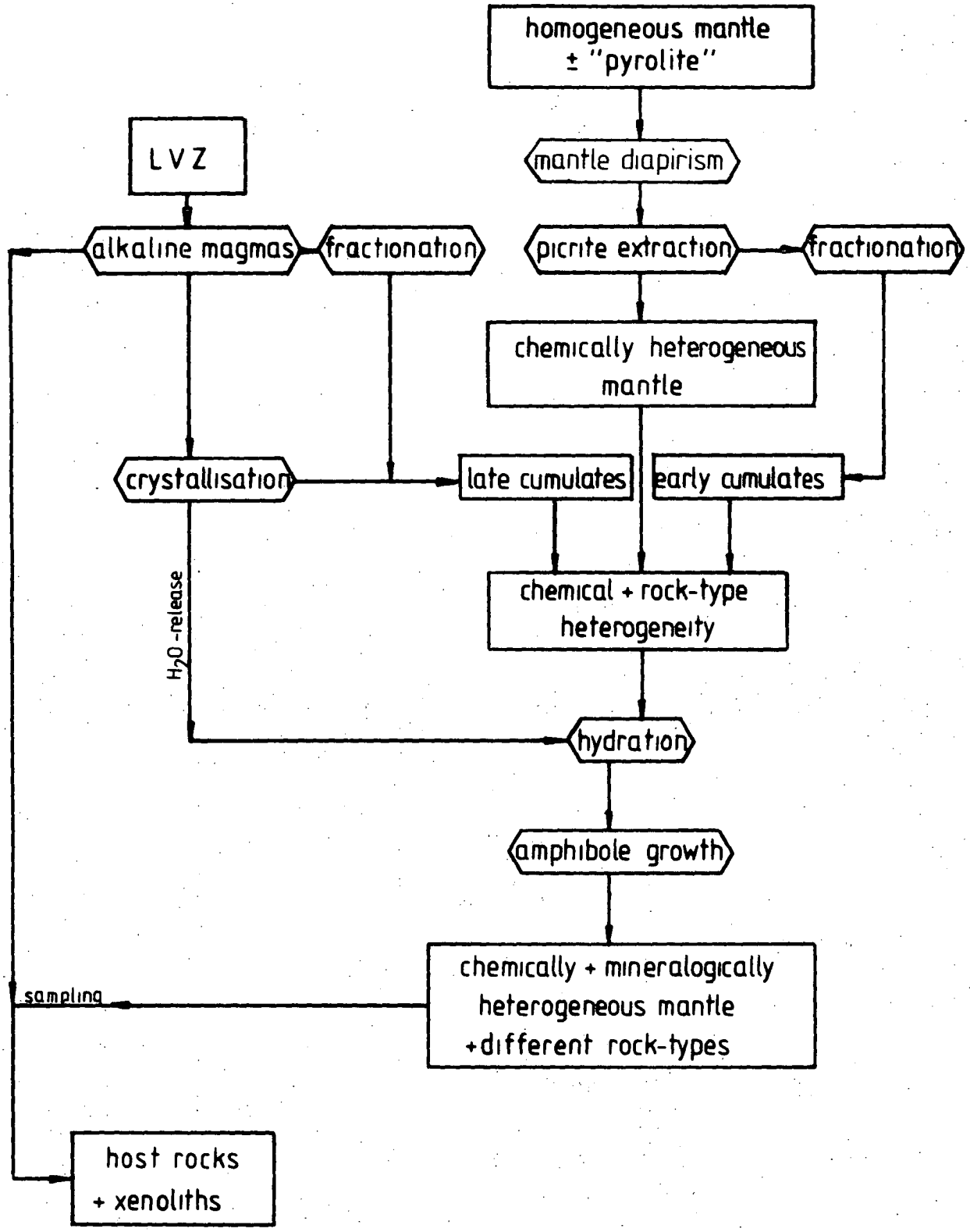

igure 11: Flow diagram illustrating the model for the evolution of the uppermost mantle beneath the sampled area.

PART II

AN EXPERIMENTAL STUDY BEARING ON PHASE RELATIONSHIPS IN THE SYSTEM CMAS (CaO-MgO-Al_2O_3-SiO_2).

9. INTRODUCTION

The CMAS system differs from the MAS system in that the addition of Ca leads to the formation of clinopyroxene in experimental runs and thus all four major phases of garnet lherzolites-olivine, ortho- and clinopyroxene and garnet can be synthesized. CMAS is therefore much closer to the mineralogy of natural upper mantle samples and provides better starting points for the extrapolation of experimental results to natural rocks.

In CMAS the calibration of the widely used cpx-opx thermometers (Wells, 1977; Wood & Banno, 1973; Davis & Boyd, 1966) can be checked for aluminous pyroxenes. The spinel-garnet transition in this system is a univariant reaction and provides information on the mineralogical stratification of the uppermost mantle, even though the results cannot be applied directly to natural rocks as shown in the following chapters.

The great effect of Ca on the solubility of Al_2O_3 in pyroxene has been recognized by Akella (1976) and has been confirmed in Fe-bearing systems (Ellis & Green, 1979; Wood, 1974; Harley, 1981; Harley & Green, 1982).

While experimental results on the solubility of Al_2O_3 in orthopyroxene coexisting with garnet in the system MAS are in good agreement with each other (McGregor, 1974; Perkins *et al.*, 1981; Harley, 1981), this is not the case for CMAS. The values derived by Akella (1976) have been disputed by Howells & O'Hara (1978), who claimed lower values of Al_2O_3 in orthopyroxene for a given P-T condition to be in equilibrium with garnet.

Therefore experiments in the system CMAS have been performed in the range 950-1400°C and 15-30 kb. Subsequently more data on CMAS have been published by Perkins & Newton (1980), which provide a check on the results of this study with those of an independent laboratory.

Thermodynamic formulations and conventional solution models used in this and subsequent parts follow those outlined by Wood & Fraser (1978).

10. EXPERIMENTAL TECHNIQUES

Experiments were carried out using a 12.7 mm (0.5 inch) piston cylinder apparatus at the Geology Department, University of Tasmania. The experimental techniques were similar to those described by Green & Ringwood (1967b).

Temperatures were measured using a $Pt/Pt_{90}Rh_{10}$ thermocouple and controlled to within ± 7°C of the set point. Experimental studies on the apparent temperature drift of $Pt/Pt_{90}Rh_{10}$ thermocouples with time (Presnall *et al.*, 1973) show that drifting occurs to a measurable degree only above 1400°C (fig. 4 of Presnall *et al.*, 1973). The range of the experimental temperatures extends only to 1400°C, hence the recorded temperatures are regarded as the true temperatures. During runs over prolonged times the input current required to maintain the temperature at the set point had to be increased. This is attributed to changes in the characteristics of the graphite heater/talc sleeve by water relased from dehydrating talc. Calibration of thermocouples after experiments and DTA experiments carried out before and after long run times demonstrate that there has been no degradation of thermocouples under run conditions matching those of this study (Harley, 1981). Confirmation of this conclusion comes from runs where NaCl cells were used (see Chapter 19). In these assemblages no increases in EMF and input current were necessary even for long durations.

The runs were performed by using the "piston-in" technique, i.e. the assemblage was brought close to the final temperature and pressure, then the temperature was brought to the set point and the pressure subsequently increased to the nominated value. This method requires -10% correction to calculate real pressures from measured load pressures. The accuracy of this method is ± 1 kb (Green *et al.*, 1966; Johannes *et al.*, 1971).

High pressure cells used are shown in figure 12. The large capacity or "buffer" assemblage was used to synthesize minerals in order to serve as

Figure 12: High pressure cells used for experiments in the CMAS system. Shown are cross sections through the cells and the material of the individual parts. Cell names "dry". "wet" and "buffer" refer to the common use of the assemblages, i.e. "dry" cells were used in experiments with no or only traces of H_2O present, "wet" cells for experiments containing H_2O sealed into the capsule, and "buffer" cells were used for large capacity runs for the synthesis of minerals.

Experimental Assemblages

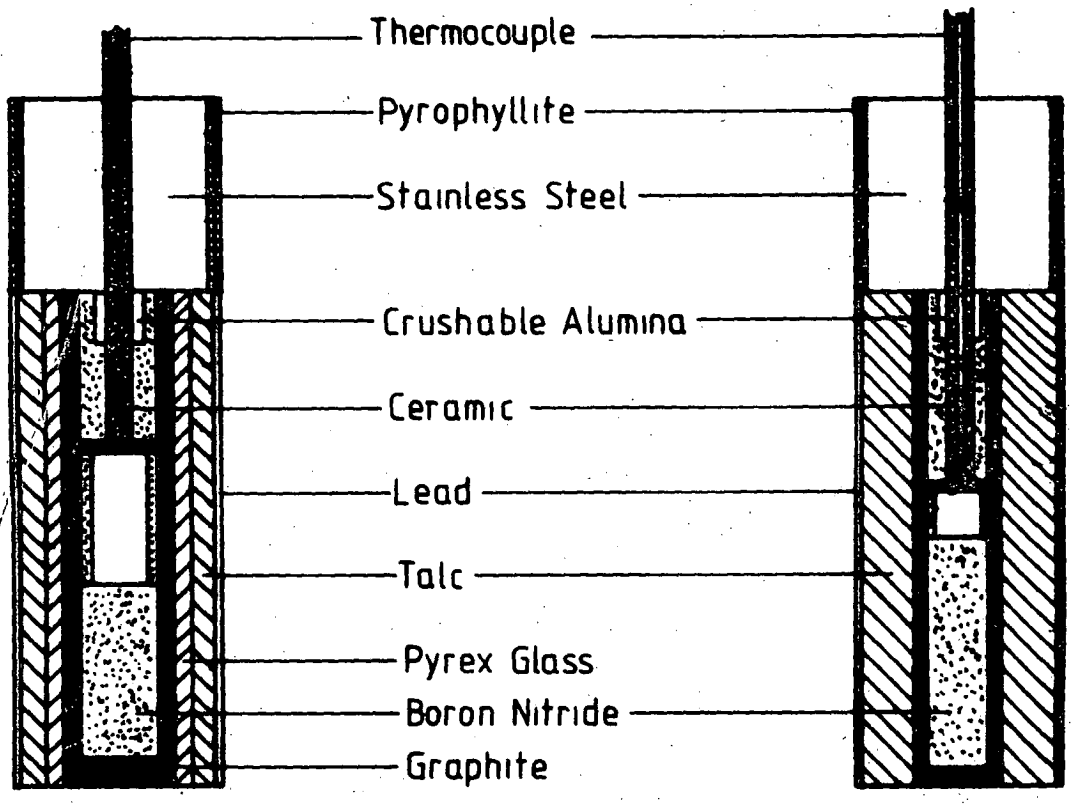

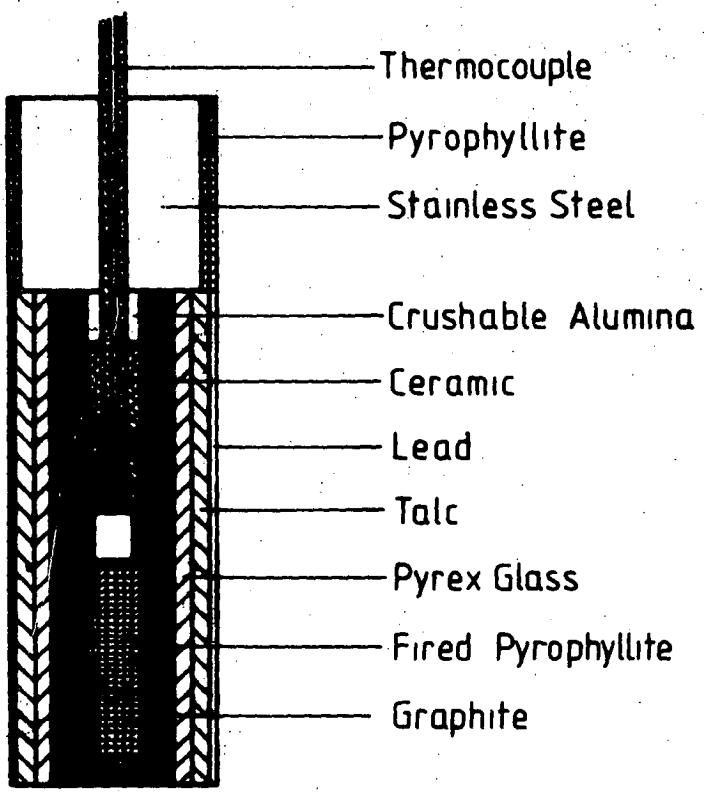

seeds. $Ag_{50}Pd_{50}$ capsules were used for low temperatures (1000°C or less) in CMAS, all others were performed with Pt capsules. The capsules were sealed by welding. In the case of the Ag-Pd capsules this was done under an argon stream.

The low temperature runs contained water sealed into the capsule (≈5-10 wt.%) to serve as a flux. The sealing was checked by weighing before and after heating at 110°C for several minutes.

Initial experiments of varying duration were carried out to establish suitable run durations. The established conditions are similar to those used by Harley (1981) at similar temperatures. In the evaluation experiments, shorter run times resulted in greater inhomogeneity of Al_2O_3 contents in orthopyroxene, compositional zoning of minerals and smaller grain size.

11. STARTING MATERIALS

The starting material for CMAS runs was prepared from pure oxide reagents. The oxides were ground together in an agate mortar under acetone. The grinding procedure was repeated three to four times to achieve homogeneity. The mixture was then pelletised and sintered in a 1 atm. furnace at 990°C overnight. Subsequently the pellet was reground and a part of this mixture was then converted to a glass by melting on an iridium-strip heater, resulting in a clear glass. The glass was then ground under acetone.

For mineral syntheses of pyrope, enstatite, diopside and spinel a stoichiometric mix of pure oxides was treated as described for the sintering process. The material was then loaded into large capacity $Ag_{50}Pd_{50}$ or Pt capsules and subjected to P and T listed in table 7. The resulting minerals were checked optically and by XRD. Only minor impurities (<5%) were detected.

Table 7: Conditions of synthesis of minerals.

Mineral	Capsule	Duration (hrs)	Temperature (°C)	Pressure (kb)
pyrope	$Ag_{50}Pd_{50}$	3	1100	25
enstatite	Pt	5	1150	15
diopside	$Ag_{50}Pd_{50}$	5	1150	15
spinel	Pt	5	1350	15

The synthesized phases were then added to the oxide mixture, each seed mineral as 1% of the mix. The seeded mixture was reground to achieve homogeneous distribution of the seeds. The seeding, especially with garnet, is regarded as necessary, because of nucleation problems (Howells & O'Hara, 1978). The chemical composition of the starting material as mixed is listed below (table 8).

Table 8: CMAS starting material.

SiO_2	45.7 wt.%
MgO	30.2 wt.%
Al_2O_3	18.3 wt.%
CaO	5.8 wt.%

The composition was checked by regularly analysing run products for bulk composition under the microprobe with a wide area scan. A small excess of SiO_2 ($\simeq$47 wt.% SiO_2 by analysis) is present, most probably due to the contamination of the mixture with SiO_2 from the agate mortar during the repeated grinding procedures. The composition of the CMAS mixture is similar to that used by Akella (1976).

12. ANALYSIS OF RUN PRODUCTS

After completion of high pressure runs the sealed capsules were opened and several fragments from each capsule were mounted in epoxy resin. Fragments come from different levels inside the capsule relative to the position of the thermocouple. No changes of compositions from fragment to fragment were detected, confirming assembly calibration experiments which show negligible (<10°) temperature gradients over the sample length.

Analyses of the phases were obtained using an energy-dispersive system with a JEOL-JXA 50A microprobe. All analyses were made at 15 kv and 2.1×10^{-9} A. (EDAX detector, calibrated on spec pure Cu). Standards to calibrate the microprobe were clinopyroxene, olivine, and garnet of known composition. Analytical and data reduction procedures used are given by Griffin (1979).

The poikilitic character of many garnet crystals makes analysis of this phase difficult in many runs. Even though inclusions within garnet can be distinguished by means of back scattered electron image or secondary electron images, the volume effect of the primary beam often results in analyses representing mixtures of garnet and inclusion. The beam has a spot mode diameter of <1 μm, however a larger volume of ≃2 μm diameter is penetrated by the beam and analysed. Mixtures between olivine and garnet are apparent from deviations of the garnet structural formula from 8.000 (based on 12 oxygen). For mixtures between garnet and pyroxenes this criterion is not valid, but differences in the internal structure (Si > 3, Al < 2) indicate contamination. Small deviations from an ideal garnet structure may however also be due to limitations in the accuracy of the microprobe.

Most garnet analyses and accordingly the mean of the analyses do show evidence for some contamination, but a rather uniform Ca/Ca+Mg ratio. As discussed in chapter 21 large contaminations are required before there is

a major change of the Ca/Ca+Mg ratio of the garnet and this ratio only is used for calculations in the following chapters. Where evidence for a major contamination in any single analysis was detected, this analysis was discarded.

13. RUN PRODUCTS - CMAS

Average analyses of run products, normalised to 100%, are listed in table 9. Run products in CMAS have generally a typical subsolidus texture with polygonal to lobate mosaics of pyroxenes and garnet. The grainsize is variable and dependent on temperature and run time, correlating positively with both. This is only a general trend and within any run there is a range in grainsize and only the maximum grainsizes are different. The range is generally between 3 and 50 μm, but poikilitic garnets may be as large as 100 μm.

Garnet is usually poikilitic with numerous inclusions of pyroxenes and/or olivine. The lack of evidence for the persistence of pyrope seeds argues that the reaction has gone to completion and that garnet is not zoned.

Orthopyroxenes in runs at higher temperatures (1200°C and above) have a small spread in Al_2O_3 content which is either within or slightly above the precision of microprobe analysis. This and the absence of mineral zoning are regarded as further evidence for the completeness of the reaction. At lower temperatures the spread in Al_2O_3 of orthopyroxene is higher (cf. standard deviations given in table 9). Although this spread may stem from Al_2O_3 zoning in pyroxene, the small grainsize makes it impossible to establish this unambiguously. It is believed that the small grainsize makes it more likely that the range in analyses represents a contamination by another phase such as clinopyroxene or garnet. Owing to the long run

Table 9: Run products CMAS.

RUN: T-690, seeded sintered oxide mix, $Ag_{50}Pd_{50}$ capsule, wet assemblage, water added. Conditions: 950°C, 30 kb, 120 hours.

Phases	opx		cpx		gt	
MgO	39.04(.41)	1.947	20.16(1.2)	1.075	25.67(.54)	2.608
Al_2O_3	1.83(.18)	0.072	1.22(.52)	0.051	24.59(.04)	1.975
SiO_2	58.72(.37)	1.964	55.17(.26)	1.974	44.17(.20)	3.011
CaO	0.41(.01)	0.014	23.45(1.4)	0.899	5.55(.35)	0.405
		3.999		4.000		8.000

RUN: T-726, seeded glass mix, $Ag_{50}Pd_{50}$ capsule, wet assemblage, water added, Fo present. Conditions: 1000°C, 20 kb, 71 hours.

Phases	opx		cpx		gt	
MgO	37.97(.90)	1.895	20.13(.95)	1.070	25.28(.62)	2.565
Al_2O_3	3.85(1.0)	0.151	3.08(.53)	0.129	24.83(1.4)	1.992
SiO_2	57.53(.84)	1.926	54.38(.46)	1.939	44.37(1.5)	3.021
CaO	0.64(.18)	0.022	22.41(1.3)	0.856	5.51(.70)	0.402
		3.997		3.995		7.982

RUN: T-685, seeded sintered oxide mix, $Ag_{50}Pd_{50}$ capsule, wet assemblage, water added. Conditions: 1000°C, 30 kb, 96 hours.

Phases	opx		cpx		gt	
MgO	38.92(.59)	1.942	20.15	1.075	26.23(.16)	2.658
Al_2O_3	1.97(.86)	0.077	1.80	0.075	24.74(.10)	1.982
SiO_2	58.62(.41)	1.962	54.59	1.955	44.29(.12)	3.011
CaO	0.46(.21)	0.016	23.46	0.900	4.72(.18)	0.343
		3.998		4.006		7.996

RUN: T-723, seeded glass mix, $Ag_{50}Pd_{50}$ capsule, wet assemblage, water added, Fo present. Conditions: 1000°C, 30 kb, 98 hours.

Phases	opx		cpx		gt	
MgO	38.90(.55)	1.938	19.93(.26)	1.063	25.35(.11)	2.571
Al_2O_3	1.49(.44)	0.050	1.10(.28)	0.046	24.87(.12)	1.994
SiO_2	59.24(.31)	1.980	55.36(.01)	1.981	44.41(.08)	3.022
CaO	0.37(.06)	0.013	23.61(.49)	0.905	5.37(.06)	0.391
		3.999		3.995		7.980

RUN: T-607, seeded oxide mix, Pt capsule, dry assemblage, slightly moist, Fo present. Conditions: 1200°C, 20 kb, 48 hours.

Phases	opx		cpx		gt	
MgO	36.28(.33)	1.814	19.64(1.2)	1.040	24.63(.37)	2.520
Al_2O_3	6.98(.30)	0.276	7.00(.30)	0.293	24.92(.04)	1.967
SiO_2	55.59(.25)	1.865	52.37(.39)	1.860	44.19(.13)	3.033
CaO	1.14(.22)	0.040	20.97(.84)	0.798	6.26(.34)	0.460
		3.996		3.992		7.982

Table 9 cont.

RUN: T-601, seeded sintered oxide mix, Pt capsule, dry assemblage, slightly moist. Conditions: 1200°C, 25 kb, 24 hours.

Phases	opx		cpx		gt	
MgO	36.51(.64)	1.831	21.14(1.3)	1.113	25.65	2.601
Al_2O_3	5.50(.38)	0.218	5.04(.56)	0.209	25.45	2.040
SiO_2	55.96(.32)	1.883	54.24(.22)	1.915	43.90	2.986
CaO	2.03(.48)	0.073	19.56(1.0)	0.740	5.00	0.364
		4.007		3.979		7.992

RUN: T-597, seeded sintered oxide mix, Pt capsule, dry assemblage, Fo present. Conditions: 1400°C, 25 kb, 24 hours.

Phases	opx		cpx		gt	
MgO	34.82(.14)	1.745	21.75(.26)	1.137	25.22(.01)	2.564
Al_2O_3	7.94(.32)	0.314	8.34(.26)	0.345	25.23(.50)	2.028
SiO_2	55.05(.29)	1.851	52.67(.16)	1.848	43.71(.57)	2.982
CaO	2.18(.22)	0.078	17.21(.20)	0.647	5.84(.43)	0.426
		3.990		3.978		8.003

RUN: T-613, seeded sintered oxide mix, Pt capsule, dry assemblage, slightly moist. Spinel present, garnet absent. Conditions: 1200°C, 15 kb, 48 hours.

Phases	opx		cpx	
MgO	35.03(.34)	1.752	19.73(.97)	1.042
Al_2O_3	9.11(.37)	0.360	8.14(.41)	0.340
SiO_2	54.48(.47)	1.828	51.84(.36)	1.838
CaO	1.40(.19)	0.050	20.27(1.0)	0.770
		3.991		3.991

RUN: T-609, seeded sintered oxide mix, Pt capsule, dry assemblage, slightly moist. Spinel present, garnet absent. Conditions: 1400°C, 20 kb, 24 hours.

Phase	opx	
MgO	35.13(.10)	1.757
Al_2O_3	9.53(.20)	0.377
SiO_2	54.13(.20)	1.816
CaO	1.20(.11)	0.043
		3.994

durations it is assumed that the reaction is complete and mean values are taken as equilibrium values.

Clinopyroxene is a minor phase and in some cases is difficult to find. Analyses show a higher spread in CaO contents, reflecting likely contamination with other neighbouring phases. Forsterite is a minor or accessory phase of the assemblages and could not be found in all cases.

Spinel and garnet exclude each other in the system CMAS in the presence of pyroxenes and forsterite. Both spinel and garnet together were only found in few unequilibrated runs performed to establish run conditions.

Melting occurred in some runs. Optically some carbonates were found in those runs. This is regarded as being introduced by acetone, which was used to grind the mixture and to clean the metal capsules. Initially mixes were not dried by heating following grinding. Under the conditions of the runs acetone will decompose to water and CO_2 and serve as a flux, but also lower the solidus. Excessive melting occurred at 1400°C and 20 kb. No clinopyroxenes other than possible quench (sub-calcic) pyroxenes were found in this run. Due to quenching problems the composition of the melt could not be satisfactorily established.

14. SPINEL-GARNET TRANSITION

Spinel and garnet are incompatible with each otner in the presence of olivine and two pyroxenes in the CMAS system apart from conditions at the univariant reaction

$$\underset{\text{spinel}}{MgAl_2O_4} + 2\underset{\text{pyroxene}}{(Ca,Mg)MgSi_2O_6} = \underset{\text{garnet}}{(Ca,Mg)_3Al_2Si_3O_{12}} + \underset{\text{forsterite}}{Mg_2SiO_4} \qquad (A)$$

Determinations of this boundary have been given by Jenkins & Newton (1979), O'Hara *et al.* (1971), and O'Neill (1981) on the basis of experiments in CMAS. Theoretical calculations were published by Herzberg (1978b) and Obata (1976). At low temperatures (1000°C and less) some uncertainty persists, but the boundary is fairly well established within a 3 kb bracket, rendering Obata's (1976) model as inadequate for low temperatures. No further bracketing has been attempted in this study, but the unreversed experiments in CMAS confirm the studies mentioned above within a wide bracket (fig. 13).

The garnet-spinel transition has some relevance to the mineral facies of the upper mantle, because basaltic rocks commonly contain spinel lherzolites, whereas inclusions in kimberlites are dominated by garnet-bearing types. In natural systems and Cr-bearing systems this reaction is no longer univariant, but also dependent on bulk chemistry. Thus determinations of the reaction in CMAS cannot be directly applied to natural rocks. This problem is discussed in chapter 24.

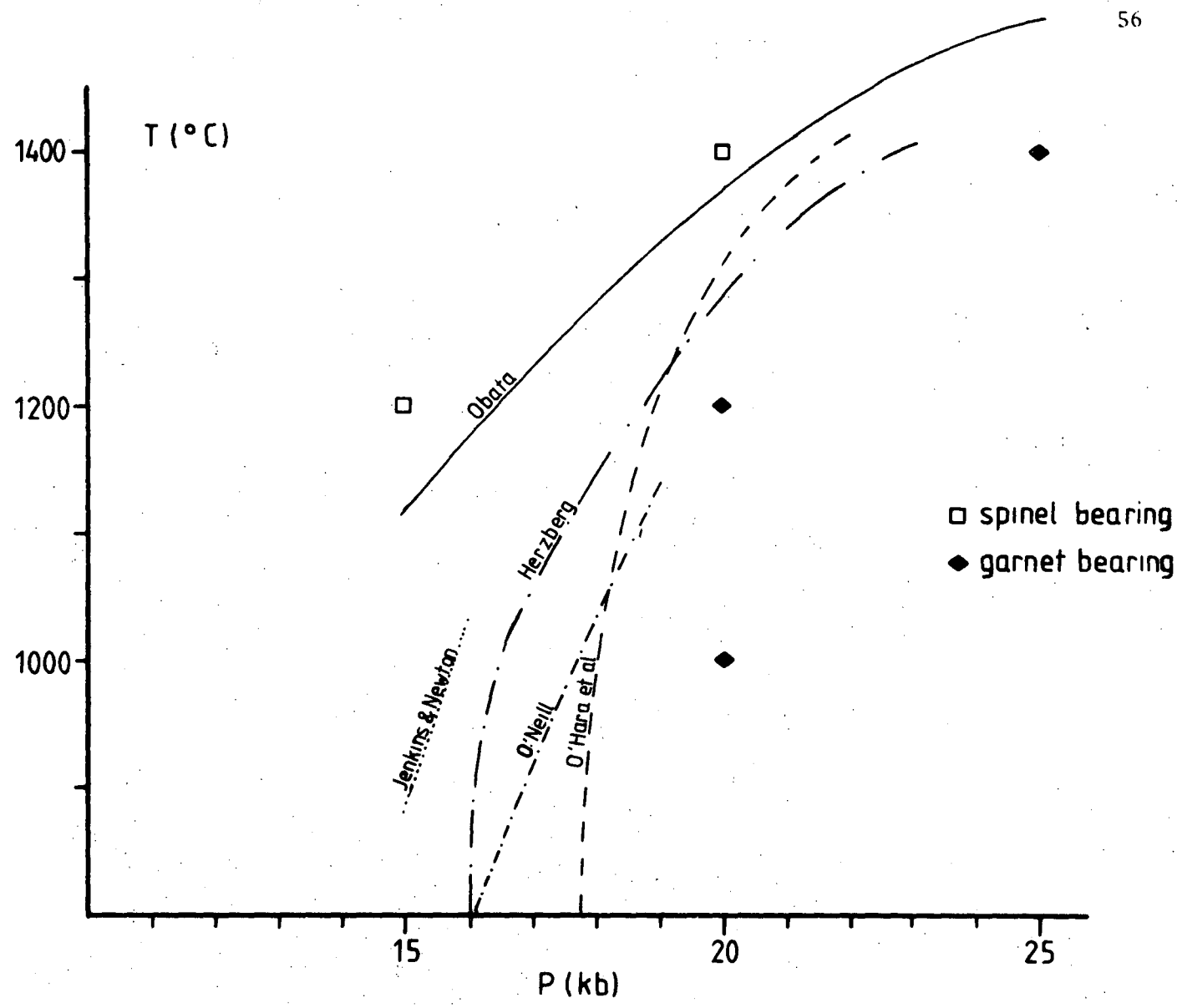

Figure 13: Character of the aluminous phase coexisting with two pyroxenes ± forsterite in CMAS runs compared to experimental determinations (Jenkins & Newton, 1979; O'Hara *et al.*, 1971; O'Neill, 1981) and theoretical calculations (Herzberg, 1978; Obata, 1976) of the univariant reaction sp + (opx,cpx) = gt + fo in the CMAS system.

15. Ca-Mg EXCHANGE BETWEEN PYROXENES

The miscibility gap between coexisting ortho- and clinopyroxene is the basis for the most widely used geothermometer for upper mantle rocks. Determinations of this gap in the system CMS (CaO-MgO-SiO_2) (Boyd & Schairer, 1964; Davis & Boyd, 1966; Lindsley & Dixon, 1976; Mori & Green, 1975; Nehru & Wyllie, 1974) showed the sensitivity of the two-pyroxene solvus to temperatures above about 900°C. While P effects are still ambiguous (Mori & Green, 1976, 1978; Lindsley *et al.*, 1981; Brey, 1982), but will be important only at higher temperatures (1300°C and above), compositional effects on the solvus are known for Fe.

In the CMS system the Ca/Ca+Mg ratios of the pyroxenes are an adequate expression of their relationship in respect to the miscibility gap. In the CMAS system, where Al substitutes in both pyroxenes (MgSi-AlAl) to form Mg-tschermak's and Ca-tschermak's molecules, the thermodynamic formulation of the reaction en(opx) = en(cpx) requires activity composition models to be formulated. Models have been presented by Wood & Banno (1973) and Wells (1977) defining the activity of enstatite in both ortho- and clinopyroxene as the product of the mole fractions of Mg in the M1 and M2 position. The new experiments in CMAS confirm the now widely acknowledged superiority of Wells (1977) formulation (Carswell & Gibb, 1980) (fig. 14). The new data presented here suggest, but do not convincingly demonstrate a pressure effect with $ln\ (a_{en}^{cpx}/a_{en}^{opx})$ increasing with increase in pressure at constant temperature. However the difficulty in clinopyroxene analyses which may bias the data to low a_{en}^{cpx} has previously been noted. The data thus may be said to be supportive of the Wells (1977) geothermometer but do not permit refinement of it.

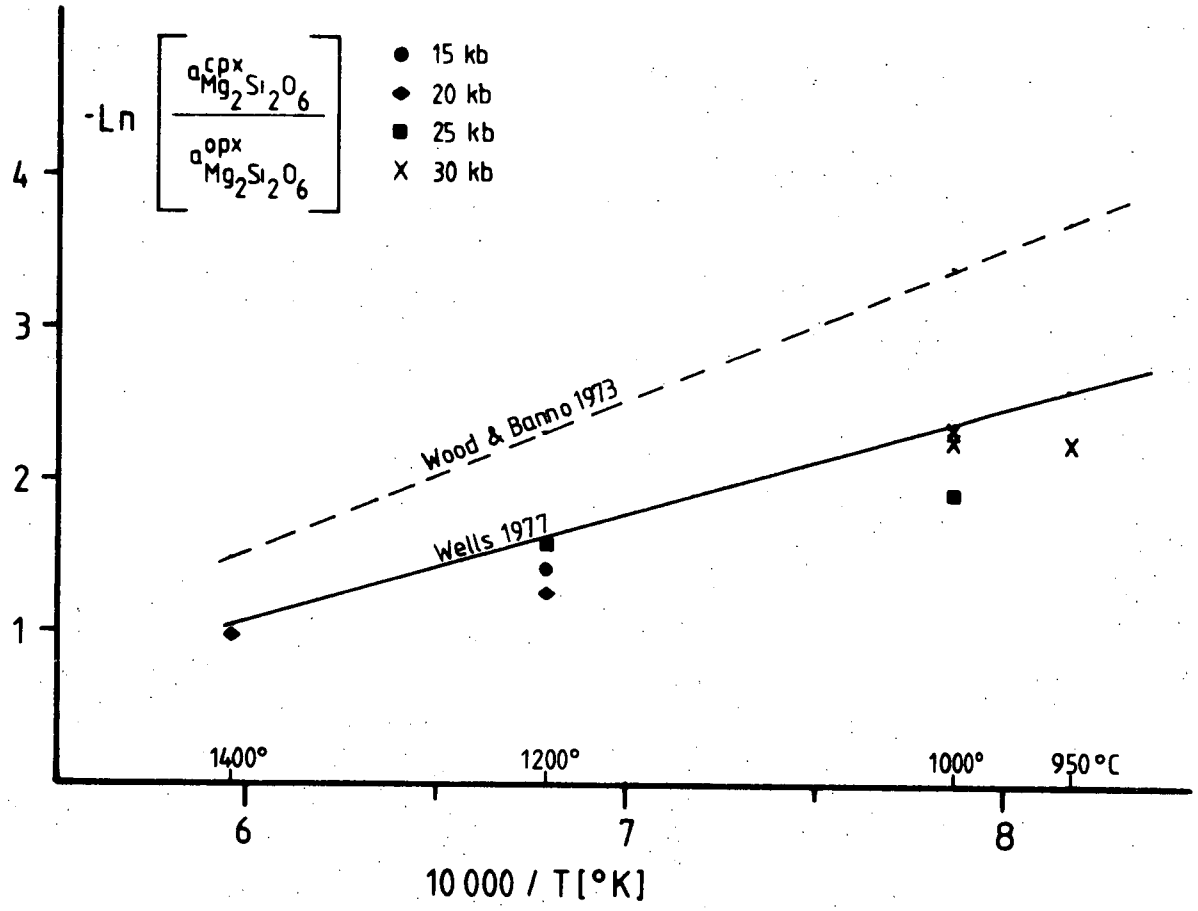

Figure 14: Plot of $-ln(a^{cpx}_{en}/a^{opx}_{en})$ vs. 10,000/T for CMAS data of this study compared to calibrations of the cpx-opx thermometer by Wood & Banno (1973) and Wells (1977). The activity of enstatite in either of the pyroxenes is defined as the product of mole fractions of Mg in M1 and M2 site. For CMAS $X^{M1}_{Mg} = [1 - (Al/2)]$ and $X^{M2}_{Mg} = (1 - Ca)$.

16. SOLUBILITY OF Al_2O_3 IN ORTHOPYROXENE

Thermodynamic considerations

The solubility of Al_2O_3 in orthopyroxene can be described by the reaction

$$Mg_2Si_2O_6 + MgAl_2SiO_6 = Mg_3Al_2Si_3O_{12} \qquad (B)$$

enstatite Mg-tschermaks pyrope

In the system CMAS the orthopyroxene contains Ca. Following Wood & Banno (1973) the Al in the octahedral sites is attributed to the M1 position, Ca to M2 position. Therefore the pyroxene consists of the three endmembers

	Position				
	M2	M1	B	A	
enstatite	Mg	Mg	Si	Si	O_6
Mg-tschermaks	Mg	Al	Al	Si	O_6
diopside	Ca	Mg	Si	Si	O_6

It follows that $X_{Al}^{M1} = \frac{\Sigma Al}{2}$, $X_{Mg}^{M1} = 1-X_{Al}^{M1}$ and $X_{Mg}^{M2} = 1-X_{Ca}$. In reality, there will be a fraction of Ca-tschermaks ($CaAl_2SiO_6$) present, but assuming a similar distribution for diopside:Ca-tschermaks as given for enstatite: Mg-tschermaks, this fraction will be small and is neglected. The treatment which follows differs from that of Wood (1974) and Harley (1981) in that the diopside fraction is not neglected in thermodynamic formulations, because the temperatures of experiments are up to 1400°C, where a substantial amount of CaO is present.

Based on this model for orthopyroxene, activities for enstatite and Mg-tschermaks can be formulated. Assuming coupling of tetrahedral and octahedral Al we have

$$a_{en}^{opx} = X_{Mg}^{M1} \times X_{Mg}^{M2} \times \gamma_{en} \qquad (1)$$

$$a_{MgTs}^{opx} = X_{Al}^{M1} \times X_{Mg}^{M2} \times \gamma_{MgTs} \qquad (2)$$

where X denotes the mole fraction in the indicated site and γ = activity coefficient, due to non-idealities.

Similarly the garnet is modelled to consist of the two endmembers pyrope ($Mg_3Al_2Si_3O_{12}$) and grossular ($Ca_3Al_2Si_3O_{12}$) and, because no mixing occurs in the M 3+ - site of the garnet in CMAS, the activity of garnet is defined as

$$a_{Py}^{gt} = (X_{Mg}^{M2+})^3 \times \gamma_{py} = (1 - X_{Ca}^{M2+})^3 \times \gamma_{py} \qquad (3)$$

Thus the K for reaction (B) is

$$K_B = \frac{(1 - X_{Ca}^{gt})^3 \gamma_{py}}{[X_{Mg}^{M1} (X_{Mg}^{M2})^2 X_{Al}^{M1}]^{opx} \gamma_{en} \gamma_{MgTs}} \qquad (4)$$

Non-idealities of mixing between Mg and Al on the M1 site have to be considered. This can be done by treating enstatite and Mg-tschermaks as binary regular solutions on the M1 site, so that

$$RT \ln \gamma_{en}^{M1} = (X_{Al}^{M1})^2 W_{MgAl} \qquad (5)$$

$$RT \ln \gamma_{MgTs}^{M1} = (X_{Mg}^{M1})^2 W_{MgAl} \qquad (6)$$

(W = Margules or interaction parameter).

Alternatively Mg-Al interactions can be taken into account by an excess volume of mixing term for orthopyroxene, assuming ideal mixing at 1 bar (Wood & Banno, 1973; Harley, 1981; Harley & Green, 1982). The volume term of Wood & Banno (1973) was derived from experimental data of Skinner & Boyd (1964) and Chatterjee & Schreyer (1972). Harley (1981) combined the latter with more recent data (Danckwerth & Newton, 1978) and derived the formula

$$-dV_r = 183.3 + 178.98 (1 - X_{Al}^{M1}) X_{Al}^{M1} \quad \text{(cals/kb)} \qquad (7)$$

where dV_r denotes the volume change of reaction (B). The derived values of dV_r are very similar to those obtained by the method of Wood & Banno (1973). The method of Harley (1981) has been adopted.

Rigorous thermodynamic formulation of the non-idealities of orthopyroxene requires a model for mixing between diopside and enstatite/Mg-tschermaks on the M2 site and reciprocal terms. A formulation for mixing of Ca and Mg as a binary regular solution has the form

$$RT\ ln\ \gamma_{en}^{M2} = RT\ ln\ \gamma_{MgTs}^{M2} = (X_{Ca}^{M2})^2\ W_{CaMg} \qquad (8)$$

It is apparent that this term will be small because of the squared form of X_{Ca}^{M2}, even where a substantial amount of Ca ($\geq$ 2 wt.%) is present. The small size of X_{Ca}^{M2} renders it also unlikely that a reciprocal term is of great importance. Non-idealities due to the mixing of Ca with Mg and reciprocal interactions are therefore neglected.

Garnet in CMAS contains a substantial amount of Ca in equilibrium with orthopyroxene and clinopyroxene. A binary regular solution model has been applied and thus

$$RT\ ln\ \gamma_{py} = 3(X_{Ca}^{gt})^2\ W_{CaMg} \qquad (9)$$

is applicable. The value for W_{CaMg} is still somewhat in dispute and different estimates have been given (Dahl, 1980; Ganguly & Kennedy, 1974; Jenkins & Newton, 1979; Oka, 1978; Saxena, 1981; Wood & Nicholls, 1978), but most estimates are in the range between 2000 and 4000 cals/mol. The value adopted here is 3000 cals/mol (Wood & Nicholls, 1978).

At equilibrium the relations

$$dG_{P,T} = -RT\ ln\ K \qquad (10)$$

$$dG_{1,T} = -RT\ ln\ K - PdV = dH - TdS \qquad (11)$$

are valid, where dG is the change in Gibbs free energy of reaction (B) at P and T or at 1 bar and T respectively, dH is the enthalpy change and dS is the entropy change for the reaction.

For reaction (B) we thus have

$$-\left[RT\ ln\left(\frac{(1 - X_{Ca}^{gt})^3}{X_{Mg}^{M1}\ (X_{Mg}^{M2})^2\ X_{Al}^{M1}}\right) + 3(X_{Ca}^{gt})^2\ W_{CaMg}\right] - PdV_r = dH - TdS \qquad (12)$$

The form of equation (12) is that of a linear equation, so that a linear relationship between dG and 1/T exists. This is shown in fig. 15. A least-square fit to the data yields values for dH of -6047 cals and dS = -3.23 e.u. (entropy units = cal $mol^{-1}deg^{-1}$). The values of dG determined with the new data are compared with the estimates of Wood (1974) and Harley & Green (1982) in table 10.

Table 10: Predictions of $dG_{P,T}$ (cals/mol) for three T conditions, based on estimates for dH and dS of -6047 cal, -3.23 e.u. (this study), -5650 cal, -2.93 e.u. (Harley & Green, 1982), -7012 cal, -3.89 e.u. (Wood, 1974).

T (°C)	this study	Harley	Wood
1000	1935	1920	2060
1200	1289	1334	1282
1400	643	748	504

The comparison shows that the derived values at low temperatures (≦ 1000°C) are in good agreement with Harley & Green (1982), who performed almost all experiments at T below 1200°C. At higher temperatures, estimates deviate from predictions by Harley & Green (1982) in the direction of the predictions of Wood (1974), whose values were derived via experiments performed generally at T of 1100°C and above. Thus derived values are in good agreement with the best constrained experimental ranges of both workers. It is concluded that the values are a close approximation to equilibrium values are are used in further treatments.

Rearranging equation (12) gives the formulation of a barometer for the system CMAS:

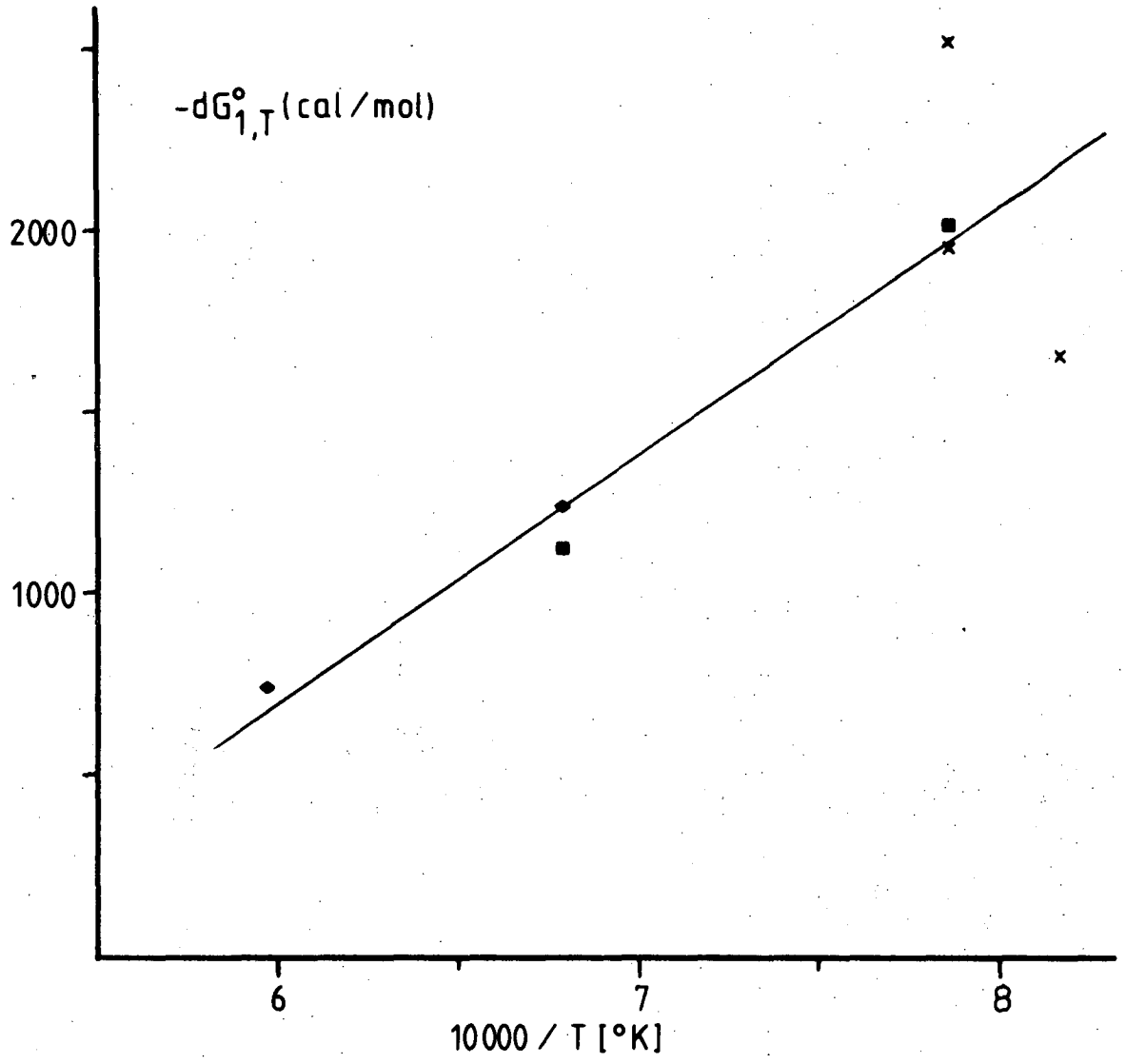

gure 15: Plot of $-dG_{1,T}$ vs. 10,000/T for the reaction En + MgTs = py in CMAS. $dG_{1,T}$ is the standard state energy change of this reaction at 1 bar and temperature of interest in cal/mol and is calculated as

$$[(-RT\ ln\ K_D(B) - 3(X_{Ca}^{gt})^2\ W_{CaMg}) - PdV_r].$$

Symbols as in figure 14.

$$P(kb) = \frac{1}{dV_r}\left(-\left[RT\ ln\ K_D + 3(X_{Ca}^{gt})^2\ W_{CaMg}\right] - dH + TdS\right) \qquad (13)$$

which becomes, substituting derived and adopted values,

$$P(kb) = \frac{-RT\ ln\left(\frac{(1-X_{Ca}^{gt})^3}{X_{Mg}^{M1}\ (X_{Mg}^{M2})^2\ X_{Al}^{M1}}\right) - 9000(X_{Ca}^{gt})^2 + 6047 - 3.23T}{-[183.3 + 178.98\ X_{Al}^{M1}\ (1-X_{Al}^{M1})]} \qquad (14)$$

Application of equation (14) to the data yields good agreement as shown in fig. 16. Error levels of predictions naturally rise with decreasing X_{Al}^{M1}, because for identical accuracy of analysis the relative error increases. Thus a higher spread in estimates is expected at lower temperatures and higher pressures, both corresponding to a decrease in X_{Al}^{M1}.

17. COMPARISON WITH OTHER STUDIES IN CMAS

To compare other studies in CMAS with the present results, pressures have been estimated by applying equation (14) to published experimental data. The result is shown in fig. 17. The data of Akella (1976) yield generally lower estimates than nominal run pressures. Akella (1976) used both "piston-in" and "piston-out" techniques in his experiments. In the light of the studies of Green *et al.* (1966) a friction correction of -10% should be applied to runs performed with assemblages using talc as a pressure medium under "piston-in" conditions. In the same study it is suggested that a smaller correction is necessary for the "piston-out" technique, the size of which remains unclear (Johannes *et al.*, 1971). Akella (1976) applied a ± 1 kb correction to the nominal run pressures, corresponding to about 2.5 to 4%. It is not obvious from his data, which run was performed with which technique, but it is envisaged that part of the disagreement between estimates and nominal pressures is due to different friction corrections applied.

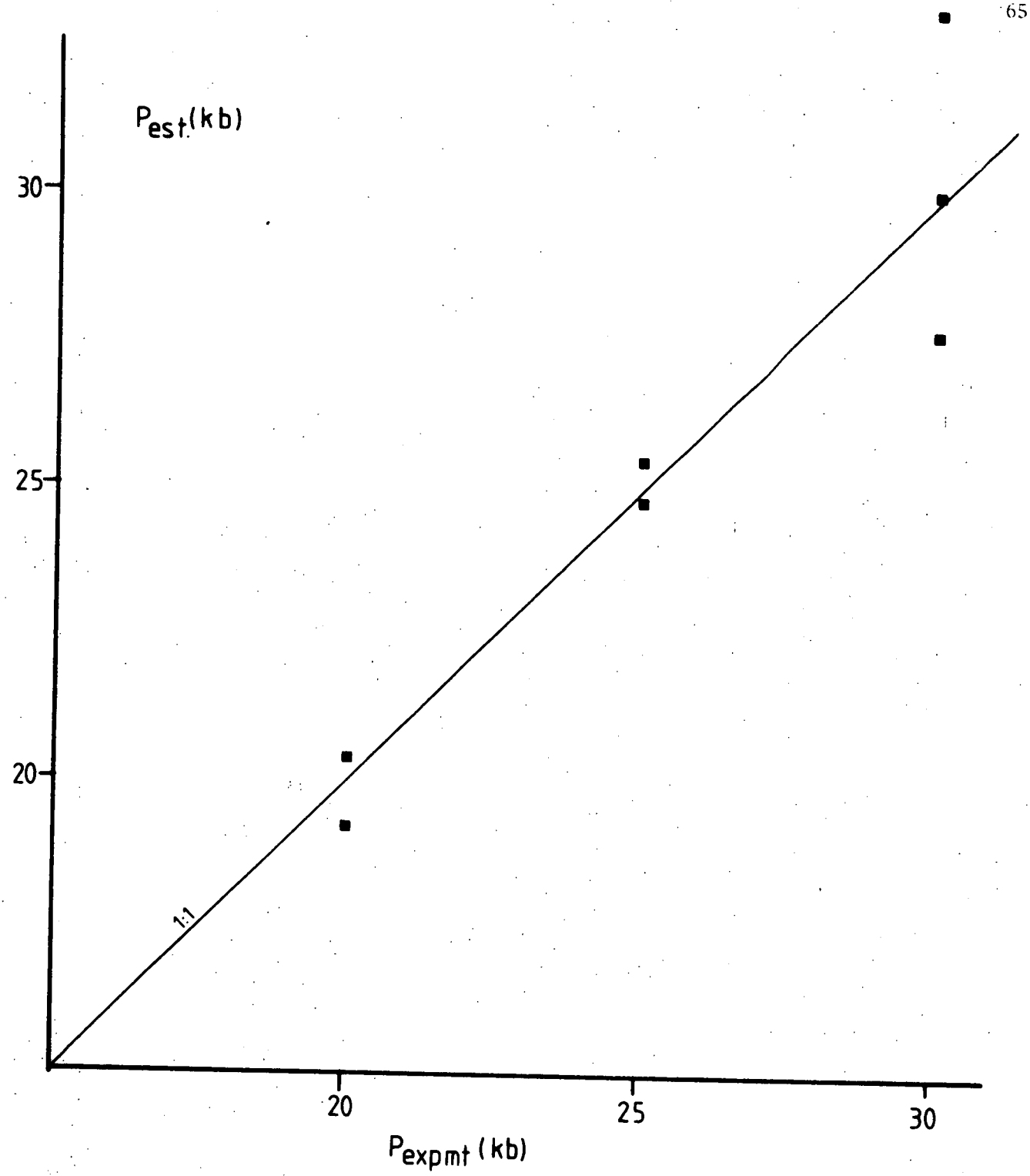

Figure 16: Comparison of estimated (P_{est}) and nominal (P_{expmt}) run pressure for CMAS. P_{est} was calculated applying equation (14) to experimental data of this study.

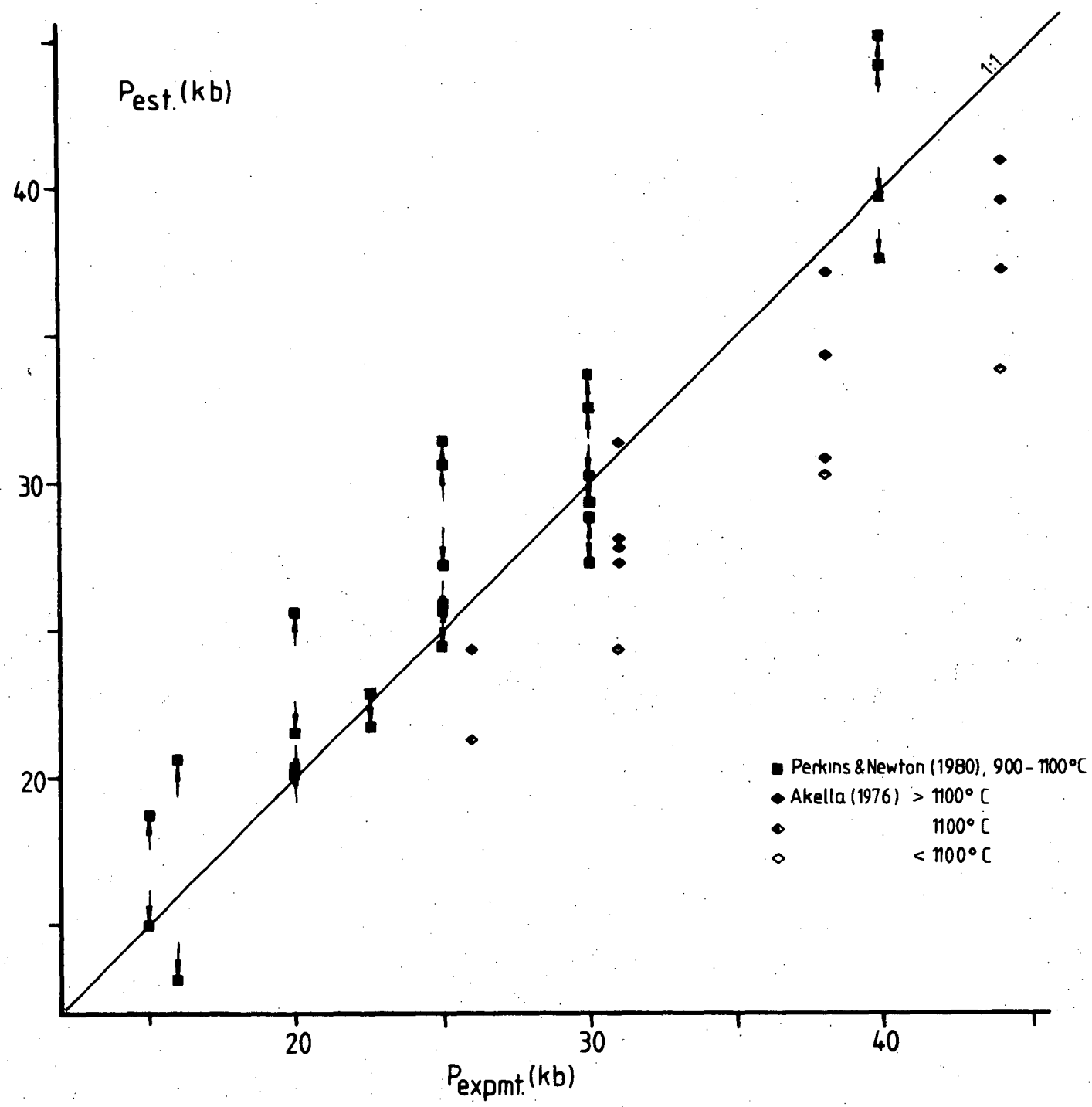

igure 17: Comparison of pressures estimated via equation (14) (P_{est}) and nominal (P_{expmt}) run pressures for CMAS data of Akella (1976) and Perkins & Newton (1980). Arrows indicate direction of approach to equilibrium by Perkins & Newton (1980); arrows pointing to lower pressure estimates are for the bracket where pure En was part of the starting material, arrows pointing to higher pressure estimates are for the bracket using highly aluminous pyroxenes as part of the starting material.

Additionally there is a systematic deviation of the estimates with temperature with lower temperature runs yielding lower estimates (fig. 17). This supports Howells & O'Hara (1978), who argued for lower solubilities of Al_2O_3 in orthopyroxene, particularly at lower temperatures. Reaction rates in experimental runs are very much dependent on temperature, so that long run durations are required to reach equilibrium at low temperature, even with a flux present. Akella's (1976) experiments were kept at the conditions for less than 31 hours, a relatively short time for low temperature runs when compared to Perkins & Newton (1980), Harley (1981), Wood (1974), and this study. Thus it is believed that the time was insufficient to reach equilibrium at low temperatures and analysed pyroxenes reflect incomplete exsolution of Al_2O_3 and incomplete growth of garnet. Runs at higher temperatures approach equilibrium more closely.

Perkins & Newton (1980) attempted to bracket the values of Al-solubility in orthopyroxene by performing experiments with different starting materials containing either a pure enstatite or a highly aluminous orthopyroxene as one component. In most of the pairs of runs they record an overlap in the final values for Al_2O_3 in orthopyroxene and attributed this to "path-looping". Assuming this process to occur in every run they argue that the equilibrium value is within the overlap range. In most of their runs the overlap region is quite small and there is good agreement between the calculated pressure from equation (14) for each of the brackets and the nominal run pressure. In some cases however their bracket is wide (e.g. a 3 wt.% Al_2O_3 bracket for 1000°C, 16 kb) and accordingly the estimates for the individual brackets differ more widely. In these cases a better agreement between estimates via equation (14) and nominal run pressures is given for the experiment approaching the equilibrium from the low-Al side (pure enstatite in starting material) and going towards higher values of Al_2O_3. The reason for this is not understood.

Summarizing the agreement between calculated and experimental pressure is sufficiently good to argue in favour of the dH and dS values derived and the thermodynamic model adopted in this study.

PART III

AN EXPERIMENTAL STUDY BEARING ON PHASE RELATIONSHIPS IN THE SYSTEM SMACCR (SiO_2-MgO-Al_2O_3-CaO-Cr_2O_3).

18. INTRODUCTION

In terms of bulk rock chemistry, Cr_2O_3 is only a minor constituent of natural garnet lherzolites with a level of about 0.4 wt.%. Nonetheless it has to be considered with reference to phase equilibria, because it is a major component of garnet (typically between 2 and 7 wt.%) and spinel (≃20-55 wt.%). In orthopyroxenes from garnet lherzolites, Cr_2O_3 is generally only present as a minor oxide component with typical contents between 0.2 and 0.5 wt.%. However, even here it has considerable influence on phase equilibria, because it is competing with Al_2O_3 and the latter is the base of the most widely used geobarometer for lherzolites. In most inclusions in kimberlites, orthopyroxene contains small quantities of Al_2O_3 (in the order of 1 wt.%), hence even small quantities of Cr_2O_3 can be significant for calculations of site distributions of Al in orthopyroxene with possible effects on P-T estimates.

Like Al_2O_3, the solubility of Cr_2O_3 in orthopyroxene was found to be dependent on pressure and temperature. Accordingly an empirical barometer utilizing these observations has been developed.

For a number of P-T-X conditions in SMACCR, garnet coexists with spinel. This is consistent with observations on some natural garnet lherzolites from kimberlites and leads to an analysis of garnet/spinel compositional relationships.

Previous studies in Cr-bearing systems mainly considered phase relations at atmospheric pressures (Glasser & Osborn, 1958; Muan, 1975; Stubican & Greskovich, 1975; Warshaw & Keith, 1954) or investigated stabilities of oxides and silicates (Chatterjee *et al.*, 1982; Ikeda & Ohashi, 1974; Ikeda & Yagi, 1972, 1977, 1982; Irfune *et al.*, 1982; Ringwood, 1977; Vredevoogd & Forbes, 1975; White & Roy, 1975; Yoder & Kullerud, 1971). Studies in the system SMACCR were performed at pressures below the garnet stability limit (Dickey & Yoder, 1970; Dickey *et al*, 1971; Onuma & Tohara,

1981) or with extremely low Cr contents (O'Neill, 1981) and no published sets of data from such experiments are available. Earlier studies on natural systems with emphasis on the influence or relationships involving Cr (McGregor, 1970, 1982; Mysen, 1976) are discussed in later sections.

19. EXPERIMENTAL TECHNIQUES

Experimental techniques employed in this study are in most cases identical to those already described (Chapter 10). Some runs at pressures of 35 kb and higher were performed with assemblages which are similar to the dry assemblage of fig. 12, but the outer talc sleeve was replaced by a NaCl sleeve. The physical properties of NaCl at high pressures and temperatures are such as to reduce the friction between assemblage and apparatus (Mirwald *et al.*, 1975). Hence no friction correction was applied in these runs and the run pressure was equated with the measured load pressure.

The NaCl sleeve did not contain water and accordingly no water was present to degrade the graphite heater. It was found that the recorded temperature at the set point was stable with time, without requiring increase in input current to maintain the recorded temperature. This provides supportive evidence for the reliability of $Pt/Pt_{90}Rh_{10}$ thermocouples under the conditions of the runs performed.

In a variation from the methods of the CMAS experiments, a number of runs used capsules containing two different starting mixtures. The two mixtures were separated from each other by a tightly fitting disc of noble metal. Longitudinal sections through these capsules show that the disc stayed in position during the run and prevented compositional exchange other than that of a volatile phase (trace of water, etc.).

20. STARTING MATERIALS

A number of different starting materials were used and their compositions are listed in table 11. Three basic types were prepared: (i) seeded sintered oxide mixes (SSO), (ii) sintered oxides + crystalline pure pyrope + crystalline pure picotite (SOGP) and (iii) seeded glass mixes (SGL).

The SSO materials were prepared from pure oxide and carbonate reagents as described in chapter 11. One starting material prepared this way contained large amounts of coarse corundum, which persisted in a series of runs. The corundum may have been formed because of overheating during the sintering process. Runs with this starting material were discarded and repeated with the SSO mix prepared as follows.

Alternative mixtures were prepared by utilizing aluminium sulphate [$Al_2(SO_4)nH_2O$] or aluminium nitrate [$Al(NO_3)_3\ 9H_2O$] as starting components along with chromium oxide, magnesium oxide and calcium carbonate, for the sintering process. During prolonged heat treatment the Al compounds convert by giving off SO_2 or NO_2 respectively, and react to form more complex Al compounds. This method makes the appearance of large amounts of coarse corundum unlikely, but has the disadvantage that Al sulphides (or, under favourable conditions, Al nitrides respectively) may be formed, both of which are highly temperature resistant. It was found that long heating times (in excess of 24 hours) were needed to drive off the sulphur effectively and that small amounts of sulphur still persisted within the mixture.

Apart from the failure of the one mixture mentioned above, no advantage of mixtures of SSO, SOGP or SGL type over each other were observed (i.e. similar results, grain sizes, etc. were obtained).

Attempts were made to produce glasses from oxide mixtures, but no clear glass was obtained, even at the highest permissible temperatures on

Table 11: Compositions of starting materials used in experiments (wt.%).

	SSO-LC	SOGP-LC	SSO-MC	SOGP-MC	SOGP-MC2	SSO-HC
MgO	35.4	35.4	35.0	34.9	35.7	29.4
Al_2O_3	10.0	10.1	10.0	10.0	8.7	12.4
SiO_2	46.1	45.9	44.2	44.6	45.0	44.9
CaO	7.0	7.0	7.0	6.7	7.1	5.6
Cr_2O_3	1.5	1.6	3.8	3.8	3.5	7.7
Cr/Cr+Al	0.091	0.096	0.203	0.203	0.213	0.294

	SOGP-HC	SSO-HC2	SOGP-HC2	SGL-HC	SGL-HCF
MgO	30.0	35.0	35.1	29.4	43.2
Al_2O_3	11.3	8.5	8.5	12.4	6.3
SiO_2	45.0	44.0	43.7	44.9	43.8
CaO	5.8	7.0	7.2	5.6	2.8
Cr_2O_3	7.9	5.5	5.5	7.7	3.9
Cr/Cr+Al	0.319	0.302	0.302	0.294	0.293

an Ir strip heater. The product was still turbid and mottled with tiny dark spots, due to the failure to dissolve Cr_2O_3 completely into the melt. These "glass" mixtures have only been used in a few runs.

The SOGP type starting material was prepared by sintering oxides and carbonates of Ca, Mg and Si in the manner described, to which were added pre-synthesized pure pyrope and pure picotite.

The compositional differences between the mixtures are differing Cr/Cr+Al ratios in order to investigate compositional effects on phase equilibria. This was necessary because in the five-component system SMACCR a divariant (P,T) equilibrium exists for a five-phase assemblage. Most run products in fact consisted of four coexisting phases.

The extensively used mixtures SSO-HC and SOGP-HC are lower in MgO and yield run products without forsterite. Garnet as a stable phase with spinel and two pyroxenes appeared under forsterite-absent conditions at lower pressures relative to forsterite-present conditions. Thus garnet-orthopyroxene equilibria could be investigated over a wider pressure range appropriate to the piston-cylinder apparatus.

The experimental strategy behind the mixtures is as follows. In the strict sense it is not possible to reverse the compositions of phases with more than one degree of compositional freedom. Phase boundaries however can be reversed in complex systems. Therefore the pairs of results on the garnet stability (garnet growth from garnet-free mixtures, disappearance of garnet from runs with garnet as a major constituent of the mixture) bracket the boundary.

The growth of pyroxenes from oxide mixtures and glasses is a very rapid process (Green & Ringwood, 1967a; Mori, 1976; Howells & O'Hara, 1978). Howells & O'Hara (1978) studied the solubility of Al_2O_3 in orthopyroxene in relation to differing starting materials. They used both crystallized gel type starting materials (essentially very fine grained oxide mixes which have been sintered and recrystallized to give a micro-

crystalline product) and glasses. The two types are thus comparable to the SSO and SGL mixes of this study. The SSO material may however be somewhat coarser than the gel-type starting material of Howells & O'Hara (1978). These authors showed that both types produced pyroxenes even at run durations as short as 30 seconds, resulting in pyroxenes with a large range of Al_2O_3 contents, including very high Al_2O_3 contents (cf. Howells & O'Hara, 1978, fig. 5). Glass-type starting material was shown to approach low Al_2O_3 limits in orthopyroxene more sluggishly than gel-type starting material with increasing run duration. Modal amounts of garnet were found to increase with increasing run duration. Garnet thus grew from aluminous pyroxenes with time, garnet nucleation and growth is a sluggish process. It is assumed that the SSO and SGL mixes used in this study show a similar behaviour. Rapid growth of initially highly heterogeneous (in Al_2O_3) pyroxenes is thus inferred for these mixes as well, followed by garnet growth and equilibration. The majority of orthopyroxenes in runs with SSO and SGL starting material are thus believed to approach equilibrium from the high-Al_2O_3 side, but at least some orthopyroxenes with low Al_2O_3 contents should be present as well, at least in the SSO starting materials. The net result in the SSO and SGL mixes is thus a homogenization process where orthopyroxenes approach equilibrium from both sides, but mostly from the high-Al_2O_3 side.

By contrast the SOGP mixture of this study had initially all Al_2O_3 in garnet and all Cr_2O_3 in the spinel phase, the rest of the mixture being a sintered oxide mix (CMS). Assuming the same process of rapid growth of pyroxenes from the oxide mix part of the charge, the initially formed pyroxenes should contain no, or very little, Al_2O_3 (and Cr_2O_3). Thus the SOGP material may be used to bracket the equilibrium content of orthopyroxene from the low-Al_2O_3 side. However, Lane & Ganguly (1980) and Perkins & Newton (1980) argued that some orthopyroxenes may be formed as nucleii within or bordering garnet and thus have high initial Al_2O_3 contents.

This problem, that the pyroxenes may approach equilibrium from both the high- and low-Al_2O_3side and only have the major part of reacting pyroxenes on the one or the other side, is known as "path-looping" and was encountered in studies in CMAS and MAS (Perkins & Newton, 1980; Lane & Ganguly, 1980) as well. Thus both approaches used here are not to be seen as strict reversals in respect to the Al_2O_3 content of orthopyroxene. The achievement of equilibrium has to be judged by the degree of homogeneity of the phases and the similarity or dissimilarity of the results for differing starting materials.

21. ANALYSES OF RUN PRODUCTS

Run products in the system SMACCR were analysed with the methods and equipment described previously. In runs containing two mixes in one capsule, the whole capsule was embedded in epoxy resin and a longitudinal section was polished. Compositions within the run products along the sections were found to be homogeneous, no influence of a thermal gradient over the length of the capsule was detected.

The run products are described in the following chapter. The appearance of Cr-bearing spinel within a poikilitic phase, particularly garnet, enhanced the problems of analysis discussed in chapter 12. Wide area scans to check the bulk composition mostly show some scatter. Nevertheless the analysed compositions from the wide scans showed a close proximity to the intended values, with only excess Si in a number of cases, again attributed to contamination of the mixture by Si from the agate mortar used in grinding processes.

To evaluate the quality of the analytical data for garnet, which showed nearly always some evidence for contamination by other phases, model calculations illustrating contamination are shown in table 12. The model was based on a typical garnet with a near-stoichiometric composition, to

Table 12: Models for contamination of garnet by other phases.

	garnet		+10% fo		+5% fo		+10% sp	
	wt.%	struc	st.%	struc	wt.%	struc	wt.%	struc
MgO	23.15	2.417	26.27	2.744	24.79	2.589	23.35	2.479
Al_2O_3	20.00	1.651	18.18	1.502	19.05	1.573	20.32	1.706
SiO_2	42.80	2.999	42.77	2.998	42.79	2.998	38.92	2.772
CaO	7.65	0.574	6.95	0.521	7.29	0.547	6.96	0.531
Cr_2O_3	6.40	0.354	5.82	0.322	6.09	0.337	10.46	0.589
Total		7.997		8.089		8.045		8.079
100Ca/Ca+Mg		19.19		15.98		17.44		17.64
100Cr/Cr+Al		17.67		17.67		17.67		25.66

	+5% sp		+2% sp		+10% cpx	
	wt.%	struc	wt.%	struc	wt.%	struc
MgO	23.25	2.449	23.19	2.430	22.79	2.385
Al_2O_3	20.17	1.680	20.07	1.663	18.36	1.520
SiO_2	40.77	2.881	41.96	2.951	43.80	3.076
CaO	7.29	0.551	7.50	0.565	9.05	0.680
Cr_2O_3	8.52	0.476	7.27	0.404	6.00	0.333
Total		8.040		0.015		7.996
100Ca/Ca+Mg		18.38		18.86		22.21
100Cr/Cr+Al		22.08		19.55		17.98

which amounts of contaminating phases were hypothetically added and the resulting structural formulae based on 8 oxygen were calculated. The contaminating phases were chosen to show maximum influence on the two important ratios of the garnet, Cr/Cr+Al and Ca/Ca+Mg. Hence a high-Cr spinel (Cr/Cr+Al = 0.6) and a high-Ca clinopyroxene were used. Forsterite contains practically no Ca, so that contamination by forsterite changes the Ca/Ca+Mg ratio and therefore this was also modelled.

From the calculated structural formulae of contaminated garnets it is apparent that major contaminations result in significant changes in the structural formula. A 5% addition of forsterite leads to a total of 8.045 (based on 12 oxygen) accompanied by a change in the 100Ca/Ca+Mg ratio of only 1.8. Similarly an addition of 5% spinel yields a cation total of 8.040 and the internal structure is grossly distorted with Si of 2.881 and Al+Cr of 2.156. Even where only 2% spinel was added, the structural formula would show a significant deviation towards low Si and high Al+Cr values. Analyses of garnets in experiments which show deviations of this type were dismissed. Most analyses of garnet show rather a positive deviation in Si from the theoretical 3.000 (cf. appendix 5), which may be the influence of contamination by pyroxene. As shown in table 12, a 10% contamination of garnet by clinopyroxene results in a change of the 100Ca/Ca+Mg ratio of about 3 and a large deviation in Si and Al+Cr. The garnet analyses taken into account in this study show less indication for contamination than the modelled contaminations. It is therefore concluded that the ratios used in the calculations in the following chapters are accurate to within ±2 (of 100Ca/Ca+Mg and 100Cr/Cr+Al).

The generally very small grainsize of the spinels of the run products leads to similar problems in the analysis of spinels. Contamination by other phases is apparent because all other phases contain SiO_2 as a major component and SiO_2 was recorded in the spinel analyses. In most cases the amount of SiO_2 in the analyses could be limited to less than 6%, with a

mean value of 3.5% (std. dev. 2.6). It is impossible to establish in each case by which phase (olivine, orthopyroxene, clinopyroxene or garnet) the spinel was contaminated. The high $MgO:(Al_2O_3+Cr_2O_3)$ ratio of all possible contaminating phases results in MgO contents too high for spinel and accordingly the structural formula of normalised spinel analyses (based on 4 oxygen and MgO, Cr_2O_3 and Al_2O_3 recordings) yields values greater than 1 for MgO. The only characteristic of spinel of importance for further treatment is the Cr/Cr+Al ratio. The influence of contamination on this ratio is shown in fig. 18. The positions of the mean spinel analyses on the basis of MgO, Cr_2O_3 and Al_2O_3 recordings is shown for two experiments (T-1068: 1200°C, 27 kb; T-855: 1400°C, 35 kb) along with the points for the coexisting phases. Run T-1068 was chosen, because it shows the worst normalised structural formula of all spinels coexisting with garnet. The analysis from run T-855 is a more typical case. Projections from the coexisting phases through the point for the mean analyses of spinel on to the ideal-spinel plane are shown. The points of intersection with this spinel plane represent the possible true spinel compositions, assuming contamination of the spinel analyses by any one of the coexisting phases. Projection from the MgO corner through these projection points on to the Cr_2O_3-Al_2O_3 plane give the Cr/Cr+Al ratio of the possible true spinel composition. It is apparent that a contamination by olivine has no influence on this ratio and that contaminations by either of the pyroxenes result in only minimal changes. Only where garnet is the contaminating phase a noticable difference exists. As shown in fig. 18 a contamination of all spinel analyses by garnet only has the result of shifting the "true" Cr/Cr+Al ratio from the nominal (0 correction) ratio by 5 units of 100Cr/Cr+Al for the worst spinel analyses. In cases with spinel compositions closer to the ideal this maximum possible error reduces to about 2 units. It seems highly unlikely that all contamination should be solely those by garnet. It is therefore concluded that the nominal Cr/Cr+Al ratios are accurate to within approximately 2 or 3 units.

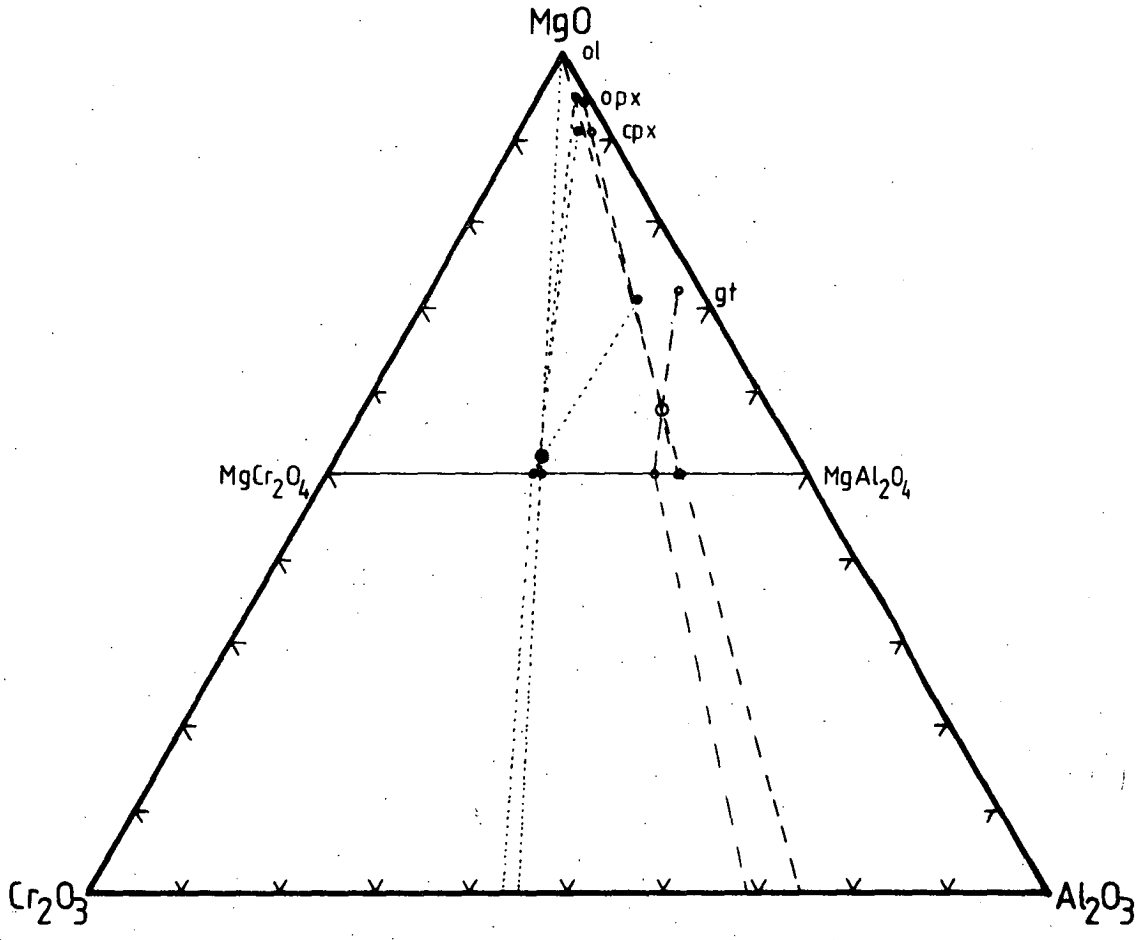

Figure 18: Plot of MgO-Cr_2O_3-Al_2O_3 (mole %) for coexisting phases, mean spinel analyses and projection points. Open symbols are for run T-1068, filled symbols for run T-855 (see text). Shown are tie lines between spinel and the coexisting phases as analysed by microprobe and their projection points on to the spinel plane (dashed lines: T-1068, dotted lines: T-855). Lines from the projection points on to the Cr_2O_3-Al_2O_3 base are lines projected from the MgO corner of the triangle showing differences in Cr/Cr+Al ratios for the projection points.

22. RUN PRODUCTS - SMACCR

Average analyses of run products, normalised to 100%, are listed in appendix 5. Run products in SMACCR are similar to those in CMAS, showing a subsolidus texture with polygonal to lobate mosaics of pyroxenes, garnets, spinel and forsterite.

Spinel shows a strong tendency to occur as tiny grains, usually not larger than about 5 μm and often too small for analysis. The distribution of the spinel grains is fairly even, but it has a tendency to be included in large poikilitic garnets. In runs with starting material of the SSO- or SGL-type the composition was found to be homogeneous within the limitations discussed. In runs where picotite was part of the starting composition, a range of Cr/Cr+Al was found, providing examples of zonation in Cr. The lowest Cr/Cr+Al ratios analysed for these runs are listed in appendix 5. These values approach, but often not very closely, the values of the runs with the SSO or SGL material. Because of the small grainsize of the spinels a proper rim analysis cannot be obtained and thus it is believed that the Cr/Cr+Al values reached in the SSO runs are a better approximation to equilibrium values.

Garnets are strongly poikilitic with numerous inclusions of other phases. Most run products show a homogeneous composition of the garnet within the analytical limitations discussed before. In some runs, however, pyrope was found either zoned or nearly unreacted. This was the case for some lower temperature runs, where time or flux were insufficient to allow completion of the reactions. In the case of zoned garnets, maximum values (i.e. analyses with maximum content of CaO and Cr_2O_3) are given in appendix 5. The poikilitic character of the garnet often makes it impossible to establish clear zonation patterns.

23. Ca-Mg EXCHANGE BETWEEN PYROXENES

As for CMAS the two pyroxene solvus in SMACCR is not adequately expressed by the ratio Ca/Ca+Mg because of the presence of tschermak-type molecules in both pyroxenes. Therefore a plot of $ln\ (a_{en}^{cpx}/a_{en}^{opx})$ vs. 1/T has been chosen to describe the Ca-Mg exchange between pyroxenes (fig. 19). The data for experiments performed at 1200°C or higher temperatures represent the great majority of runs and show three main features:

(a) The values for $ln\ K_D$ are, despite some scatter, in good agreement with the calibration of the geothermometer by Wells (1977). Hence calculations of temperatures by the method of Wells (1977) yield values of within ±60°C of the nominal run temperatures, i.e. within the limits of accuracy envisaged by Wells (1977).

(b) Within the spread of $ln\ K_D$ there is little evidence for an influence of pressure on this exchange. This is in contrast to the theoretical model of Lindsley *et al.* (1981), where a pressure effect should become important at least at $\geq$ 1400°C. However, it may be noted that the P-effect at 1400°C calculated by Lindsley *et al.* (1981) is also in disagreement with published data on the Ca-Mg exchange in simpler systems (Lindsley & Dixon, 1976; Mori & Green, 1976) for this temperature.

(c) The pyroxenes generated in the experiments cover a large range of Al and Cr contents (cf. section 25.1 and appendix 5). The good agreement with the predicted values from CMS and other systems argues against a significant influence of both Al and Cr on the temperature-activity relationships between diopside and enstatite.

At temperatures of 1050°C and lower deviations from the predicted values of Wells (1977) are apparent and some are very large deviations. The deviations are systematically towards higher values of K_D (thus the negative $ln\ K_D$ shows lower values in fig. 19). The calibration of the geothermometer of Wells (1977) was based on the then available data on the

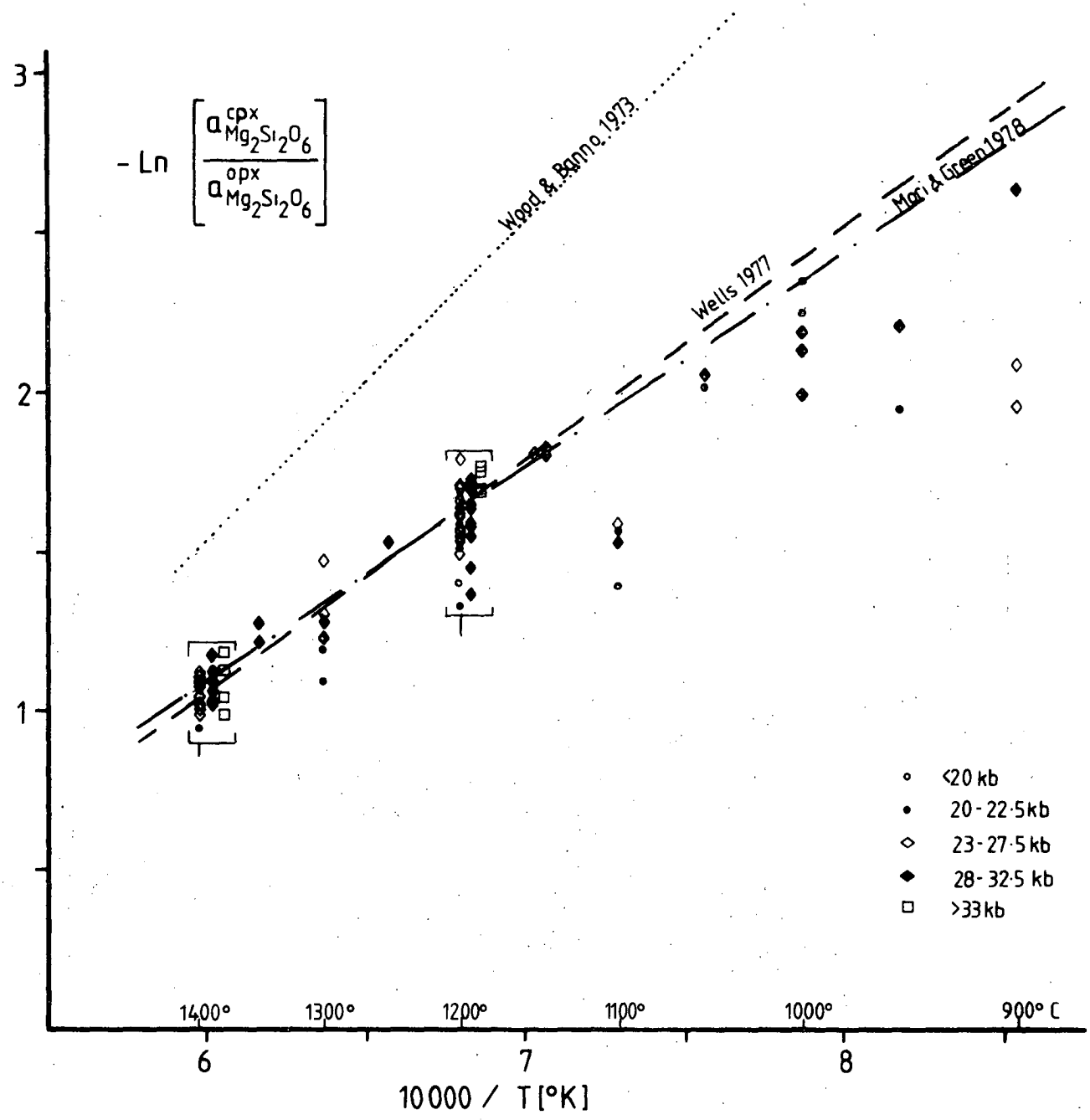

Figure 19: Plot of $-ln(a_{en}^{cpx}/a_{en}^{opx})$ vs. 10000/T (K) for data in the SMACCR system compared to calibrations by Mori & Green (1978), Wells (1977) and Wood & Banno (1973). Activities of the pyroxenes are defined as $X_{Mg}^{M1}X_{Mg}^{M2}$ and the values are calculated as $X_{Mg}^{M1} = 1 - [(Al+Cr)/2]$ and $X_{Mg}^{M2} = 1 - Ca$ (from the structural formula based on 6 oxygens). Data points for 1400°C and 1200°C have plotted so that the symbols for runs with increasing pressure are placed to the right for clarity. Note that the calibration of Mori & Green (1978) was based on experiments with low-Fe content (Mg/Mg+Fe ≅·9) in pyroxenes.

solvus and the bulk of those data are from experiments at temperatures of 1100°C and higher. From fig. 1 of Wells (1977) it is apparent that the published data in CMS (Lindsley & Dixon, 1976; Mori & Green, 1975, 1976) also show systematic deviation towards lower values of $-ln\ K_D$ at temperatures lower than about 1050°C [see also Ehrenberg (1982) and Evans & Trommsdorff (1978)]. Accordingly Kretz (1982) argued for a different behaviour of the Ca-Mg exchange between pyroxenes above and below ≈1080°C. The results of the present study would favour such a model. However, it should be noted that the Ca-Mg exchange becomes less sensitive with decreasing temperature, so that a experimental calibration is likely to involve larger errors. This is enhanced by the slowing down of reaction rates at low temperatures, making an experimental determination more difficult.

Summarizing, the experimental results of this study show good agreement with data from studies in other systems especially at higher temperatures but are supportive of suggestions of inaccuracy in the Wells (1977) calibration of the geothermometer at low temperatures. Some deviations are however very large (lower P runs at 900° and 950°C) and cast doubt on the quality of these analyses.

As is readily seen from fig. 19, the results at 1100°C deviate strongly from predicted values and also from data in other systems. This condition is experimentally difficult, because the addition of flux results very quickly in extensive melting, whereas without sufficient flux reaction rates are slow. The deviation is therefore not seen as significant in respect to the two-pyroxene solvus and results at this temperature condition are to be treated with great caution.

24. SPINEL AND GARNET STABILITY

As shown by MacGregor (1970) in natural systems the appearance of garnet as a stable phase is dependent on bulk composition. The complexity of the natural system, where both FeO and Fe_2O_3 are present, makes a quantitative determination of compositional effects on the garnet stability impossible. Nevertheless qualitatively it was shown that an increase in the $Cr/Cr+Al+Fe^{3+}$ ratio shifted the "garnet-in-boundary" to higher pressures and that a region of coexisting garnet and chromiferous spinel existed.

In the SMACCR system the only variable contributing to changes in the minimum stability of a two pyroxene-garnet-olivine spinel assemblage is the varying ratio of Cr/Cr+Al of the bulk composition. Therefore the effect of Cr on this boundary can be assessed.

Forsterite-free assemblages do show a different stability region relative to fo-bearing assemblages. Under fo-free conditions garnet is stable to lower pressures than in the fo-bearing system with equal Cr/Cr+Al ratio, but is formed at higher pressures than in CMAS (fig. 20). In one run at 1300°C and 25 kb garnet was eliminated from the SOGP charge, a result apparently inconsistent with the other data. It is believed that undetected forsterite was present in this run.

The stability limit of garnet coexisting with forsterite, two pyroxenes and spinel for varying Cr/Cr+Al ratios is shown in fig. 21. At low Cr/Cr+Al ratio of the bulk composition (LC, approx. 100Cr/Cr+Al = 9.5, comparable to model mantle compositions) the minimum pressure to stabilize garnet is increased by about 5 kb relative to a pure CMAS system. A further increase in the Cr/Cr+Al ratio to levels of 100Cr/Cr+Al ≃ 20 (MC, comparable to depleted garnet lherzolites) or 30 (HC, comparable to strongly depleted garnet lherzolites and harzburgites) yields a further increase in this minimum pressure, but not to a proportionate degree.

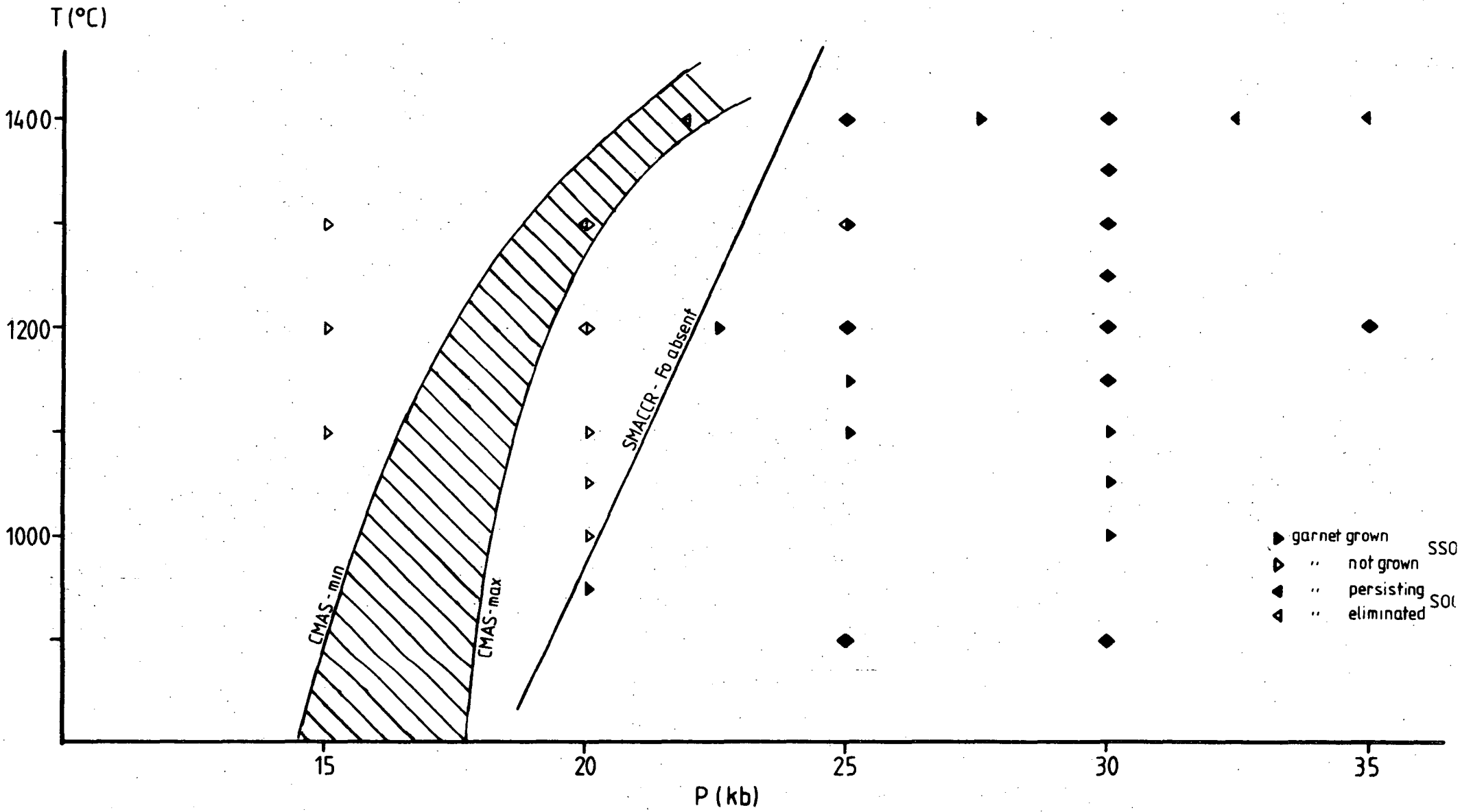

Figure 20: Stability limit of garnet in the system SMACCR coexisting with two pyroxenes under fo-absent conditions compared to (fo-present) garnet stability limit in CMAS. Spinel present in all runs. Range in CMAS from fig. 13.

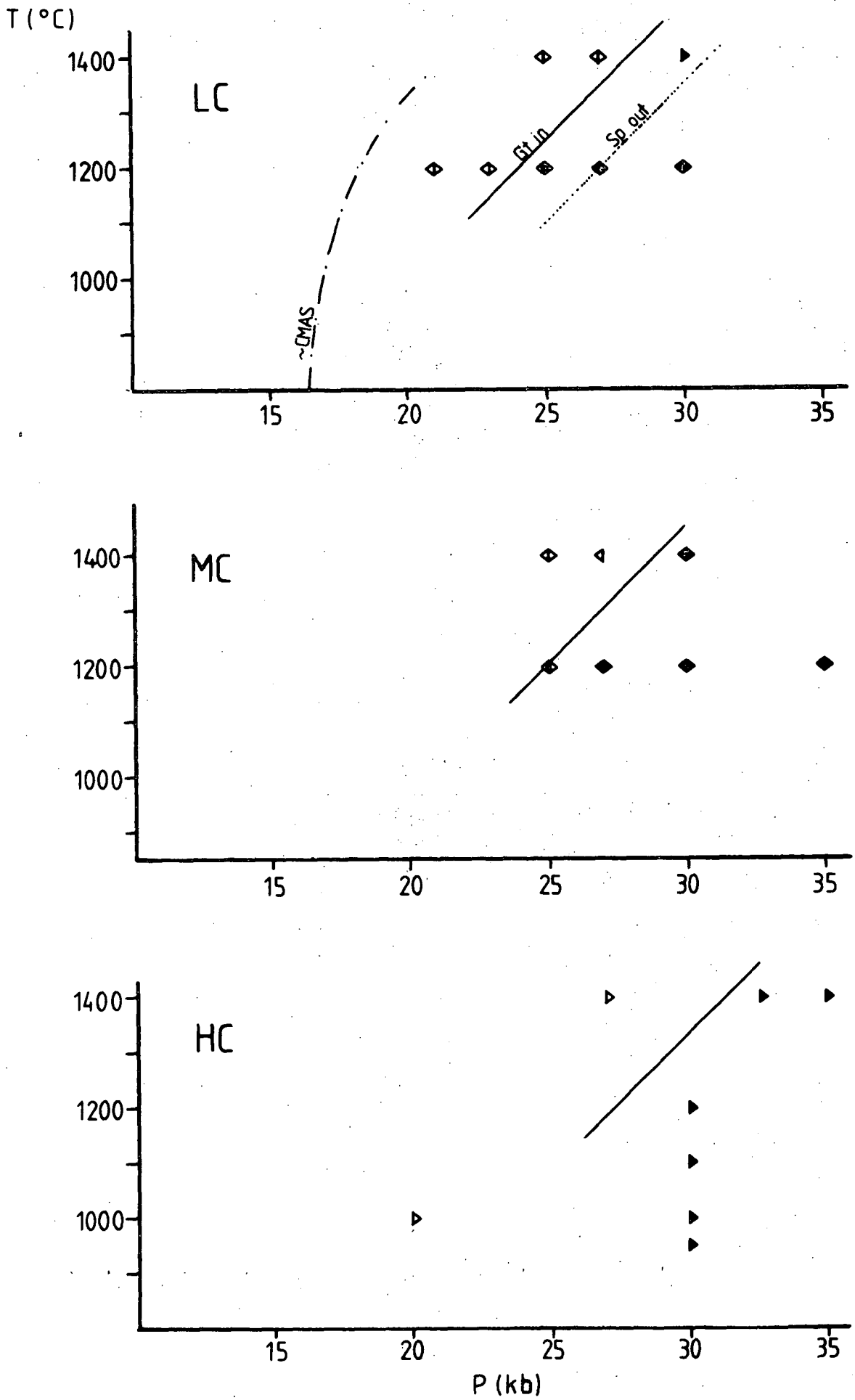

Figure 21: Stability limits for garnet in the SMACCR system coexisting with two pyroxenes and forsterite, for varying Cr/Cr+Al ratios of the bulk composition. LC = low Cr/Cr+Al = 9.5, MC =medium Cr/Cr+Al = 20, HC = high Cr/Cr+Al = 30. Approximate boundary for CMAS in (a) drawn from fig. 13, symbols as in fig. 20.

The increase in pressure needed to stabilize garnet over the values in CMAS is thus not a linear function of the Cr/Cr+Al ratio of the bulk composition.

It must be emphasized that the results on the garnet stability in the system SMACCR cannot be applied directly to natural rocks. Experimental studies and theoretical calculations (Evans & Trommsdorff, 1978; Jenkins & Newton, 1979; Green & Ringwood, 1967a; O'Neill, 1981) argue strongly for an influence of the Mg/Mg+Fe value of the bulk composition on the stability of garnet. O'Neill's (1981) calculation shows that the pressure required to stabilize garnet may be lowered by several kb depending on the Mg/Mg+Fe of the coexisting olivine. This may explain the large discrepancies of "garnet-in" boundaries between the studies in complex systems of Green & Ringwood (1967a) and Jenkins & Newton (1979), because the latter worked with a composition, where the Cr/Cr+Al ratio was extremely low (1.1) and the Mg/Mg+Fe value also lower (84.6) compared to Green & Ringwood (1967a) (Cr/Cr+Al = 7.5, Mg/Mg+Fe = 89.2).

The second result in respect to garnet-spinel stability is the confirmation of the existence of a P-T-X space where garnet and chromiferous spinel coexist. The width of this field is again dependent on the Cr/Cr+Al ratio of the bulk composition, becoming wider with increasing values of Cr/Cr+Al. A spinel-out boundary could only be located in the investigated system with the lowest Cr/Cr+Al ratio. In all other runs within the stability limit of garnet, spinel crystallized up to the highest pressures employed. This is consistent with the observation that some natural garnet lherzolites from kimberlite inclusions, usually depleted in basaltic components, show coexisting primary garnet and spinel (Nixon & Boyd, 1973a; Carswell *et al.*, 1979).

25. Cr-Al EXCHANGE

Reactions for an exchange of Cr and Al can be formulated for pyroxene-pyroxene, spinel-pyroxene and garnet-spinel pairs. Reactions between garnet and pyroxenes are discussed separately because of their potential for geobarometry.

25.1 Cr-Al EXCHANGE BETWEEN ORTHO- AND CLINOPYROXENE

Both ortho- and clinopyroxene dissolve Al and Cr. Discussion exists on the site occupancy of Cr in pyroxenes. Cr occurs in oxidation states ranging from 0 to +6, but under the fO_2 conditions of upper mantle and the experiments it is restricted to the +2 and +3 state. The +2 state may be neglected and is believed to occur only at very low fO_2 and high pressure-temperature conditions (Haggerty *et al.*, 1970; Haggerty, 1979). Cr as Cr^{+++} competes with Al^{+++} and is thus capable of replacing the latter in pyroxenes. Al occupies both octahedral and tetrahedral sites in pyroxenes, whereas Cr has a high octahedral site preference (Burns, 1970, 1975). Natural minerals contain Cr^{+++} almost exclusively in octahedral sites (Burns & Burns, 1975). Some experimental studies report tetrahedrally coordinated Cr in clinopyroxenes, but this is accompanied by a change in colour to give blue diopside (Dickey *et al.*, 1971; Ikeda & Yagi, 1977, 1978, 1982; Schreiber, 1977). No such blue diopsides have been observed in the present study and therefore Cr is regarded as restricted to the octahedral site. In the system SMACCR it occurs thus as a tschermak-type molecule in pyroxenes $(Ca,Mg)CrAlSiO_6$ [named Mg-Cr-tschermaks (MgCrTs) or Ca-Cr-tschermaks (CaCrTS)].

Solubilities of Al_2O_3 and Cr_2O_3 are different for ortho- and clinopyroxenes in simple systems. Perkins & Newton (1980) report that orthopyroxene contains more Al_2O_3 than coexisting clinopyroxene in the system CMAS and this is true for most of the data of Akella (1976) as well.

The new results in both CMAS and SMACCR confirm this trend for low to moderately high Al_2O_3 contents (fig. 22a) in pyroxenes, but data for pyroxenes with very high Al_2O_3 (i.e. in excess of approx. 7 wt.%) do not show this behaviour. Cr_2O_3 on the other hand is more concentrated in clinopyroxene (fig. 22b), a trend becoming more pronounced with increasing Cr_2O_3 and more obvious in garnet-bearing assemblages relative to garnet-free assemblages. The combined effect of lower Al- and higher Cr-solubility in clinopyroxene is a balancing of tetrahedral Al (fig. 23). Tetrahedral Al is nearly evenly distributed between ortho- and clinopyroxene with only a weak tendency to deviate at very low or very high Al contents.

The Cr-Al exchange between pyroxenes in the system SMACCR may be expressed by the reaction

$$\underset{\text{MgCrTs}}{\underset{\text{(opx)}}{MgCrAlSiO_6}} + \underset{\text{CaTs}}{\underset{\text{(cpx)}}{CaAlAlSiO_6}} = \underset{\text{CaCrTs}}{\underset{\text{(cpx)}}{CaCrAlSiO_6}} + \underset{\text{MgTs}}{\underset{\text{(opx)}}{MgAlAlSiO_6}} \qquad \text{(C)}$$

The K of this reaction is therefore

$$K(C) = \frac{a_{CaCrTs}\ a_{MgTs}}{a_{MgCrTs}\ a_{CaTs}} \qquad (15)$$

In the simplest form, adopting an ideal mixing model and assuming coupling of tetrahedral Al with octahedral Al and Cr, the activities may be expressed as

$$a_{CaCrTs} = X_{Cr}^{M1}\ X_{Ca}^{M2}\ \text{(cpx)} \qquad (16)$$

$$a_{MgCrTs} = X_{Cr}^{M1}\ X_{Mg}^{M2}\ \text{(opx)} \qquad (17)$$

$$a_{CaTs} = X_{Al}^{M1}\ X_{Ca}^{M2}\ \text{(cpx)} \qquad (18)$$

$$a_{MgTs} = X_{Al}^{M1}\ X_{Mg}^{M2}\ \text{(opx)} \qquad (19)$$

so that the K_D (C) is

$$K_D\ (C) = \frac{(X_{Cr}^{M1}X_{Ca}^{M2})^{cpx}\ (X_{Al}^{M1}X_{Mg}^{M2})^{opx}}{(X_{Cr}^{M1}X_{Mg}^{M2})^{opx}\ (X_{Al}^{M1}X_{Ca}^{M2})^{cpx}} \qquad (20a)$$

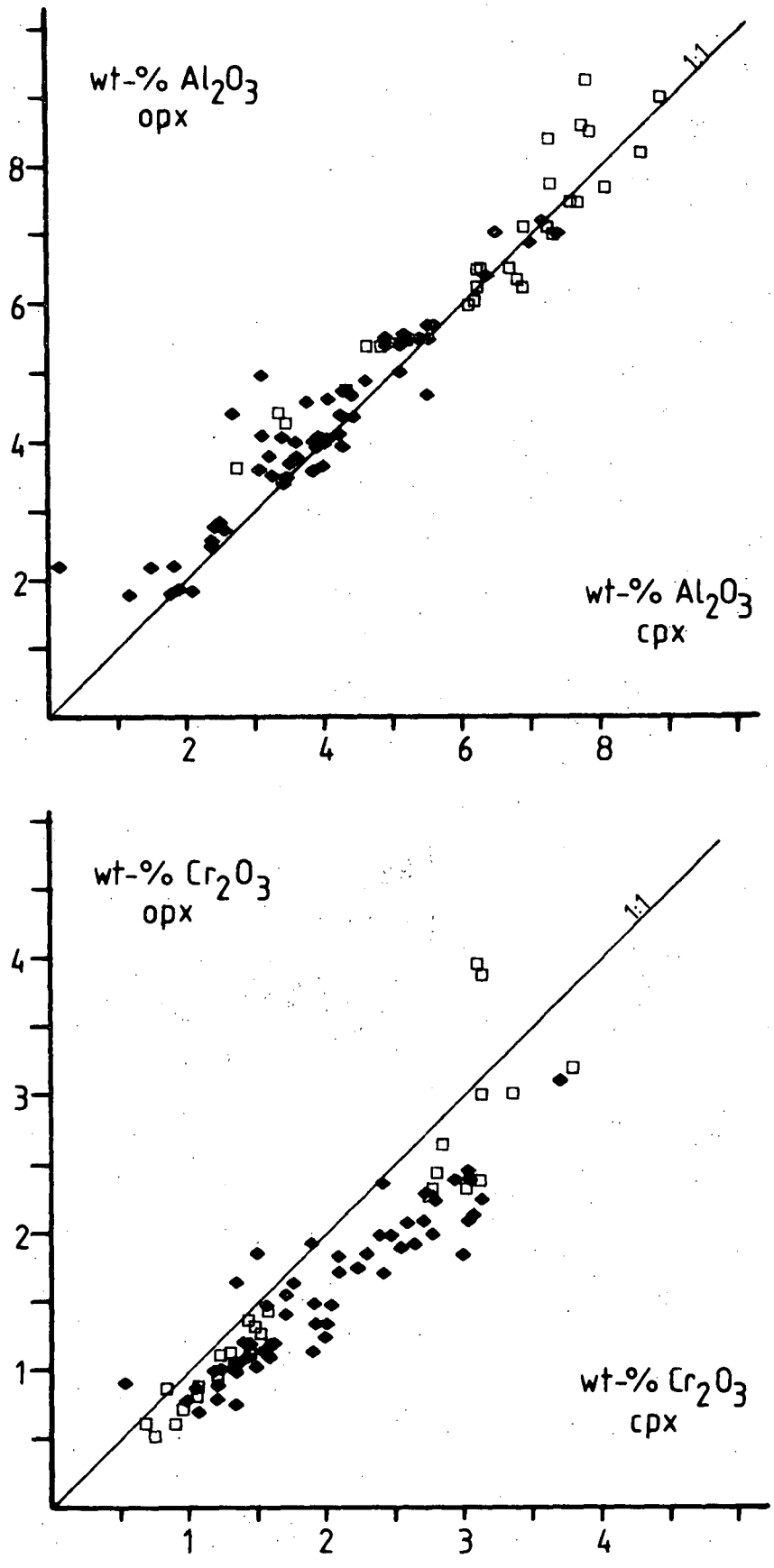

Figure 22: Comparison of solubilities of Al_2O_3 and Cr_2O_3 in ortho- and clinopyroxene (wt.%) from experiments in SMACCR. Open symbols = garnet-free assemblages, filled symbols = garnet-bearing assemblages.

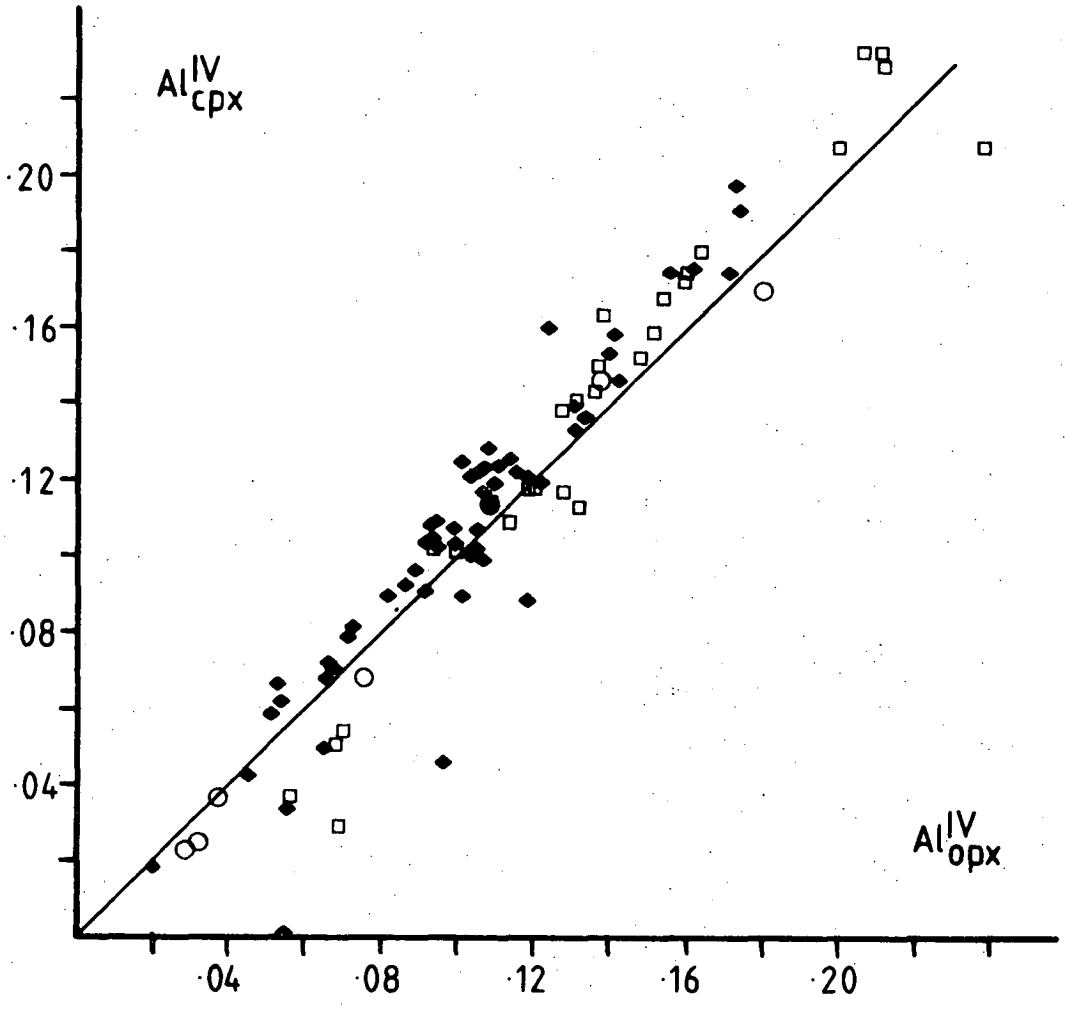

Figure 23: Relative distribution of tetrahedral Al in ortho- and clinopyroxene in experimental run products. Filled diamonds = garnet-bearing assemblages from SMACCR, open squares = garnet-free assemblages from SMACCR, open circles = from CMAS. Al^{IV} is calculated as (Al+Cr)/2.

X_{Mg} and X_{Ca} terms are identical in nominator and denominator and hence cancel each other. K_D (C) is therefore simplified to

$$K_D\ (C) = \frac{(X_{Cr}^{M1})^{cpx}\ (X_{Al}^{M1})^{opx}}{(X_{Cr}^{M1})^{opx}\ (X_{Al}^{M1})^{cpx}} \qquad (20b)$$

or, rewritten

$$K_D\ (C) = \frac{Al(M1)/Cr(M1)^{opx}}{Al(M1)/Cr(M1)^{cpx}} \qquad (20c)$$

As discussed before, Cr is placed entirely into the M1 position and hence $X_{Cr}^{opx} = (X_{Cr}^{M1})^{opx}$ and $X_{Cr}^{cpx} = (X_{Cr}^{M1})^{cpx}$. X_{Al}^{M1} for both pyroxenes is calculated as $(X_{Al}^{total}-X_{Cr})/2$ for reasons outlined in chapter 26. The M1 position is an octahedral position and hence the Al in M1 is in six-fold coordination. Equation (20c) can therefore be equally written as

$$K_D\ (C) = \frac{(Al^{VI}/Cr)^{opx}}{(Al^{VI}/Cr)^{cpx}} \qquad (20d)$$

This K_D has been used by Mysen (1976) to calibrate a geothermometer. A plot of this K_D (C) vs. 1/T is shown in fig. 24. The spread of values is high and the weak tendency of averages for $ln\ K_D$ (C) to increase with decreasing temperature is insignificant. The line given by Mysen (1976) for the variation of $ln\ K_D$ (C) with 1/T bears little resemblance to the data obtained. However, Mysen's (1976) experiments were performed in a natural system, containing Na. In Na-bearing systems Cr is contained in ureyite (= kosmochlor), $NaCrSi_2O_6$, the existence of which and its high solubility in diopside has been demonstrated experimentally by a number of workers (Ikeda & Ohashi, 1974; Ikeda & Yagi, 1972; Vredevoogd & Forbes, 1975; Yoder & Kullerud, 1971). In contrast to orthopyroxene, natural clinopyroxene usually contains sufficient Na to balance all of the Cr (usually more, which is then present as jadeite, acmite, etc.). No information is available on the distribution between ureyite and CaCrTs in

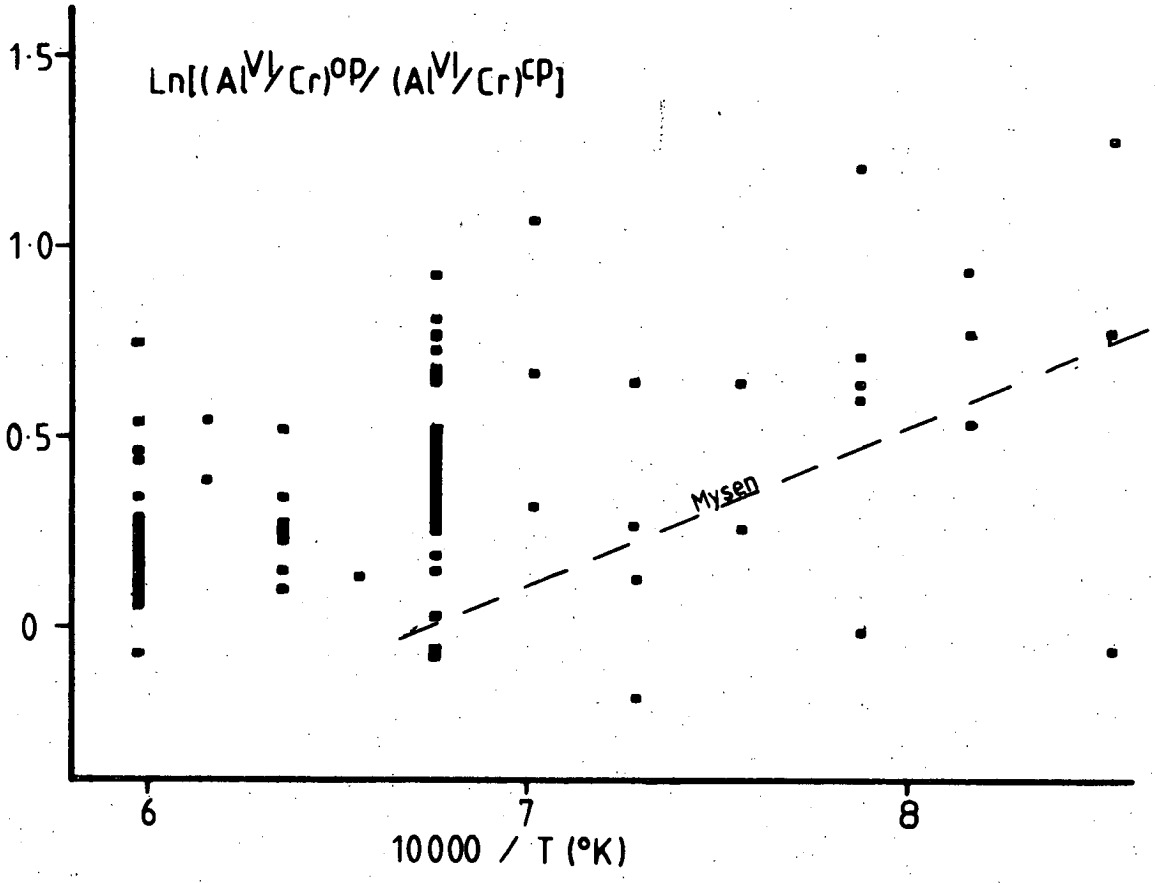

Figure 24: Plot of $ln[(Al^{VI}/Cr)^{opx}/(Al^{VI}/Cr)^{cpx}]$ for run products in SMACCR vs. 10000/T (K) compared to the calibration of Mysen (1976) based on experiments in a complex system.

diopside and it seems possible that most of the Cr in clinopyroxene exists in the form of a ureyite molecule. The problem of Na-Cr compounds in clinopyroxene was not discussed by Mysen (1976). The data obtained in SMACCR suggest that, if Mysen's (1976) experiments represent equilibrium conditions, the temperature dependence of the Cr-Al distribution between pyroxenes in his data is due to the Na contained in clinopyroxene. If this is so, the K_D (C) in the form used is not an adequate expression for the actual reaction.

Furthermore it seems likely that compositional parameters do have an influence on the Cr-Al exchange between pyroxenes. This is plausible from comparison of the rather regular behaviour of the Al-Al and Cr-Cr distribution between the pyroxenes (fig. 28a,b) with the $ln\ K_D$ (C) vs. 1/T plot (fig. 24). No attempt has been made to explore any compositional dependencies of the Cr-Al distribution between pyroxenes, because any application to natural rocks is unlikely to be relevant for several reasons: (i) the unknown NaCr-CrAl relations in clinopyroxene, (ii) the general low level of Cr_2O_3 in natural orthopyroxenes, which will require very exact data for both Al and Cr, and (iii) the low spread in Cr/Al-Cr/Al (opx vs. cpx) for natural rocks (cf. fig. 7 of this thesis).

The gross disagreement between temperatures obtained by Mysen's (1976) method and temperature estimation of natural rocks with those by other thermometers (Carswell & Gibb, 1980) suggests that even on a purely empirical basis Mysen's (1976) calibration is not correct and the experimental data are suspect.

Summarizing, the distribution of Cr-Al between pyroxenes does not have the potential for calibration as a useful geothermometer in the system SMACCR and casts strong doubts on the validity of geothermometers derived from experiments in natural systems.

25.2 Cr-Al EXCHANGE BETWEEN PYROXENES AND SPINEL

Spinels in the system SMACCR show differences in experiments with SSO and SOGP type starting material. Spinels starting off as the pure-Cr endmember picotite (SOGP mix) show a range of compositions from high-Cr to low-Cr values. Even though it could not be directly established, this is seen as evidence for a zonation of the spinels from high-Cr cores to low-Cr rims. The rims will approach equilibrium and this is shown in fig. 25 where the Cr minima are compared to the composition of the more homogeneous spinels obtained in runs with SSO starting material at the same P-T-X condition.

The Cr/Al ratios of spinels were calculated directly from values recorded in appendix 5. The uncertainties due to difficulties in spinel analyses have been discussed previously.

In a few runs picotite was nearly unreacted. The much better homogeneity of other phases in runs with SOGP starting material show spinel to be the most sluggishly reacting phase of the assemblage. Given the sluggishness of reactions involving spinel, it must be emphasized that the composition of spinels in SSO runs may not represent equilibrium values but an approach from a low-Cr side. In this case the equilibrium value would lie between spinels from SSO and SOGP experiments. The greater homogeneity (within the analytical uncertainties) for spinels from SSO material argues however for a closer approach to equilibrium of these spinels and it may be seen from fig. 25 that in quite a number of cases the approach from both sides is sufficiently close to ensure the achievement of near-equilibrium. The investigation of Cr-Al exchanges involving spinel has therefore been based on the values of spinels from SSO starting material.

Since reaction rates decrease with decreasing temperature and the spinel has been shown to react slowly even at high temperatures, there has

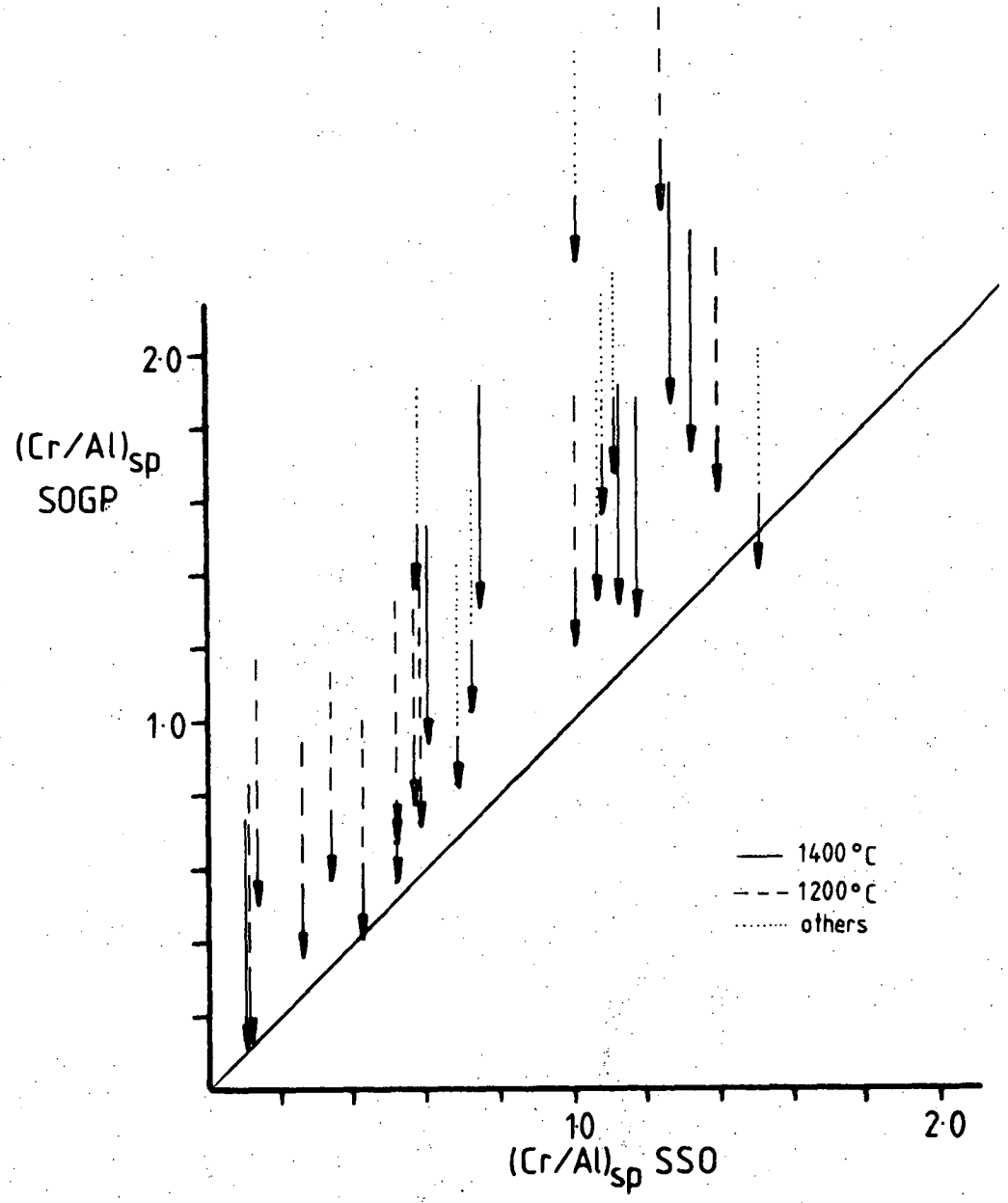

Figure 25: Cr/Al ratios of spinels from SMACCR experiments, comparing different starting materials. Arrows represent direction of approach of equilibrium value for SOGP starting material (pure picotite as one reactant) and point to the Cr/Al ratio of the spinel from SSO starting material, produced at identical P,T,X (bulk composition) conditions. Tip of arrow is the minimum value of Cr/Al analysed for the SOGP charge. Solid line is the 1:1 line (perfect agreement between runs).

been no attempt (with two exceptions) to establish equilibrium with an SOGP type starting material at temperatures below 1150°C. The values for spinels in these runs are to be examined with great caution and may not be equilibrium values because of the reaction rate problem. Any discussion of Cr-Al relationships involving spinel has therefore to be founded on experiments at temperatures in excess of approx. 1100°C.

It has been claimed (McGregor, 1982) that the exchange of Cr and Al between pyroxenes and spinel is sensitive to temperature and that thermometers can be based on this exchange. McGregor's (1982) experiments were performed in a natural system and the problems discussed before, particularly where clinopyroxene is involved, may invalidate such a calibration. Results in SMACCR show a very uniform temperature-independent correlation between (Cr/Al) of pyroxenes and spinel (fig. 26). Unspecific scatter in this correlation is introduced mainly by low-temperature experiments. The data presented in fig. 26 argue very strongly against the usefulness of the Cr-Al exchange between spinel and pyroxenes to serve as the basis of a geothermometer in SMACCR. Any attempt at calibration has therefore not been pursued.

25.3 Cr-Al EXCHANGE BETWEEN GARNET AND SPINEL

The discussion of the Cr-Al exchange between garnet and spinel in SMACCR has to bear in mind the analytical limitations of spinel and garnet (cf. chapter 21). Nevertheless it can be shown that systematic differences exist for Cr-Al exchange with temperature (fig. 27). As shown in fig. 27 the values for garnet-spinel pairs at temperatures below 1100°C are only slightly different from the 1200°C data. This may be interpreted as either an insensitivity of this exchange to temperatures below about 1200°C or as an expression for non-equilibrium data for spinel. From fig. 27 it is also apparent that regression lines for one temperature will not go through the origin of the plot. Rotating lines from the origin

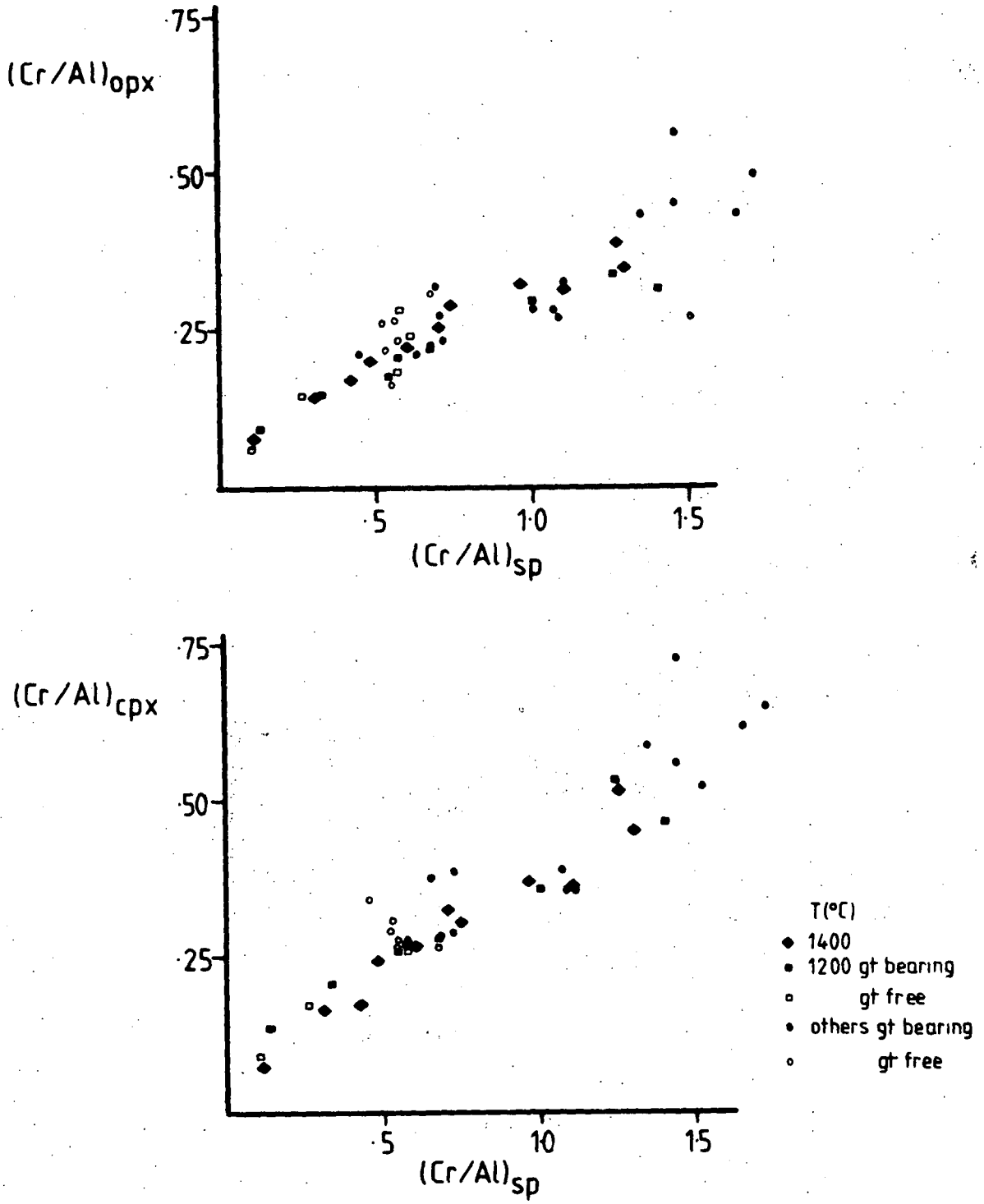

Figure 26: Plot of Cr/Al ratio of spinel vs. ortho- and clinopyroxene. Data points are those of runs with SSO-type starting material.

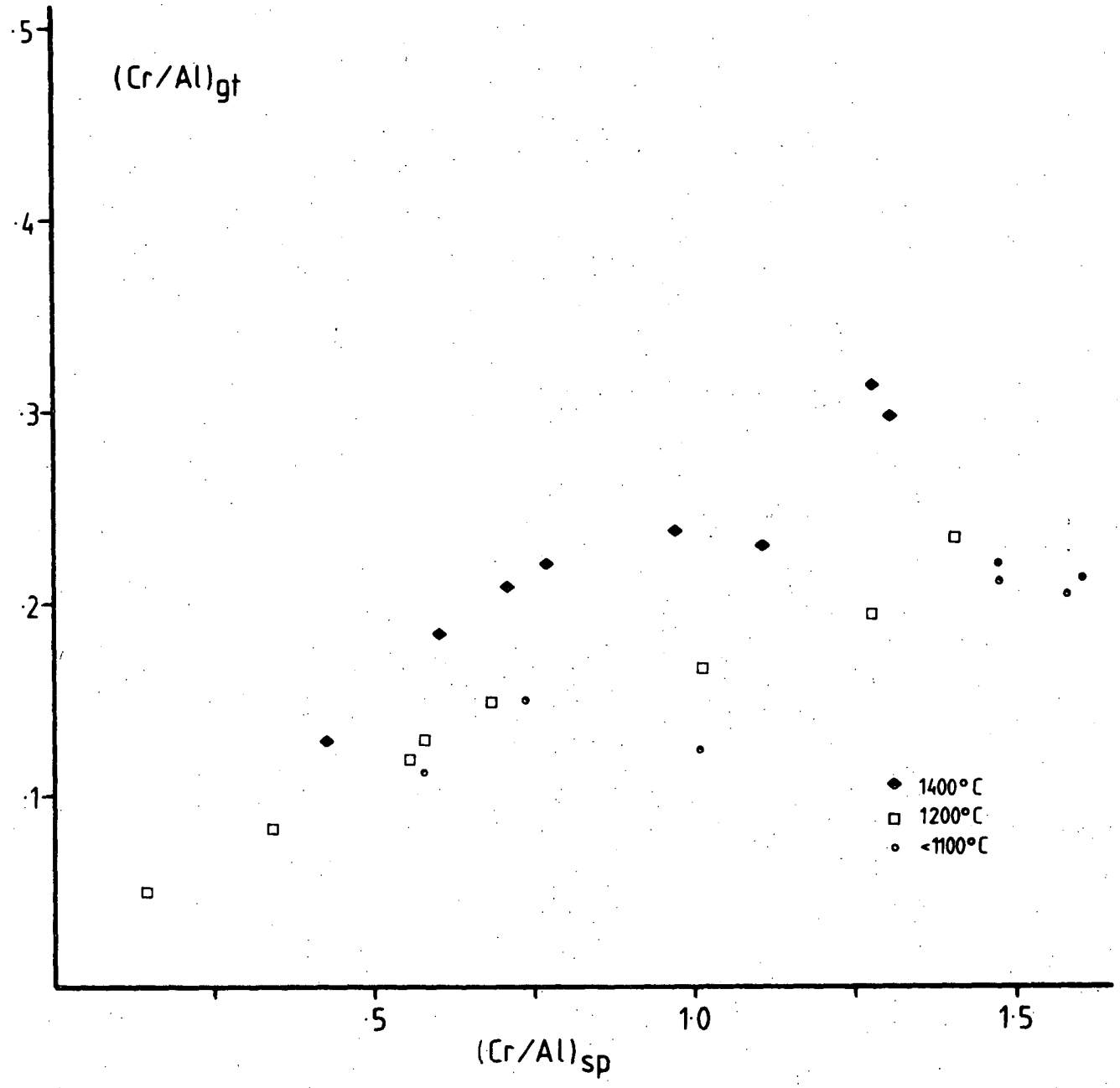

Figure 27: Cr/Al ratio of garnet vs. Cr/Al of coexisting spinel for varying temperature-composition conditions. Pairs of spinel and garnet are from SSO-type starting material.

(which are lines of equal K_D) will pass through variable values of K_D at one temperature. This is indicative for the influence of other parameters on this exchange.

The reaction for the exchange of Cr and Al between garnet and spinel in SMACCR is given by

$$\underset{\text{pyrope}}{Mg_3Al_2Si_3O_{12}} + \underset{\text{picotite}}{MgCr_2O_4} = \underset{\text{knorringite}}{Mg_3Cr_2Si_3O_{12}} + \underset{\text{spinel s.s.}}{MgAl_2O_4} \qquad (D)$$

A K for reaction (D) may thus be formulated as

$$K(D) = \frac{a_{sp}\, a_{Kn}}{a_{pi}\, a_{py}} \qquad (21)$$

The activities are defined by

$$a_{sp} = X_{Mg}^{sp}(X_{Al}^{sp})^2\gamma_{sp} \qquad (22)$$

$$a_{pi} = X_{Mg}^{sp}(X_{Cr}^{sp})^2\gamma_{pi} \qquad (23)$$

$$a_{py} = (X_{Mg}^{gt})^3(X_{Al}^{gt})^2\gamma_{py} \qquad (24)$$

$$a_{kn} = (X_{Mg}^{gt})^3(X_{Cr}^{gt})^2\gamma_{kn} \qquad (25)$$

where γ denotes activity coefficient. The K_D is thus

$$K_D(D) = \frac{[X_{Mg}(X_{Al})^2]^{sp}\,[(X_{Mg})^3(X_{Cr})^2]^{gt}}{[X_{Mg}(X_{Cr})^2]^{sp}\,[(X_{Mg})^3(X_{Al})^2]^{gt}} \qquad (26)$$

Both the X_{Mg}^{sp} and X_{Mg}^{gt} terms are identical in nominator and denominator and hence cancel each other. Therefore

$$K_D(D) = \frac{(X_{Al}^{sp})^2\,(X_{Cr}^{gt})^2}{(X_{Cr}^{sp})^2\,(X_{Al}^{gt})^2} \qquad (27)$$

being equivalent to

$$K_D(D) = \left(\frac{X_{Al}^{sp}\,X_{Cr}^{gt}}{X_{Cr}^{sp}\,X_{Al}^{gt}}\right)^2 \qquad (28)$$

Now non-idealities are discussed. Garnet is treated as a binary regular solution on both Mg-Ca and Cr-Al sites with reciprocal terms. The appropriate expressions are then

$$RT\ ln\ \gamma_{py} = 3(X_{Ca})^2 W_{CaMg} + 2(X_{Cr})^2 W_{CrAl} + X_{Ca}X_{Cr}dG_{rec} \quad (29)$$

$$RT\ ln\ \gamma_{kn} = 3(X_{Ca})^2 W_{CaMg} + 2(X_{Al})^2 W_{CrAl} + X_{Ca}X_{Al}dG_{rec} \quad (30)$$

where W = Margules or interaction parameter and dG_{rec} the change in free energy due to reciprocal relationships or relationships across sites. The size and temperature-dependence of the parameter dG_{rec} is derived and discussed in chapter 27.

Similarly spinel is modelled as a binary regular solution and thus the expressions for non-idealities are

$$RT\ ln\ \gamma_{sp} = 2(X_{Cr})^2 W_{CrAl} \quad (31)$$

$$RT\ ln\ \gamma_{pi} = 2(X_{Al})^2 W_{CrAl} \quad (32)$$

The full expression for the free energy change of the exchange reaction (D) is then

$$\begin{aligned} dG_{1,T} = -[&RT\ ln\ K_D + 3(X_{Ca}^{gt})^2 W_{CaMg} + 2(X_{Al}^{gt})^2 W_{CrAl} + X_{Ca}^{gt}X_{Al}^{gt}dG_{rec} \\ &- 3(X_{Ca}^{gt})^2 W_{CaMg} - 2(X_{Cr}^{gt})^2 W_{CrAl} - X_{Ca}^{gt}X_{Cr}^{gt}dG_{rec} \\ &+ 2(X_{Cr}^{sp})^2 W_{CrAl} - 2(X_{Al}^{sp})^2 W_{CrAl}] - PdV \end{aligned} \quad (33)$$

For exchange reactions it is generally true that little volume differences exists between products and reactants and hence only a very limited pressure-dependence is expected. Calculating a volume difference by taking the molar volume datum on pure knorringite of Irfune *et al.* (1982) (which is practically identical to the value for knorringite extrapolated by Ringwood (1977)) and the volume data of Robie *et al.* (1978) for the other endmembers a dV_r (i.e. $V^0_{kn}+V^0_{sp}-V^0_{py}-V^0_{pi}$) of 0.35 cm^3 is derived and used in further calculations. Under the assumption that W_{CrAl} is identical for garnet and spinel, equation (33) is reformulated to

$$dG_{1,T} = -\Big(RT\ ln\ K_D(D) + (X_{Ca}^{gt}X_{Al}^{gt} - X_{Ca}^{gt}X_{Cr}^{gt})\ dG_{rec} + 2[(X_{Al}^{gt})^2 + (X_{Cr}^{sp})^2 - (X_{Cr}^{gt})^2 - (X_{Al}^{sp})^2]W_{CrAl}\Big) - PdV \quad (34)$$

The value for W_{CrAl} can now be determined by plotting the compositional parameter

$$2[(X_{Al}^{gt})^2 + (X_{Cr}^{sp})^2 - (X_{Cr}^{gt})^2 - (X_{Al}^{sp})^2]$$

$$\text{vs. } -[RT\ ln\ K_D + (X_{Ca}^{gt}X_{Al} - X_{Ca}^{gt}X_{Cr}^{gt})]dG_{rec}] - PdV.$$

This is done in fig. 28. A regression yields a value of 3400 cal for W_{CrAl} and lines of this slope are shown in fig. 28. Even though uncertainties exist on the values for low temperatures, the value obtained for W_{CrAl} is quite well established by the experimental data.

The derived W_{CrAl} is substituted in equation (34) and the plot of $dG^0_{1,T}$ vs. 1/T is shown in fig. 29. An apparent disagreement exists between regressions for temperatures above and below 1100°C. Again it is impossible at this stage to decide whether a change in the behaviour of the Cr/Al exchange occurs at low temperatures or if the low temperature data are due to non-equilibrium data for spinel. However, regressions for low temperature runs on the basis of dG = dH - TdS + PdV would require unrealistically low values of dS (in the order of -15 e.u.). Regression of data at temperatures above 1100°C yields values of dH = -4673 cals and dS = -5.46 e.u.

Values derived for dH and dS of reaction (D) make it possible to give estimates of the as yet undetermined values of $H_{f,298}$ and S_{298} for knorringite. This can be done by solving the equations

$$H_{f,298}^{knorringite} + H_{f,298}^{spinel} - H_{f,298}^{pyrope} - H_{f,298}^{picotite} = dH\ (reaction\ D) = -4673\ cals \quad (35)$$

$$S_{298}^{knorringite} + S_{298}^{spinel} - S_{298}^{pyrope} - S_{298}^{picotite} = dS\ (reaction\ D) = -5.46\ e.u. \quad (36)$$

for the unknown quantities. Taking the values of dH (D) = -4673 cals

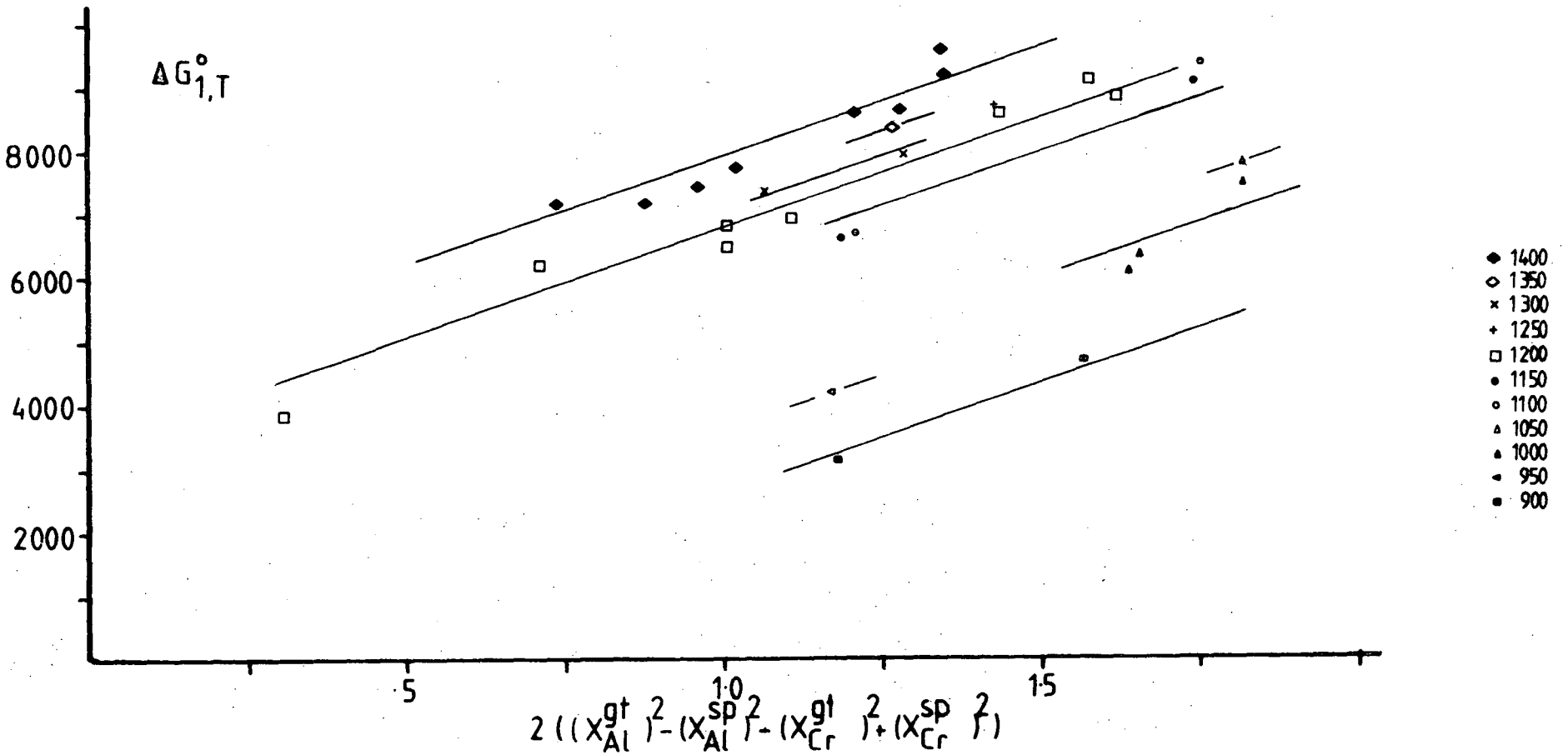

Figure 28: Plot of $dG_{1,T}$ of reaction (D) vs. the parameter $2[(X^{gt}_{Al})^2-(X^{sp}_{Al})^2+(X^{sp}_{Cr})^2 -(X^{gt}_{Cr})^2]$. $dG_{1,T}$ in this plot is defined as $- RT\ ln\ K_D(D) + (X^{gt}_{Ca}X^{gt}_{Al} - X^{gt}_{Ca}X^{gt}_{Cr})dG_{rec}(E)]-PdV_r$. Data points from runs with SSO-type starting material, temperatures of runs are in °C and indicated by symbols. Slope of the drawn lines comes from regression of high temperature data.

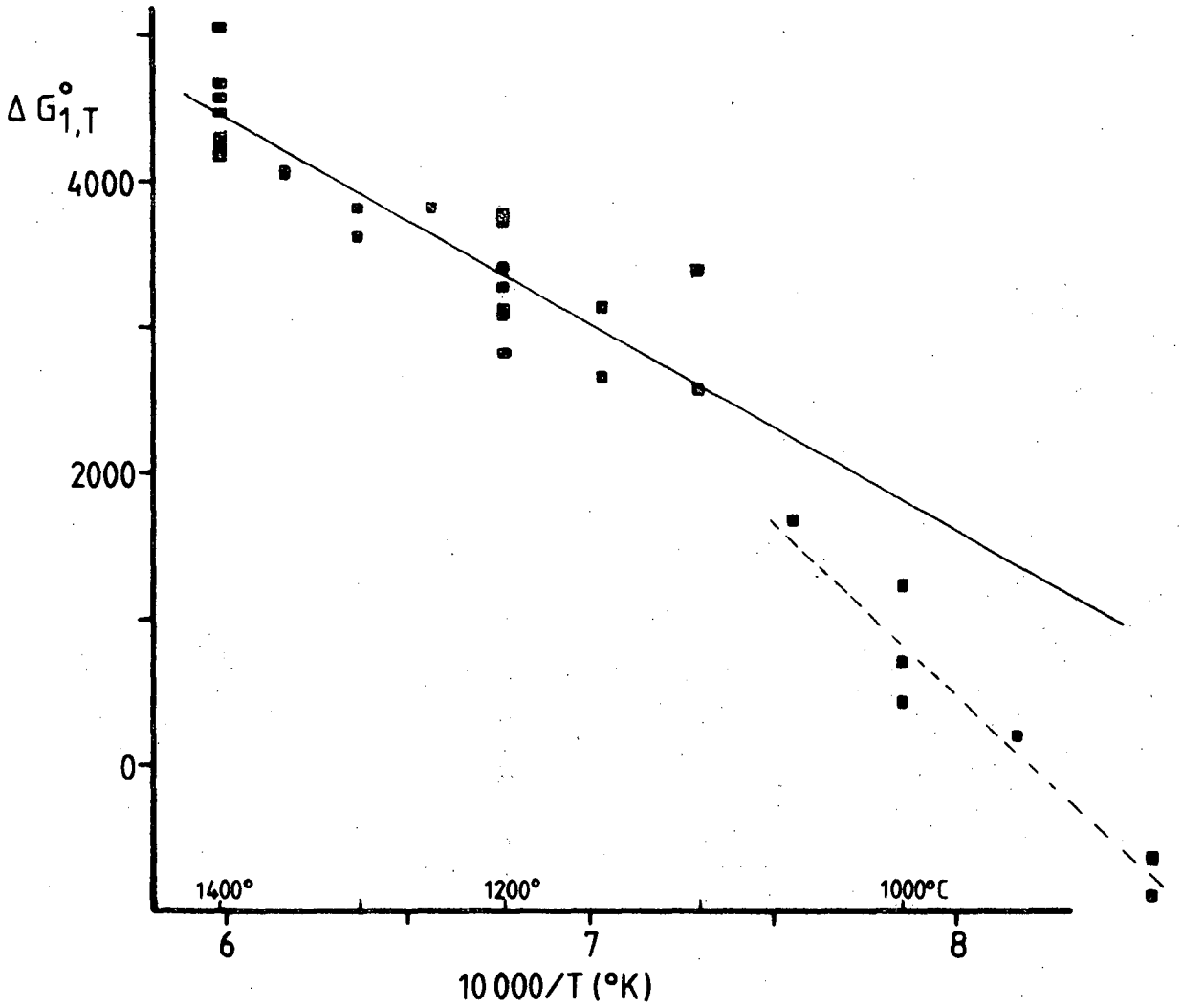

Figure 29: Plot of $dG_{1,T}(D)$ vs. 10000/T (K). $dG_{1,T}$ is defined by $-[RT\ ln\ K_D(D) + (X^{gt}_{Ca}X^{gt}_{Al} - X^{gt}_{Ca}X^{gt}_{Cr})dG_{rec}(E) + 2[(X^{gt}_{Al})^2+(X^{sp}_{Cr})^2 -(X^{gt}_{Cr})^2-(X^{sp}_{Al})^2]W_{CrAl}] - PdV_r$ (see text). Solid line is regressed from high temperature data, dashed line from low temperature data.

and dS (D) = -5.46 e.u., values of $H_{f,298}^{knorringite}$ = -5788.5 (kJ/mol) and $S_{298}^{knorringite}$ = 224.5 (J/mol K) are derived. The values of $H_{f,298}$ and S_{298} for pyrope, spinel and picotite were taken from Robie *et al.* (1978) and are listed in table 13.

Table 13: $H_{f,298}$ (kJ/mol) and S_{298} (J/mol K) values for garnets and spinels.

	$H_{f,298}$	S_{298}
spinel	-2299.3	80.63
picotite	-1783.6	106.02
pyrope	-6284.6	222.0
knorringite	-5788.5	224.5

From table 13 it is apparent that the derived values for knorringite relative to the measured values for pyrope are consistent with the differences for the respective Al and Cr endmembers of the spinel group. Spinel has the higher $H_{f,298}$ and the lower S_{298} relative to picotite. The estimates for the Cr-garnet are lower in $H_{f,298}$ and higher in S_{298} relative to the Al-garnet.

A rough estimate of the expected size of $H_{f,298}$ for garnets can also be obtained by the summation of the $H_{f,298}$ values of the oxides. Adding the appropriate oxides for pyrope (data from Robie *et al.*, 1978) a value of -6212 kJ/mol is obtained, which compares well with the measured value of -6284 kJ/mol. Adding the appropriate oxide values for knorringite yields -5671 kJ/mol compared to the estimate of -5788 kJ/mol. S_{298} values for phases and oxides are more than three orders of magnitude smaller in absolute numbers and hence a small absolute difference represents a large relative difference. Therefore a summation of S_{298} values for the oxides is less meaningful, unless appropriate corrections are made (Fyfe, Turner & Verhoogen, 1958), but point also to higher values for S_{298} for knorringite relative to pyrope.

Consideration of calorimetric measurements of thermodynamic quantities of oxides and minerals are therefore supportive of the dH and dS values derived for reaction (D).

Substituting dH-TdS for $dG_{1,T}$ equation (34) becomes

$$dH - TdS = -RT\ ln\ K_D - (X_{Ca}^{gt}X_{Al}^{gt} - X_{Ca}^{gt}X_{Cr}^{gt})dG_{rec} - 2W_{CrAl}\ [(X_{Al}^{gt})^2-(X_{Cr}^{gt})^2+(X_{Cr}^{sp})^2-(X_{Al}^{sp})^2] - PdV \quad (37)$$

The reciprocal term for the garnet is more fully expressed (derived in chapter 27) as

$$dG_{rec} = dH_{rec} - TdS_{rec} \quad (38)$$

where dH_{rec} and dS_{rec} denote the enthalpy and entropy change of the cross-site interaction. Thus equation (37) becomes

$$dH - TdS = -RT\ ln\ K_D - (X_{Ca}^{gt}X_{Al}^{gt} - X_{Ca}^{gt}X_{Cr}^{gt})(dH_{rec} - TdS_{rec}) - 2W_{CrAl}[(X_{Al}^{gt})^2-(X_{Cr}^{gt})^2+(X_{Cr}^{sp})^2-(X_{Al}^{sp})^2] - PdV \quad (39)$$

which is equivalent to

$$dH - TdS = -RT\ ln\ K_D - dH_{rec}(X_{Ca}^{gt}X_{Al}^{gt} - X_{Ca}^{gt}X_{Cr}^{gt}) + TdS_{rec}(X_{Ca}^{gt}X_{Al}^{gt} - X_{Ca}^{gt}X_{Cr}^{gt}) - 2W_{CrAl}[(X_{Al}^{gt})^2-(X_{Cr}^{gt})^2+(X_{Cr}^{sp})^2-(X_{Al}^{sp})^2] - PdV \quad (40)$$

Reformulation of this equation gives then the thermometric formulation

$$T = \frac{-dH_{rec}(X_{Ca}^{gt}X_{Al}^{gt}-X_{Ca}^{gt}X_{Cr}^{gt})-2W_{CrAl}[(X_{Al}^{gt})^2-(X_{Cr}^{gt})^2+(X_{Cr}^{sp})^2-(X_{Al}^{sp})^2]-dH-PdV}{R\ ln\ K_D - dS_{rec}(X_{Ca}^{gt}X_{Al}^{gt}-X_{Ca}^{gt}X_{Cr}^{gt})-dS} \quad (41)$$

Substituting the values for the parameters derived in this chapter (W_{CrAl} = 3400 cals, dH(D) = -4673 cals/mol, dS(D) = -5.46 e.u., dV_r = 8.37 cals/kb) and in chapter 27 (dH_{rec} = 90 853 cals/mol, dS_{rec} = -52.1 e.u.), equation 41 becomes

$$T(^{\circ}K) = \frac{-90853(X_{Ca}^{gt}X_{Al}^{gt}-X_{Ca}^{gt}X_{Cr}^{gt})-6800[(X_{Al}^{gt})^2-(X_{Cr}^{gt})^2+(X_{Cr}^{sp})^2-(X_{Al}^{sp})^2]+4673-8.37P}{R\ ln\ K_D - 52.1(X_{Ca}^{gt}X_{Al}^{gt}-X_{Ca}^{gt}X_{Cr}^{gt})+5.46} \quad (42)$$

Application of this equation (42) to the experimental data is shown in fig. 30. The data for experiments carried out at temperatures above 1100°C with the SSO-type starting material are reproduced within approx. ±70°C with a mean dT (i.e. $T_{expmt}-T_{est}$) of 42°C. A number of data obtained from runs with SOGP-type starting material comply with these limits, but others show large discrepancies according to the closeness of approach for spinel compositions for different starting materials.

Calculations of low-temperature runs (below 1100°C) yield large over-estimations with a calculated temperature being constant at about 1150°C. The possible reasons for this have been discussed previously.

Summarizing, the exchange of Cr and Al between garnet and spinel is sensitive to temperature at least above 1200°C. A thermometer has been calculated for these conditions in the system SMACCR based on SSO-type starting material. The uncertainties for both attempeted reversals and low-temperature runs have to be borne in mind when applying the expressions to natural rocks (chapter 35).

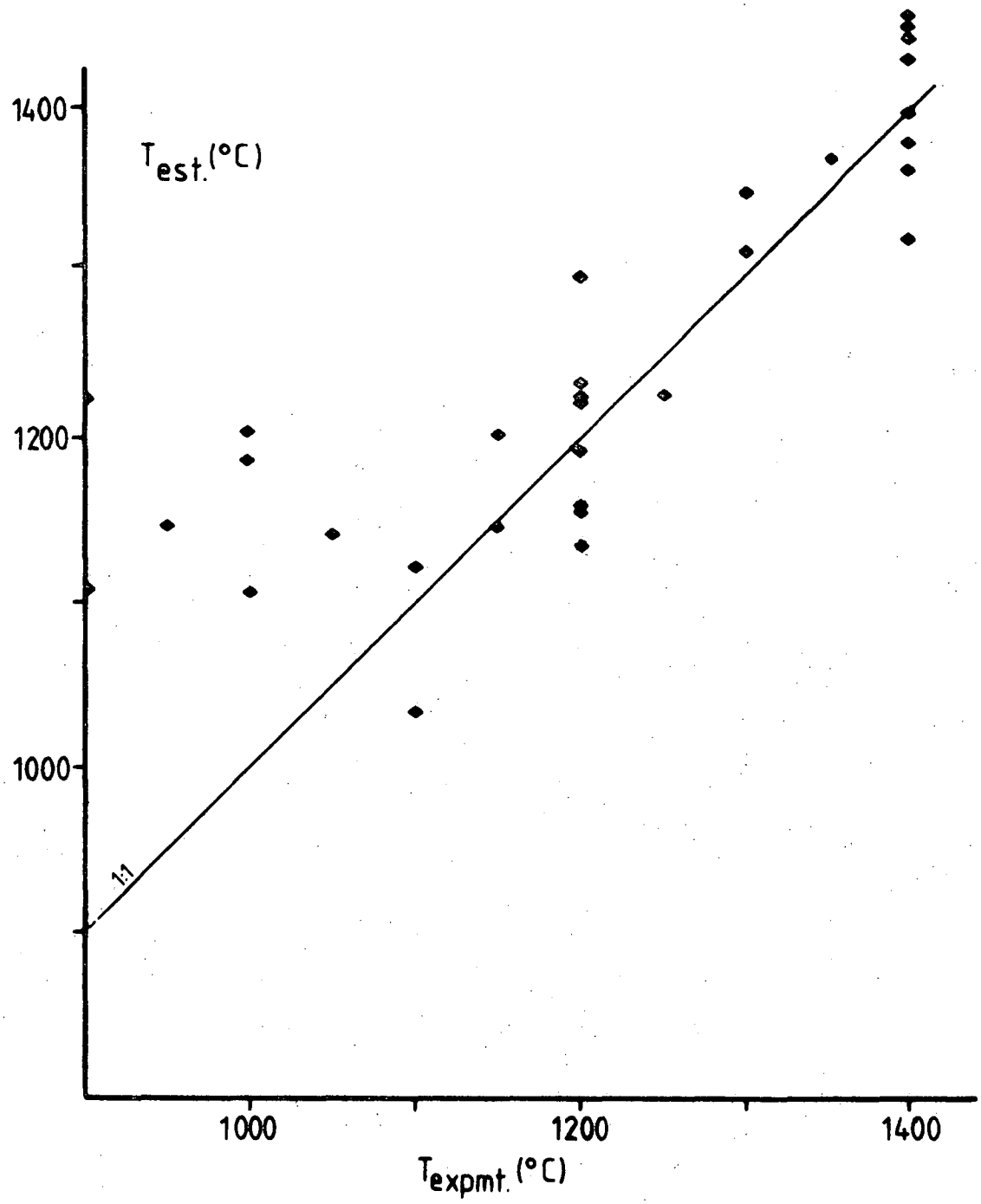

Figure 30: Comparison of temperature estimated via equation (42) and nominal run temperatures. Estimates shown are for SSO-type starting material.

26. SOLUBILITY OF Al_2O_3 AND Cr_2O_3 IN ORTHOPYROXENE COEXISTING WITH GARNET

As outlined before, the experimental strategy adopted here is based on the rapidity of pyroxene growth in experimental charges, but that it is not possible to reverse the compositions *sensu stricto*. The quality of data for the solubility of Al_2O_3 and Cr_2O_3 is evaluated in figs. 31 and 32. There is no preference for data obtained from SSO or SOGP starting material, the choice of taking the data from SSO runs as a reference is purely arbitrary. Fig. 31 illustrates two points: (i) both SSO and SOGP charges show good clustering around a mean value. The error bar has the length of two standard deviations for each individual run. The variance is often within the limits of the accuracy of probe analyses (approx. ± 0.25 wt.% Al_2O_3), and (ii) the values for the pairs (SSO and SOGP at identical P-T conditions and of identical composition) approach each other very closely.

If the assumption is correct that SSO material approaches equilibrium from high-Al_2O_3 contents and SOGP material from low-Al_2O_3 contents in orthopyroxene, then all possible cases of a "reversal" are present: incomplete closure, identical data points, or overstepping. This was expected in the light of possible, but not necessarily always given, "path-looping" (Lane & Ganguly, 1980; Perkins & Newton, 1980).

It is impossible to determine whether for an individual pair of runs an overlap is due to overstepping of equilibrium from both sides or only one. Equally impossible is the determination of a possible assymetry of the approach of the equilibrium where a gap exists. Both bracketing values have therefore been used in calculations instead of a "preferred" value within an overlap or between gaps.

The solubility of Cr_2O_3 (fig. 32) may be discussed in the same way. However, some standard deviations are relatively large, so that compositional zonation cannot be excluded in respect to Cr_2O_3 in a few runs. There is a

Figure 31: Comparison of Al_2O_3 contents in orthopyroxenes in SMACCR experiments between different starting material. The value for Al_2O_3 obtained in runs with SSO material is taken as reference and is shown as filled circles on a 1:1 line. The error bar has the length of two standard deviations. The values from SOGP-type starting material from runs at identical P,T,X conditions are as open symbols, the error bar points towards the corresponding SSO value. Two diagrams drawn for clarity.

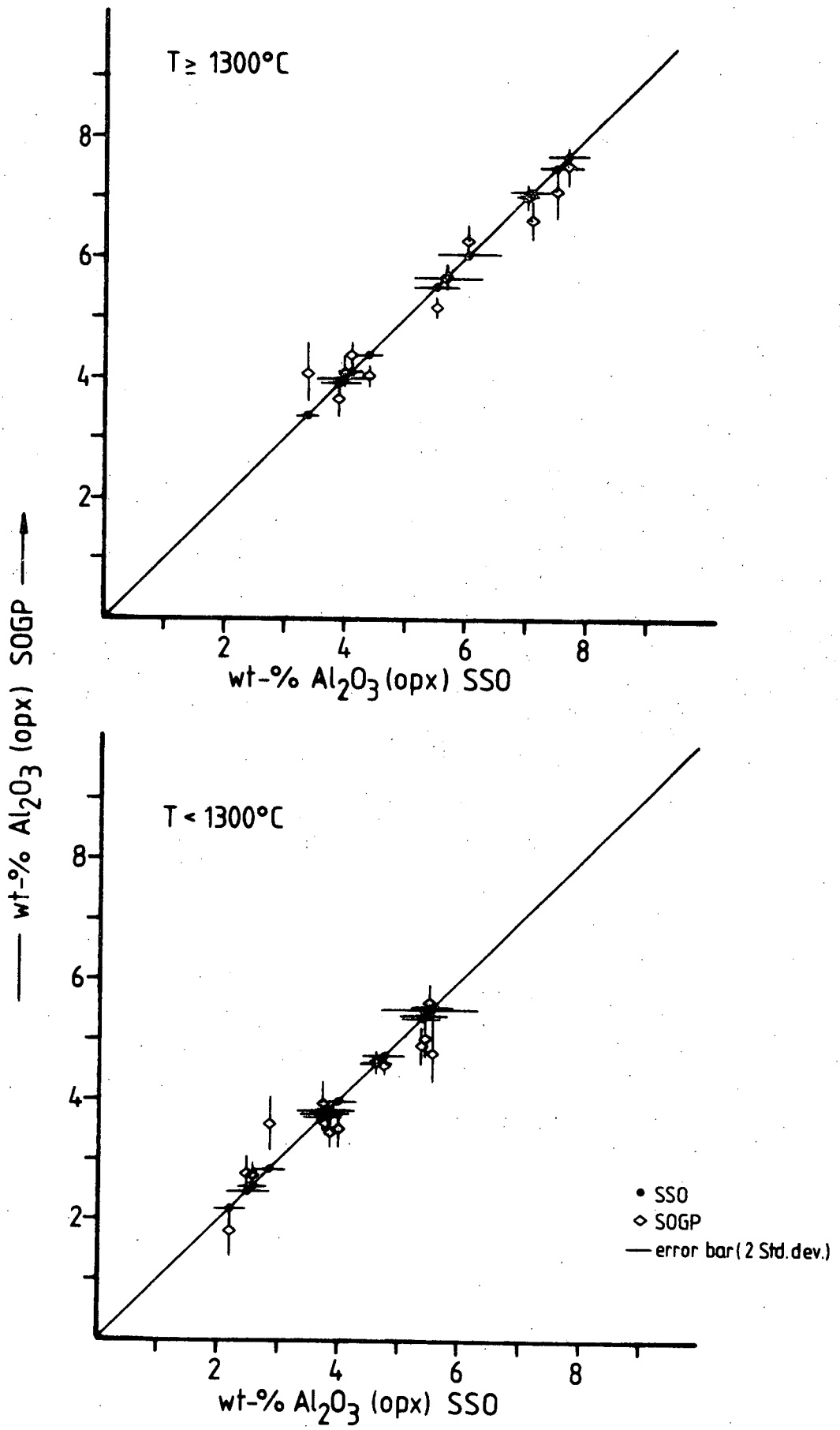
T ≥ 1300°C
T < 1300°C
wt-% Al2O3 (opx) SOGP
wt-% Al2O3 (opx) SSO
wt-% Al2O3 (opx) SSO
2
4
6
8
• SSO
◇ SOGP
— error bar (2 Std. dev.)

Figure 32: Comparison of Cr_2O_3 contents in orthopyroxene in SMACCR experiments between different starting materials. The technique of display is identical to fig. 31.

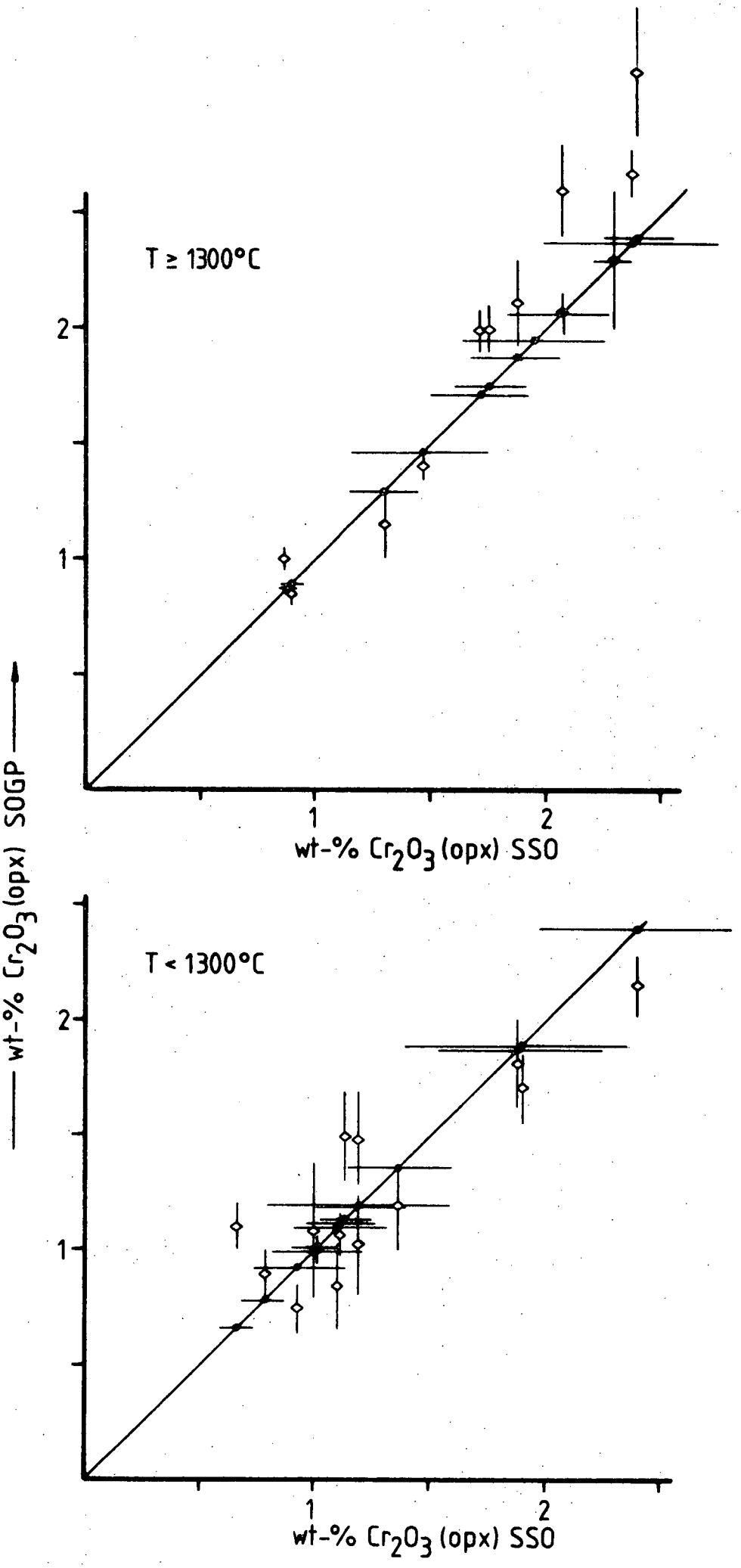
T ≥ 1300°C
T < 1300°C
wt-% Cr_2O_3 (opx) SOGP
wt-% Cr_2O_3 (opx) SSO
wt-% Cr_2O_3 (opx) SSO
1
2
1
2
1
2
1
2

tendency for high temperature runs with high Cr contents of orthopyroxene to give overlapping results, while this is not apparent for lower temperature runs. This is interpreted as due to the change of reaction rates with temperature.

In figs. 31 and 32 only pairs of runs are shown. A number of runs have been performed with only one starting material (mostly SSO) and are hence "unreversed". This is true especially for experiments at low temperatures, where crystalline starting material is likely to be too sluggish to reach or approach equilibrium closely. The closeness of approach of pairs of runs makes it likely that unreversed data are a good approximation of equilibrium values at least at higher temperatures. Therefore unreversed data are considered, but uncertainties, particularly at low temperatures, are likely to be higher.

Cr is interpreted as entering orthopyroxene in the form of a Mg-Cr-tschermaks molecule with the formula $MgCrAlSiO_6$ and Cr is placed completely into the M1 site (cf. section 25.1). This leads to the formulation of $X_{Al}^{M1} = (X_{Al}^{total} - X_{Cr})/2$ for the amount of Al present on the M1 site. It should be noted that this formulation yields identical results with $X_{Al}^{M1} = X_{Al}^{total} - (2-Si)$ only where the structural formula is exactly 4.000 (based on 6 oxygen). Most analyses show minor deviation of the sums of structural formulae from 4.000 and hence slightly different values for X_{Al}^{M1} may be calculated. A relatively small error in Si analyses will result in a relatively large error for Al^{IV} (calculated as 2-Si). Therefore values for Al in M1 of orthopyroxene have been calculated on the basis of the recorded Al and Cr values.

The amount of X_{Al}^{M1} in orthopyroxene present at any one P-T condition is strongly dependent on the amount of Cr present in coexisting garnet (fig. 33). This is expected if CrAl substitutes for AlAl in orthopyroxene and regular relationships between orthopyroxene and garnet exist. However, the data in fig. 33 suggest that the slopes of X_{Al}^{M1} vs. X_{Cr}^{gt} are not identical

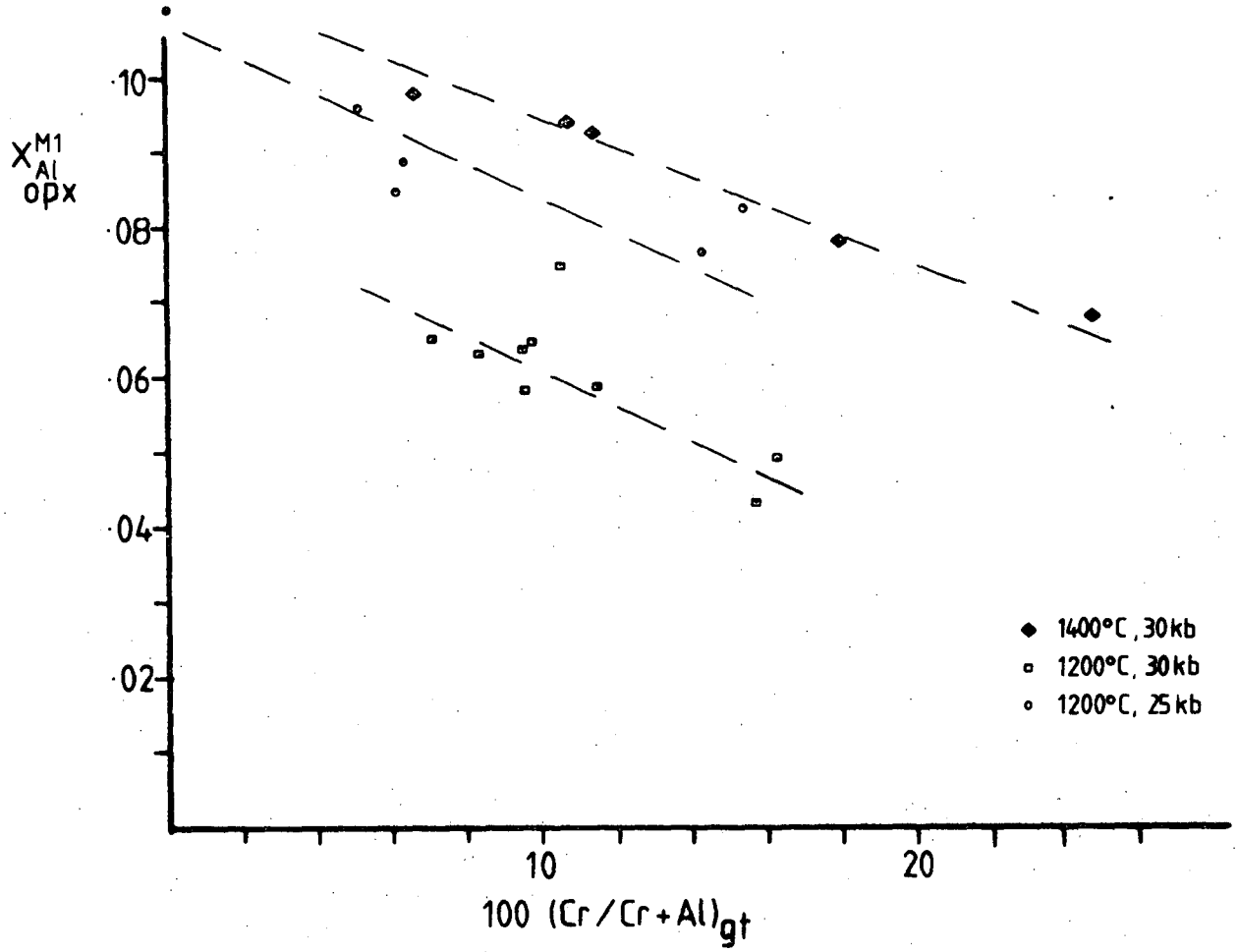

Figure 33: Dependence of X^{M1}_{Al} of orthopyroxene on the Cr/Cr+Al ratio (= X^{gt}_{Cr}) of garnet. X^{M1}_{Al} of orthopyroxene is in the system SMACCR equal to (Al-Cr)/2. Dashed lines are handfitted trendlines.

for different temperatures. Translated into a pressure-temperature space it is only possible to specify isopleths of X_{Al}^{M1} for a given coexisting garnet. A schematic picture of the influence of varying garnet compositions on Al isopleths is shown in fig. 34. Both in the system SMACCR and natural rocks substantial differences in garnet compostions are present. A grid of X_{Al}^{M1} isopleths cannot therefore be a good tool for the estimation of pressure-temperature conditions.

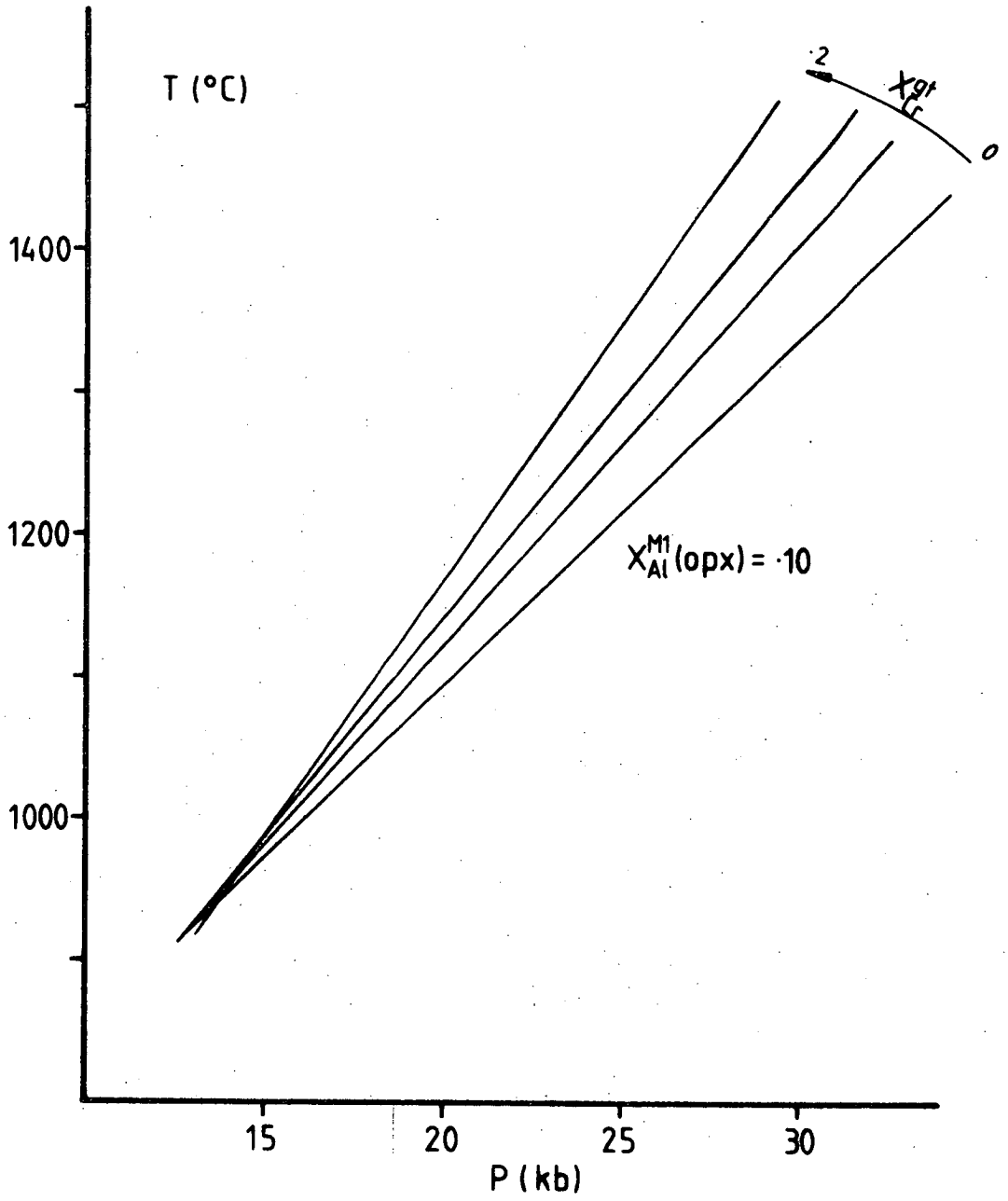

Figure 34: Influence of X_{Cr}^{gt} on X_{Al}^{M1} in orthopyroxene in P-T space. Shown as solid lines are schematic isopleths of X_{Al}^{M1} = 0.1 for varying Cr content of coexisting garnet. The picture is schematic because X_{Ca}^{gt} has to be specified for the correct location of X_{Al}^{M1} in SMACCR.

27. GEOBAROMETRY BASED ON THE SOLUBILITY OF Al_2O_3 IN ORTHOPYROXENE

As in the system CMAS, the reaction on which pressure estimations are based is

$$\underset{\text{enstatite}}{Mg_2Si_2O_6} + \underset{\text{Mg-tschmk}}{MgAl_2SiO_6} = \underset{\text{pyrope}}{Mg_3Al_2Si_3O_{12}} \qquad (B)$$

and accordingly the activities are expressed as

$$a^{opx}_{Mg_2Si_2O_6} = X^{M1}_{Mg} X^{M2}_{Mg} \gamma_{Mg_2Si_2O_6} \qquad (43)$$

$$a^{opx}_{MgAl_2SiO_6} = X^{M1}_{Al} X^{M2}_{Mg} \gamma_{MgAl_2SiO_6} \qquad (44)$$

$$a^{gt}_{Mg_3Al_2Si_3O_6} = (X^{gt}_{Mg})^3 (X^{gt}_{Al})^2 \gamma_{Mg_3Al_2Si_3O_{12}} \qquad (45)$$

Neglecting possible small quantities of Ca-tschermaks or Ca-Cr-tschermaks, orthopyroxene in the system SMACCR consists of the four endmembers enstatite, Mg-tschermaks molecule, Mg-Cr-tschermaks molecule and diopside. Ca terms in expressions for non-ideal behaviour of orthopyroxene have been neglected for reasons discussed in CMAS. Therefore the non-ideal contribution of diopside has not been included in the modelling and this reduces the mixing model to the M1 site, where Mg, Al and Cr mix. A model for a ternary regular solution has been adopted and so

$$RT\ ln\ \gamma_{en} = (X^{M1}_{Al})^2 W_{MgAl} + (X^{M1}_{Cr})^2 W_{CrAl} + X^{M1}_{Al} X^{M1}_{Cr} (W_{MgAl} + W_{MgCr} - W_{CrAl}) \qquad (46)$$

$$RT\ ln\ \gamma_{MgTs} = (X^{M1}_{Mg})^2 W_{MgAl} + (X^{M1}_{Cr})^2 W_{CrAl} + X^{M1}_{Mg} X^{M1}_{Cr} (W_{MgAl} + W_{CrAl} - W_{MgCr}) \qquad (47)$$

As for CMAS the interaction between Mg and Al is taken into account by the excess volume term of Harley & Green (1982). This approach is adopted for SMACCR also. It is assumed here that Cr-Mg interactions are also taken into account by use of this term. The activity expressions thus reduce to

$$RT\ ln\ \gamma_{en} = (X^{M1}_{Cr})^2 W_{CrAl} + X^{M1}_{Al} X^{M1}_{Cr} (-W_{CrAl}) \qquad (48)$$

$$RT\ ln\ \gamma_{MgTs} = (X^{M1}_{Cr})^2 W_{CrAl} + X^{M1}_{Mg} X^{M1}_{Cr}\ W_{CrAl} \qquad (49)$$

which on combination yield

$$RT\ ln\ \gamma_{en} + RT\ ln\ \gamma_{MgTs} = [2(X_{Cr}^{M1})^2 + X_{Mg}^{M1}X_{Cr}^{M1} - X_{Al}^{M1}X_{Cr}^{M1}]W_{CrAl} \quad (50)$$

Garnet consists of four endmembers: pyrope, grossular, knorringite and uvarovite. Non-ideal contributions to the changes in free energy for reaction (B) may be modelled as being a combined effect of two binary regular solutions and reciprocal or cross-site interactions.

The contribution of the on-site non-ideality of mixing is then

$$RT\ ln\ \gamma_{py}^{on\text{-}site} = 3(X_{Ca}^{gt})^2\ W_{CaMg} + 2(X_{Cr}^{gt})^2\ W_{CrAl} \quad (51)$$

Cross-site interactions come from the reaction of the endmembers

$$Mg_3Al_2Si_3O_{12} + Ca_3Cr_2Si_3O_{12} = Ca_3Al_2Si_3O_{12} + Mg_3Cr_2Si_3O_{12} \quad (E)$$

pyrope uvarovite grossular knorringite

Adopting the model of Wood & Nicholls (1978) the activity of pyrope in SMACCR becomes

$$RT\ ln\ a_{py} = RT\ ln\ [(X_{Mg}^{gt})^3 (X_{Al}^{gt})^2] + 3(X_{Ca}^{gt})^2 W_{CaMg} + 2(X_{Cr}^{gt})^2 W_{CrAl} + X_{Ca}^{gt}X_{Cr}^{gt}dG_{rec} \quad (52)$$

where dG_{rec} is the change in free energy for the exchange reaction (E). Combining these expressions for non-idealities with the formulation for reaction (B) we have

$$dG_{1,T}(B) = -\Big(RT\ ln\ K_D(B) + 3(X_{Ca}^{gt})^2 W_{CaMg} + [2(X_{Cr}^{gt})^2 - 2(X_{Cr}^{M1})^2 - X_{Mg}^{M1}X_{Cr}^{M1} + X_{Al}^{M1}X_{Cr}^{M1}]W_{CrAl} + X_{Ca}^{gt}X_{Cr}^{gt}dG_{rec}\Big) - PdV \quad (53)$$

An estimation of the size of $dG_{rec}(E)$ can now be made by plotting $RT\,ln\,K_D(B)$ + on-site terms + PdV vs. the parameter $X_{Ca}^{gt}X_{Cr}^{gt}$. This is shown in fig. 35. It is apparent from the change in slope of these lines with temperature that $dG_{rec}(E)$ is temperature-dependent. The sizes of the parameters dH(B), dS(B), W_{CaMg} and W_{CrAl} are known from CMAS and section 25.3 respectively. An error in the estimation of W_{CrAl} will have little influence on the calculation of dH_{rec} and dS_{rec} because the parameters associated with W_{CrAl} in equation (53) tend to cancel each other. The temperature-dependence of reaction (E) has been modelled by means of stepwise and multiple regression as $dG_{rec} = dH_{rec} - TdS_{rec}$. The experiments at low temperatures are unreversed and thus likely to include larger errors than the high temperature data. The regression was therefore based on the latter data.

The regression yields values of dH_{rec} = 90,853 cals/mol and dS = 52.1 e.u. and thus the size of dG_{rec} is 3690, 14110 and 24530 cals/mol at 1400°, 1200° and 1000°C respectively. Slopes of the appropriate value are drawn in fig. 35.

The values for dH_{rec} and dS_{rec} are very large and physically improbable. They have therefore to be discussed. Wood & Nicholls (1978) argued for the likelihood of a large $dG_{rec}(E)$ on the basis of the high pressures needed to synthesize pure knorringite. They estimated the size of dG_{rec} on the basis of the correlation between Ca and Cr in natural garnets from lherzolite inclusions in kimberlite and derived apparent values between 26000 and 18000 cals/mol (depending on the consideration of on-site terms). A second estimate by Wood & Nicholls (1978) of $dG_{rec}(E)$ was based on calorimetric measurements of garnets and stability ranges of pyrope and knorringite and yielded 12000 cals/mol. However, this estimate was based on the knorringite synthesis of Ringwood (1977). Ringwood's (1977) data have been disputed by Irfune *et al.* (1982), who showed that a much higher pressure is required to produce knorringite (at 1400°C:

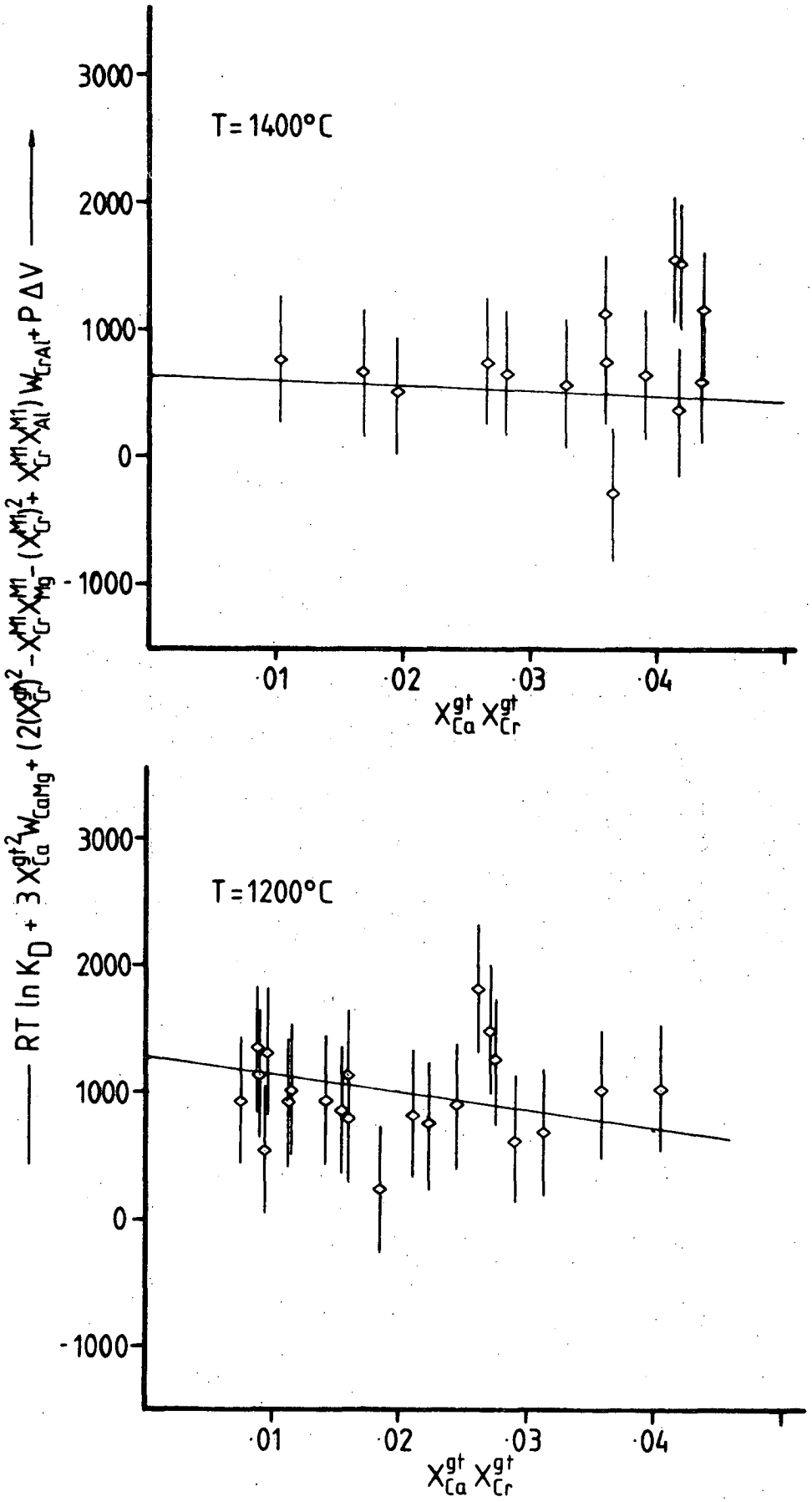

Figure 35: Plot of RT ln K_D(B) + on-site terms + PdV_r vs. the parameter $X_{Ca}^{gt} X_{Cr}^{gt}$ for experiments in SMACCR at 1400° and 1200°C. Solid lines are slopes from multiple regressions. Error bar is equal to an estimated error of ±500 cals/mol for the term on the y-axis.

Ringwood (1977) approx. 70 kb, Irfune *et al.* (1982) approx. 120 kb). Thus consideration of stabilities of garnet endmembers and calorimetric measurements is likely to yield very high values for $dG_{rec}(E)$ as well in the light of the new data (Irfune *et al.*, 1982).

The estimate of $dG_{rec}(E)$ of Wood & Nicholls (1978) based on the Ca-Cr correlation in garnets took into account mainly garnets from nodules, which show low equilibration temperatures [900-1100°C, based on Wells (1977) geothermometer]. Sobolev (1977) also noted the correlation between Ca and Cr in garnets from lherzolite inclusions in kimberlite. His data from the Udachnaya pipe indicate a different slope for this correlation (fig. 36). Most lherzolites studied by Sobolev (1977) equilibrated at higher temperatures [1100-1200°C, based on Wells (1977) geothermometer] than those of Wood & Nicholls (1978). The slope of the Ca-Cr correlation based on Sobolev's (1977) data is less steep than that of Wood & Nicholls (1978), indicating a smaller size of $dG_{rec}(E)$. Natural rocks thus show evidence for a temperature dependence of an apparent $dG_{rec}(E)$. The data in SMACCR are consistent with this observation and different slopes of the Ca-Cr correlation in garnet are obtained for different temperatures, becoming less steep at higher temperatures (fig. 36). In particular, the 1000°C and 1200°C slopes are very similar to the slopes of Wood & Nicholls (1978) and Sobolev (1977) respectively (fig. 36). Thus the observations on natural rocks are consistent with the data obtained in the SMACCR system and provide evidence for both the correct size and temperature dependence of the $dG_{rec}(E)$ derived in this study.

Nonetheless, the derived values for $dH_{rec}(E)$ and $dS_{rec}(E)$ seem physically improbable. Wood & Nicholls (1978) showed that a large size of $dG_{rec}(E)$ argues for the presence of substantial short-range order in garnet. At this stage it cannot be distinguished between a "true" temperature dependence of $dG_{rec}(E)$ and the influence of increasing short-range order with decreasing temperature. The modelled values of dG_{rec}, dH_{rec} and

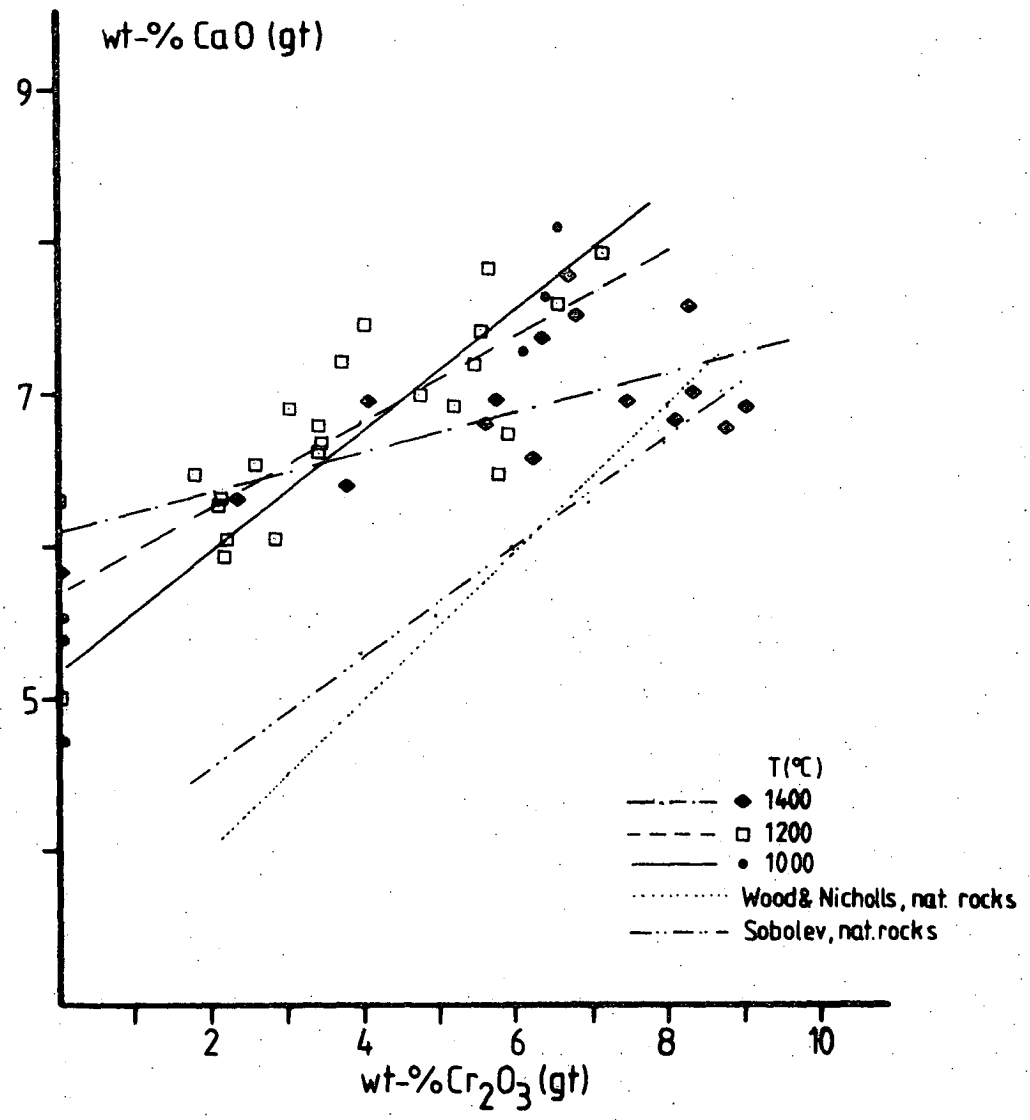

Figure 36: Comparison of Ca-Cr correlations in garnets from experimental runs and natural rocks. Slopes for garnets from natural garnet lherzolites are from Sobolev (1977) and Wood & Nicholls (1978). Data points and (regressed) trends are for experiments in SMACCR and CMAS. Correlation coefficient r is 0.63, 0.79 and 0.97 for the experimental data at 1400, 1200 and 1000°C respectively.

dS_{rec} are therefore regarded as apparent values and thus should not be confused with straightforward thermodynamic data, which may be derived by calorimetric measurements. The model presented is thus semi-empirical.

Substuting now dH-TdS for $dG_{1,T}$ of reactions (B) and (E), equation (53) becomes

$$dH(B)-TdS(B) = -\Big(RT\ ln\ K_D + 3(X_{Ca}^{gt})^2 W_{CaMg} + [2(X_{Cr}^{gt})^2 - 2(X_{Cr}^{M1})^2 - X_{Mg}^{M1}X_{Cr}^{M1} + X_{Al}^{M1}X_{Cr}^{M1}]W_{CrAl} + X_{Ca}^{gt}X_{Cr}^{gt}(dH_{rec}-TdS_{rec})\Big) - PdV_r \quad (54)$$

which is reformulated to give a solution for P:

$$P = \frac{1}{dV_r}\Big(-RT\ ln\ K_D - 3(X_{Ca}^{gt})^2 W_{CaMg} - [2(X_{Cr}^{gt})^2 - 2(X_{Cr}^{M1})^2 - X_{Mg}^{M1}X_{Cr}^{M1} + X_{Al}^{M1}X_{Cr}^{M1}]W_{CrAl} - X_{Ca}^{gt}X_{Cr}^{gt}(dH_{rec}-TdS_{rec})\Big) - dH(B) + TdS(B) \quad (55)$$

The values for parameters derived in this study (W_{CrAl} = 3400 cals, dH_{rec} = 90853 cals/mol, dS_{rec} = 52.1 e.u., dH(B) = -6047 cals/mol, dS(B) = -3.23 e.u.) and those adopted from the literature [W_{CaMg} = 3000 cal, Wood & Nicholls (1978), $dV_r = -(183.3 + 178.98\ X_{Al}^{M1}(1-X_{Al}^{M1}))$, Harley & Green (1982)] are substituted into equation (55) and thus the barometer for the SMACCR system is given by -

$$P(kb) = \frac{1}{dV_r}\left(-RT\ ln\left(\frac{(X_{Mg}^{gt})^3 (X_{Al}^{gt})^2}{X_{Mg}^{M1}(X_{Mg}^{M2})^2 X_{Al}^{M1}}\right) - 9000(X_{Ca}^{gt})^2 - 3400[2(X_{Cr}^{gt})^2 - 2(X_{Cr}^{M1})^2 - X_{Mg}^{M1}X_{Cr}^{M1} + X_{Al}^{M1}X_{Cr}^{M1}] - X_{Ca}^{gt}X_{Cr}^{gt}(90853 - 52.1T) + 6047 - 3.23T\right) \quad (56)$$

Application of equation (56) to the experimental data is shown in fig. 37. Due to the complexity of formulations and the limitations for the analysis of garnets the accuracy is not expected to be better than about ±3-4 kb. In fig. 37 such a limit of ±3.5 kb is shown and most data fall within this limit and almost all would fall within a 4 kb limit. Some runs show larger deviations. These are three runs at 900°C and 1000°C and three results at 1400°C. The discrepancies for the low temperature runs may be explained by the fact that besides the problem of slow reaction rates a small analytical error will result in comparatively large under- or over-estimations, because of the low levels of Al and Cr in orthopyroxene. The run at 1400°C and 45 kb may not have reached the nominal run pressure. 45 kb is close to the pressure limit of the apparatus and the pressure vessel used in this experiment was found to have a cracked and partly extruded core on completion of this run. The deviation of two runs at 32.5 and 35 kb is not well understood, but in the 32.5 kb run no clinopyroxene was found and the coexisting clinopyroxene of the 35 kb run shows a higher content of Al_2O_3 than orthopyroxene. Since for these levels of Al_2O_3 the clinopyroxene usually has the lower content, it is concluded that the run failed to approach equilibrium closely. If these runs are excluded, the mean deviation of the calculated pressure from the nominal run pressure is 1.67 kb.

There are no published data of other workers in SMACCR, so that the derived formula cannot be applied to results of an independent laboratory. However, differences in estimations of pressure can be shown by calculating pressures by the methods of published barometers based on the solubility of Al_2O_3 in orthopyroxene. Harley (1981) and Harley & Green (1982) neglect Cr in both orthopyroxene and garnet, so that the "X_{Al}^{M1}" used is equal to $X_{Al}^{total}/2$. This is an incorrect formulation in the light of crystallographic studies (Burns, 1970, 1975) and approaches reality only for very low Cr contents. Accordingly Harley (1981) recommends the

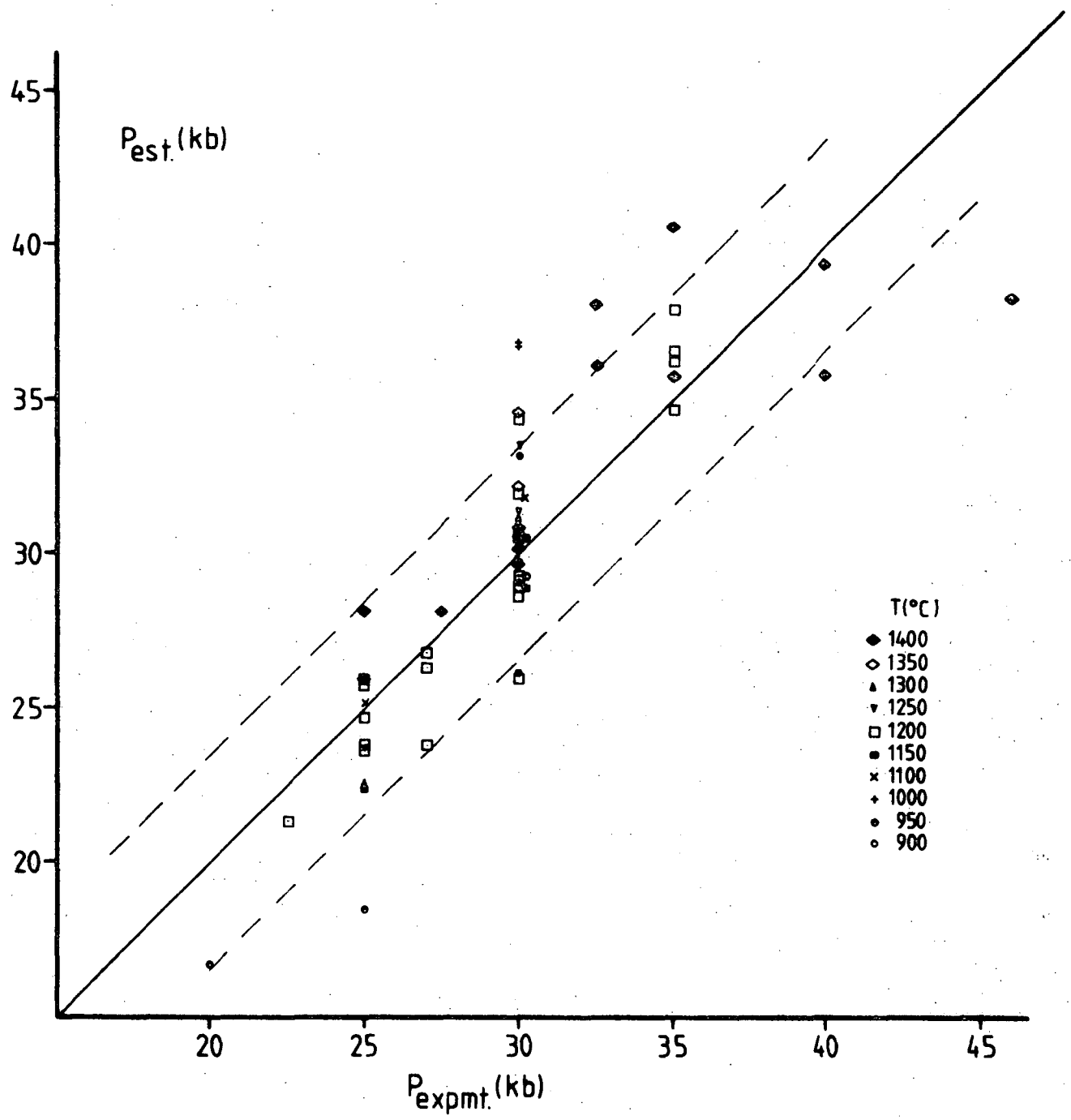

Figure 37: Comparison of pressures estimates via equation (56) and nominal run pressures for data in SMACCR. Dashed lines enclose a ±3.5 kb interval.

use of his formulation only for assemblages, where garnet has a content of less than 2 wt.% Cr_2O_3. None of the experimental data (and very few of the available data for natural garnet lherzolites) comply with that condition, so that the barometer should strictly not be applied to experiments and garnet lherzolites from inclusions in kimberlites. The diagram in fig. 38 is only drawn to show the effect of total neglect of Cr, even where present in large amounts. Systematic and partly very large underestimations result in applying Harley & Green's (1982) equation.

Wood (1974) recognized the necessity of incorporation of an $(X_{Al}^{gt})^2$ term in the $K_D(B)$, where a substantial amount of Cr is present. Wood & Banno (1973) placed Cr also entirely into the M1 site. However no correction for non-idealities due to Cr and reciprocal interactions were made. The result is shown in fig. 38b. Again a systematic and partly large under-estimation of pressures is given. This is seen as evidence for the necessity to consider the demonstrated effects of Cr in barometric formulations.

It may be noted that a "mixed" approach utilizing Harley & Green's (1982) or Wood's (1974) equations reproduces the experimental pressures better: If X_{Al}^{M1} is calculated as in the present study and hence Cr is taken into account for orthopyroxene, but Cr is neglected in garnet [no $(X_{Al}^{gt})^2$ term in the $K_D(B)$], a better agreement with nominal run pressures is obtained. The changes thereby introduced in the size of the $K_D(B)$ tend to cancel against the interaction terms. Approaches of this type are, even though they give better results, principally incorrect formulations. The equation derived in this study is thus seen as a step further towards modelling physical realities although it remains semi-empirical.

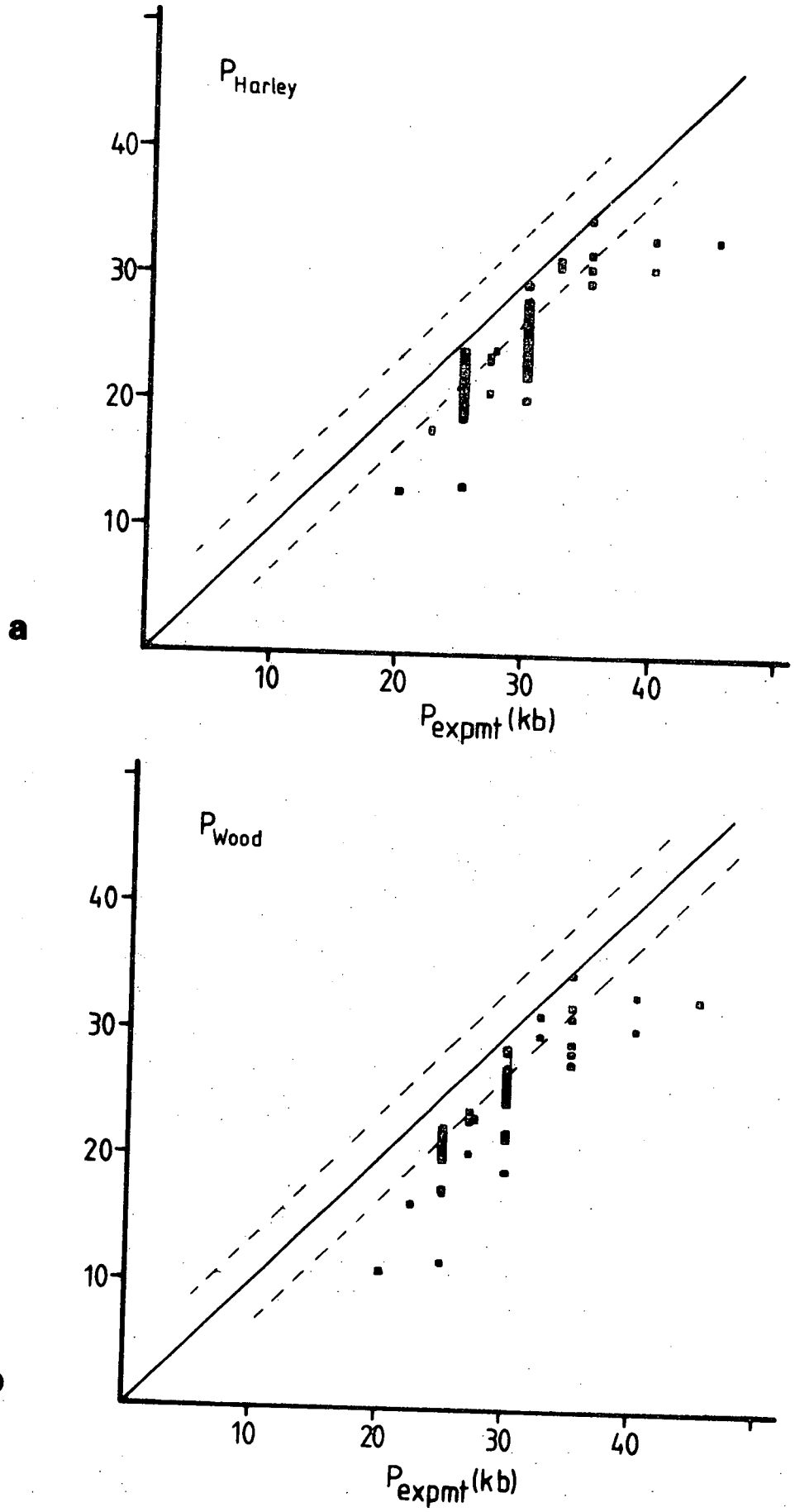

Figure 38: Pressure estimates for SMACCR data applying the barometers of Wood (1974, eq. 12) and Harley (1981) (the latter is identical to Harley & Green, 1982). Dashed lines are ±3.5 kb from nominal run pressures.

28. GEOBAROMETRY BASED ON THE SOLUBILITY OF Cr_2O_3 IN ORTHOPYROXENE

The discrimination of Cr^{+++} against tetrahedral site occupancy (cf. section 25.1) necessitates a more complex formulation of a reaction relating garnet and orthopyroxene relative to the reaction of the previous chapter. The reaction is

$$2Mg_2Si_2O_6 + 2MgCrAlSiO_6 = Mg_3Al_2Si_3O_{12} + Mg_3Cr_2Si_3O_{12} \qquad (F)$$

enstatite Mg-Cr-tsch. pyrope knorringite

and the activities of the phases are expressed as

$$a_{Mg_2Si_2O_6} = X_{Mg}^{M1} X_{Mg}^{M2} \gamma_{Mg_2Si_2O_6} \qquad (57)$$

$$a_{MgCrAlSiO_6} = X_{Cr}^{M1} X_{Mg}^{M2} \gamma_{MgCrAlSiO_6} \qquad (58)$$

$$a_{Mg_3Al_2Si_3O_{12}} = (X_{Mg}^{gt})^3 (X_{Al}^{gt})^2 \gamma_{Mg_3Al_2Si_3O_{12}} \qquad (59)$$

$$a_{Mg_3Cr_2Si_3O_{12}} = (X_{Mg}^{gt})^3 (X_{Cr}^{gt})^2 \gamma_{Mg_3Cr_2Si_3O_{12}} \qquad (60)$$

The K of reaction (F) has therefore the form

$$K(F) = \frac{a_{pyrope}\, a_{knorringite}}{(a_{enst.})^2 (a_{MgCrTs})^2} \qquad (61)$$

and the K is therefore

$$K(F) = \frac{(X_{Mg}^{gt})^3 (X_{Al}^{gt})^2 \gamma_{py} (X_{Mg}^{gt})^3 (X_{Cr}^{gt})^2 \gamma_{kn}}{(X_{Mg}^{M1})^2 (X_{Mg}^{M2})^2 (\gamma_{en})^2 (X_{Cr}^{M1})^2 (X_{Mg}^{M2})^2 (\gamma_{MgCrTs})^2} \qquad (62)$$

which becomes for the case of ideal mixing

$$K(F) = K_D(F) = \left(\frac{(X_{Mg}^{gt})^3 (X_{Al}^{gt}) (X_{Cr}^{gt})}{X_{Mg}^{M1} (X_{Mg}^{M2})^2 X_{Cr}^{M1}} \right)^2 \qquad (63)$$

A plot of $ln\ K_D(F)$ vs. pressure is shown in fig. 39. Three features are apparent:

a) $K_D(F)$ is sensitive to pressure,

b) the spread is partly due to differences in temperature but also due to differences in bulk composition, and

c) the runs at 1400°C and 40 and 45 kb are inconsistent with the others.

The good sensitivity to pressure shows the potential of the reaction for geobarometry. Differing bulk compositions cause different solubility limits of Cr_2O_3 in both orthopyroxene and garnet. Therefore it is not possible to use X_{Cr} isopleths as pressure indicators, because the composition of the coexisting garnet would have to be specified. The positive correlation of X_{Cr}^{gt} with X_{Cr}^{opx} has a limited tendency to cancel in the $K_D(F)$ (because a decrease in X_{Cr}^{gt} will make $K_D(F)$ smaller while a simultaneous decrease in X_{Cr}^{opx} will make it larger). The mixing is non-ideal and appropriate terms have to be used in barometric expressions.

The inconsistency of the runs at 45 kb was discussed in the previous section and doubts of this run as not having reached nominal pressure conditions are reinforced. The inconsistency of the 40 kb experiments are however not well understood. The orthopyroxene analyses may have been contaminated by spinel inclusions, which would account for too high values for both Al and Cr (and indeed a lower value in Al would be more consistent with the Al barometer), but the structural formula shows no evidence for this. The problem thus remains and has to be kept in mind when applying the barometer to pressures greater than 35 kb.

The non-idealities in the mixing behaviour of the phases is modelled following the methods employed in the previous chapters. Thus orthopyroxene is modelled to be a ternary regular solution between Mg, Al and Cr on the M1 site neglecting the non-ideal Ca contribution. Garnets are regarded as two binary regular solutions plus reciprocal interaction. Therefore the expressions become

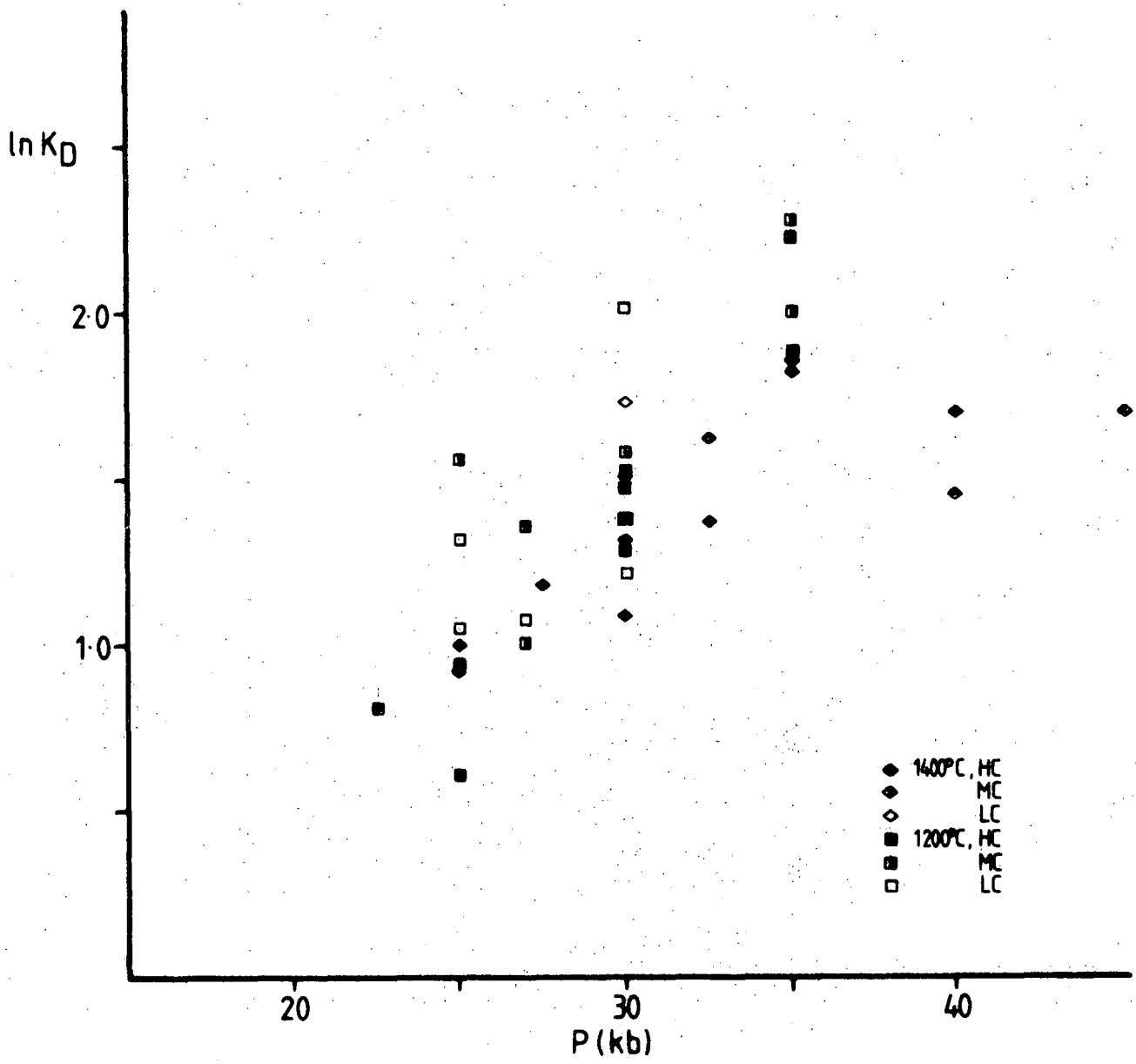

Figure 39: Plot of $ln\ K_D(F)$ vs. P for experiments in SMACCR at 1400° and 1200°C. Symbols represent different temperatures and bulk compositions. HC = 30, MC = 20, LC = 9.5 of 100Cr/Cr+Al of the bulk composition.

$$RT\,ln\,\gamma_{en} = (X^{M1}_{Al})^2 W_{MgAl} + (X^{M1}_{Cr})^2 W_{CrAl} + X^{M1}_{Al} X^{M1}_{Cr} (W_{MgAl} + W_{MgCr} - W_{CrAl}) \quad (64)$$

$$RT\,ln\,\gamma_{MgCrTs} = (X^{M1}_{Mg})^2 W_{MgCr} + (X^{M1}_{Al})^2 W_{CrAl} + X^{M1}_{Mg} X^{M1}_{Al} (W_{MgCr} + W_{CrAl} - W_{MgAl}) \quad (65)$$

$$RT\,ln\,\gamma_{py} = 3(X^{gt}_{Ca})^2 W_{CaMg} + 2(X^{gt}_{Cr})^2 W_{CrAl} + X^{gt}_{Ca} X^{gt}_{Cr} (dH_{rec} - TdS_{rec}) \quad (66)$$

$$Rt\,ln\,\gamma_{kn} = 3(X^{gt}_{Ca})^2 W_{CaMg} + 2(X^{gt}_{Al})^2 W_{CrAl} + X^{gt}_{Ca} X^{gt}_{Al} (dH_{rec} - TdS_{rec}) \quad (67)$$

The molar volume of $MgCrAlSiO_6$ is unknown. This poses a serious problem for the development of a geobarometer based on the solubility of Cr_2O_3 in orthopyroxenes. Assumptions can only be made by analogy with known relations and empirical modelling. The octahedral ionic radius of Cr^{+++} (Shannon & Prewitt, 1969) is greater than that of Al^{+++}. This results in a greater molar volume of knorringite (Irfune *et al.*, 1982; Ringwood, 1977) relative to pyrope, even though knorringite is denser. By analogy it is envisaged that $MgCrAlSiO_6$ has a greater molar volume than $MgAl_2SiO_6$. The difference in molar volumes between products and reactants of reaction (F) is therefore expected to be roughly twice the molar volume difference of reaction (B), because two moles of garnet and four moles of pyroxene are involved. Mixing between enstatite and Mg-tschermaks has an excess volume and it may be envisaged that this is true for the mixing of enstatite and Mg-Cr-tschermaks as well. Whether this excess is positive or negative and of what size is impossible to say due to the lack of X-ray studies. The method adopted here to circumvent this problem is similar to the approach of Wood & Banno (1973). If non-ideal mixing of MgAl can be taken into account by formulating $dV_r(B) = a+b(X^{M1}_{Al})(1-X^{M1}_{Al})$ (Harley, 1981; Harley & Green, 1982) an analog of this is to formulate $dV_r(F) = a+b(X^{M1}_{Cr})(1-X^{M1}_{Cr})$ for the reaction (F). The W_{MgAl} and W_{MgCr} are then treated as being 0. It must be emphasized that this is only a very crude analogy, because the dV_r formulation of Harley (1981) and Wood & Banno (1973) were based on actual volume measurements, while the assumptions here are not constrained. The validity of the method employed

may be judged by the closeness of the derived values for $dV_r(F)$ to those predicted from the analogy (i.e. $dV_r(f)$ = approx. 2 $dV_r(b)$).

Under those assumptions the expressions for non-idealities in orthopyroxene are simplified to

$$RT\ ln\ \gamma_{opx'} = RT\ ln\ \gamma_{en} + RT\ ln\ \gamma_{MgTs} =$$

$$[(X_{Cr}^{M1})^2+(X_{Al}^{M1})^2+X_{Mg}^{M1}X_{Al}^{M1}-X_{Al}^{M1}X_{Cr}^{M1})W_{CrAl} \quad (68)$$

and those for garnet remain

$$RT\ ln\ \gamma_{gt's} = RT\ ln\ \gamma_{py} + RT\ ln\ \gamma_{kn} =$$

$$6(X_{Ca}^{gt})^2W_{CaMg}+[2(X_{Cr}^{gt})^2+2(X_{Al}^{gt})^2]W_{CrAl}$$

$$+ (X_{Ca}^{gt}X_{Cr}^{gt} + X_{Ca}^{gt}X_{Al}^{gt})(dH_{rec}-TdS_{rec}) \quad (69)$$

Because

$$dG_{1,T} = dH - TdS + PdV = -RT\ ln\ K_D \quad (70)$$

we can now formulate for reaction (F)

$$P = \frac{1}{[a+b(X_{Cr}^{M1})(1-X_{Cr}^{M1})]}[-(RT\ ln\ K_D + RT\ ln\ \gamma_{gt's} - 2RT\ ln\ \gamma_{opx'})$$

$$- dH + TdS] \quad (71)$$

and solve for the parameters a, b, dH, and dS by means of multiple regression. The best fit yielded values of dH = -17716 cals, dS = -10.51 e.u., a = -392.1 and b = 1346. The barometer therefore has on substituting values derived here and previously the form

$$P = \frac{1}{[-392.1+1346(X_{Cr}^{M1})(1-X_{Cr}^{M1})]} \left(- \left[RT \ ln \left(\frac{(X_{Mg}^{gt})^3 (X_{Al}^{gt})(X_{Cr}^{gt})}{(X_{Mg}^{M1})(X_{Mg}^{M2})^2 (X_{Cr}^{M1})} \right)^2 \right.$$

$$+ 18000(X_{Ca}^{gt})^2 + (90853 - 52.1T)X_{Ca}^{gt}$$

$$+ 6800[(X_{Al}^{gt})(X_{Cr}^{gt})^2 + X_{Al}^{M1}X_{Cr}^{M1} - (X_{Cr}^{M1})^2 - (X_{Al}^{M1})^2 - X_{Mg}^{M1}X_{Al}^{M1}]$$

$$\left. + 17716 - 10.51T \right] \Bigg) \qquad (72)$$

The expression for the reciprocal interaction is simplified to $dG_{rec}(E)\ X_{Ca}^{gt}$, because in the system SMACCR (as for natural garnets without Fe^{+++}) $X_{Al}^{gt} = 1 - X_{Cr}^{gt}$ and so $(X_{Ca}^{gt}X_{Cr}^{gt} + X_{Ca}^{gt}X_{Al}^{gt}) = X_{Ca}^{gt}$.

The size of dV_r for reaction (F) ranges between about -12 and -16 cm^3 depending on the composition of the pyroxene. For reaction (B) the volume difference varies between approx. -8 and -9 cm^3. The magnitude of the derived $dV_r(F)$ is thus in marginal agreement with the prediction from the analogy.

The application of equation (72) to the experimental data is shown in fig. 40. The agreement is generally very good with the exceptions of the runs at 40 and 45 kb, previously discussed. The misfit of the runs at 1100°C and one at 950°C is not unexpected in the light of the discussion in chapter 26. Excluding the 45 kb run and those at 1100°C, the mean deviation of the predicted value from the nominal run pressure is 1.8 kb.

It must be emphasized that because of the nature of the assumptions made the barometer is basically empirical and derived by curve-fitting.

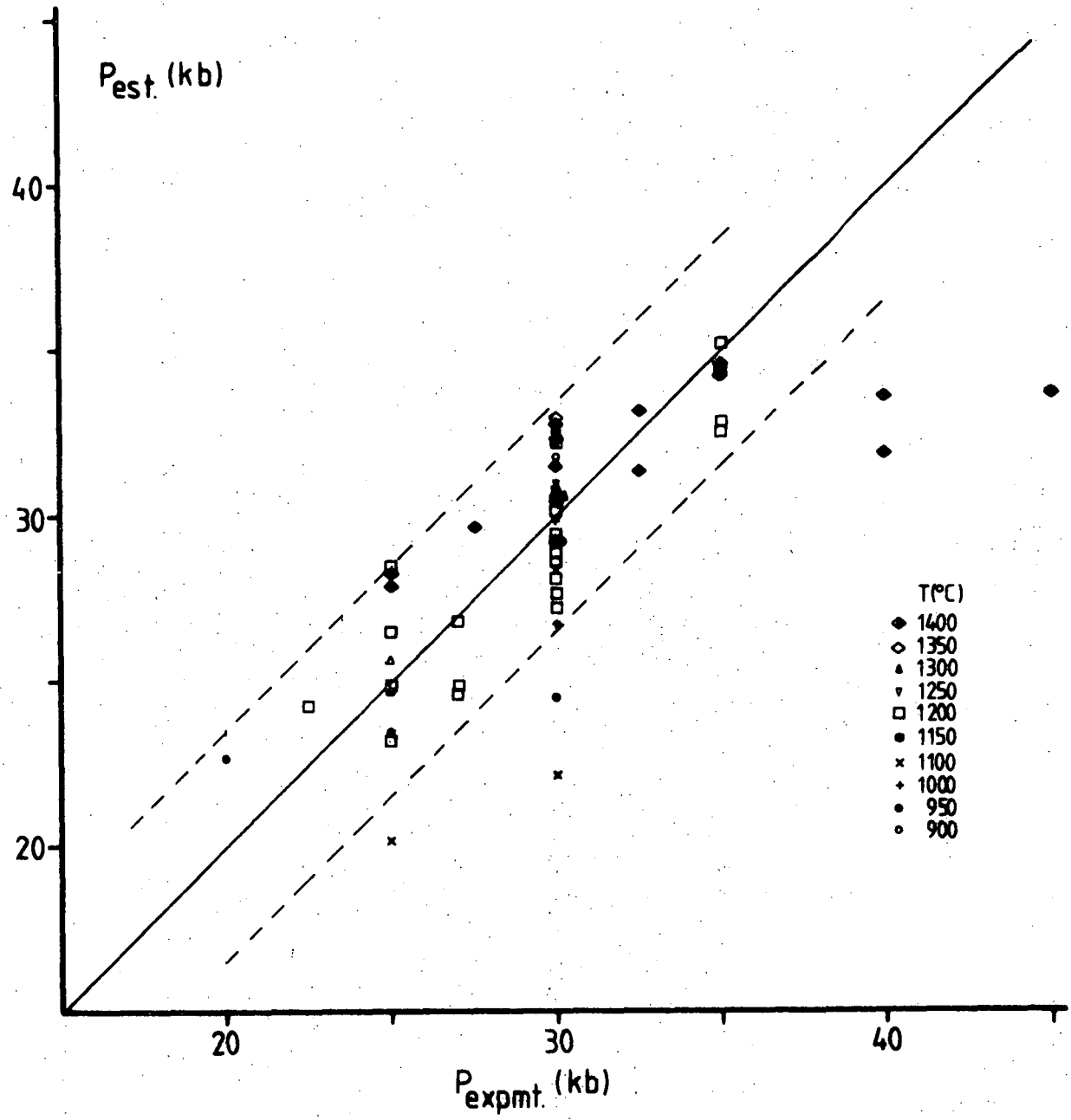

Figure 40: Comparison of pressures estimated via equation (72) and nominal run pressures for experiments in SMACCR. Dashed lines enclose a ±3.5 kb interval relative to ideal agreement (solid line).

PART IV

STUDY IN MULTICOMPONENT ("NATURAL") SYSTEMS AND APPLICATION OF GEOBAROMETERS TO Fe-BEARING SYSTEMS AND NATURAL GARNET LHERZOLITES.

29. INTRODUCTION

Any model for extension of data from simple to more complex systems requires the validation of the model by experimental study of the more complex systems. The main difference between the mineral chemistry of natural garnet peridotites and the system SMACCR is the existence of Fe as a major component of the coexisting phases. The application of the barometers derived for the SMACCR system to natural rocks requires thus a model for the effect of Fe on the equilibria. This is done by applying correction factors mainly derived by Harley (1981). Up to this time the experimental data for Fe-bearing systems have been interpreted by an empirical formulation of the influence of Fe on phase equilibria (Wood & Banno, 1973; Wood, 1974; Harley, 1981; Harley & Green, 1982). This study adopts those empirical factors and thus remains empirical and does not provide a strict thermodynamic model.

Experiments have been carried out at conditions where the Al and Cr contents of the minerals of interest were high enough to ensure the analytical data to be significant relative to the error of analysis, and also close to conditions estimated for natural garnet lherzolite xenoliths. The starting materials were based on the composition of a natural lherzolite (Tinaquillo peridotite - 40% olivine, Jaques & Green, 1980). Cr/Cr+Al ratios were chosen to be comparable with fertile and moderately depleted mantle compositions.

The P-T estimates for crystallization conditions of garnet lherzolite xenoliths from kimberlite have been discussed in the literature since Boyd (1973) interpreted them as outlining a mantle geotherm. Extensive discussion exists in the literature on the validity of such geotherms and the meaning of the P-T estimates (Irving, 1976; Harte, 1978; Gurney & Harte, 1980; Thompson & Harley, 1982). The new estimates for some suites of xenoliths are presented and discussed.

30. EXPERIMENTAL TECHNIQUES

Experimental techniques used in this study are similar to those described before (chapters 10 and 15) for runs at or below 1200°C. NaCl or pyrex-NaCl high pressure cells contained 2-sample capsules made from $Ag_{50}Pd_{50}$ or $Ag_{75}Pd_{25}$. The two mixes were separated by a metal disc of the same material. Iron loss to the silver-palladium capsule was experienced in the runs at 1100° and 1200°C, while this effect seems to be small in the 1000°C run. To prevent more Fe loss in runs at higher temperatures, a different assemblage was used (fig. 41a). The capsule consisted of inner graphite capsules and an outer platinum capsule. The inner container was made by stacking two individual graphite cylinders, each containing a different mix, on top of each other. A dome-shaped graphite was placed on top to seal the second mixture against the platinum (fig. 41b). The platinum capsule was then sealed by welding.

As for SMACCR, no friction correction was applied in cells using NaCl assemblages.

In a run at 1400°C and 45 kb, lead intruded into cracks in the core of the pressure vessel, resulting in continuous extrusion of the core. Accordingly the nominal run pressure had to be monitored and adjusted continuously and unlike runs at lower pressure, this experiment did not attain the normal extremely stable pressure-temperature setting characteristic of the apparatus using NaCl pressure cells.

Figure 41: (top) cross section of high pressure cell used in experiments with TP-40 and TP-40C starting material.
(bottom) sample capsule and surrounding used in these experiments.
Note that the graphite part consists of three sections (two mixture containers and a dome-shaped lid), which are stacked inside the Pt capsule.

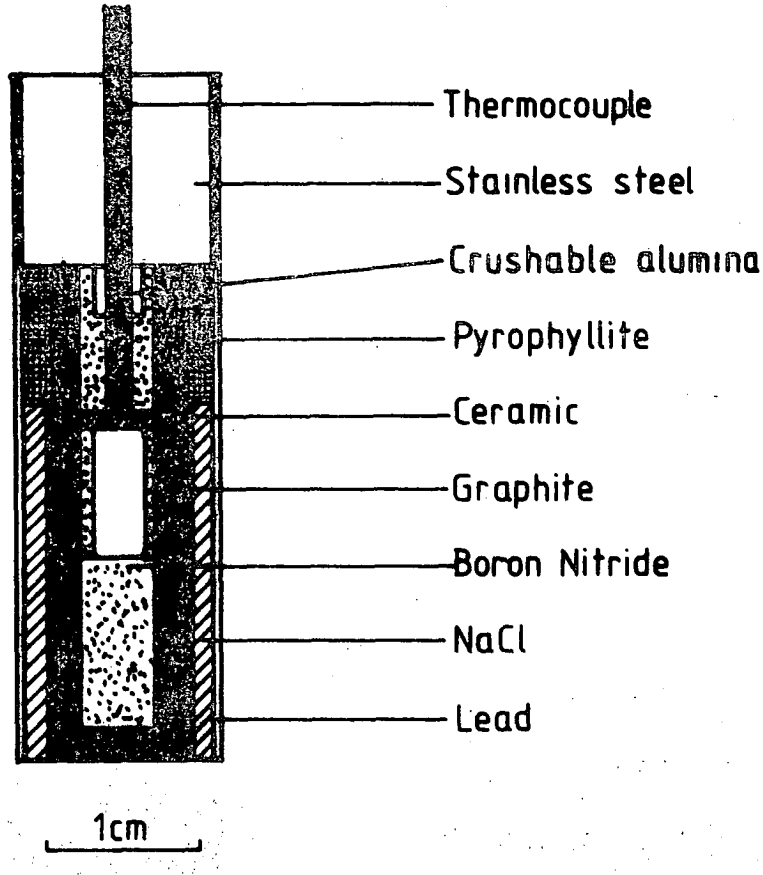
Thermocouple
Stainless steel
Crushable alumina
Pyrophyllite
Ceramic
Graphite
Boron Nitride
NaCl
Lead
1cm

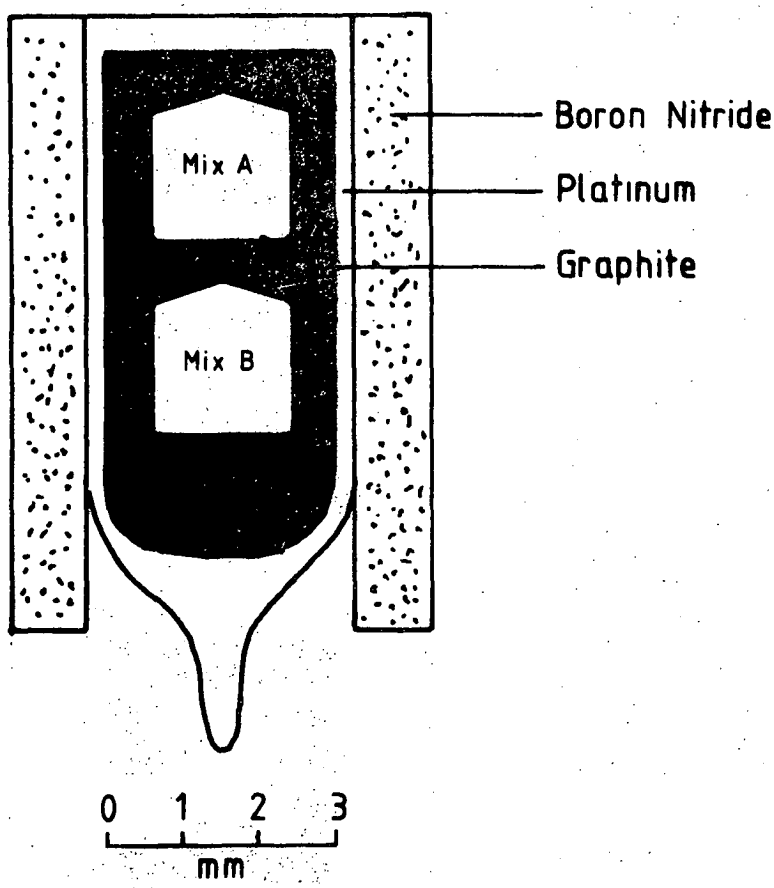
Boron Nitride
Platinum
Graphite
Mix A
Mix B
0 1 2 3
mm

31. STARTING MATERIAL

The peridotite mix was prepared by C. Hatton in this Department in the manner described by Jaques & Green (1980). The composition of mix TP-40 is that of Tinaquillo peridotite minus 40% olivine, to which 1.6% Cr_2O_3 was added for mix TP-40C (table 14).

Because the mixture was exposed to laboratory atmosphere for some time, the Fe^{++}/Fe^{+++} ratio is not as mixed, but contains a higher relative amount of Fe^{+++}. However, under the conditions of the runs most of the Fe^{+++} is reduced again to Fe^{++}. No evidence for large amounts of Fe^{+++} was found in any of the analyses of minerals produced in the runs. Calculation of spinel stoichiometry confirms the reduced nature of the charges, whether in graphite or AgPd capsules.

Table 14: Starting materials for experiments in multicomponent systems.

	TP-40	TP-40C
SiO_2	47.51	46.76
TiO_2	0.13	0.13
Al_2O_3	5.35	5.27
Cr_2O_3	0.75	2.31
Fe_2O_3	0.15	0.15
FeO	7.38	7.26
MnO	0.18	0.18
MgO	32.80	32.28
CaO	4.97	4.89
Na_2O	0.30	0.30
K_2O	0.03	0.03
P_2O_5	0.02	0.02
NiO	0.43	0.42
Mg'	88.8	88.8
Cr'	8.6	22.7

$Mg' = 100(Mg/Mg+Fe^{++})$
$Cr' = 100(Cr/Cr+Al)$

32. RUN PRODUCTS - TINAQUILLO PERIDOTITE

Analyses of run products are listed in appendix 6. The textures of the run products are similar to those described previously. Melting occurred in runs at 1100°, 1200° and possibly to a very small degree at 1300°C. Due to the small amount of melt and quenching problems of silicate melts the compositions of the melt could not be established. Melting was insufficient to eliminate garnet, clinopyroxene or spinel from the assemblage.

Garnet is poikilitic with numerous inclusions of other phases (fig. 42a), which makes it difficult to obtain good analyses for garnet. Nevertheless a chemical zoning pattern could be established in the run at 1000°C, which showed an increase of Cr in garnet towards the rim, accompanied by a decrease in Al (fig. 42b,c). It was possible to obtain good analyses for cores of garnets and analyses with only minor contamination near rims of the same garnet, showing both the zonation in Cr and Al and that there is no significant amount of Fe^{+++} present (table 15). No evidence for chemical zoning in Ca/Ca+Mg or Mg/Mg+Fe was found.

The best obtainable rim analyses of garnet were then taken as the closest approach to equilibrium and the mean of these is listed as "gt (max)" in appendix 6. It should be stressed that this value is a minimum for Cr in garnet, because the zoning pattern is continuous and no good analyses from the very edge could be obtained; in those analyses it is impossible to distinguish contamination from zonation.

In runs above 1000°C, a spread in Cr/Cr+Al in garnet analyses was found, which decreased with increasing temperature. The spread is interpreted as being due to some compositional zoning and accordingly the analyses showing the highest Cr/Cr+Al ratio have been taken as the closest approach to equilibrium compositions.

Figure 42: Three pictures of run T-1148 (1000°C, 35 kb, mixture TP-40C), showing the same area. The large garnet grain in the central part of the pictures has a maximum diameter of about 12 μm. Top: secondary electron image showing differing mean atomic numbers as different shades of grey, lighter colours indicating higher mean atomic numbers. Edges of garnets appear lighter because of increased Cr content. Middle and bottom: X-ray distribution maps for Al and Cr respectively. The large garnet (outlined) shows clear chemical zonation with Al decreasing towards the rim and an accompanying increase in Cr.

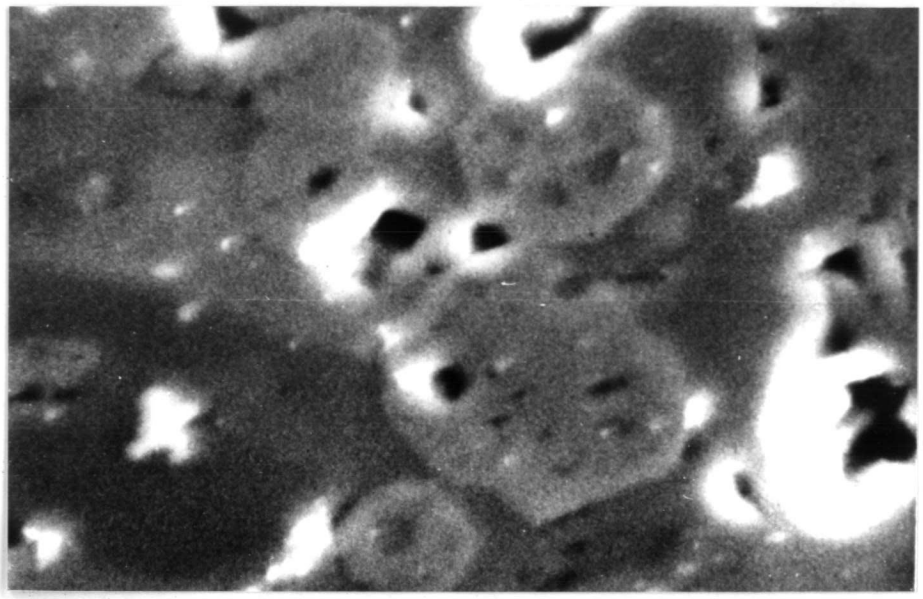

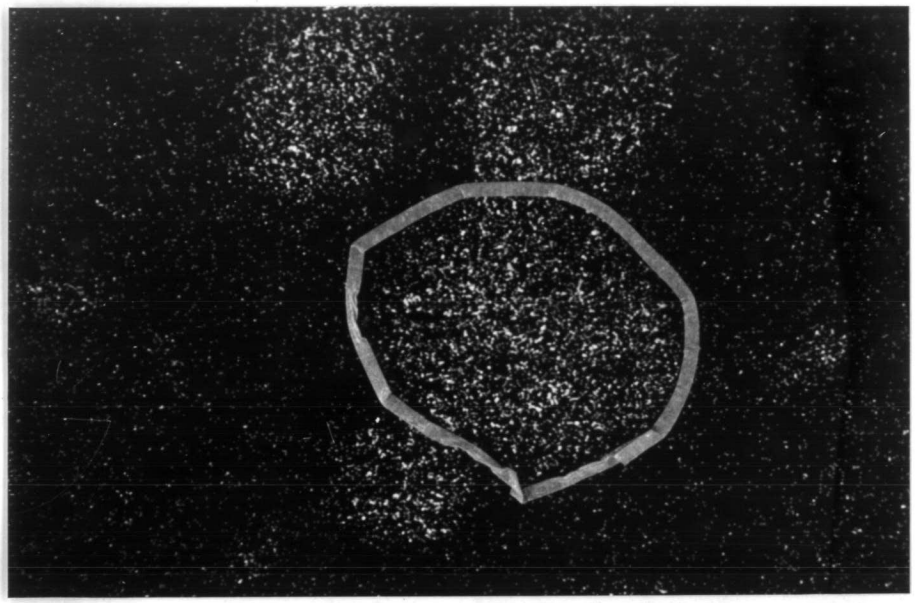

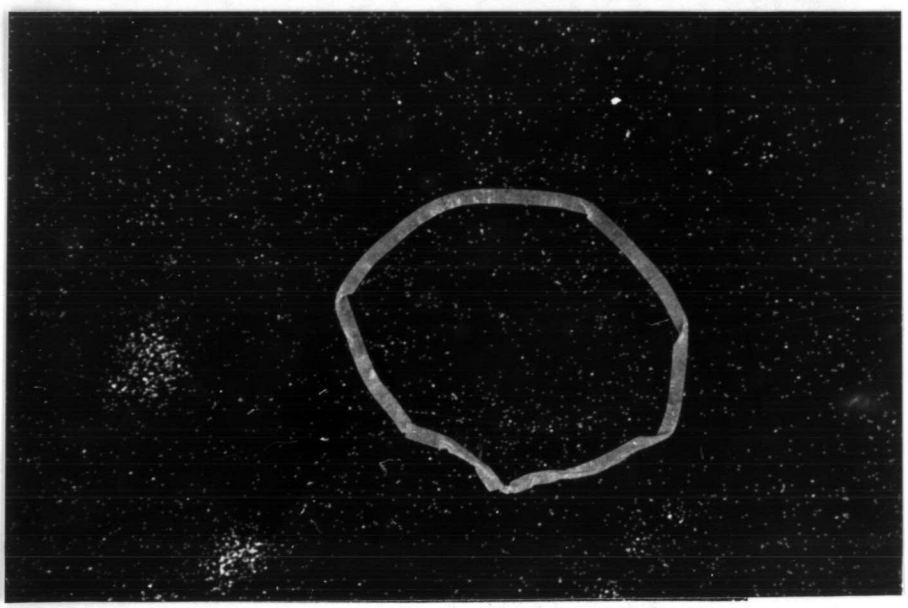

Table 15: Analyses of zoned garnet in run T-1148 (1000°C, 35 kb), mix TP-40C. Normalised to 100%.

	core		rim	
	wt.%	struc	wt.%	struc
MgO	19.02	2.021	19.33	2.083
Al_2O_3	22.82	1.917	19.43	1.655
SiO_2	42.26	3.013	41.93	3.030
CaO	6.00	0.458	6.17	0.478
TiO_2	0.20	0.011		
Cr_2O_3	0.76	0.043	4.01	0.229
FeO	8.56	0.510	8.77	0.530
MnO	0.38	0.023	0.35	0.022
Total		7.996		8.027
Ca/Ca+Mg		0.1532		0.1546
Mg/Mg+Fe		0.7985		0.7912
Cr/Cr+Al		0.0219		0.1215

Pyroxenes and olivines were found to be homogeneous. In runs performed at 1100° and 1200°C Fe loss occurred. Differences in Fe loss rate of different minerals (Jaques & Green, 1979; Ellis & Harris, pers. comm.) prevented the evaluation of geothermometers based on Fe-Mg exchange, but the loss is small enough to allow the use of the data to evaluate the barometers and thermometers based on other reactions.

Spinels are present in runs with the starting mixture TP-40C (high Cr/Cr+al ratio). With the exception of a run at 1400°C and 45 kb, spinels are generally very small and no zonation within the accuracy limits of the analyses was detected. In runs at 1400°C patches of intergrowths of spinel and garnet were found. The spinel of this intergrowth is not identical to the spinel outside those patches. It is a highly aluminous and highly magnesian spinel. Discrete grains of this spinel could not be found and in the run at 45 kb no good garnet analyses were obtained either. Fig. 43 shows the chemical composition of the intergrowth for the 45 kb run in an $(Al_2O_3+Cr_2O_3)$-FeO-MgO plot (mol %). The data points constitute a tie-line between projected garnet and Al-rich spinel. The Cr-rich spinel, which occurs as distinct, partly large but anhedral grains is zoned in Al

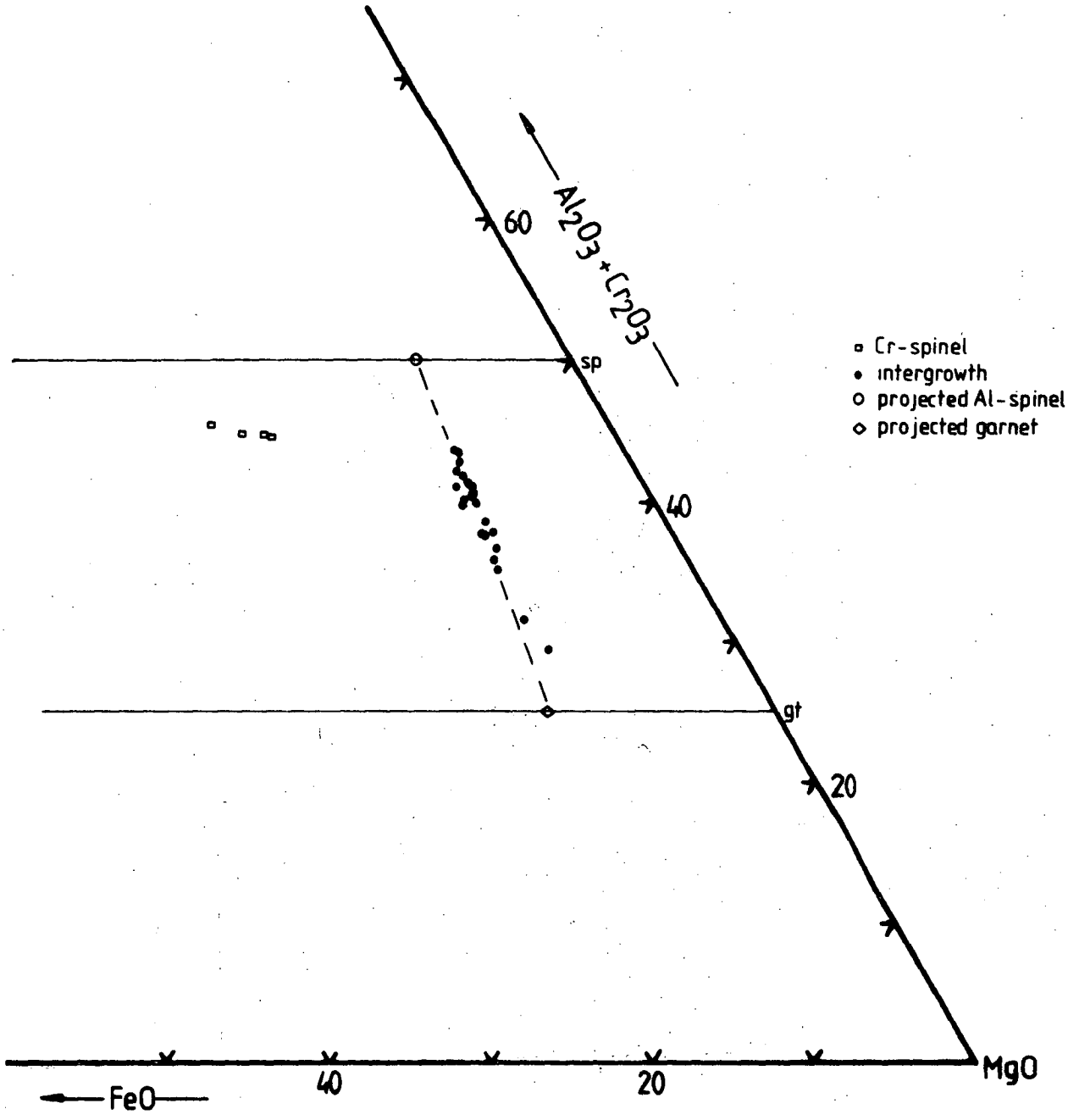

Figure 43: Analyses of (Al)-spinel-garnet intergrowth in a molar $(Al_2O_3+Cr_2O_3)$-FeO-MgO plot compared to analyses of discrete spinels. Chemical variation of the intergrowth analyses constitutes a tie line between projection points of the respective endmembers.

(Cr/Cr+Al 80-60 from core to rim) and analyses show high levels of contamination by other phases. The appearance of the intergrowth and zonation is not understood, possibly the run time was insufficient to reach equilibrium. The run at 1400°C and 45 kb has therefore been discarded from the data set. The run at 1400°C and 35 kb has been included in the data set because good garnet analyses were obtained and Cr spinels did not show evidence for zonation.

33. SITE DISTRIBUTIONS IN NATURAL PYROXENES AND GARNETS

In natural systems a great variety of possible pyroxene endmembers exists because a number of minor elements are accommodated in the structure of pyroxenes. This complexity is commonly treated by making assumptions such as $(Mg/Mg+Fe)_{mineral} = (Mg/Mg+Fe)_{site}$ or the restriction of Al^{VI} to the M1 site. These assumptions are to some extent incorrect in the light of crystallographic studies (Fleet, 1974; Ganguly & Ghose, 1979; Sack, 1980). However the complexities inferred in the latter studies cannot be resolved by the experimental methods employed in this study. As emphasized previously, it is possible to derive empirical relationships which are of use in practical thermometry and barometry. Thus even where some assumptions do not adequately incorporate all information on site occupancy, this does not render a geobarometer or geothermometer inaccurate, because a number of complexities can be encompassed by the empirical, experimentally determined factors. Such empirical factors and the P-T equations based on them remain empirical and without theoretical basis and should not be extrapolated far beyond the experimentally calibrated P-T-X range.

The formulation of site distributions in complex pyroxenes follows mainly that of Wood & Banno (1973) and hence we have as endmembers

site				
M2	M1	B	A	Oxygen
(Mg,Fe,Mn)	(Mg,Fe,Mn)	Si	Si	O_6
(Mg,Fe,Mn)	Al	Al	Si	O_6
(Mg,Fe,Mn)	Cr	Al	Si	O_6
Ca	(Mg,Fe,Mn)	Si	Si	O_6
Na	Ti	Al	Si	O_6
Na	Cr	Si	Si	O_6
Na	Al	Si	Si	O_6
(Mg,Fe,Mn)	Ti	Al	Al	O_6

The assumption $(Mg/Mg+Fe)_{opx} = (Mg/Mg+Fe)_{M1,M2}$ (Wood & Banno, 1973) is here extended to include Mn, which can be a minor component in natural orthopyroxenes from garnet lherzolite. Fe denotes in each case Fe^{++}. There is no evidence for the presence of large quantites of Fe^{+++} in natural orthopyroxenes from lherzolites and therefore Fe^{+++} is neglected here. It must be emphasized that this treatment is not valid for those crustal rocks in which Fe^{+++} is significant and the molecules $MgFe^{+++}AlSiO_6$ or $NaFe^{+++}Si_2O_6$ must be considered.

The calculation scheme for site distributions in natural orthopyroxenes from lherzolites involves the following steps: Ti is first allocated to Na to form $NaTiAlSiO_6$, or, where there is insufficient Na, to form $(Mg,Fe,Mn)TiAl_2O_6$. Any excess Na is then taken to form ureyite ($NaCrSi_2O_6$) followed by jadite ($NaAlSi_2O_6$). Where Na is insufficient to take into account all of the Cr this is expressed as Mr-Cr-tschermaks type molecule [$(Mg,Fe,Mn)CrAlSiO_6$] and the remaining Al is expressed as Al-tschermaks type molecule [$(Mg,Fe,Mn)Al_2SiO_6$]. Ca in orthopyroxene is calculated only as the molecule $Ca(Mg,Fe,Mn)Si_2O_6$.

From this formulation it follows that $X_{Al}^{M1} = (Al-Cr-2Ti+Na)/2$ is equivalent to $X_{Al}^{M1} = Al-(2-Si)$. This is true only if the sum of cations on the basis of 6(O) per formula unit of the pyroxene is exactly 4.000, in all other cases the two expressions yield different results. In the

energy dispersive X-ray spectrum of minerals being analysed by electron microprobe, the size and location of the Si peak may lead to errors in Si analysis and thus in the calculation of X_{Al}^{M1} as Al-(2-Si). If small amounts of Al are present in orthopyroxene, as is the case for most garnet lherzolite nodules, the differences in calculation of X_{Al}^{M1} are significant and many published analyses of orthopyroxenes yield negative values of X_{Al}^{M1}, when calculated as Al-(2-Si). Thus the first expression is adopted and the site distribution for the elements are calculated as follows:

$$X_{Al}^{M1} = (Al-Cr-2Ti+Na)/2$$

$$X_{Mg}^{M1} = (1-X_{Al}^{M1}-Cr-Ti)\ (Mg/Mg+Fe+Mn)$$

$$X_{Mg}^{M2} = (1-Ca-Na)\ (Mg/Mg+Fe+Mn)$$

$$X_{Fe}^{M1} = (1-X_{Al}^{M1}-Cr-Ti)\ (Fe/Mg+Fe+Mn)$$

$$X_{Mg,Fe,Mn}^{M1} = X_{MF}^{M1} = (1-X_{Al}^{M1}-Cr-Ti) = X_{Mg}^{M1}/(Mg/Mg+Fe+Mn)$$

$$X_{Mg,Fe,Mn}^{M2} = X_{MF}^{M2} = (1-Ca-Na) = X_{Mg}^{M2}/(Mg/Mg+Fe+Mn)$$

Clinopyroxenes are similarly calculated but with the difference that Ti, Cr and Al excess over Na is calculated into the appropriate Ca endmember, i.e. $CaTiAl_2O_6$, $CaCrAlSiO_6$ and $CaAl_2SiO_6$.

Natural garnets from garnet lherzolites have the main endmembers $Mg_3Al_2Si_3O_{12}$ (pyrope), $Mg_3Cr_2Si_3O_{12}$ (knorringite), $Ca_3Al_2Si_3O_{12}$ (grossular), $Ca_3Cr_2Si_3O_{12}$ (uvarovite), $Fe_3Al_2Si_3O_{12}$ (almandine), and potentially $Fe_3Cr_2Si_3O_{12}$. Additional minor elements are Mn, Ti and Fe^{+++}. The divalent Mn substitutes for Mg and Fe^{++}, while Fe^{+++} substitutes for Al and Cr. Theoretically, the possible Ti endmembers are (Ca,Mg,Fe,Mn) (Al,Fr,Fe^{+++}) (Si,Ti)$_3O_{12}$ or (Ca,Mg,Fe,Mn)$_2Ti_2Si_3O_{12}$ or even[(Ca,Mg,Fe,Mn)(Al,Cr,Fe^{+++})] [Ti(Al,Cr,Fe^{+++})]Si_3O_{12}. Analytical uncertainties for garnet data from both experiments and natural garnet lherzolites make it impossible to decide on the endmember, because Si in structural formulae of garnet ranges from below to above 3 (based on 12 oxygen). Most garnets do however

contain Ti only to a very limited extent (usually <0.5 wt.%) and Ti is thus negelcted without introducing major uncertainties.

Analytical uncertainties also prevent an exact calculation of Fe^{+++} in garnet. Even where Fe^{+++} can be determined, it is not clear whether this represents a primary feature of the garnet or is of secondary origin as most garnets in natural rocks have kelphytic rims, suggesting late-stage alteration which may well influence the Fe^{++}/Fe^{+++} ratio. In view of the very limited amount of Fe^{+++} present in garnets from experiments all Fe is taken to be Fe^{++}.

Therefore site distributions are calculated as follows:

$$X_{Mg}^{gt} = Mg/Mg+Fe+Mn+Ca$$

$$X_{Ca}^{gt} = Ca/Mg+Fe+Mn+Ca$$

$$X_{Fe}^{gt} = Fe/Mg+Fe+Mn+Ca$$

$$X_{Mg,Fe,Mn}^{gt} = X_{MF}^{gt} = 1 - X_{Ca}^{gt}$$

$$X_{Al}^{gt} = Al/Al+Cr$$

$$X_{Cr}^{gt} = Cr/Al+Cr$$

34. Ca-Mg EXCHANGE BETWEEN PYROXENES

Barometry based on the solubility of either Al or Cr in orthopyroxene is very sensitive to temperature estimates. Hence it is necessary to have an estimate of the temperatures of natural rocks. It has been shown in both CMAS and SMACCR that temperature estimates by the method of Wells (1977) are reliable in the range from approx. 1050° to 1400°C. This is also true for those experiments performed at 35 kb, T = 1000-1300°C with natural system starting materials (fig. 44). As discussed before and pointed out by Ehrenberg (1982) there is considerable doubt as to the reliability of this thermometer at low and very low temperatures and large under-estimations may result in the use of this thermometer below about 900°C.

There are also uncertainties with the temperature estimation by this method at high temperatures (at or exceeding 1400°C) combined with high pressures (exceeding about 35 kb), because of the possible pressure effect on the Ca-Mg exchange reaction (Lindsley *et al.*, 1981; Brey, 1982). At these conditions the Wells geothermometer may over-estimate temperatures by approx. 50°C (fig. 44). Most garnet lherzolites from inclusions in kimberlite however are well within the range of P-T conditions where the experiments show a good agreement between predicted and experimental temperature (figs. 19 and 44). In these data it is particularly noteworthy that there is apparently no difference between data from the Cr-poor and Cr-rich compositions.

In conclusion, the geothermometer of Wells (1977) may be used for the estimation of temperatures with considerable confidence for most natural garnet lherzolite nodules.

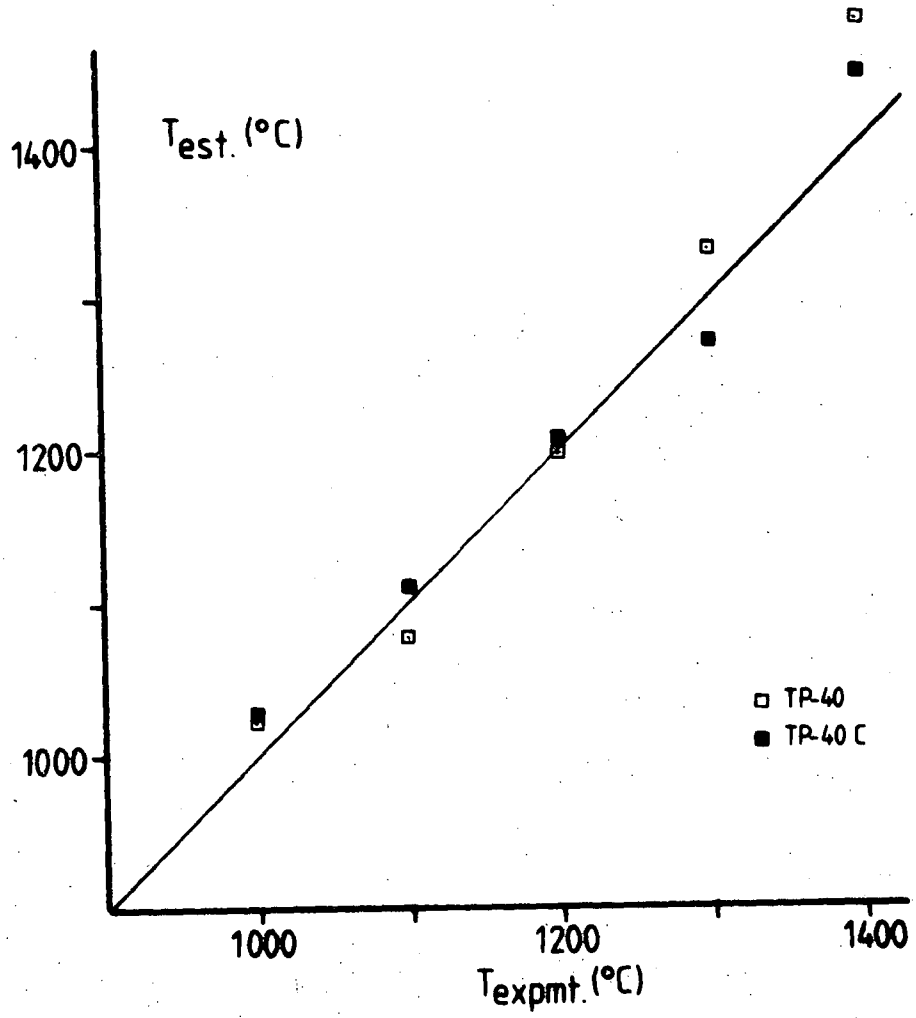

Figure 44: Temperature estimates by the method of Wells (1977) for experiments with TP-40 and TP-40C starting material at 35 kb compared to experimental conditions. The solid line is for perfect agreement between estimate and nominal temperature.

35. Cr-Al EXCHANGE BETWEEN SPINEL AND GARNET

In fig. 45 a plot of $ln(X^{gt}_{Cr}X^{sp}_{Al}/X^{gt}_{Al}X^{sp}_{Cr})^2$ [the K_D reaction (D)] vs. 1/T is shown. It is apparent that the $ln\ K_D$ becomes very insensitive to temperatures even at levels of about 1300°C. The values of $ln\ K_D$(D) are shifted towards lower values in experiments in the complex "natural" system starting material relative to the simple system (SMACCR). The two data sets produce $ln\ K_D$ vs. 1/T curves of very similar character and in the light of these data it is inferred that spinel compositions of the simple system represent equilibrium, even at the lower temperatures, and are a reflection of an increasing insensitivity of the K_D(D) to temperature with decreasing temperature. In the simple system the segment between about 1200° and 1400°C can be approximated by a straight line and accordingly a thermometer for SMACCR was calibrated (section 25.3). For the TP-40 and TP-40C compositions also, it is possible to approximate the relationship between $ln\ K_D$(D) and 1/T by a straight line at least for segments of the temperature range, but as fig. 45 shows, this would result in a very flat slope in the range of interest. Additionally, the very large shift between the SMACCR system and the Fe-bearing system (TP-40 and TP-40C) suggests that small variations in Fe/Mg may produce variations in $ln\ [(X^{sp}_{Cr}X^{sp}_{Al})/(X^{gt}_{Al}X^{gt}_{Cr})]$ greater than the changes due to temperature differences of ≅100°C. A thermometer of this type would yield very large uncertainties (in the order of 200°C), and is thus of no practical value.

Data from natural garnet lherzolites confirm this interpretation. Four lherzolites from Thaba Putsoa (Nixon & Boyd, 1973a) and one each from the Thumb (Ehrenberg, 1982), the Sloan pipe (McCallum & Eggler, 1976), and Pipe 200 (Carswell *et al.*, 1979) fall into the narrow range of -5 to -5.8 ($ln\ K_D$), but cover a range of (cpx-opx) temperatures from about 900° to 1100°C.

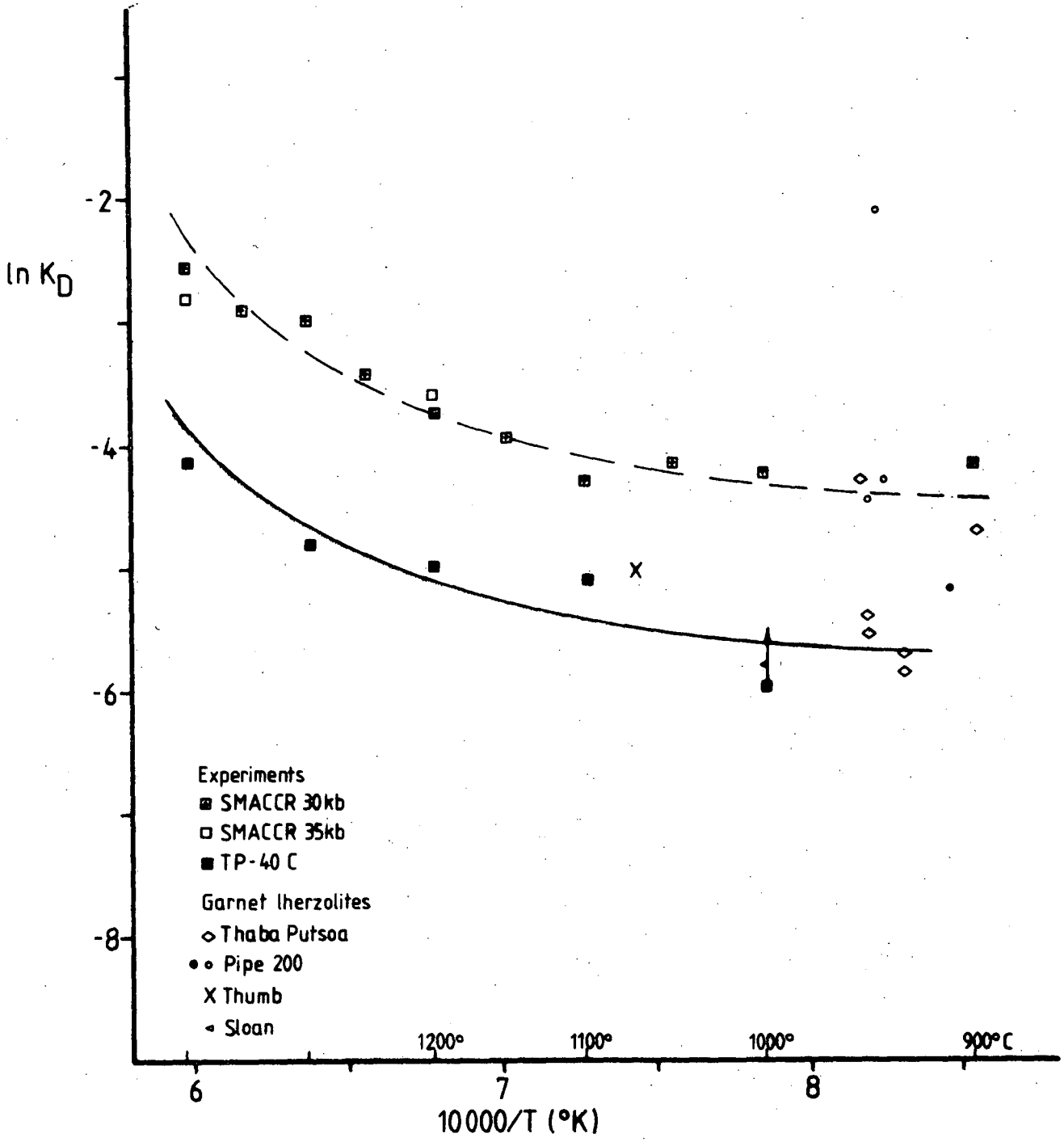

Figure 45: Plot of $ln(X_{Cr}^{gt}X_{Al}^{sp}/X_{Al}^{gt}X_{Cr}^{sp})^2$ vs. 10000/T (K) for experimental data in the SMACCR system, the multicomponent system TP-40C and some natural garnet lherzolites from kimberlite. The temperatures for the natural rocks were estimated by the method of Wells (1977). The filled circle represents the data for a garnet lherzolite with primary spinel (class "a", see text) from Pipe 200 (Carswell *et al.*, 1979), open circles for garnet-spinel pairs, where the spinel belongs to the "d" class (see text) from this locality (Carswell *et al.*, 1979). The other data for rocks from Thaba Putsoa (Nixon & Boyd, 1973), Thumb (Ehrenberg, 1982) and Sloan pipe (McCallum & Eggler, 1976) are reported as apparently primary spinel.

Fig. 45 illustrates another problem in the natural rocks. It is not always clear whether a spinel found in garnet lherzolite is primary or secondary. Spinels in garnet lherzolites have been described as occurring as a) large discrete, apparently primary grains

b) small idioblastic grains associated with clusters of clinopyroxenes and phlogopite grains,

c) small grains associated with kelphytic breakdown of garnet,

d) spinels, typically outside, although still adjacent to kelphytic zones,

e) rounded grains, mainly included in olivine and enstatite, and

f) inclusions in garnet.

(Boyd & Nixon, 1978; Carswell *et al.*, 1979; Ortez, pers. comm.). While spinels of groups b and c are obviously secondary and as such are not in equilibrium with the primary garnet assemblage, spinels of groups e and f may or may not be in equilibrium with the whole assemblage. Carswell *et al.* (1979) reported spinels of types a, b, c and d. Plotted in fig.45 are those of groups a and d, where temperatures could be estimated via the cpx-opx thermometer of Wells (1977). Only the spinel which has been described as primary plots in the region of the K_D's for primary garnet and spinel coexisting in the experiments on natural starting material, while the others have higher K_D's. This is seen as evidence for them being secondary or being affected by the breakdown of garnet. It is concluded that it is very difficult to establish on textural or petrographic grounds, whether a spinel is primary or not. Judging from the experiments and the values of $ln\ K_D$ for apparently primary spinels, two of the samples from Thaba Putsoa are also of secondary origin or have been altered at a late stage.

36. GEOBAROMETRY BASED ON THE SOLUBILITY OF Al_2O_3 IN ORTHOPYROXENE

36.1 Fe-BEARING SIMPLE SYSTEM

The extension of the modelling for the CMAS and SMACCR systems to Fe-bearing simple systems and natural rocks has to take account of the effect of Fe on the equilibria. The significance of this effect has been demonstrated in FMAS and CFMAS systems by Wood (1974), Harley (1981) and Harley & Green (1982). However, the treatment of their experimental data by these authors must be discussed because of the nature of the assumptions made by them.

The K_D of reaction (B) is

$$K_D = \frac{(X^{gt}_{Mg})^3 (X^{gt}_{Al})^2}{X^{M1}_{Mg} (X^{M2}_{Mg})^2 X^{M1}_{Al}} \qquad (73)$$

In Fe-free simple systems such as MAS, CMAS and SMACCR the expression for garnet site distribution $X^{gt}_{Mg} = (1 - X^{gt}_{Ca})$ is valid. In Fe-bearing systems $(1 - X^{gt}_{Ca})$ is equivalent to $(X^{gt}_{Mg} + X^{gt}_{Fe})$. The extension of the term $(1 - X^{gt}_{Ca})$ in K_D(B) from MAS to Fe-bearing systems is thermodynamically not valid. The use of this term in the K_D for reaction (B) (Wood, 1974; Harley, 1981; Harley & Green, 1982) implies that Mg and Fe are thermodynamically indistinguishable. If this were true there could be no dependence of X^{M1}_{Al} on Mg/Mg+Fe of the garnet and the authors quoted have shown that the opposite is true.

Similarly the expression X^{M1}_{Mg} in orthopyroxene = $(1 - X^{M1}_{Al})$ is only correct for MAS and CMAS systems and not in Fe-bearing systems. Again the use of a $(1 - X^{M1}_{Al})$ term in K_D(B) implies a thermodynamically incorrect assumption of identical characteristics of Fe and Mg.

Furthermore the assumptions made by Wood (1974) and Harley (1981) that Mg-Al and Fe-Al relationships in pyroxenes yield identical changes in terms of partial molar volumes is unconstrained and may be incorrect.

As mentioned before, other assumptions concerning Fe-Mg exchanges like $(Mg/Mg+Fe)_{mineral} = (Mg/Mg+Fe)_{site}$ are likely to be incorrect as well (Fleet, 1974; Ganguly & Ghose, 1979; Sack, 1980), but this partitioning problem requires a considerable amount of site occupancy data from crystallographic studies of a range in pyroxene compositions and at a range of temperatures.

A re-interpretation of the experimentally determined Fe-Mg relationships and their influence on phase equilibria in a strict thermodynamic sense is beyond the scope of this work and requires use of data as yet unpublished. Therefore the algebraic conventions used by Wood (1974), Harley (1981) and Harley & Green (1982) must also be maintained here. The $K_D(B)$ is therefore changed to

$$K_D(B') = \frac{(1 - X_{Ca}^{gt})^3 (X_{Al}^{gt})^2}{[X_{MF}^{M1} (X_{MF}^{M2})^2 X_{Al}^{M1}]} \qquad (74)$$

Thus two approaches were adopted here for the analyses of experimental data. Treatment of P-T-X relations in the CMAS and SMACCR systems employs conventional thermodynamic reasoning. In particular, activity-composition relations for within-site non-ideal interactions have been modelled using binary and ternary regular solution models. Extension of this work to Fe-bearing systems has to rely on the thermodynamically incorrect formulations of Wood (1974), Harley (1981) and Harley & Green (1982) which are curve-fitting only. As the data used by these authors are not published in sufficient numbers it is necessary to use their curve-fitting terms for the Fe-bearing systems and hence, unfortunately, my final equation is also a curve-fitting equation only.

Nonetheless thermodynamic expressions (e.g. ternary regular solutions) will be used in the further treatment to derive correction parameters. This is done because these formulations may be of use in thermodynamic modelling once appropriate models for Fe-Mg relationships become available.

I wish to emphasize again that non-thermodynamic (empirical) formulations are not invalid as such, if their accuracy and practical usefulness can be demonstrated. However they are empirical and the curve-fitting terms do not strictly reflect thermodynamic quantities.

Following the procedures of Wood (1974), Harley (1981) and Harley & Green (1982) we have for the simplest Fe-bearing systems, FMAS, the endmembers or rather endmember groups

$$(Mg,Fe)\ (Mg,Fe)\ Si\ Si\ O_6$$

$$(Mg,Fe)\quad Al\quad Al\ Si\ O_6$$

A ternary regular solution model for the M1 site, where Al, Mg and Fe mix has the form

$$RT\ ln\ \gamma_{en} = (X_{Al}^{M1})^2 W_{MgAl} + (X_{Fe}^{M1})^2 W_{MgFe} + X_{Fe}^{M1} X_{Al}^{M1} (W_{MgAl} + W_{MgFe} - W_{FeAl}) \quad (75)$$

$$RT\ ln\ \gamma_{MgTs} = (X_{Mg}^{M1})^2 W_{MgAl} + (X_{Fe}^{M1})^2 W_{FeAl} + X_{Mg}^{M1} X_{Fe}^{M1} (W_{MgAl} + W_{FeAl} - W_{MgFe}) \quad (76)$$

The assumptions of the above authors include the following:

(a) $W_{MgFe} = 0$,

(b) Mg-Al interactions are taken into account by the excess volume term,

(c) Fe-Al exchange reactions yield identical changes in partial molar volumes as Mg-Al exchange reactions.

With these assumptions equations (75) and (76) are simplified to

$$RT\ ln\ \gamma_{en} = X_{Fe}^{M1} X_{Al}^{M1}\ (-W_{FeAl}) \quad (77)$$

$$RT\ ln\ \gamma_{MgTs} = (X_{Fe}^{M1})^2\ W_{FeAl} + X_{Mg}^{M1} X_{Fe}^{M1}\ W_{FeAl} \quad (78)$$

which may be combined to give

$$RT\ ln\ \gamma_{en} + RT\ ln\ \gamma_{MgTs} = [(X_{Fe}^{M1})^2 + X_{Mg}^{M1} X_{Fe}^{M1} - X_{Fe}^{M1} X_{Al}^{M1}]\ W_{FeAl} \quad (79)$$

Wood (1974) took account of Fe-Al non-idealities and those of Fe-Mg by a term of the form $10450(Fe/Fe+Mg)(1-2X_{Al}^{M1})$. Harley (1981) applied an apparent W_{FeAl} for the same purpose, which is $W_{FeAl} = 5157$. In the following discussions this apparent W_{FeAl} is adopted.

In FMAS, garnet consists of the two endmembers almandine and pyrope. As pointed out previously, the use of $K_D(B')$ (eq. 74) implies a grouping of Fe and Mg in both garnet and pyroxenes. In FMAS $X_{Mg}^{gt} + X_{Fe}^{gt} = (1 - X_{Ca}^{gt}) = 1$, $X_{Al}^{gt} = 1$, $X_{Mg}^{M2} = 1$ and $X_{Mg,Fe}^{M1} = (1 - X_{Al}^{M1})$ and thus equation (74) is simplified to

$$K_D(B')_{FMAS} = \frac{1}{X_{Al}^{M1}(1 - X_{Al}^{M1})} \tag{80}$$

Rearranging equation (11) to give a solution for P we derive the barometric expression for FMAS

$$P_{FMAS} = \frac{1}{dV_r}\left(\left(-RT\ ln\ K_D(B')_{FMAS} - [(X_{Fe}^{M1})^2 + X_{Mg}^{M1}X_{Fe}^{M1} - X_{Fe}^{M1}X_{Al}^{M1}]W_{FeAl}\right) - dH(B) + TdS(B)\right) \tag{81}$$

In CFMAS the Ca in garnet has to be considered. With the assumption that $W_{FeMg} = 0$ the garnet is modelled as a ternary regular solution, so that by analogy to the orthopyroxene the non-ideal contribution of garnet to the change in free energy becomes

$$RT\ ln\ \gamma_{py} = 3(X_{Ca})^2 W_{CaMg} + 3X_{Fe}X_{Ca}(W_{CaMg} - W_{FeCa}) \tag{82}$$

and the barometric formulation for CFMAS is

$$P_{CFMAS} = \frac{1}{dV_r}\left(\left(-RT\ ln\ K_D(B') - [(X_{Fe}^{M1})^2 + X_{Mg}^{M1}X_{Fe}^{M1} - X_{Fe}^{M1}X_{Al}^{M1}]^{opx} W_{FeAl} + 3(X_{Ca}^{gt})^2 W_{CaMg} + 3X_{Fe}^{gt}X_{Ca}^{gt}(W_{CaMg} - W_{CaFe})\right) - dH(B) + TdS(B)\right) \quad (83)$$

The size of the parameter $(W_{CaMg} - W_{CaFe})$ under the assumption that $W_{FeMg} = 0$ and with a volume correction for $X_{Al}(opx)$, has been estimated by Harley (1981) to be 2530 cals. This value has been adopted.

It should be emphasized that the parameters used here (i.e. $[(X_{Fe}^{M1})^2 + X_{Mg}^{M1}X_{Fe}^{M1} - X_{Fe}^{M1}X_{Al}^{M1}]$ and $[3(X_{Ca}^{gt})^2 W_{CaMg} + 3X_{Fe}^{gt}X_{Ca}^{gt}(W_{CaMg} - W_{FeCa})]$ are different from Harley (1981, 1982) who used $(1-X_{Al}^{M1})$ $(1-2X_{Al}^{M1})$ [1-(Mg/Mg+Fe)] and $3X_{Ca}^{gt}[1-(1-X_{Ca}^{gt})(Mg/Mg+Fe)]$ to describe the non-idealities. The formulation used here comes from the straightforward application of ternary regular solution models for both orthopyroxene and garnet. All other contributions are assumed to be taken into account by the values of the apparent interaction parameters. The validity of this empirical approach is evidenced by the good agreement between calculated and experimental pressures, when equations (81) and (83) are applied to the experimental data of Harley (1981) and Wood (1974). This is shown in figs. 46 and 47.

Major differences between calculated and nominal run pressures exist for the experiment (T-821) at 1200°C and 30 kb of Harley (1981) and the four experiments of Wood (1974) in FMAS at pressures greater or equal to 25 kb. Run T-821 of Harley was performed with a multibore capsule containing four different mixes. It is for this reason that several estimates appear in figs. 46 and 47 for this experiment. Harley (1981) reported melting and partial chemical exchange between the mixes. Hence there may be good reasons for disagreement of calculated and run pressure and the date are not necessarily in conflict with the barometric formulations.

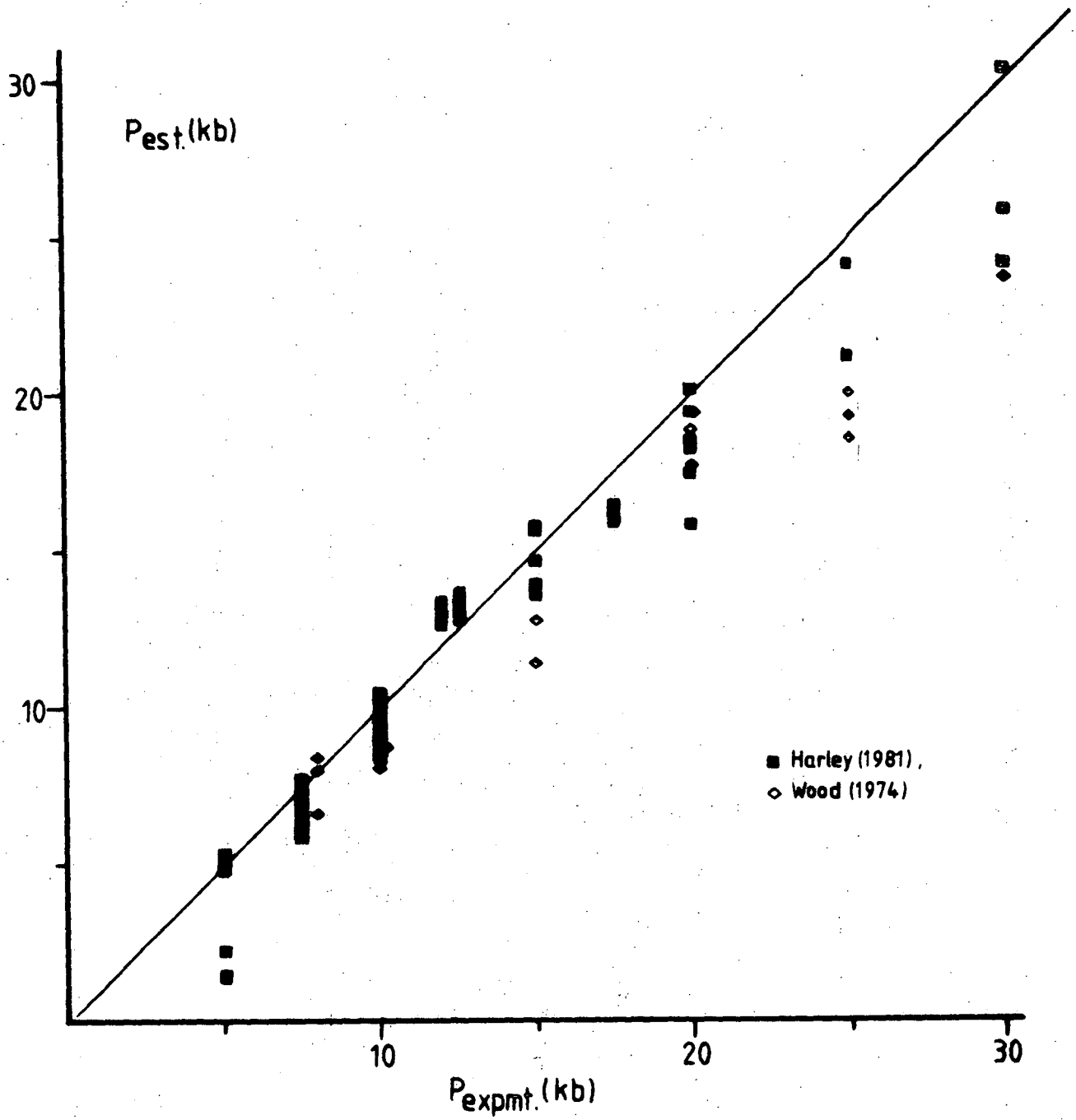

Figure 46: Comparison of pressures estimated via equation (81) and nominal run pressures for data in FMAS by Harley (1981) and Wood (1974).

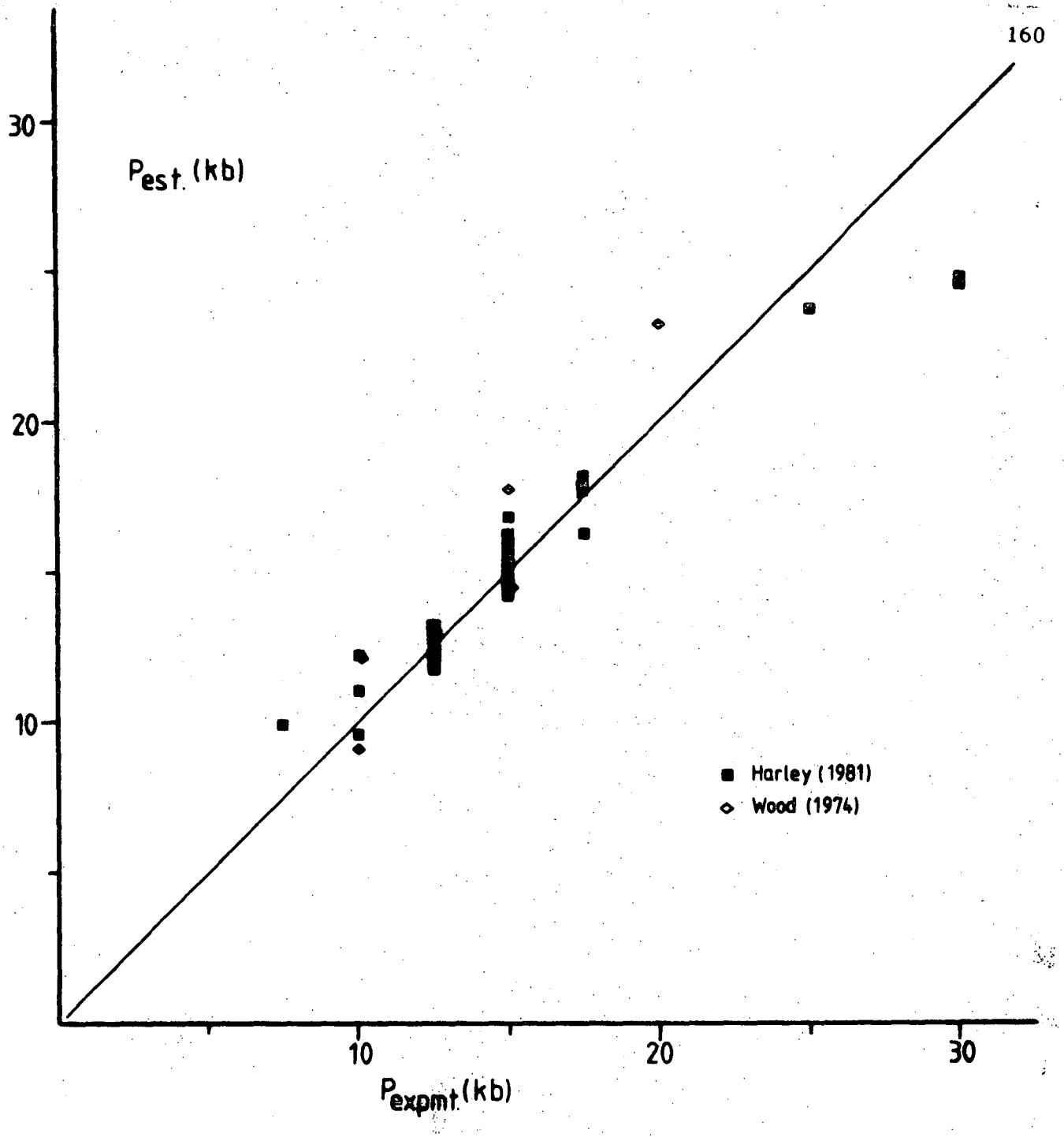

Figure 47: Comparison of pressure estimates via equation (83) and nominal run pressures for data in CFMAS of Harley (1981) and Wood (1974).

Figure 17: Comparison of pressure estimates via equation (83) and nominal rim pressures for data in CYMAS of Morley (1981) and Wood (1974).

The differences between estimated and nominal run pressures in the four experiments of Wood (1974) in FMAS are not well understood and cast some doubt on the validity of the approach used herein for FMAS. However, Wood's (1974) experiments are greatly outnumbered by those of Harley (1981) and there is good agreement between both data sets in CFMAS and accordingly in estimated pressures using equation (83).

36.2 MULTICOMPONENT SYSTEMS

The appearance of Cr in both orthopyroxene and garnet leads to somewhat more complex formulations than in the CFMAS and SMACCR systems, and introduces new parameters in thermodynamic equations.

Under the same assumptions as for simple systems, i.e. neglect the non-ideal contribution of Ca in orthopyroxene and assuming that Mg-Fe cross-site interactions are taken into account by the apparent W_{FeAl}, the orthopyroxene is modelled as a quarternary regular solution, where Mg, Fe Al and Cr mix on the M1 site. Thus we have

$$\begin{aligned} RT\ ln\ \gamma_{Mg_2Si_2O_6} = {} & (X^{M1}_{Fe})^2 W_{MgFe} + (X^{M1}_{Al})^2 W_{MgAl} + (X^{M1}_{Cr})^2 W_{MgCr} \\ & + X^{M1}_{Fe} X^{M1}_{Al} (W_{MgFe} + W_{MgAl} - W_{FeAl}) \\ & + X^{M1}_{Fe} X^{M1}_{Cr} (W_{MgFe} + W_{MgCr} - W_{FeCr}) \\ & + X^{M1}_{Al} X^{M1}_{Cr} (W_{MgAl} + W_{MgCr} - W_{CrAl}) \end{aligned} \tag{84}$$

$$\begin{aligned} RT\ ln\ \gamma_{MgAl_2SiO_6} = {} & (X^{M1}_{Mg})^2 W_{MgAl} + (X^{M1}_{Fe})^2 W_{FeAl} + (X^{M1}_{Cr})^2 W_{CrAl} \\ & + X^{M1}_{Mg} X^{M1}_{Fe} (W_{MgAl} + W_{FeAl} - W_{MgFe}) \\ & + X^{M1}_{Mg} X^{M1}_{Cr} (W_{MgAl} + W_{CrAl} - W_{MgCr}) \\ & + X_{Fe} X_{Cr} (W_{FeAl} + W_{CrAl} - W_{FeCr}) \end{aligned} \tag{85}$$

While assumptions regarding the Mg-Al interaction and Fe-Mg relationships have been discussed and the W_{MgFe} and the W_{MgAl} are set to be 0, little is known about Mg-Cr and Fe-Cr interactions. By analogy with the Mg-Al interaction one may assume that the Mg-Cr contribution is taken into account by the volume term and hence is treated as being 0 as well. The size of W_{FeCr} is however unknown. The assumption is made here that $W_{FeCr} = W_{FeAl}$. The expressions for non-ideal mixing thus become

$$RT\ ln\ \gamma_{Mg_2Si_2O_6} = X^{M1}_{Fe}X^{M1}_{Al}[-W_{Fe(Cr,Al)}] + X^{M1}_{Fe}X^{M1}_{Cr}(-W_{Fe(Cr,Al)}) + X^{M1}_{Al}X^{M1}_{Cr}(-W_{CrAl}) \quad (86)$$

$$RT\ ln\ \gamma_{MgAl_2SiO_6} = (X^{M1}_{Fe})^2W_{Fe(Cr,Al)} + (X^{M1}_{Cr})^2W_{CrAl} + X^{M1}_{Mg}X^{M1}_{Fe}\,W_{Fe(Cr,Al)} + X^{M1}_{Mg}X^{M1}_{Cr}\,W_{CrAl} + X^{M1}_{Fe}X^{M1}_{Cr}\,W_{CrAl} \quad (87)$$

On combining the two expressions we have

$$RT\ ln\ \gamma_{en} + RT\ ln\ \gamma_{MgTs} = [(X^{M1}_{Cr})^2+X^{M1}_{Mg}X^{M1}_{Cr}+X^{M1}_{Fe}X^{M1}_{Cr}-X^{M1}_{Al}X^{M1}_{Cr}]W_{CrAl} + [(X^{M1}_{Fe})^2+X^{M1}_{Mg}X^{M1}_{Fe}-X^{M1}_{Fe}X^{M1}_{Cr}-X^{M1}_{Fe}X^{M1}_{Al}]W_{Fe(Cr,Al)} \quad (88)$$

Comparing the sizes of the parameters $[(X^{M1}_{Cr})^2+X^{M1}_{Fe}X^{M1}_{Cr}]$ with $X^{M1}_{Al}X^{M1}_{Cr}$ and also $(X^{M1}_{Fe})^2$ with $(X^{M1}_{Fe}X^{M1}_{Al}+X^{M1}_{Fe}X^{M1}_{Cr})$, which appear in equation (88) with opposite signs, it is apparent that they will be of little influence, because most garnet lherzolite orthopyroxenes contain only small amounts of Fe, Al or Cr in the M1 position. Accordingly, they may be neglected without introducing much uncertainty as long as only the highly magnesian lherzolites are concerned. The equation for the contribution of non-ideal mixing of pyroxenes to the change of free energy of reaction (B) is then simplified to

$$RT\ ln\ \gamma_{en} + RT\ ln\ \gamma_{MgTs} = X_{Mg}^{M1}X_{Cr}^{M1}\ W_{CrAl} + X_{Mg}^{M1}X_{Fe}^{M1}\ W_{Fe(Cr,Al)} \quad (89)$$

The incorporation of Fe in garnet changes the activity coefficient expressions for this phase as well. On the dedecahedral (or A) site we now have a mixing of Mg, Fe and Ca. Modelled as a ternary solution this results in

$$RT\ ln\ \gamma_{py}^{A} = 3(X_{Fe}^{gt})^2W_{FeMg} + 3(X_{Ca}^{gt})^2W_{CaMg} + 3\ X_{Fe}^{gt}X_{Ca}^{gt}(W_{FeMg}+W_{CaMg}-W_{FeCa}) \quad (90)$$

and simplifies with the assumption of ideal mixing of Mg and Fe to

$$RT\ ln\ \gamma_{py}^{A} = 3(X_{Ca}^{gt})^2W_{CaMg} + 3\ X_{Fe}^{gt}X_{Ca}^{gt}(W_{CaMg}-W_{FeCa}) \quad (91)$$

A volume-corrected estimation of the size of $(W_{CaMg}-W_{FeCa})$ term for garnet has been given by Harley (1981) and this value (2530 cals) is adopted.

The B-site (octahedral) remains a binary solution, because Fe^{+++} is neglected and is thus

$$RT\ ln\ \gamma_{py}^{B} = 2(X_{Cr}^{gt})^2W_{CrAl} \quad (92)$$

The reciprocal terms would have to consider Fe, because of the additional reaction

$Ca_3Cr_2Si_3O_{12}$	+	$Fe_3Al_2Si_3O_{12}$	=	$Ca_3Al_2Si_3O_{12}$	+ $Fe_3Cr_2Si_3O_{12}$ (G)
uvarovite		almandine		grossular	Fe-Cr garnet

Adopting the model of Wood & Nicholls (1978), this could be taken into account by an additional parameter of the form $X_{Fe}^{gt}X_{Cr}^{gt}dG_{rec}(G)$, where the $dG_{rec}(G)$ term is the standard change in Gibbs free energy of reaction (G). Wood & Nicholls argued on the basis of similar crystallochemical behaviour of Mg and Fe^{++} for an approximately equal size of dG of reactions (E) and (G). Yet one of the arguments of Wood & Nicholls (1978) for a large

size of $dG_{rec}(E)$ was that the endmember knorringite cannot be synthesized at low pressures. The minimum pressure needed to synthesize the endmember $Fe_3Cr_2Si_3O_{12}$ should thus be an indicator for the relative sizes of $dG_{rec}(E)$ and $dG_{rec}(G)$. Fursenko (1981) synthesized the Fe-Cr garnet at 80 kb. The lower limit of its stability was not established, but attempts at pressures $\leqq$40 kb failed to produce Fe-Cr garnet (Fursenko, 1981). The stability limit is therefore somewhere between 40 and 80 kb and thus much lower than that the knorringite (Irfune *et al.*, 1982; in excess of 100 kb). This is consistent with the differences in stabilities for the Mg and Fe endmembers pyrope and almandine. Pyrope cannot be synthesized at pressures below about 14 kb (Schreyer, 1967), whereas almandine has been synthesized at 2 kb and is predicted to be stable at atmospheric pressures below 785°C (Yoder, 1955). Studies on the join $Fe_3Al_2Si_3O_{12}$-$Mg_3Al_2Si_3O_{12}$ (Hsu & Burnham, 1969) confirm that only Fe-rich garnets are stable at low pressures.

A much lower stability limit for the Fe-Cr garnet relative to knorringite suggests a much smaller size of $dG_{rec}(G)$ compared to $dG_{rec}(E)$. Empirically a treatment of $dG_{rec}(G)$ as equal to $dG_{rec}(E)$ leads to pressure over-estimations for a number of the experiments performed in this study and to unreasonably high pressure estimates for natural rocks. It is therefore concluded that either $dG_{rec}(G)$ is indeed very small or that the influence of it is taken into acccount by the apparent $dG_{rec}(E)$ obtained in the study in the system SMACCR (chapter 27).

Garnet non-idealities of mixing are therefore expressed as

$$RT\ ln\ \gamma_{py} = 3(X_{Ca}^{gt})^2 W_{CaMg} + 3\ X_{Fe}^{gt} X_{Ca}^{gt} (W_{CaMg} - W_{FeCa}) + 2(X_{Cr}^{gt})^2 W_{CrAl} + X_{Ca}^{gt} X_{Cr}^{gt}\ dG_{rec}(E) \qquad (93)$$

so that the barometer takes the form

$$P = \frac{1}{dV_r} = \Big\{ -RT\ ln\ K_D(B') - 3(X_{Ca}^{gt})^2 W_{CaMg} - [2(X_{Cr}^{gt})^2 - X_{Mg}^{M1}X_{Cr}^{M1}]W_{CrAl} - 3\ X_{Fe}^{gt}X_{Ca}^{gt}(W_{CaMg} - W_{FeCa}) + X_{Mg}^{M1}X_{Fe}^{M1}\ W_{FeAl} - X_{Ca}^{gt}X_{Cr}^{gt}[dH_{rec}(E) - TdS_{rec}(E)] - dH(B) + TdS(B) \Big\} \quad (94)$$

Previously the following values were derived and adopted

$dH(B)$	=	-6047 cals	chapter 16 (this work)
$dS(B)$	=	-3.23 e.u.	" 16
W_{CrAl}	=	3400 cals	" 25.3
$dH_{rec}(E)$	=	90853 cals	" 27
$dS_{rec}(E)$	=	52.1 e.u.	" 27
W_{CaMg}	=	3000 cals	(Wood & Nicholls, 1978)
W_{FeAl}	=	5157 cals	(Harley, 1981)
$(W_{CaMg} - W_{FeCa})$	=	2530 cals	(Harley, 1981)
dV_r	=	$-(183.3 + 178.98\ X_{Al}^{M1}(1 - X_{Al}^{M1}))$	(Harley, 1981)

These values are substituted into equation (94) and thus we have

$$P = \frac{1}{[-(183.3 + 178.98\ X_{Al}^{M1}(1 - X_{Al}^{M1}))]} \Big\{ -RT\ ln \left[\frac{(1 - X_{Ca}^{gt})^3 (X_{Al}^{gt})^2}{X_{MF}^{M1}(X_{MF}^{M2})^2 X_{Al}^{M1}} \right] - 9000(X_{Ca}^{gt})^2 - 3400[2(X_{Cr}^{gt})^2 - X_{Mg}^{M1}X_{Cr}^{M1}] - 7590X_{Fe}^{gt}X_{Ca}^{gt} + 5157X_{Mg}^{M1}X_{Fe}^{M1} - X_{Ca}^{gt}X_{Cr}^{gt}(90853 - 52.1T) + 6047 - 3.23T \Big\} \quad (95)$$

37. GEOBAROMETRY BASED ON THE SOLUBILITY OF Cr_2O_3 IN ORTHOPYROXENE

As for the barometry based on the solubility of Al_2O_3 in orthopyroxene, the application of the Cr barometer requires the consideration of Fe. Accordingly enstatite and Mg-Cr-tschermaks are modelled as quarternary regular solutions. The expression for enstatite is then the same as before

$$RT\ ln\ \gamma_{Mg_2Si_2O_6} = X_{Fe}^{M1}X_{Al}^{M1}(-W_{FeAl}) + X_{Al}^{M1}X_{Cr}^{M1}(-W_{CrAl}) + X_{Fe}^{M1}X_{Cr}^{M1}(-W_{Fe(Cr,Al)}) \quad (86)$$

The full formulation for Mg-Cr-tschermak as a quarternary regular solution is

$$\begin{aligned} RT\ ln\ \gamma_{MgCrAlSiO_6} = {} & (X_{Mg}^{M1})^2W_{MgCr} + (X_{Al}^{M1})^2W_{CrAl} + (X_{Fe}^{M1})^2W_{FeCr} \\ & + X_{Mg}^{M1}X_{Al}^{M1}(W_{MgCr}+W_{CrAl}-W_{MgAl}) + X_{Mg}^{M1}X_{Fe}^{M1}(W_{MgCr}+W_{FeCr} \\ & -W_{MgFe}) + X_{Fe}^{M1}X_{Al}^{M1}(W_{CrAl}+W_{FeCr}-W_{FeAl}) \end{aligned} \quad (96)$$

Again it is assumed that W_{MgAl}, W_{MgCr} and W_{MgFe} can be treated as being 0 and $W_{FeCr} = W_{FeAl} = W_{Fe(Cr,Al)}$. This simplifies equation (96) to

$$\begin{aligned} RT\ ln\ \gamma_{MgCrAlSiO_6} = {} & (X_{Al}^{M1})^2W_{CrAl} + (X_{Fe}^{M1})^2W_{Fe(Cr,Al)} + X_{Mg}^{M1}X_{Al}^{M1}W_{CrAl} \\ & + X_{Mg}^{M1}X_{Fe}^{M1}\ W_{Fe(Cr,Al)} + X_{Fe}^{M1}X_{Al}^{M1}\ W_{CrAl} \end{aligned} \quad (97)$$

Combining the activity expressions (86) and (97) we have

$$\begin{aligned} RT\ ln\ \gamma_{en} + RT\ ln\ \gamma_{MgCrTs} = {} & [(X_{Al}^{M1})^2+X_{Mg}^{M1}X_{Al}^{M1}+X_{Fe}^{M1}X_{Al}^{M1}-X_{Al}^{M1}X_{Cr}^{M1}]W_{CrAl} \\ & + [(X_{Fe}^{M1})^2+X_{Mg}^{M1}X_{Fe}^{M1}-X_{Fe}^{M1}X_{Al}^{M1}-X_{Fe}^{M1}X_{Cr}^{M1}]W_{Fe(Cr,Al)} \end{aligned} \quad (98)$$

As for the Al barometry, the sizes and signs of the minor parameters in equation (98) [i.e. $((X^{M1}_{Al})^2+X^{M1}_{Fe}X^{M1}_{Al})$ vs. $-X^{M1}_{Al}X^{M1}_{Cr}$ and $(X^{M1}_{Fe})^2$ vs. $-(X^{M1}_{Fe}X^{M1}_{Al}+X^{M1}_{Fe}X^{M1}_{Cr})$] allow neglect of these terms. Equation (98) is then simplified to

$$RT\ ln\ \gamma_{en} + RT\ ln\ \gamma_{MgCrTs} = X^{M1}_{Mg}X^{M1}_{Al}\ W_{CrAl} + X^{M1}_{Mg}X^{M1}_{Fe}\ W_{Fe(Cr,Al)} \qquad (99)$$

The expression for non-ideal behaviour of pyrope has already been discussed and the equation

$$RT\ ln\ \gamma_{py} = 3(X^{gt}_{Ca})^2W_{CaMg} + 3X^{gt}_{Fe}X^{gt}_{Ca}(W_{CaMg}-W_{FeCa}) + 2(X^{gt}_{Cr})^2W_{CrAl} + X^{gt}_{Ca}X^{gt}_{Cr}\ dG_{rec}(E) \qquad (93)$$

was derived. The analogous formulation for knorringite is

$$RT\ ln\ \gamma_{kn} = 3(X^{gt}_{Ca})^2W_{CaMg} + 3X^{gt}_{Fe}X^{gt}_{Ca}(W_{CaMg}-W_{FeCa}) + 2(X^{gt}_{Al})^2W_{CrAl} + X^{gt}_{Ca}X^{gt}_{Al}\ dG_{rec}(E) \qquad (100)$$

Arranging the expressions in the manner appropriate to their position in the equation for the reaction (F), bearing in mind that two pairs of $Mg_2Si_2O_6$ + $MgCrAlSiO_6$ are involved, we have

$$\Sigma RT\ ln\ \gamma's_{reac(F)} = 6(X^{gt}_{Ca})^2W_{CaMg} + 6X^{gt}_{Fe}X^{gt}_{Ca}(W_{CaMg}-W_{FeCa}) + 2W_{CrAl}[(X^{gt}_{Al})^2+(X^{gt}_{Cr})^2-X^{M1}_{Mg}X^{M1}_{Al}] - 2W_{Fe(Cr,Al)}X^{M1}_{Mg}X^{M1}_{Fe} + X^{gt}_{Ca}(X^{gt}_{Al}+X^{gt}_{Cr})\ dG_{rec}(E) \qquad (101)$$

Neglecting Fe^{+++} as before, $X^{gt}_{Al}+X^{gt}_{Cr} = 1$, so that

$$\Sigma RT\ ln\ \gamma's_{reac(F)} = 6(X_{Ca}^{gt})^2 W_{CaMg} + 6X_{Fe}^{gt}X_{Ca}^{gt}(W_{CaMg}-W_{FeCa}) + X_{Ca}^{gt}(dH_{rec}-TdS_{rec}) + 2W_{CrAl}[(X_{Al}^{gt})^2+(X_{Cr}^{gt})^2 - X_{Mg}^{M1}X_{Al}^{M1}] - 2W_{Fe(Cr,Al)}X_{Mg}^{M1}X_{Fe}^{M1} \quad (102)$$

Therefore the barometer is formulated as

$$P = \frac{1}{dV_r}\left\{-RT\ ln\ K_D(F) - 6(X_{Ca}^{gt})^2 W_{CaMg} - 6X_{Fe}^{gt}X_{Ca}^{gt}(W_{CaMg}-W_{FeCa}) - X_{Ca}^{gt}(dH_{rec}-TdS_{rec}) - 2W_{CrAl}[(X_{Al}^{gt})^2+(X_{Cr}^{gt})^2-X_{Mg}^{M1}X_{Al}^{M1}] + 2W_{Fe(Cr,Al)}X_{Mg}^{M1}X_{Fe}^{M1} - dH(F) + TdS(F)\right\} \quad (103)$$

The following values have been derived and adopted previously:

$dH(F)$	=	-17716 cals	chapter 28 (this work)
$dS(F)$	=	-10.51 e.u.	" 28
$dH_{rec}(E)$	=	90853 cals	" 27
$dS_{rec}(E)$	=	52.1 e.u.	" 27
W_{CrAl}	=	3400 cals	" 25.3
$dV_r(F)$	=	$[-392.1 + 1346\ X_{Cr}^{M1}(1-X_{Cr}^{M1})]$ cals/kb	chapter 28
W_{CaMg}	=	3000 cals	(Wood & Nicholls, 1978),
		hence $6W_{CaMg}$ = 18000 cals	
W_{FeAl}	=	5157 cals	(Harley, 1981),
		hence $2W_{FeAl}$ = 10314 cals	
$(W_{CaMg}-W_{FeCa})$	=	2530 cals	(Harley, 1981),
		hence $6(W_{CaMg}-W_{FeCa})$ = 15180 cals.	

Substituting these values into equation (103) we have

$$P = \frac{1}{[-392.1 + 1346\ X_{Cr}^{M1}(1-X_{Cr}^{M1})]} \left\{ -RT\ ln \left(\frac{(1-X_{Ca}^{gt})^3\ X_{Al}^{gt}\ X_{Cr}^{gt}}{[X_{MF}^{M1}(X_{MF}^{M2})^2\ X_{Cr}^{M1}]} \right)^2 \right.$$

$$- 18000(X_{Ca}^{gt})^2 - 15180\ X_{Fe}^{gt}X_{Ca}^{gt} - X_{Ca}^{gt}(90853 - 52.1T) - 6800[(X_{Al}^{gt})^2$$

$$\left. + (X_{Cr}^{gt})^2 - X_{Mg}^{M1}X_{Al}^{M1}] + 10314\ X_{Mg}^{M1}X_{Fe}^{M1} + 17716 - 10.51T \right\} \qquad (104)$$

38. APPLICATION OF THE BAROMETERS TO EXPERIMENTAL AND NATURAL ROCKS

The results of the application of the two barometers to the experiments performed with complex natural rock starting compositions are listed in table 16 and shown in fig. 48.

Table 16: P estimates for experimental runs with mixes TP-40 and TP-40C at at 35 kb.

Mix	T(°C)	P(Al)	P(Cr)	ϕ P
TP-40	1000	34.2	32.4	33.3
TP-40C	1000	37.3	30.7	34.0
TP-40	1100	35.2	34.0	34.6
TP-40C	1100	37.9	33.9	35.9
TP-40	1200	32.9	32.5	32.7
TP-40C	1200	34.6	30.0	32.3
TP-40	1300	35.3	35.8	35.6
TP-40C	1300	36.4	31.1	33.7
TP-40	1400	34.0	34.8	34.4
TP-40C	1400	36.9	31.1	34.0

P(Al) = P estimated via eq. (95)
P(Cr) = P estimated via eq. (104)
ϕ P = mean of estimates.

From both table 16 and fig. 48, five features are apparent:

(a) estimates for the mixture with low Cr/Cr+Al ratio (TP-40) are closer to nominal run pressures for both Al and Cr barometers than for experiments with TP-40C (bimodal distribution of estimates between Al and Cr barometry in fig. 48).

(b) Al and Cr estimates are closer to each other in runs with TP-40 relative to those with TP-40C.

(c) estimates via Al barometry for runs with TP-40C have a small tendency to over-estimate pressures, becoming greater at lower temperatures.

(d) estimates via Cr barometry for runs with TP-40C have a greater tendency to under-estimate pressures (bimodal distribution within Cr barometry estimates in fig. 48).

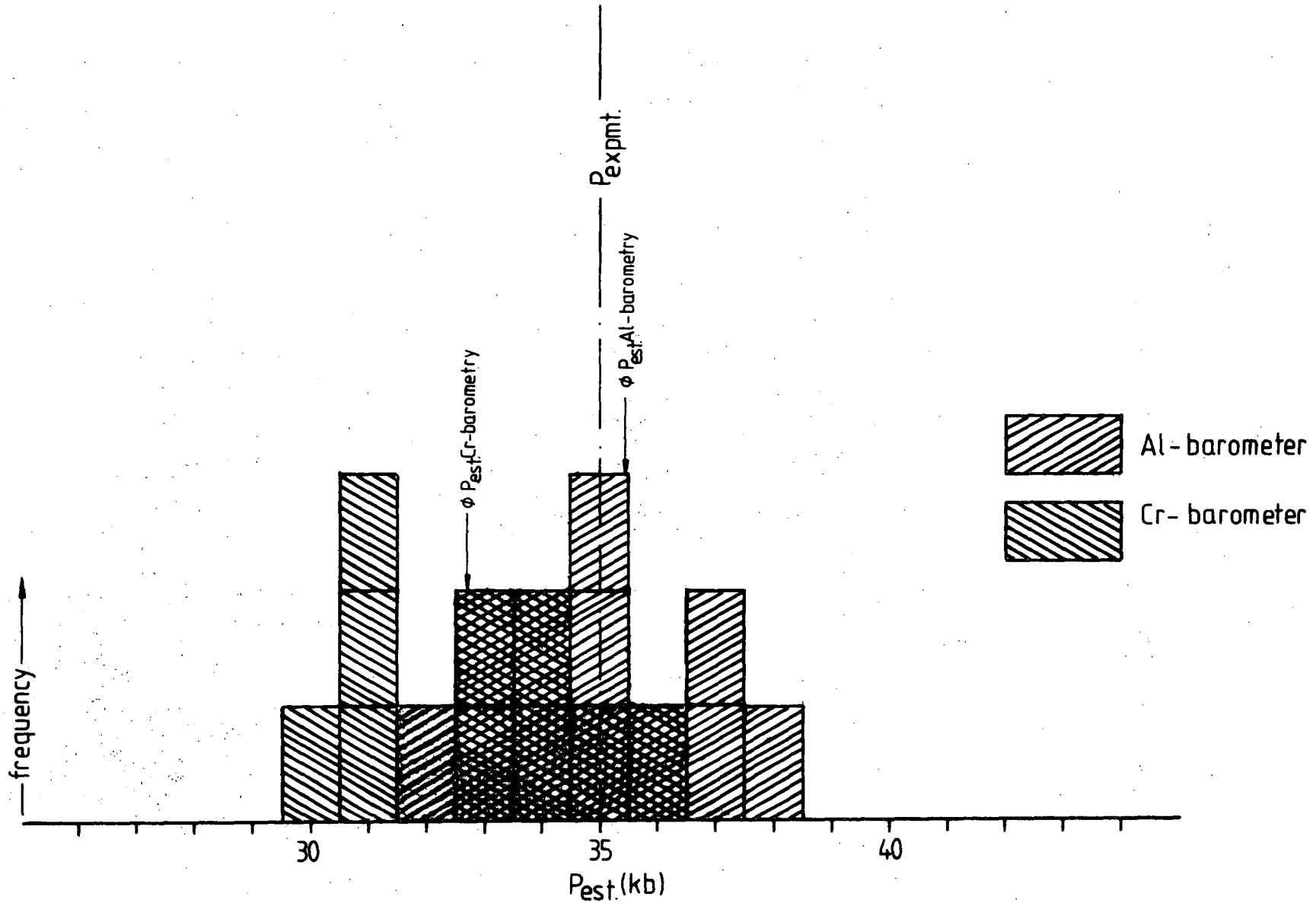

Figure 48: Histogram for pressure estimates via equations (95) (Al barometer) and (104) (Cr barometer) for experiments with TP-40 and TP-40C starting materials at 35 kb. Mean estimates for the individual barometers are indicated (ϕ P_{est}). The distribution and values of estimates are discussed in the text.

(e) differences in estimates between Al and Cr barometry tend to increase with decreasing temperature.

All five features result from a single cause, the chemical zoning of garnet. In runs with TP-40 (low Cr/Cr+Al) the garnets contain less Cr and so the difference between true rim composition and measured maximum Cr is smaller than in runs with TP-40C (high Cr/Cr+Al). Thus the relative error is smaller and this accounts for both better estimates and closeness of estimates. As pointed out before, garnet zoning is greater at low temperatures because reaction rates decrease. Thus it is expected that the difference between true rim composition and measured maximum should increase with decreasing temperature. The direction of zonation is towards higher Cr contents in the rims. Measured Cr contents of garnets which are lower than real rim compositions will lead to a higher K_D for Al barometry (because X_{Al}^{gt} is higher) and to a lower K_D for Cr barometry (because of the X_{Cr}^{gt} term). The relative error for X_{Al}^{gt} is smaller than for X_{Cr}^{gt}, because the first term is much larger than the second. Thus the error in estimation of pressures is such that the Cr barometer underestimates for the same reason that the Al barometer will over-estimate and the effect will be stronger on the Cr barometer relative to the Al barometer.

Applying the barometers to natural rocks one has to bear in mind the restrictions resulting from analytical uncertainties, calibration range and the empirical character of the barometers. The empirical character of the barometers implies that they should not be extrapolated far outside the calibrated range. Thus they should yield good results for the range 900-1400°C and 20-45 kb. Below 900°C uncertainties increase because of the increasing unreliability of the thermometer and because of extrapolation without experimental control, and thus estimates outside the 900-1400°C, 20-45 kb range should be treated with caution. The barometers are designed for garnet lherzolites. Low P/T rocks such as granulites

may be estimated by the method of Harley & Green (1982), which was calibrated at lower P-T conditions and was based on assemblages richer in Fe.

Analytical uncertainties become important when Al or Cr become small. For these cases both because of the position of the Al peak in the energy-dispersive spectrum utilized for microprobe analysis and the involvement of other minor elements in the calculation of X_{Al}^{M1} in orthopyroxene, analytical uncertainties will have an important effect on the accuracy of the pressure estimate. Minerals in which Al is only a very minor element ($\leqq$0.5 wt.%) are often inaccessible to the experimental set-up used (very low T, or higher P) and it is not certain whether the assumptions made for the relation between X_{Al}^{M1} and pressure/temperature can be extrapolated to these conditions. It is therefore recommended to use the Al barometer only if X_{Al}^{M1} exceeds 0.01 ($\cong$ 0.5 wt.%). Cr_2O_3 measurements have less problems and the Cr barometer may be used for X_{Cr}^{M1} as low as 0.005 ($\cong$ 0.2 wt.%). The third restriction due to the analytical uncertainties comes from garnet analysis. It is envisaged that the Cr barometer will yield good results where X_{Cr}^{gt} in garnet exceeds about .08 ($\cong$ 1.5 wt.%).

As far as garnet lherzolites are concerned few nodules will fall outside these restrictions and at least one barometer can be applied to almost all published data. In fig. 49 estimates for 100 nodules are plotted, which comply with the restrictions mentioned. If the two barometers work independently and each has an accuracy of about ±3.5 kb then it is expected that the estimates will scatter evenly around the 1:1 line. The difference in estimates is likely to range between 0 and 7 kb. This is confirmed by fig. 49. There is no good evidence for a systematic under- or over-estimation of either of the barometers and very few gross inconsistencies are present. Also there is no evidence for preferential under- or over-estimation with temperature. This is taken as evidence for the

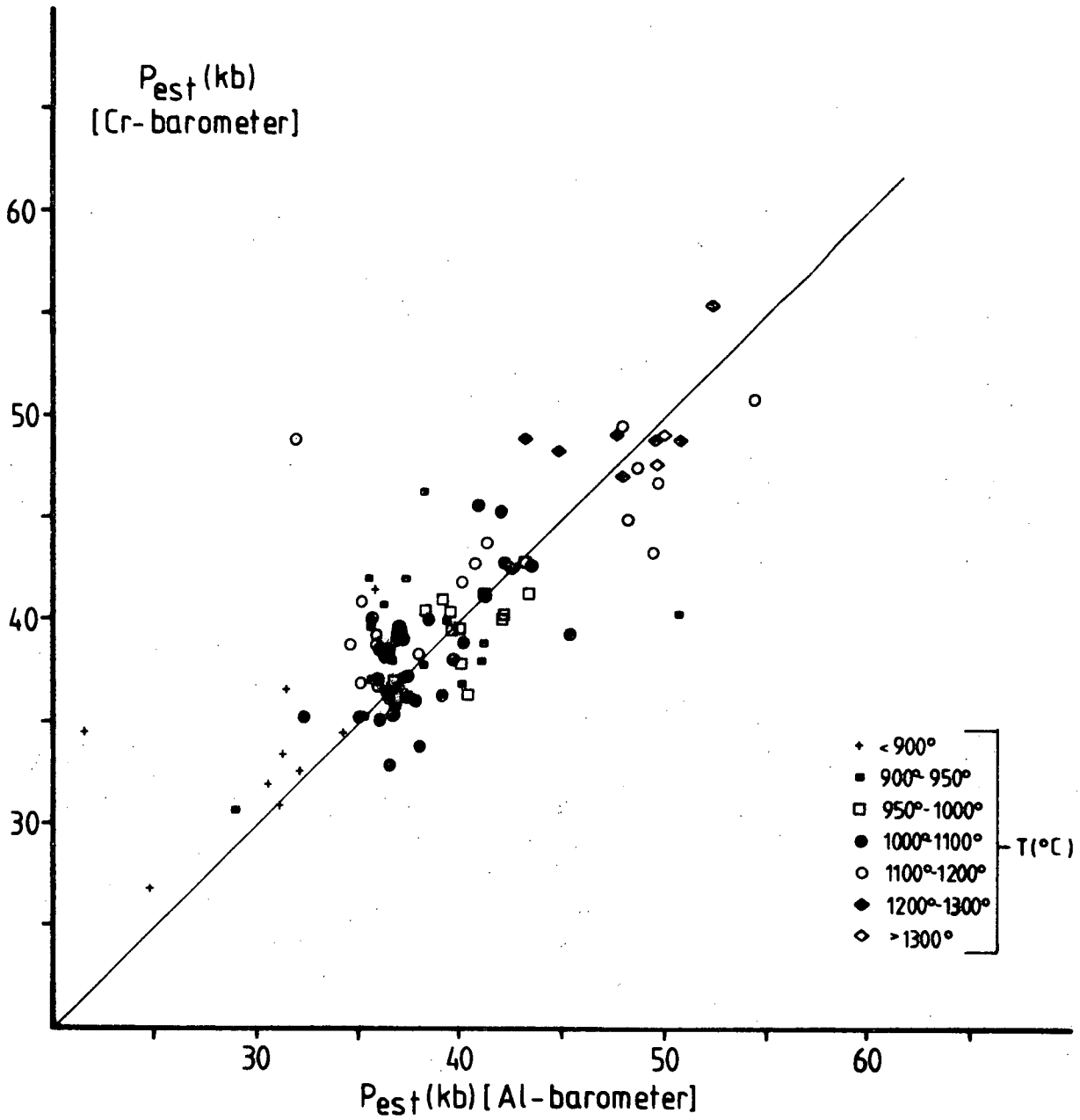

Figure 49: Comparison of pressure estimations via equations (95) (Al barometer) and (104) (Cr barometer) for natural garnet lherzolites from kimberlite and lamprophyre inclusions. Indicated temperatures are calculated by the method of Wells (1977). Data were obtained from Boyd (1974), Boyd & Nixon (1973, 1978), Boyd *et al.* (1976), Carswell *et al.* (1979), Carter Hearn & Boyd (1975), Cox *et al.* (1973), Danchin & Boyd (1976), Dawson *et al.* (1970), Ehrenberg (1979, 1982), Gurney *et al.* (1975), Mitchell (1977), Mori (1976), Reid *et al.* (1975), Sobolev (1977).

correct formulation of the barometers and that the systematic differences in estimates for the experiments are indeed the result of zonation in garnets.

This result is also demonstrated in fig. 50. In fig. 50 the estimates for five natural garnet lherzolites from South Africa are shown, which give a very narrow range of temperature estimates (930-960°C, using the Wells (1977) thermometer), but cover a large range of Cr contents in garnet. If these samples represent wallrock to kimberlite magma which was equilibrated at conditions typical for the province (i.e. under a similar geothermal gradient) then similar depths of origin are expected for all five samples. Both the Al barometer (eq. 95) and the Cr barometer (eq. 104) and their mean values $[(P_{Al\ barom} + P_{Cr\ barom})/2]$ give pressures indicating a similar pressure within the error level expected. A larger data set confirms that the pressure estimate does not correlate with the Cr content of the garnet (discussed later, see also fig. 56). The pressure estimates by the method of Wood (1974, eq. 12) show by contrast a correlation with the Cr content of the garnet. This was expected, because increasing Cr in garnet has a dilution effect on the $(X_{Al}^{gt})^2$ term in Wood's (1974) K_D, but is uncorrected for the influence of Cr on phase equilibria. Systematic and partly large under-estimations were already demonstrated using Wood's (1974) equation in the simple system (fig. 38b).

Summarizing, pressure-temperature conditions for garnet lherzolite xenoliths may be estimated by applying the cpx-opx thermometer in the form of Wells' (1977) equation and pressures via both barometers. If the mineral data comply with all restrictions, a mean pressure should be given as best estimate. Where only one barometer complies with the mineral composition constraints this estimate is likely to be better and should be taken as the preferred value. This procedure can easily be computerized and a simple example is given in appendix 7.

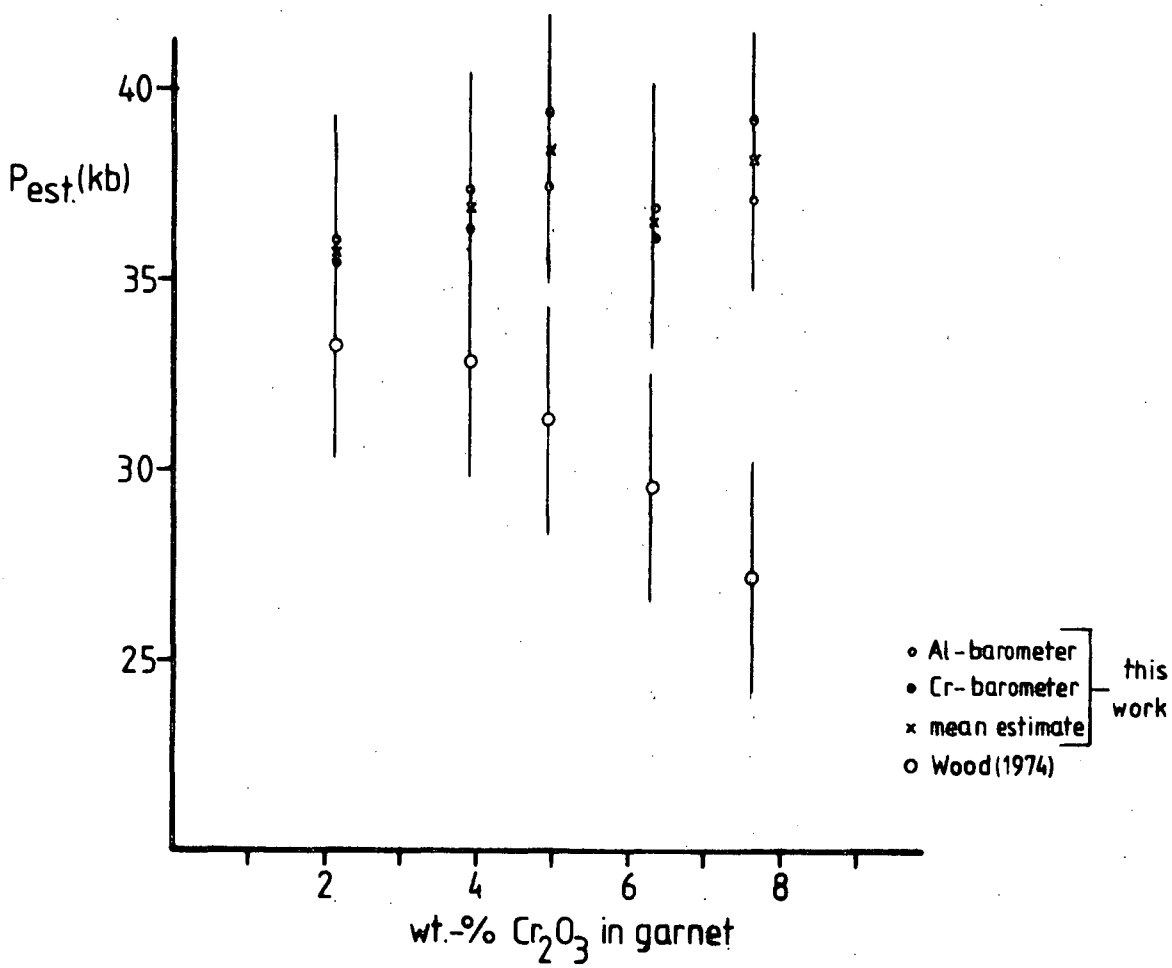

Figure 50: Plot of pressure estimates using equations (95) and (104) and mean values thereof and Wood's (1974) equation 12 in relation to the Cr content of garnet. The drawn error bars are ±3.5 kb for the barometry of this study and ±3 kb for Wood's (1974) method. All samples used come from South Africa and give temperature estimates (Wells, 1977) between 930-960°C. The samples are RVD-155, PTH 405, PTH 407, PHN 2767/1 and 1570 from Danchin & Boyd (1976), Carswell *et al.* (1979), Boyd & Nixon (1978) and Nixon & Boyd (1973a) respectively.

39. P-T ESTIMATES FOR NATURAL GARNET LHERZOLITES

Figs. 51 to 54 show the estimates of P and T for various suites of garnet lherzolite and a few garnet pyroxenite inclusions from kimberlite and other basaltic rocks from South Africa, Russia, North America, and the southwestern Pacific region.

Xenoliths can be grouped into low (<1100°C) and high (>1100°C) T xenoliths. Low temperature xenoliths from South Africa and Russia (figs. 51 and 52) follow approximately the proposed steady-state geotherm for shields of Clark & Ringwood (1964).

The estimates for high temperature xenoliths from South Africa show them as being derived from essentially one depth (about 48-51 kb, equivalent to about 150-160 km), but covering a range of temperatures from 1100-1400°C. The estimates at the highest temperatures are somewhat less reliable, because of the uncertain pressure effect on the pyroxene miscibility gap at high temperatures and pressures (Lindsley *et al.*, 1980; Brey, 1982). The agreement in pressure estimates is seen as significant, even if the absolute number contains some uncertainty.

From the literature descriptions it appears that all high temperature (>1100°C) xenoliths from South Africa are texturally of the "sheared" type (Nixon & Boyd, 1973a). However, two xenoliths from the Finsch mine (Shee *et al.*, 1982), being transitional between high and low temperature xenoliths (1050° and 1100°C), have been described as granular and low temperature xenoliths include both sheared (Bultfontein floors, Boyd & Nixon, 1978) and granular types. The textural grouping thus does not correlate with P-T grouping.

The bulk of the Russian samples from the Udachnaya mine (Sobolev, 1977; Boyd *et al.*, 1976) yield temperature estimates transitional between the low and high temperature (1050-1200°C) xenoliths as defined in the South African groups. Pressure estimates for Russian samples suffer from

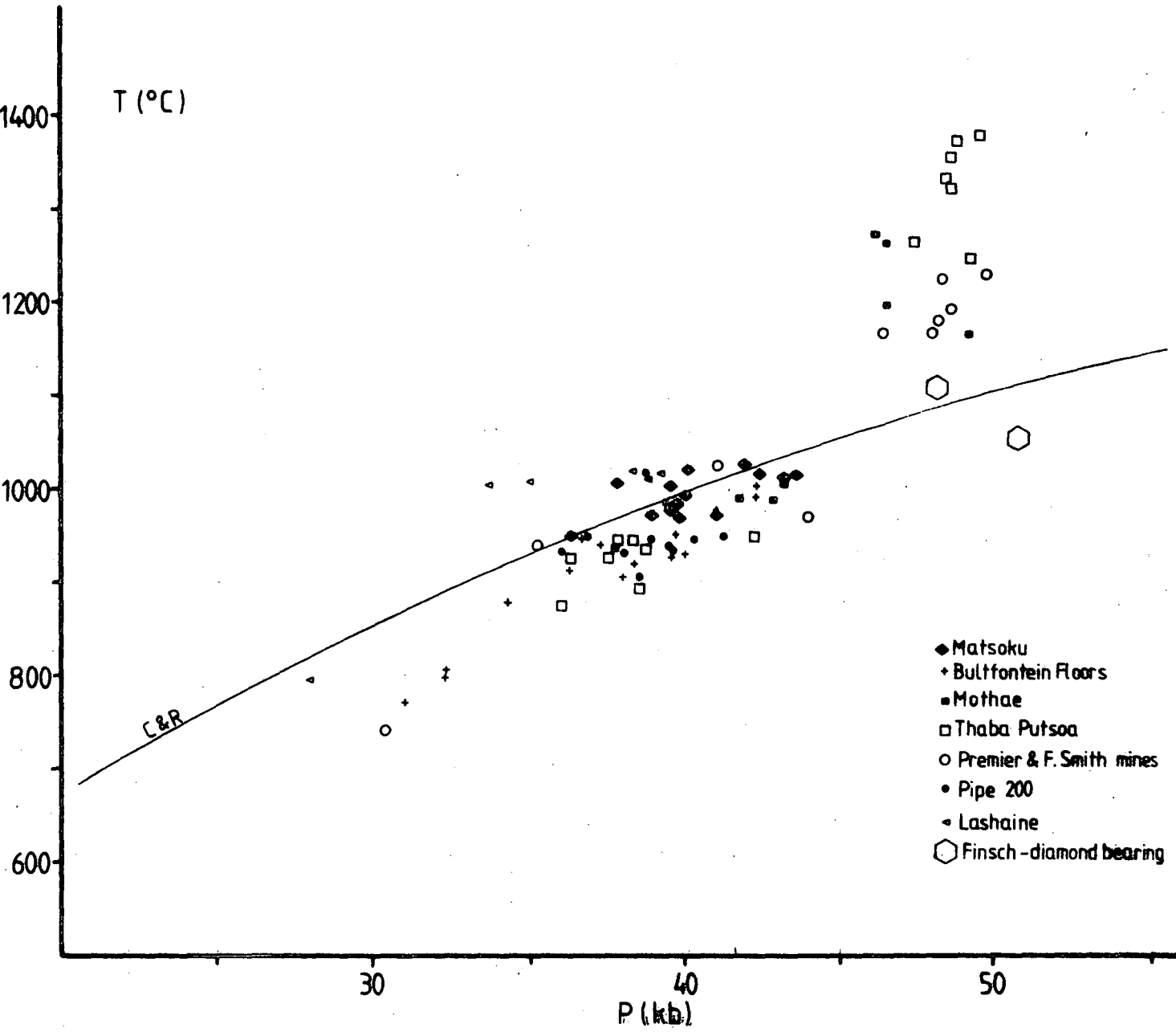

Figure 51: P,T estimates for garnet lherzolites and a few garnet pyroxenites from South Africa and Tanzania. Temperatures are estimated by the method of Wells (1977), P are estimates from Al barometry (eq. 95) and Cr barometry (eq. 104). Where compositional restrictions for the individual barometers (chapter) were met by both barometers, the mean estimate has been plotted, otherwise the value from the barometer complying with the restrictions was taken as best estimate (cf. appendix 7). Data sources: Boyd (1974), Boyd & Nixon (1978), Carswell *et al.* (1979), Cox *et al.* (1973), Danchin & Boyd (1976), Dawson *et al.* (1970), Dawson & Smith (1975), Gurney *et al.* (1975), Mori (1976), Nixon & Boyd (1973a), Reid *et al.* (1975) and Shee *et al.* (1982). Solid line is the geotherm of Clark & Ringwood (1964) for shields.

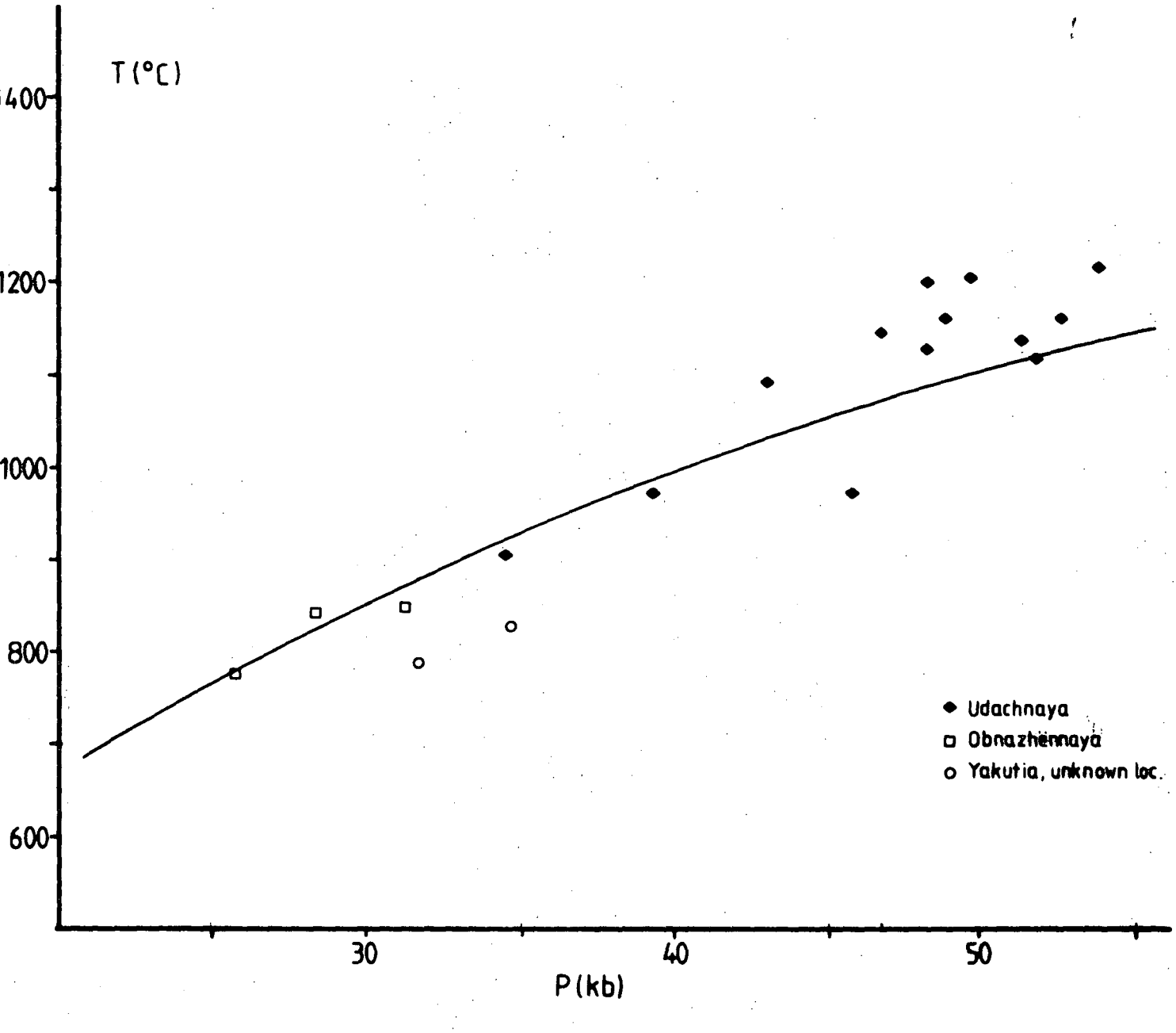

Figure 52: P,T estimates for garnet lherzolites from Russia. The plotted values were derived as outlined in fig. 50. Solid line = Clark & Ringwood (1964) geotherm for shields. Data from Boyd *et al.* (1976) and Sobolev (1977).

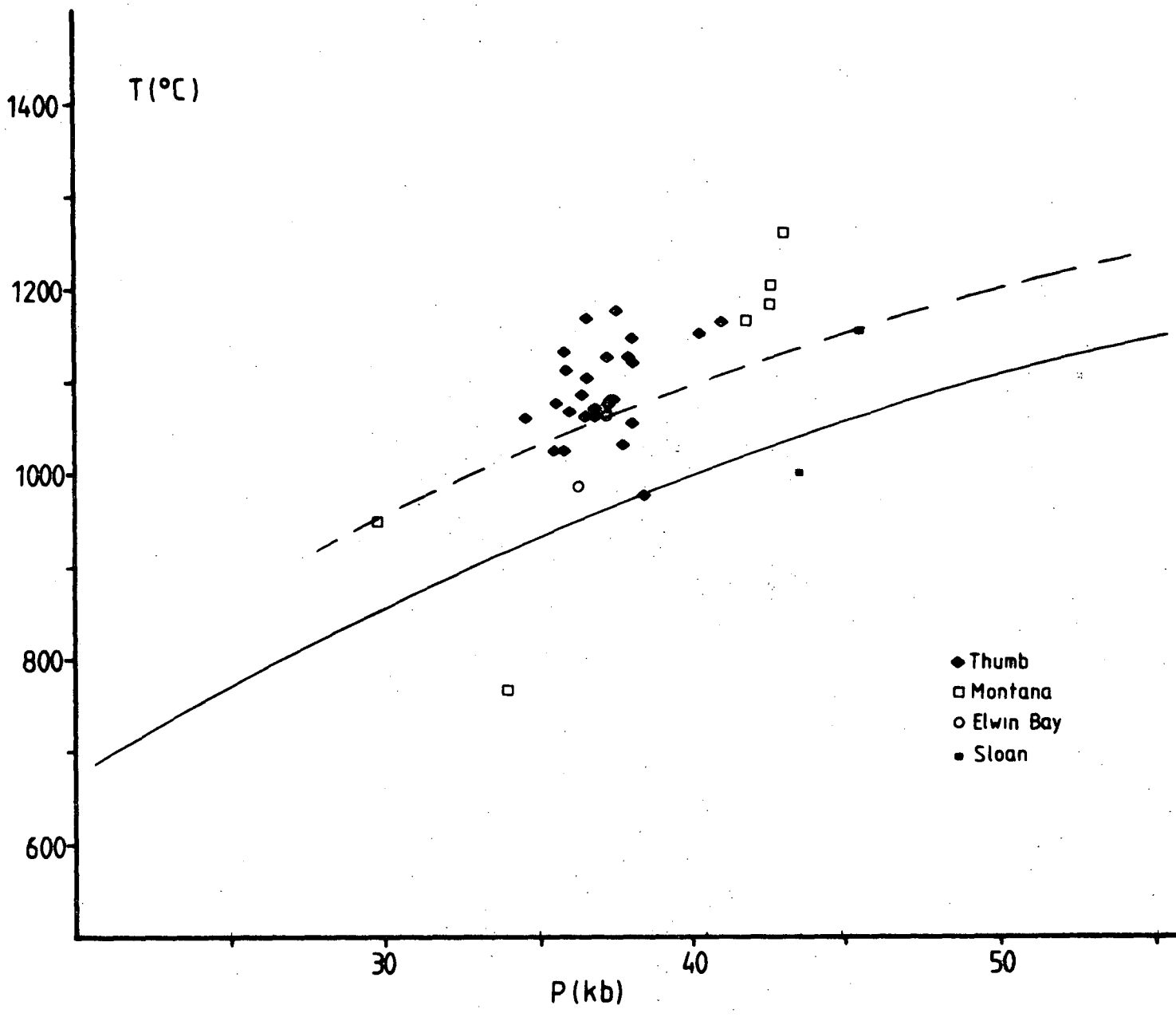

Figure 53: P,T estimates for garnet lherzolites from North America. The plotted values were derived as outlined in fig. 51. Solid line = Clark & Ringwood (1964) geotherm for shields, dashed line = Clark & Ringwood (1964) geotherm for younger continents (1.2 hfu). Data from Carter-Hearn & Boyd (1975), Ehrenberg (1979, 1982), McCallum & Eggler (1976) and Mitchell (1978).

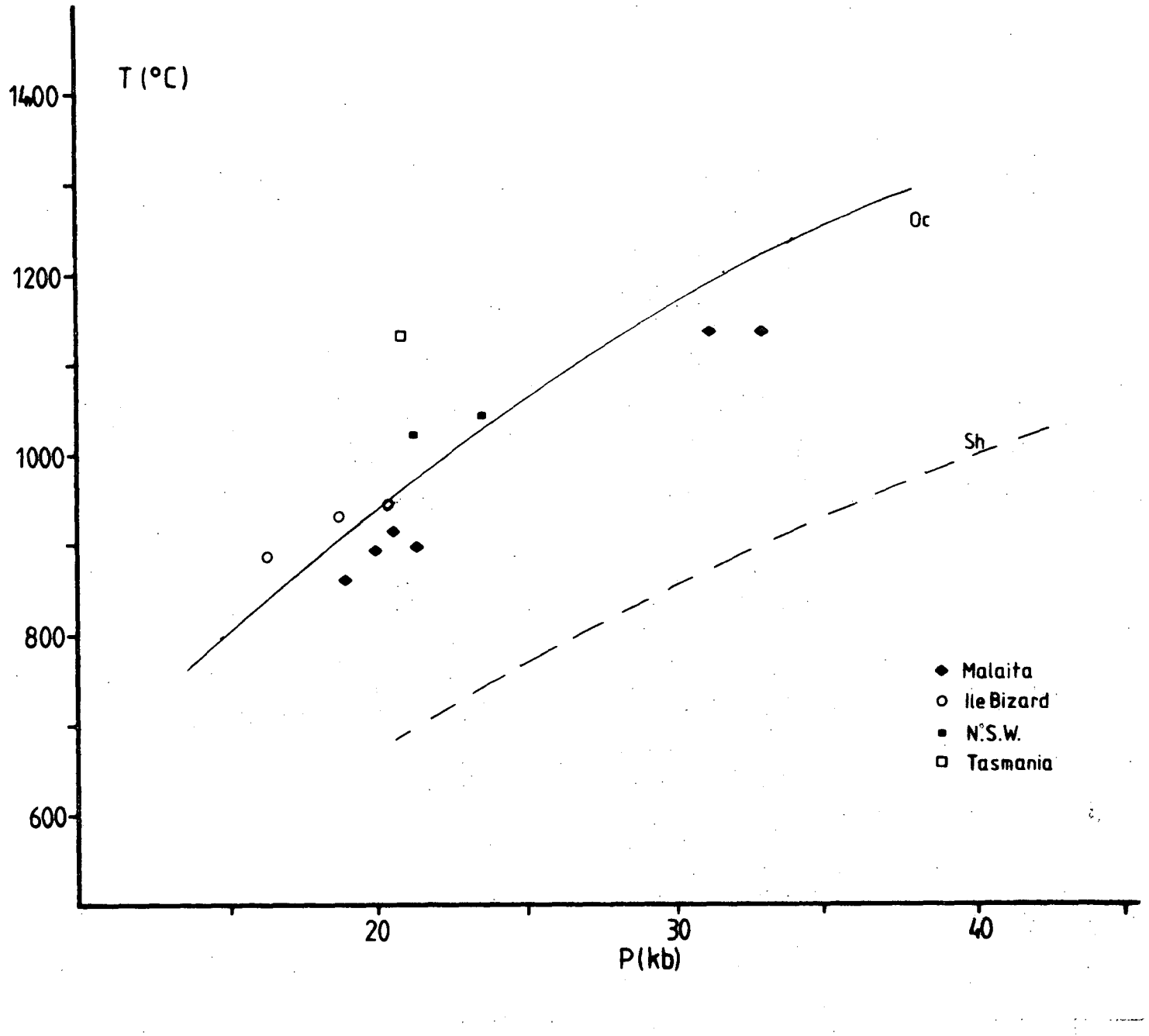

Figure 54: P,T estimates for garnet lherzolites from Ile Bizard (Canada) and the southwestern Pacific region. The plotted values were derived as outlined in fig. 51. Solid line = Clark & Ringwood (1964) geotherm for oceanic regions. Data from Ferguson & Sheraton (1979), Nixon & Boyd (1979), Raeside & Helmstaedt (1982), Sutherland & Hollis (1982).

very low Al concentrations in orthopyroxenes in many cases and accordingly only estimates based on the Cr barometer were considered in these samples. The pressure estimates for those Russian xenoliths transitional to high temperature types (1050-1200°C) are slightly higher (range of 48-54 kb) than those for South African nodules and show a systematic deviation from the Clark & Ringwood (1964) geotherm towards higher temperatures.

By contrast garnet lherzolites from minette in the Navajo volcanic district (The Thumb locality, Ehrenberg, 1979, 1982) cluster around 36-39 kb with a temperature range of approximately 1000-1200°C (fig. 53). Again no systematic differences in P-T estimates exist for different types (sheared/granular). These conditions of crystallization differ from those of the South African and Russian pipes and also from the "shield geotherm" of Clark & Ringwood (1964). The inferred P,T conditions are closer to a geotherm for younger continents with a higher heat flow. Data from garnet lherzolites in kimberlites from North America are sparse and the low number of data points (fig. 52) preclude a discussion of the Sloan, Montana and Elwin Bay examples.

Xenoliths in alnoite and basaltic rocks from the southwestern Pacific region (fig. 54) and Quebec, Canada, yield the lowest pressure estimates for xenolithic occurrences . Garnet lherzolites from Malaita (Solomon Islands), Ile Bizard (Canada) and New South Wales (Australia) are in good agreement with the steady-state geotherm for oceanic regions of Clark & Ringwood (1964). The exceptional high T/low P estimate for the sample from Tasmania (Australia) may be a reflection of its unusual occurrence (in basalt), but cannot be discussed until further information is available.

Megacryst suites have been used to infer P-T conditions from various localities (Boyd & Nixon, 1973; Eggler & McCallum, 1976; Eggler *et al.*, 1979; Garrison & Taylor, 1980). Unless a megacryst contains all phases necessary for P-T estimates (e.g. an orthopyroxene megacryst with

inclusions of clinopyroxene and garnet) there is no rational way of linking particular minerals from the megacryst suite for P,T estimates, i.e. assuming megacrysts relate to one event and one equilibrium assemblage. In particular, temperatures deduced from the composition of orthopyroxenes include very large uncertainties, because differences in X_{en}^{opx} or X_{di}^{opx} are very small for a wide range of temperatures. The barometers are very sensitive to temperature and thus the P estimates will be accordingly uncertain. Furthermore, this and the study of Harley (1981) have shown that the solubility of Al in orthopyroxene is sensitive to the composition of the coexisting garnet, not only in terms of the Ca content (which is usually fairly constant in megacrysts, Gurney *et al.*, 1979a), but also in terms of its Mg-value (correction factor $X_{Fe}^{gt}X_{Ca}^{gt}$ in barometric expressions) and its Cr content. This places further doubt on to the accuracy of P-T estimates for megacrysts. Such estimates are therefore regarded as giving a rough qualitative estimate at best and consequently no pressures or temperatures have been inferred for megacryst suites in this study.

P-T estimates for alpine-type garnet peridotite bodies are problematic for various reasons:

1. Geothermometry for alpine-type peridotites by means of the cpx-opx thermometer (Wells, 1977) yields generally low (<900°C) or very low estimates (<700°C for Norwegian peridotites, Medaris, 1980). As discussed in earlier sections and by Evans & Trommsdorff (1978) and Ehrenberg (1982), low estimates include large uncertainties. Uncertainties in temperature estimates result in uncertainties in pressure estimates.
2. The empirical nature of the barometers derived in this study placed restrictions on to the applicability (chapter 38). Pressure estimates for samples estimated to have equilibrated at ≤800°C are potentially inaccurate, because these conditions are outside the calibrated range. Additionally, garnet peridotites from the Alps (Evans & Trommsdorff, 1978) and Norway (Medaris, 1980) have orthopyroxenes with very low Al concentrations

and garnets with very low Cr contents. Thus the concentrations of X_{Al}^{M1} in orthopyroxene and Cr in garnet border or are below the calibrated range.

3. Minerals from alpine-type garnet peridotites are usually inhomogeneous and/or chemically zoned, reflecting retrograde metamorphism, secondary alteration and overprinting by later metamorphic events (Evans & Trommsdorff, 1978; Medaris, 1980; Obata, 1980). In particular, late metamorphic events involving the growth of aluminous hydrous phases at the expense of pyroxenes (Evans & Trommsdorff, 1978) may alter the chemistry of pyroxenes, so that their compositions may not reflect the earlier equilibrium with garnet.

Numerical values for the garnet peridotites from the Alps (Evans & Trommsdorff, 1978) lie between 33 and 37 kb for core compositions and 27 to 33 kb for rim compositions at temperatures around 830°C (±60°C). Even though high initial pressures of equilibration have been envisaged by Ernst (1978), it is believed that the uncertainties prohibit a better estimate than the "in excess of 20 kb" of Evans & Trommsdorff (1978).

Estimates for rocks from the garnet lherzolite facies of the Ronda Massif (Obata, 1980) can be obtained with a higher reliability, because both estimated temperatures (870-940°C) and Al contents in orthopyroxene are higher. However, opx-cpx pairs are only available from neoblasts within the assemblage and the estimates thus are values for varying stages of recrystallization during ascent and not the P,T conditions of the primary (before ascent) equilibration. The estimates range from 14-20 kb. The primary conditions of equilibration for the Ronda Massif are therefore also inferred to be in excess of 20 kb.

40. DISCUSSION OF P,T ESTIMATES FOR GARNET LHERZOLITE XENOLITHS AND A MODEL FOR THE PETROGENESIS OF LHERZOLITES, KIMBERLITES AND DIAMONDS

By far the greatest number of data for garnet lherzolite inclusions comes from kimberlite pipes of South Africa. The following discussion is therefore based primarily on these data. The good agreement between P,T estimates for the South African inclusions and the geotherm for shields of Clark & Ringwood (1964) suggests that low temperature xenoliths represent wallrock, which has equilibrated under the steady-state conditions of an old (Archaean) lithosphere. This is somewhat surprising, because the geotherm of Clark & Ringwood (1964) was calculated on the basis of heat-flow data and does not provide for any other heat source than conductive heat and internal heating due to radioactive decay, i.e. it is calculated for a non-convective model of the mantle. The data for low temperature xenoliths from South Africa thus suggest a negligible contribution of convective heat to this part of the upper mantle/ lithosphere, if the mantle beneath that region is convecting.

By contrast the high temperature xenoliths record a range of at least 300°C at practically one depth, clearly in disagreement with the steady-state conditions calculated by the shield geotherm of Clark & Ringwood (1964). Maintaining the non-convective model requires thus a heat source such as a "hot spot". In recent years, the idea of "whole mantle convection" has regained popularity and models in favour of this theory have been put forward (Rice, 1982; Peltier, 1980; Yuen *et al.*, 1981). In these models the lithosphere is behaving as a cold boundary layer (Jarvis & Peltier, 1982; Peltier & Jarvis, 1982), where vertical heat diffusion from flows is largely balanced by horizontal heat advection (Peltier, 1981). One of the results of the convection style of the authors mentioned is a temperature "overshoot" near the boundary layer over the temperature of the regions further below and above.

In this sense strongly perturbed geotherms are expected. The problem of heat and heat transfer between mantle and lithosphere is certainly far from being resolved (Jacoby & Schmeling, 1982), but the P,T distribution recorded in the South African xenoliths is in the light of the mentioned theories not necessarily inconsistent with convective mantle models.

Whatever the source of the heat, high temperature conditions existed at least temporarily at depths of about 150-160 km. Fig. 55 shows the range of P,T estimates for garnet lherzolites from South Africa, Russia and The Thumb locality (U.S.A.) in relation to the solidus for the system "pyrolite + 0.2% H_2O" (Green, 1973; Green & Liebermann, 1976). The solidus for pressures greater than 30 kb is similar for pyrolite + H_2O, pyrolite + H_2O + CO_2 or pyrolite-C-H-O (Green & Liebermann, 1976).

At the highest recorded P-T conditions for the garnet lherzolite xenoliths from South Africa partial melting of a peridotitic source would take place, if enough H_2O ± other volatiles are present. The volatile-rich character of kimberlitic magmas argues for the availability of volatiles in the source region of kimberlites. The degree of partial melting above the solidus is dependent on the amount and composition of volatiles present. For small amounts of H_2O (<0.4%) the xenoliths recording the highest temperatures of equilibration would contain partial melts (< or << 1%). At depths below the source of those xenoliths temperatures must be higher still. The liquidus for an average kimberlite composition from South Africa at about 160 km is in the vicinity of 1500°C, depending on X_{CO_2} (Eggler & Wendlandt, 1979). At these conditions the near-liquidus phases of kimberlite are those of a peridotite (olivine, orthopyroxene, clinopyroxene and garnet) (for X_{CO_2} = 0.5. Eggler & Wendlandt, 1979). Thus a kimberlite may be generated at conditions of about 1400-1500°C and at depths of about 160-180 km. These conditions are consistent with the assumption that kimberlite is formed as a small amount (≅1%) of partial melt of a peridotitic source rock (Wyllie, 1979).

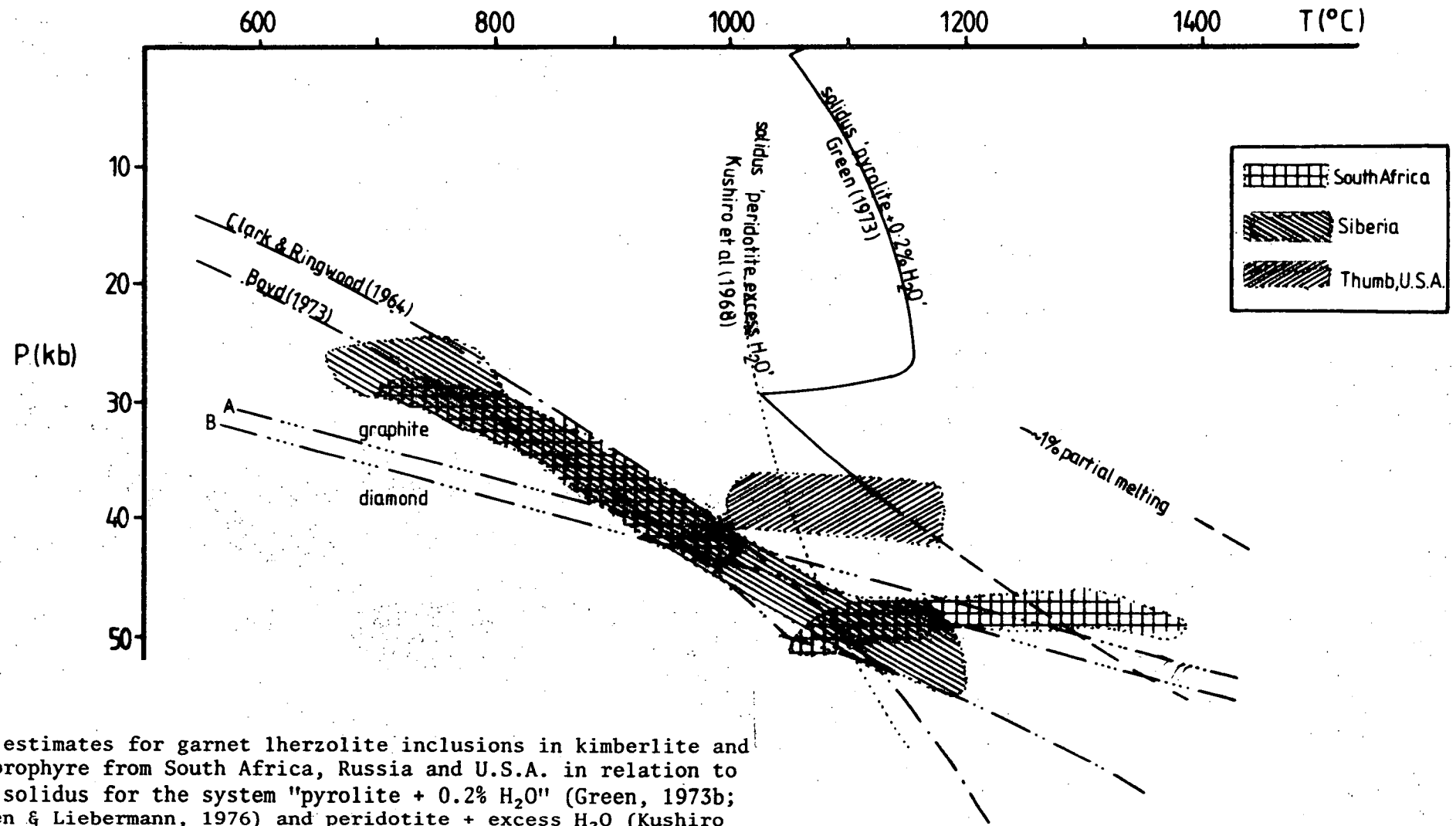

Figure 55: P,T estimates for garnet lherzolite inclusions in kimberlite and lamprophyre from South Africa, Russia and U.S.A. in relation to the solidus for the system "pyrolite + 0.2% H_2O" (Green, 1973b; Green & Liebermann, 1976) and peridotite + excess H_2O (Kushiro *et al.*, 1968). Shaded areas are ranges taken from figs.51-53.

— 1% — — approximate position of 1% partial melting of a peridotitic source with 0.2-0.05% H_2O from Green & Liebermann (1976).

— · — · — geotherm for shields (Clark & Ringwood, 1964).

— ·· — ·· — pyroxene geotherm (Boyd, 1973).

— ···· — ···· graphite-diamond stability limits after (A) Bundy *et al.* (1961) and (B) Kennedy & Kennedy (1976).

P,T conditions of approximately 1400-1500°C and 50-60 kb would produce partial melting of about 1% in the system "pyrolite + 0.2-0.5% H_2O" (Green & Liebermann, 1976). It is therefore inferred that the South African kimberlites were formed at those conditions.

The Mg-values and other characteristics of kimberlites (Dawson, 1980) suggest that kimberlite is a primitive magma with little or no fractionation. Yet one of the features commonly observed in kimberlites is the existence of large mono- or bimineralic crystals or nodules (megacrysts, discrete nodules), which show consistently lower Mg-values than the minerals of most lherzolites. Additionally, dunites with olivines with Mg-values as low as 84 (Nixon & Boyd, 1973b) are found within kimberlites. These megacryst suites point towards a fractionation/crystallization process taking place at mantle depth. Whether this process is active in a magma chamber or rather within a magma-crystal mush (Boyd & Nixon, 1978; Nixon & Boyd, 1973b; Gurney & Harte, 1980), it requires cooling of the kimberlite or protokimberlite magma. A cooling history for a magma precipitating megacrysts, diamonds and dunites may account for the wide range in chemistry found within these precipitates (Dawson, 1980; Gurney & Harte, 1980).

There are differing views on the rheologic behaviour of magmas (Sparks *et al.*, 1977; Wolff, 1980; Basu, 1980). However, slow ascent of xenolith-bearing magmas should result in an extensive re-equilibration of clino- and orthopyroxenes of lherzolite nodules to the temperature conditions of the transporting magma and would cause extensive partial melting within the nodules during ascent. As there is very little evidence for such a process and in particular the granular garnet lherzolite nodules retain a record of temperatures which are likely to be steady-state ambient mantle temperatures, it is believed that the ascent of kimberlitic magmas is a very fast process. Great speed precludes an effective fractionation process within the magma during ascent.

In analogy with the study on basanite (this work) it seems thus more likely that the megacrysts and cumulates were precipitated by earlier pulses of magmas rather than from the host kimberlite magma itself. The magma(s) precipitating those phases is not by necessity a kimberlite, nor do all megacrysts have to be precipitated from one magma or in one magmatic event, even though this has been inferred on the basis of similar chemical variations (Gurney *et al.*, 1979a). Many or most precipitates (megacrysts, diamonds, dunites) are therefore regarded as xenocrysts or xenoliths to the host kimberlite.

The inferred conditions for the formation of kimberlite and the model for the derivation of megacryst suites from pre-dating kimberlites or protokimberlitic magmas put constraints on the genesis of diamonds. At the inferred conditions of kimberlite formation (≅1400-1500°C and 50-60 kb) diamond is not stable. Any form of carbon would be concentrated into the melt in the form of a $(CO_3)^{--}$ ion, because of the high solubility of CO_2 in under-saturated magmas (Brey & Green, 1975, 1976). If a kimberlitic magma is however injected into the adjacent wallrock and cools/crystallizes there under sufficiently low fO_2, C would crystallize as diamond.

Inclusions in diamonds have several distinct features:

(a) two broad groups of inclusions occur (eclogitic and peridotitic) (Tsai *et al.*, 1979);

(b) both groups are accompanied by inclusions of sulphides and/or graphite (Gurney *et al.*, 1979);

(c) garnets from diamond inclusions of the peridotitic suite are generally more magnesian, contain more Cr and are poor in Ca relative to the minerals of garnet lherzolite inclusions from the kimberlite (Meyer & Boyd, 1972; Shee *et al.*, 1982);

(d) olivines from inclusions in diamond contain up to 10 times as much Cr as olivines from lherzolite nodules (Meyer, 1975); and

(e) P,T estimates for the peridotitic suite of diamond inclusions yield temperature values lower than most high-temperature garnet lherzolite xenoliths and pressures similar to those (Dawson, 1980; Hervig *et al.*, 1980; Shee *et al.*, 1982).

These features are explicable in the light of the model outlined above. Diamonds crystallize from a pre-dating protokimberlite or kimberlite, which has the peridotitic phases near its liquidus (Eggler & Wendlandt, 1979). Alternatively, eclogitic phases including diamonds may precipitate at a more evolved stage of kimberlite crystallization. The mineral chemistry of early crystallizing phases may have the characteristics of the inclusions found within diamond (Harte *et al.*, 1980). The fO_2 conditions for the crystallization are very low, accounting for the growth of diamond rather than carbonates and the high Cr content of olivines, which contain probably some Cr^{++} (Meyer, 1975; Hervig *et al.*, 1980). Inclusions in diamond are sheltered from re-equilibration with the further crystallizing magma, retaining the refractory character of the initial precipitates. Immiscible sulphide liquids may account for the sulphide inclusions in diamonds (Fesq *et al.*, 1975). The further crystallization of the magma leads to the formation of the megacryst suites and recent studies suggest that some megacryst assemblages in diamondiferous kimberlites fill the compositional gap between inclusions in diamonds and coarse grained xenoliths (Gurney & Harris, 1982). In rare cases a kimberlitic magma may infiltrate the wallrock along cracks and the late crystallizing phases may completely equilibrate with the wallrock under subsolidus conditions, leaving diamonds with or without inclusions within the matrix of a garnet peridotite. This process could account for the rare occurrences of diamonds in garnet lherzolites (Dawson & Smith, 1975; Shee *et al.*, 1982; Pokhilenko *et al.*, 1976). In general diamond should be more frequently associated with megacrysts and other

precipitates such as igneous eclogites, which is the case (Pokhilenko *et al.*, 1976).

This model together with the constraints that the wallrock at levels shallower than about 145 km has ambient temperatures in accord with the shield geotherm (Clark & Ringwood, 1964) and the data on the graphite-diamond inversion (Bundy *et al.*, 1961; Kennedy & Kennedy, 1976) predicts P,T conditions for the crystallization of diamond.

The conditions at which diamond may crystallize, along with its inclusions and coexisting silicate phases, are equated with the conditions of crystallization of lherzolite and eclogite xenoliths, some of which are diamond-bearing. Although the parent magmas to those crystallizing diamond may be initially at $T > 1400°C$, $P \geq 55$ kb, diamond cannot begin to crystallize at $T > 1300°C$, $P = 55$ kb (see fig. 55 for the relationship of diamond stability field and conditions of crystallization of xenoliths). Obviously, the diamond-precipitating magmas cannot cool to temperatures below the ambient conditions, i.e. 900-970°C at 40 kb. Thus, considering the range of mantle P,T conditions defined by the South African lherzolite xenoliths, including diamond-bearing examples, there is a "diamond window" of 900-1300°C and 40-55 kb in which diamond crystallization occurred. These conditions are very close to the experimentally determined diamond-graphite boundary.

Temperature and pressure estimates for inclusions in diamond are problematic, because a full set of minerals required to give an estimate via the method of this work is rarely present in one diamond. However, T estimates via methods other than cpx-opx thermometry do show the expected range (Dawson, 1980; Hervig *et al.*, 1980; Shee *et al.*, 1982) and the presence of both graphite and diamond within single eclogites of inferred igneous origin (Hatton & Gurney, 1979) suggests conditions close to the graphite-diamond inversion. This window also places limits on the geographical distribution of diamond-bearing igneous rocks.

This window also places limits on the geographical distribution of diamond-bearing igneous rocks. The relatively low temperatures required for the formation of diamond at these depths exist only in areas with an old lithosphere. Younger parts of continents have higher ambient temperatures for equal depths and will not allow the crystallization of diamonds. This explains why diamond-bearing igneous rocks are found within or adjacent to ancient shields, while those in younger areas are barren.

The characteristics of diamond and its inclusions can thus be explained without a chemical zonation of the upper mantle and/or deeper levels for diamond formation (Irfune *et al.*, 1982). Irfune *et al.* (1982) suggested that the upper mantle is chemically zoned in respect to Cr, where Cr-richer compositions are concentrated at deeper levels and that the Cr/Cr+Al value of garnet is an indicator for the equilibration pressure. Fig. 56 shows the P,T estimates for South African garnet lherzolites in respect to the Cr content of garnet. It is apparent that there is no correlation between the Cr content of garnet from lherzolites and the P,T condition of equilibration. In particular, garnets with Cr contents of up to 4 wt.% cover the entire range of P,T estimates and garnets with higher Cr contents occur also more or less evenly distributed over the greater part of the data range. It seems more likely that the Cr content of garnet is a reflection of the Cr content of the bulk rock composition and that the continental upper mantle is heterogeneous in its chemistry. In analogy with the results on spinel lherzolites from Lake Bullenmerri (Part I, this work) it is suggested that this heterogeneity is due to depletion by partial melting events with various degrees of extraction of magma. Like the uppermost mantle, all degrees of depletion may occur at any one depth. Unlike the uppermost mantle beneath areas of under-saturated basaltic volcanism containing extensive spinel lherzolite suites (cf. Part I and appendix 4) it is not

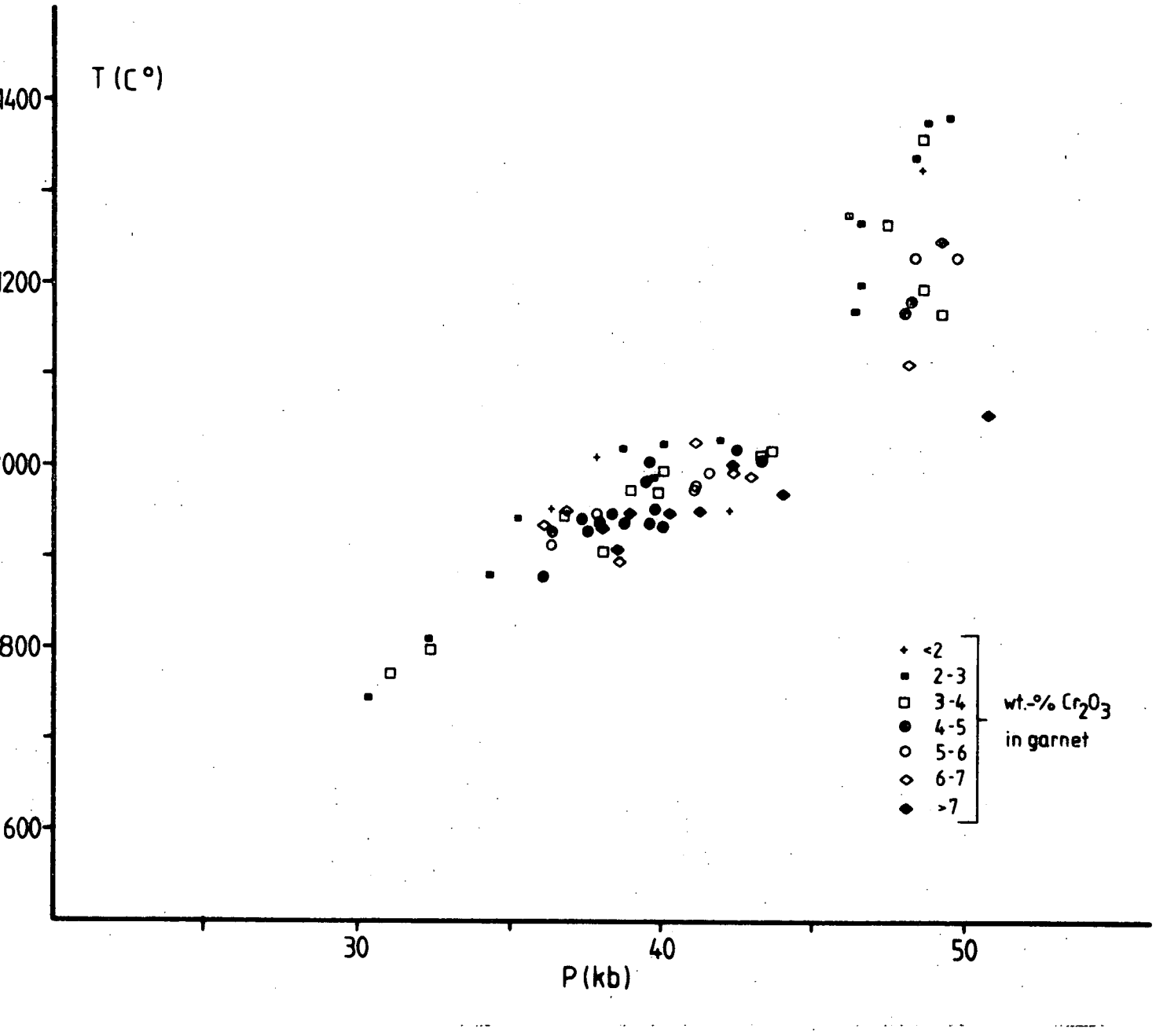

Figure 56: P,T estimates for South African garnet lherzolites from kimberlite in relation to the Cr content of the garnet. The plotted values were derived as outlined in fig. 51. Data sources see fig. 51.

yet possible to reliably infer a bulk composition for the deep upper mantle sampled by kimberlitic magmas (cf. appendix 4 for more detailed discussion).

Injection of kimberlitic magma into lherzolite wallrock may cause differing characteristics according to the P-T conditions of the wallrock. In fig. 57 a schematic diagram is drawn, in which the temperature of a portion of the mantle is raised to levels sufficient to produce kimberlite at about 160 km. The source of the heat may be attributed to a hot spot, shear heating or convective heating and has little influence on the distribution of isotherms around the heated area. The geometry of isotherms is such that a zone of partial melting exists with degrees $<<1\%$ at greater depth (region A in fig. 57), grading into a region with $<1\%$ partial melt followed by a maximum of approximately 1% partial melt, which is thought to be the region of kimberlite formation (region B in fig. 57). On top of this zone is a region (C in fig. 57) where the amount of partial melt drops again to below 1%. At somewhat shallower levels the solidus is reached and there is a region (D in fig. 57), which is completely subsolidus, but has conditions close to its solidus. This zone is followed by a region, where no influence of the heat source is experienced and the isotherms are in accord with steady-state conditions (E in fig. 57). An injection of magma into the "hot" regions C and D will favour wallrock-magma interaction and the following processes are envisaged:

- addition: infiltration metasomatism with complete/incomplete equilibration with wallrock
- subtraction: the wallrock is slightly above solidus temperatures and the partial melt may be leached into the magma
- diffusion interaction: at high temperatures diffusion could become an effective way of exchange between magma and wallrock. Hot fluids released upon crystallization of the injected magma may have a part in the process.

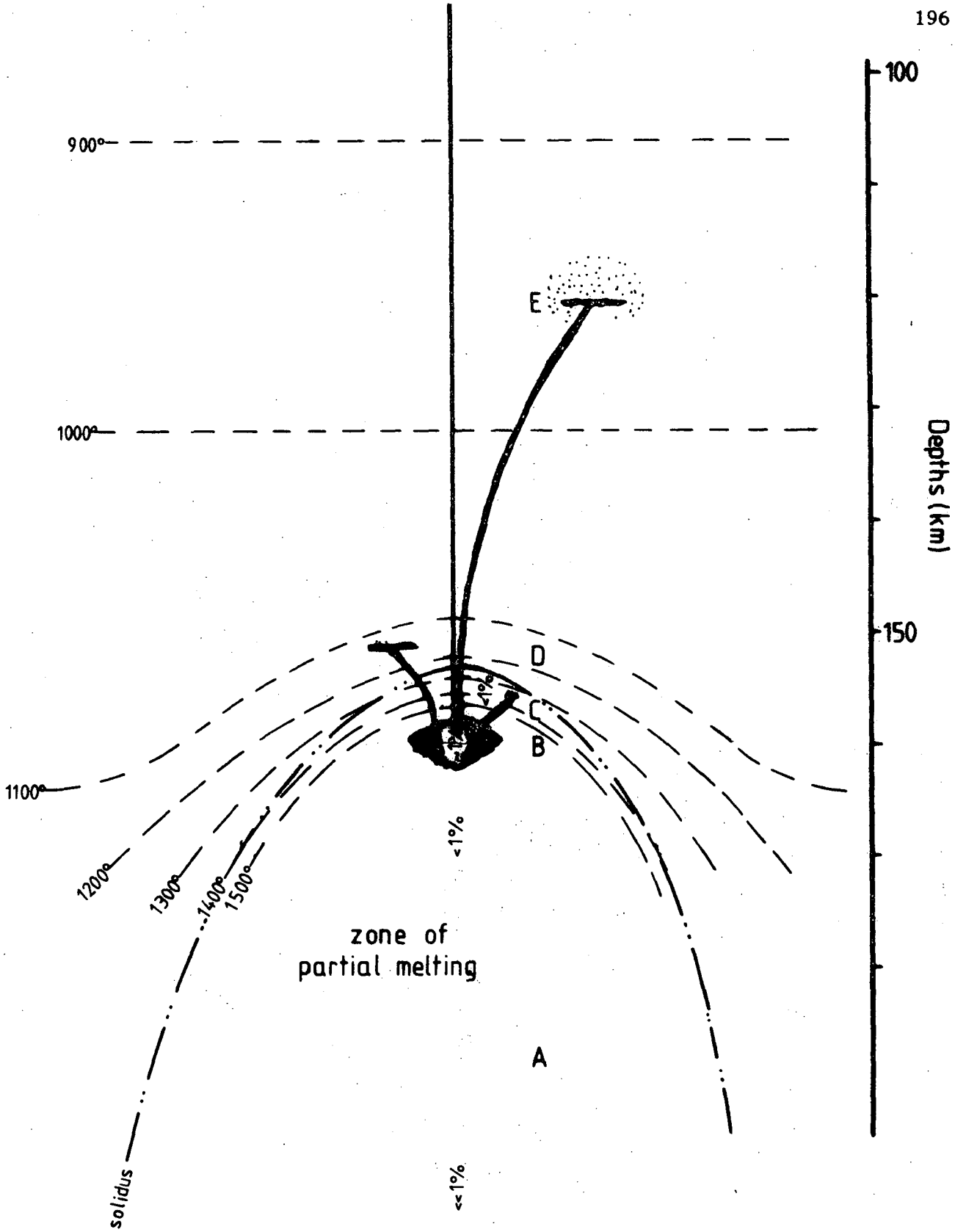

Figure 57: Schematic picture of the influence of a heat source on isotherms, partial melting, and magma-wallrock interaction. Dashed lines are isotherms in °C. 900° and 1000°C isotherms are from Clark & Ringwood (1964, shield geotherm), dash-dotted line is the solidus for the system "pyrolite + 0.2% H_2O" (Green, 1973b, Green & Lievermann, 1976). Indicated degrees of partial melting are inferred from Green & Liebermann (1976), capital letters A to E indicate regions with different degrees of partial melting and different styles of magma-wallrock interaction (see text). Blackened areas represent possible magma concentrations and paths.

- combination of processes above: multiple events may include successions such as a first addition, a leaching by a second event, and diffusion interaction in the wake of this.

If kimberlitic magma is injected into cooler regions (shallower levels, region E in fig. 57), then a direct interaction between magma and lherzolite wallrock is probably more limited, because the magma will crystallize more quickly. Processes similar to those suggested for spinel lherzolites from Lake Bullenmerri (this work) are envisaged, i.e. an interaction via released volatiles from the crystallizing magma. Simple hydration may account for secondary phlogopites in the sense of Carswell (1975). It should be noted that "hydration" is used here in a loose sense, incorporating volatiles other than H_2O (e.g. F, Cl). Solubilities of elements in fluids under the conditions of the upper mantle are largely unknown, but metasomatism by such fluids is likely to affect concentrations of minor and trace elements.

Fig. 57 is a schematic diagram showing possible relations between kimberlite formation and wallrock lherzolite. It is not implied that all processes seen in xenoliths have to be due to one single event or happening at one time. Isotopic studies show wide ranges of isotopic ratios for minerals from nodules (Menzies & Murthy, 1980b) which may be explained by isotopic disequilibrium (Erlank *et al.*, 1982; Richardson *et al.*, 1982) or by repeated metasomatic events at different times, including recent events (Menzies & Murthy, 1980b). Differences in apparent ages between diamonds and host rocks (Gurney & Harris, 1982) suggest repeated processes on a large time scale. If the theory of the lithopshere behaving as a cold boundary layer is correct and the region of approximately 160-180 km depth has usually temperatures of about 1400-1500°C, then the existence of a low-velocity zone at that depth is likely. Some geophysical constraints argue for the existence of a low-velocity zone at a depth of 150-200 km (Hales, 1981). If this is the case repeated processes of kimberlite injection into the lithosphere are most probable.

The Russian samples may be interpreted in a similar way. Low temperature xenoliths are in agreement with the shield geotherm of Clark & Ringwood (1964) to depths up to approximately 160-170 km, but most of the xenoliths recording the highest temperatures deviate from this geotherm towards higher temperatures (fig. 51). This is interpreted as the lower temperature limb of an array of deep-seated nodules with a range of temperature recordings, paralleling the South African trend. However, more data, particularly for high-temperature xenoliths, are needed to substantiate this analogy.

Samples of garnet lherzolites from The Thumb locality (U.S.A., Ehrenberg, 1979, 1982) have a record of temperatures between about 1000° and 1200°C within the narrow pressure range of 36-39 kb. Like the South African samples the equilibration conditions of the xenoliths with the highest recorded temperatures intersect the solidus for the system "pyrolite +0.2% H_2O", but in this case at shallower levels (fig. 54). The garnet lherzolites are included in a lamprophyre, not a kimberlite, and the differences in magma types are inferred to reflect different P,T conditions for the formation of the magma. The sampled area is not part of an Archaean lithosphere, but is of younger age (Condie, 1976) with a higher heat flow (1.3-1.6 h.f.u. compared to ≅1.0 of South Africa; Ehrenberg, 1982; Clarke & Ringwood, 1964). The younger age of the lithosphere may relate to a thinner lithopshere, allowing the heat source (hot spot, convecting mantle) to reach shallower levels. If the temperatures reach similar levels as suggested for South Africa (i.e. 1400-1500°C) but at shallower levels, higher degrees of partial melting of a peridotitic source are expected for equal amounts of volatiles present. This may be the reason for the difference in the chemistry of the host rock of these American samples compared to kimberlite.

Fig. 58 shows the range of P,T estimates for garnet lherzolites from alnoites and olivine nephelinite from Malaita (Solomon Islands)

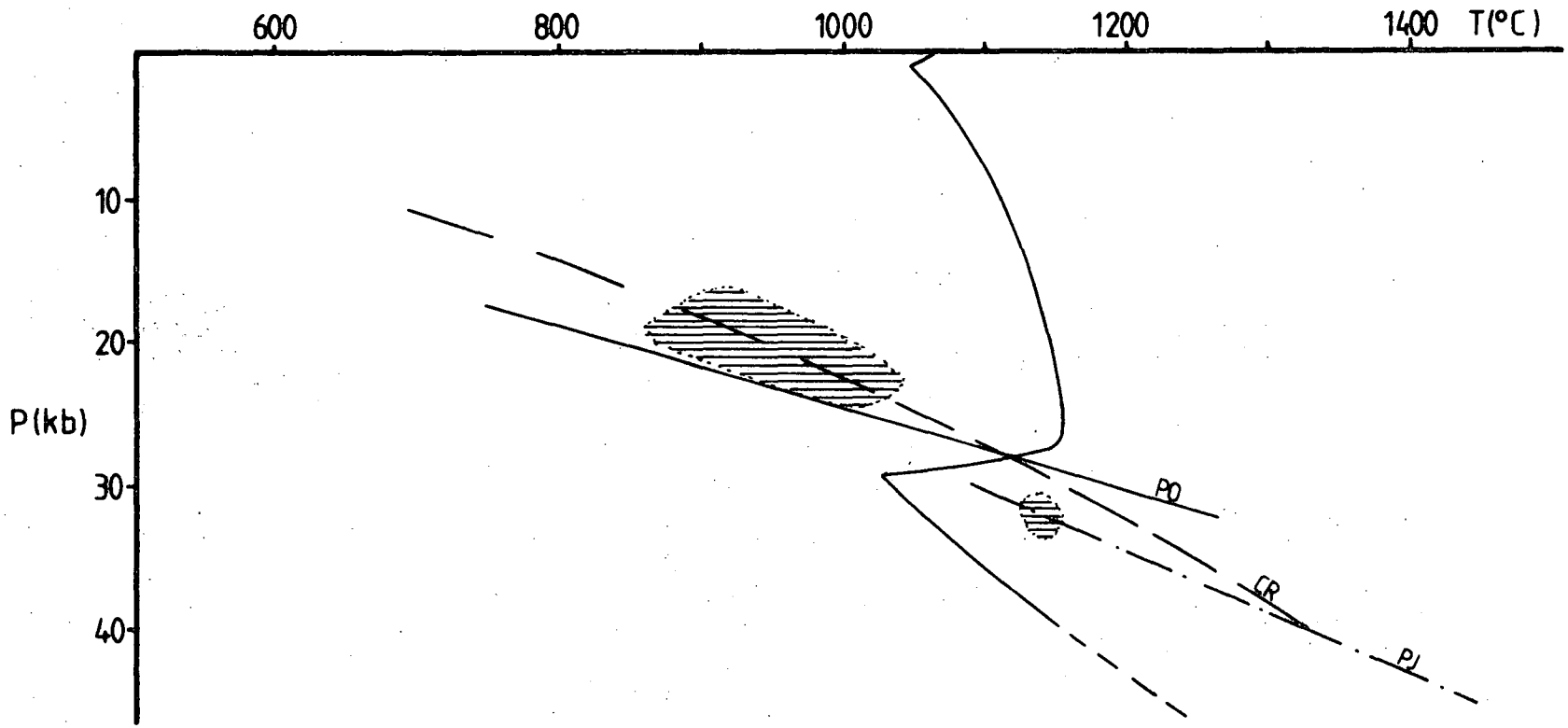

Figure 58: P,T estimates for garnet lherzolite inclusions from Malaita, Ile Bizard and New South Wales in relation to the solidus for the system "pyrolite + 0.2% H_2O" (Green , 1973b; Green & Liebermann, 1976) and geotherms for oceanic regions (PO = Parker & Oldenburg, 1973, for 100 Ma; CR = Clark & Ringwood, 1974; PJ = Peltier & Jarvis, 1982 for whole mantle convection and lherzolite model). Shaded area is the range of P,T estimates from fig. 54.

(Nixon & Boyd, 1979), N.S.W. (Australia) (Ferguson & Sheraton, 1979) and Ile Bizard (Canada)(Raeside & Helmstaedt, 1982) in comparison to the solidus for the system "pyrolite + 0.2% H_2O" and various oceanic geotherms (Clark & Ringwood, 1964; Parker & Oldenburg, 1973; Peltier & Jarvis, 1982). It is apparent that both geotherms from differing models of mantle convection (Parker & Oldenburg, 1973, for oceanic plates $\leq$ 100 Ma; and Peltier & Jarvis, 1982, for whole mantle convection) are in agreement with the steady-state (non-convective) geotherm of Clark & Ringwood (1964) for oceanic regimes in the region of interest. The P,T estimates are thus not capable of distinguishing between mantle models for oceanic regions, but show these nodules as being equilibrated in a "normal" oceanic P-T environment. It is interesting to note that all three suites show lherzolites with coexisting garnet and spinel in the range of 16-22 kb and 850-1050°C. The spinels of these assemblages are strongly aluminous compared to primary spinels from South African garnet-spinel lherzolites (Nixon & Boyd, 1973a; Carswell *et al.*, 1979). The field for coexisting garnet and spinel is therefore likely to be closer to the univariant reaction sp + px = gt + fo in the system CMAS than the South African samples. The effects of Cr/Cr+Al and Fe/Fe+Mg on this reaction tend to cancel against each other to some extent (Evans & Trommsdorff, 1978). The P,T estimates for these rocks are indeed close to this boundary (cf. fig. 13).

The two high-temperature xenoliths from Malaita would contain partial melts under the estimated P,T conditions in the presence of volatiles. The peculiar texture of these rocks (both contain "shattered" ortho- and/or clinopyroxenes, Nixon & Boyd, 1979) may be related to this, because the low-temperature garnet lherzolites of the same suite do not exhibit this feature (Nixon & Boyd, 1979). The exception of one low temperature rock with this textural characteristic may be related to an igneous history of this sample (ol-websterite).

Summarizing, the distribution of P,T estimates for equilibration conditions of garnet lherzolites differ between provinces and host rocks. Both the character of the host rocks and the differences between provinces are likely to reflect different ages and thicknesses of the sampled lithosphere.

The largest parts of the lithosphere have P,T conditions in accord with steady-state (non-convective) geotherms. This outline of the geotherms may however also be interpreted as the result of the lithosphere behaving as a cold boundary layer above a convecting mantle.

The xenoliths from continental areas with the highest recorded temperatures have equilibrated within a narrow pressure interval. These recordings are interpreted as a strong perturbation of isotherms due to a heat source, which caused partial melting at those depths and slightly deeper levels. Comparing the P,T estimates for the high-temperature xenoliths with melting studies on peridotitic rocks and liquidus studies on kimberlite, South African kimberlites are inferred to have originated at depths of about 160-180 km and at 1400-1500°C.

Megacrysts, cumulates and diamonds are regarded as precipitates from pre-dating magmas of probable kimberlitic character, fractionating and/or crystallizing under low fO_2 conditions and at mantle depths. Diamonds in particular are inferred to crystallize from those pre-dating magmas between 40-55 kb and 900-1300°C. Diamonds, megacrysts and cumulates are thus commonly xenolithic/xenocrystic to their host kimberlite.

Garnet lherzolites were wallrocks to the sampling kimberlites and their chemistry is a reflection of a complex history, involving partial melting events and partial extraction of liquids. The data do not point to primitive composition, but rather a confusing mixture of a variety of processes in modifying parental and residual mantle compositions (see also appendix 4). Apart from the complexities of multiple partial melting events, interaction between wallrock and kimberlitic magmas passing through or crystallizing seems likely.

For situations of small temperature difference between the magma and wallrock (areas C and D in fig. 57) this interaction may be a pervasive and selective chemical change, including major element variations. For situations of larger temperature difference (area E in fig. 57) then the alteration of the wallrock is largely one of hydration (phlogopite, K-richterite growth) and metasomatic addition of the most volatile (i.e. concentrated in fluid phases) of the minor and trace elements.

APPENDIX 1

Sample descriptions.
Abbreviations as in table 2.

I. LAKE BULLENMERRI

A-1: Lherzolites without hydrous phases or secondary assemblages after such.

BM-54 Porphyroclastic to equigranular-mosaic textured, medium to fine grained (0.2-2 mm) with both large and small strained ol, opx; cpx mostly as smaller grains with interstitial character, sp as partly elongated patches of light brown colour, often in contact with cpx, but with triple-junctions; elongation and setting of interstitial grains show weak developed foliation; pyroxenes show no exsolutions, all phases fresh, but some traces of pale brownish glass are present as veinlets.

BM-69 Porphyroclastic with medium to coarse grainsize (0.5-4 mm), strained ol and partly large opx, cpx dominantly interstitial and small, sp as small interstitial grains and patches of brown colour in holly-leaf shape, sp is concentrated in bands or layers; all phases fresh with no reactions or exsolutions.

BM-99 Porphyroclastic with medium to coarse grainsize (0.5-4 mm), strained ol, some opx with rounded inclusions of ol, cpx, sp, interstitial cpx, rare reddish-brown sp as small interstitial grains or small patches, mostly with cpx contact; all phases fresh with no reactions or exsolutions.

BM-160 Protogranular to porphyroclastic, coarse (0.5-4 mm), large strained ol, party large opx and dominantly interstitial cpx, interstitial small grains and partly large patches of brown sp (up to 4 mm); no reactions or exsolutions between or in minerals; some veinlets of bronwish glass are present.

A-2: Lherzolites with amphibole.

BM-9 Coarse (0.5-5 mm), porphyroclastic with strong developed foliation, large ol-with slightly flattened shape and strain features, opx, rare primary interstitial pale green cpx, primary sp is strongly elongated in direction of the foliation and holly-leaf shaped, sp is surrounded by patches of amph breakdown products (=Abdwn) with the typical assemblage cpx II, sp II, glass, ol II as described in appendix 2; inside the patches amph is partly preserved, Abdwn occurs also as often rounded or sub-euhedral

shaped individual patches without core of sp I, cpx has sometimes coronas or breakdown halos, where irregular traces of glass are visible, opx shows weakly developed exsolutions of cpx.

BM-15 Porphyroclastic to equigranular-mosaic, fine grained (1 mm, except for sp), ol with little or no strain features, common opx and cpx, sp as partly large (2-3 mm) patches of light brown colour, but also as small grains; sp is always associated with, but not surrounded by minor amph; amph occurs also as individual grains without sp-contact, all phases fresh, no exsolutions or breakdown.

BM-27 Porphyroclastic to protogranular, coarse (up to 5 mm) with strained ol, opx, cpx and sp both as small interstitial grains and large (up to several mm) patches, where sp has rounded inclusions of opx and ol; minor to rare amph in contact with larger sp, but sp mostly independent of amph present, few exsolutions in opx.

BM-58 Porphyroclastic to equigranular-tabular, fine grained (0.2-1.5 mm), some larger ol grains within abundant recrystallized small ol, opx, cpx; sp as small interstitial grains and larger patches, sometimes surrounded by Abdwn, containing amph I, some cpx breakdown halos developed, very few exsolutions.

BM-62 Protogranular to porphyroclastic, coarse (1-6 mm) with large ol, showing strong strain features, opx, common cpx; both pyroxenes show exsolutions of px and sp, cpx exsolves sometines parallel and perpendicular to cleavage, but in some cases at high angle (app. 120°) to each other; sp occurs as interstitial patches, always in contact with amph. which show weak marginal breakdown. sp has frequently rounded inclusions of ol, px and is in a number of cases completely mantled by amph ± Abkdwn.

BM-74 Protogranular to prophyroclastic, coarse (1-5 mm) with large strained ol and opx, minor cpx, small interstitial grains and larger parches of sp often, though not completely mantled or in contact with common amph; amph shows moderate marginal breakdown, cpx has sometimes exsolution of sp as platelets along cleavage.

BM-134 Porphyroclastic, medium to coarse grained (1-4 mm) with well developed foliation, large strongly strained ol, large opx, minor cpx of variable grainsize, patches and holly-leaf shaped elongated streaks of sp, mostly completely mantled by common amph, amph present with and without sp core, weak development of marginal breakdown of amph, pyroxenes show moderate development of mutual exsolution.

BM-139 Protogranular to porphyroclastic, medium grained (0.5-3 mm), strained ol, opx, cpx, sp always mantled by amph; amph is abundant and has rounded to sub- and near-euhedral shape with some development of marginal breakdown, amph grains aligned in direction of foliation, some marginal breakdown of cpx, but no exsolutions observed.

BM-147 Porphyroclastic, medium to coarse (0.5-3 mm, except for larger amph) with weak developed foliation, strained ol and opx, cpx of variable grainsize (up to 3 mm), rare sp as core of amph, amph is abundant with rounded to euhedral shape and weak marginal breakdown, cpx shows common exsolution of opx and marginal breakdown, opx exsolves cpx.

BM-161 Protogranular to porphyroclastic, coarse (0.5-4 mm), with large strained ol, opx, cpx, some patches, but mostly finely disseminated sp, mostly in contact or mantled by common amph, amph shows little breakdown at margins, some exsolutions of mutual character in pyroxenes.

A-4: Lherzolites with wites of former hydrous phases.

BM-48 Porphyroclastic, coarse to medium grained (1-4 mm) with weak fabric, strained large ol, opx, minor interstitial cpx and patchy or disseminated red-brown sp, patches of Abdwn mostly associated with sp or cpx, cpx developes marginal breakdown, opx often shows exsolution of cpx ± sp, some veinlets of brownish glass present.

BM-144 Prorogranular, coarse (1-5 mm) with large strained ol, opx, and cpx of variable grainsize, few patches and small disseminated grains of sp, minor patches of Abdwn, the glass of which appears often brownish (possible contribution of phlogopite breakdown?), veinlets of brownish glass present, some mutual exsolution of pyroxenes, cpx exsolves also sp, patches of Abdwn occur with or without contact to sp.

BM-162 Prorogranular to porphyroclastic, coarse (0.5-5 mm) with large strained ol, opx and cpx of variable grainsize, few holly-leaf shaped patches and finely disseminated grains of sp, amph is not preserved, but some patches of Abdwn are present, often in contact with sp, cpx shows minor exsolution of sp, very few cpx exsolution in opx.

A-5: Lherzolites with amphibole and phlogopite.

BM-143 Equigranular moasic to porphyroclastic, fine to medium grained (0.2-3 mm) with little or unstrained ol of variable grainsize, generally smaller opx and cpx, but clusters of small recrystallized cpx have the outline of former very large cpx grains (app. 1 cm), sp as disseminated small grains and some patches, amph occurs both as smaller insterstitial grains and larger grains with or without sp contact, rare phlo of similar character present, hydrous phases fresh, but some brownish glass as veinlets or along grain boundaries.

A-6: Fe-rich lherzolites.

BM-47 Porphyroclastic, coarse to medium grained (1-3 mm), with weak foliation, large ol with only few strain features, variable, but mostly small opx and minor cpx, large and abundant amph, amph with moderate marginal breakdown, so sp I observed, pyroxenes with some mutual exsolution.

BM-154 Protogranular to porphyroclastic, coarse (0.5-6 mm), with large ol with only few strain features, mostly small opx and cpx, rare sp as core of amph or cpx, often large and abundant amph, showing strong marginal to penetrative breakdown, no exsolutions observed.

A-7: Lherzolites with banded character.

BM-137 The specimen shows evidence for banded or layered character, zones of ol-enrichment have lherzolitic/wehrlitic mineralogy, medium grainsize (0.5-2.5 mm) containing mainly ol, cpx, some opx, rare sp, adjacent to zones of relative opx enrichment, followed by a zone dominated by large poikilitic cpx (1 cm, inclusions of opx, amph, sp) with breakdown features plus sp and amph, the amph shows some marginal breakdown; in this portion of the rock pockets exist, where large ol (1 cm) occur together with the lherzolitic/wehrlitic assemblage as described above.

B: Wehrlites

The textures of the wehrlites could be described in the majority of cases in the same terms as used for lherzolites, but at least one sample BM-152) shows evidence for cumulus processes and the others are interpreted as also originally being cumulus textured. This is supported by the hand specimens, where cpx seems to form an interstitial phase along with amph; a clear cumulus texture however has been largely eliminated by recrystallization processes.

BM-18 Granular, coarse (up to 7 mm) with large strained ol, cpx, rare interstitial opx, some coarse cpx, large and common amph have sometimes sp core and are often rimmed by cpx; large cpx show strong development of opx exsolution and partly poikilitic, rare interstitial ap, amph shows partial breakdown, discrete patches of Abdwn present.

BM-51 Strongly foliated, medium grained (0.2-2 mm, except for some large amph) with large ol with few strain features plus largely recrystallized ol and cpx, amph occurs as partly large rounded grains (up to 1 cm) and as subhedral smaller grains, showing dislocations, but no breakdown, rare sp as core of amph, cpx often in contact with amph, minor to rare interstitial ap.

BM-135 Equigranular-mosaic to porphyroclastic, fine grained (0.2-1 mm) with few larger strained ol amidst strongly recrystallized ol + cpx, abundant and partly large amph, showing strong marginal or penetrative breakdown, no opx, no sp I observed, no exsolutions.

BM-142 Porphyroclastic to equigranular mosaic, medium to fine grained (0.4-2 mm) with large and small ol (larger are strained), minor poikilitic cpx, in contact with abundant patches of Abdwn, no sp I, opx amph observed.

BM-152 Cumulate textured rock with ol of variable grainsize (0.2-6 mm) with typically rounded shape within a matrix of predominantly cpx and minor amph, cpx with exsolutions of opx; incorporated in the rock are pockets of dunitic material with rare sp and bright green cpx in contrast to the black (in hand specimen) matrix cpx; amph shows few breakdown features.

C: Harzburgites.

BM-163 Protogranular, coarse (1-7 mm) with large strained ol, common opx, sp as cores of amph, amph with minor breakdown, opx has commonly exsolutions of cpx.

D: Hornblendites.

BM-117 Coarse grained (2-5 mm), intergrowth textured, mainly amph with minor phlo and ilm, rare titanomagnetite and very rare ol; amph has frequently exsolutions of ilm, ilm occurs also as interstitial patches and as discrete grains with euhedral shape, very small grains of titanomagnetite inside or interstitial to amph; ol is associated with brownish glass.

BM-156 Coarse grained (2-10 mm) intergrowth of amph with minor phlo and ilm as BM-117, containing a pocket of fine grained (0.1-0.4 mm) cpx, opx, phlo within amph matrix and minor ilm, amph shows rare marginal breakdown.

G: Cumulate textured wehrlite.

BM-168 Cumulate textured rock, coarse (up to 8 mm) with large sub- to euhedral unstrained ol, poikilitic cpx with inclusions of ol and amph, interstitial amph and minor phlo, very rare interstitial opx, cpx and amph show some marginal breakdown, in some bigger spaces between large ol and cpx a dark brown glass contains small euhdral ol.

E/F: Composite xenoliths.

BM-109 Amphibole-bearing lherzolite cut by hornblendite vein; lherzolite: porphyroclastic to protogranular, medium to coarse (1-5 mm) with ol with few strain features, opx, cpx, minor sp partly being rimmed by amph of light brown-pale brown pleochroic character, phases fresh with rare cpx exsolution in opx; crosscutting hornblendite; intergrown amph with minor phlo, cpx, the amph is pale to dark yellowish brown pleochroic, poikilitic with numerous small inclusions of cpx, individual amph grains exceed 1 cm, phlo of variable grainsize is also poikilitic with often rounded inclusions of cpx, pockets in the vein consist of cpx and rare opx with some interstitial brownish glass; the two rock types are separated very sharply with little signs of reactions with each other.

BM-114 Gt-pyroxenite plus amph-clinopyroxenite; gt-pyroxenite: metamorphic texture, medium to large gt (1-5 mm) with sub- to euhedral shape within medium to fine grained (0.2-1 mm) cpx and minor to rare opx, gt has thick kelphytic rims, extending into the crystal along cracks, some patches of small cpx + green sp marginal to gt present, abundance of patches increases towards amph-clinopyroxenite: coarse (1-6 mm) intergrowth of cpx + amph, marginal to gt-pyroxenite, some bigger patches of green sp.

BM-116 Gt-pyroxenite + clinopyroxenite + amph-lherzolite; gt-pyroxenite: medium to large (1-5 mm) sub- to euhedral gt in a matrix of smaller (0.2-1 mm) cpx and minor to rare opx, gt has thin kelphytic rims extending into the crystal only along major cracks, marginal to gt patches of predominantly cpx + green sp of fine to very fine grainsize (0.3 mm); this zone is followed by the assemblage

cpx + amph, coarse (1-4 mm), where cpx has frequently wormy intergrowth with green sp, followed by a zone of cpx with minor brown interstitial sp, this zone is followed, sharply separated from it, by lherzolite: porphyroclastic, medium grained (1-3 mm) with strained ol, common opx and cpx, common sp; minor amph in contact with sp.

II. MT LEURA

A: Lherzolites without hydrous phases or secondary assemblages after those.

LE-50 Porphyroclastic, edium grained (0.5-4 mm) with larger little strained ol, opx, smaller insterstitial cpx, patches (up to 4 mm) of sp, elongated in direction of foliation, no exsolutions observed.

LE-532 Porphyroclastic, medium grained (0.5-3 mm) with strained ol, opx and minor small interstitial cpx, sp as small interstitial grains or patches, weakly aligned in direction of foliation, cpx often, but not exclusively in contact with sp, no exsolutions observed.

LE-539 Porphyroclastic to protogranular, medium to coarse (0.5-4 mm) with large strained ol, opx, common small cpx, sp as patches aligned along a well developed foliation, some rounded inclusions of ol in sp, sp often in contact with cpx, but also with triple-junctions, no exsolutions observed.

LE-2664 Protogranular, coarse (1-4 mm) with large strained ol, opx, common cpx of variable grainsize, minor to rare sp as small interstitial grains or patches, minor mutual exsolution of px.

A-2: Lherzolites with amphibole.

LE-2641 Protogranular, coarse (2-8 mm) with large strained ol, opx, common cpx of variable grainsize, small interstitial grains and larger patches of sp, rare amph and minor patches of Abdwn, mostly in contact with sp, cpx shows frequent exsolution of opx and sometimes of sp, opx exsolves cpx.

A-3: Lherzolites with phlogopite.

LE-67 Protogranular to porphyroclastic, coarse (1-5 mm) with large strained ol, opx, minor small cpx, sp as weakly elongated and aligned patches, rare sub- to euhedral phlo, very few exsolutions in opx.

LE-68 Porphyroclastic, coarse (0.5-7 mm) with large strained ol, opx, mostly small common cpx, sp as small interstitial patches, rare small euhedral phlo, no exsolutions observed.

A-4: Lherzolites with sites of former hydrous phases.

LE-4 Porphyroclastic, fine to medium grained (0.3-2.5 mm) with large strained ol, opx, common cpx of variable grainsize, sp patches are weakly aligned alogg a moderate developed foliation, minor patches of Abdwn, no exsolutions observed, cpx shows commonly a marginal breakdown.

LE-19 Protogranular to porphyroclastic, coarse (1-5 mm) with large strained ol, opx, minor cpx of variable grainsize, sp as patchy cores of Abdwn, those patches of Abdwn are abundant with or without sp core, opx shows frequent exsolutions of cpx.

LE-544 Protogranular to porphyroclastic, coarse (1-9 mm) with large strained ol, opx, common cpx of variable grainsize, small interstitial grains or larger, often elongated patches of sp, very rare small patches of Abdwn attached to sp, cpx and opx show mutual exsolution and exsolution of sp.

LE-2662 Porphyroclastic, edium grained (0.5-2.5 mm) with large strained ol, smaller opx and common cpx, minor to rare small interstitial sp, few patches of Abdwn, opx shows few exsolutions of cpx + ?sp, cox has moderate to large breakdown halos.

B: Wehrlites

LE-27 Granular to porphyroclastic, medium grained (1-3 mm) with strong foliation, larger strained ol and common cpx, common phlo as elongated patches in direction of foliation, minor sp occurs as small interstitial grains or as inclusions in ol, rare opx, minor patches of phlo breakdown with dark brown glass, cpx sometimes with breakdown halo.

E: Composite xenoliths.

LE-00 Lherzolite crosscut by phlogopite vein; lherzolite: porphyroclastic to equigranular-tabular (0.2-3 mm), with some larger strained ol, generally smaller opx and cpx, minor interstitial grains of sp, often in contact with or mantled by cpx, all phases fresh, except where cpx is bordering the vein, some small breakdown halos; vein: thin (app. 1 mm) line of phlo grains, crosscutting the foliation of the lherzolite nearly perpendicular.

APPENDIX 2

Breakdown of pargasitic amphibole in lherzolite nodules.

Pargasitic amphibole in lherzolitic nodules from Lake Bullenmerri shows various stages of breakdown to a secondary assemblage. The breakdown assemblage consists of clear to somewhat turbid glass, a number of clinopyroxene grains with variably developed habits, small olivine and small to very small euhedral spinel grains.

Pargasitic amphibole is distributed more or less evenly in the majority of amphibole-bearing nodules and occurs as rounded, but also as angular, subhedral or euhedral grains. The size of the grains is variable and in some cases exceeds the size of the other phases. Even though it is generally well distributed, amphibole shows often an intimate relation with spinel. Spinel is commonly, though not exclusively, in contact with amphibole and is frequently completely rimmed by it. The shape of the spinel in spinel lherzolites is often patchy, elongated, or "holly-leaf"-like (Mercier & Nicholas, 1975), interstitital to olivine and orthopyroxene. This embayed shape is also shown where amphibole is rimming spinel (fig.59). Therefore the spinel of this shape is regarded as primary, even when rimmed by amphibole.

In the majority of cases the amphibole shows partial to complete breakdown. Various stages are observed, typically starting with a marginal breakdown (fig.60). Subsequently larger parts of the grain are affected (fig.61), eventually only patches of the secondary assemblage are left (fig.62).

In anhydrous lherzolites there is often an intimate relation between spinel and clinopyroxene. The formation of secondary amphibole requires both (spinel + pyroxene + fluid = amphibole, Francis, 1976a). The patches of secondary assemblages appear therefore often close to clinopyroxene. Clinopyroxene is also likely to have breakdown halos due to heating and/or decompression (Frey & Green, 1974). The two different breakdown phenomena can be distinguished, because the breakdown of clinopyroxene yields only irregular traces of glass, typically marginal (cf. fig. 1 of Kleeman *et al.*, 1969). Some interaction between amphibole and clinopyroxene breakdown seems possible, but not generally necessary.

Microprobe analyses of the secondary phases in comparison to the primary assemblage are listed in table 17. The main differences are the higher Mg-values (= Mg/Mg+Fe) of olivine, clinopyroxene and spinel, the lower Na content of clinopyroxene and the lower Cr value (= Cr/Cr+Al) of

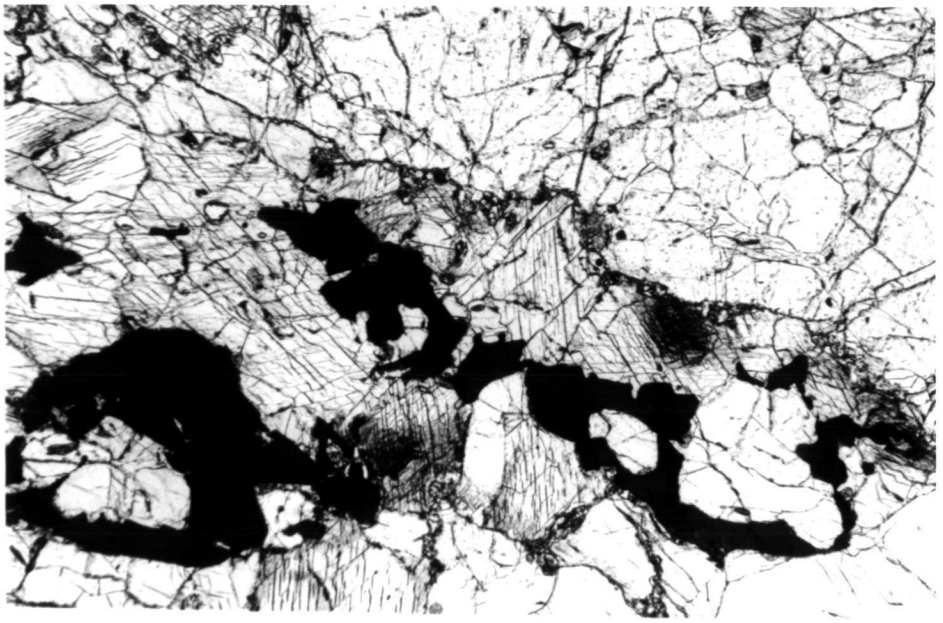

Figure 59: "Holly-leaf" shaped spinel incompletely surrounded by fresh amphibole. Sample BM-134, width of field approx. 2 mm.

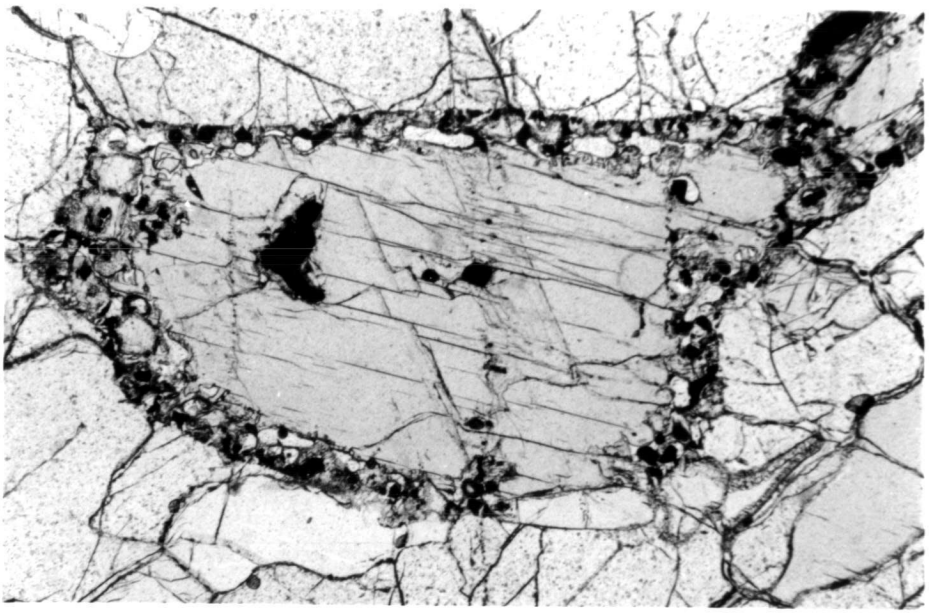

Figure 60: Amphibole with small spinels in the core and marginal breakdown. Sample BM-154, width of field approx. 2 mm.

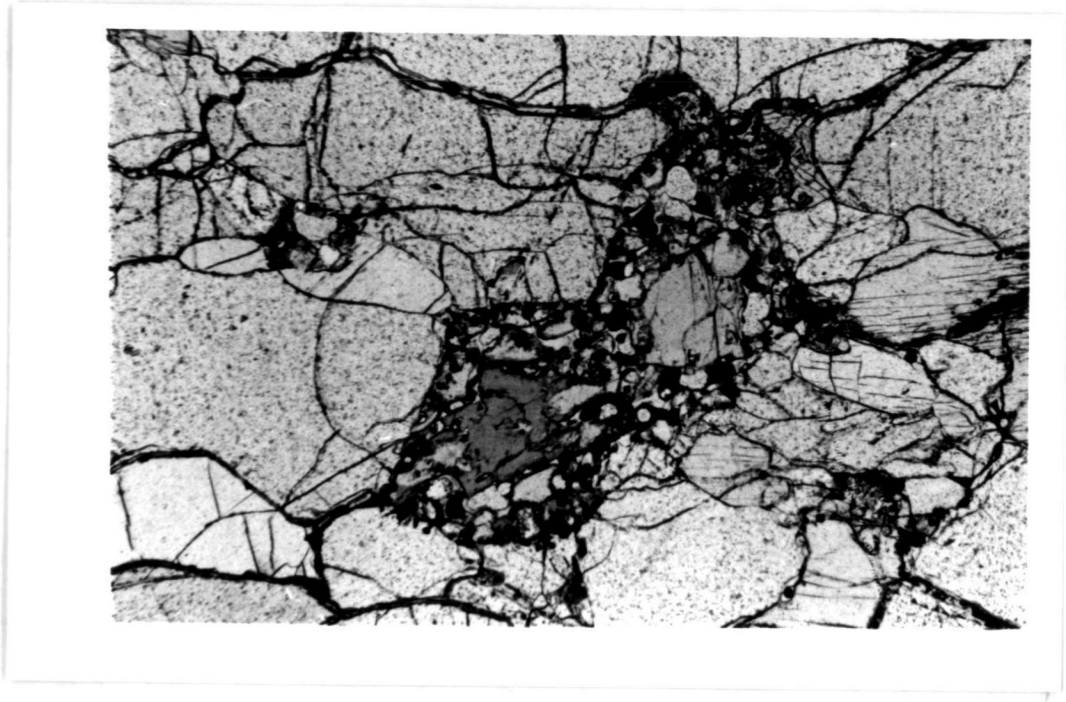

Figure 61: Largely broken-down amphibole, preserved in the centre. Sample BM-154, width of field approx. 2 mm.

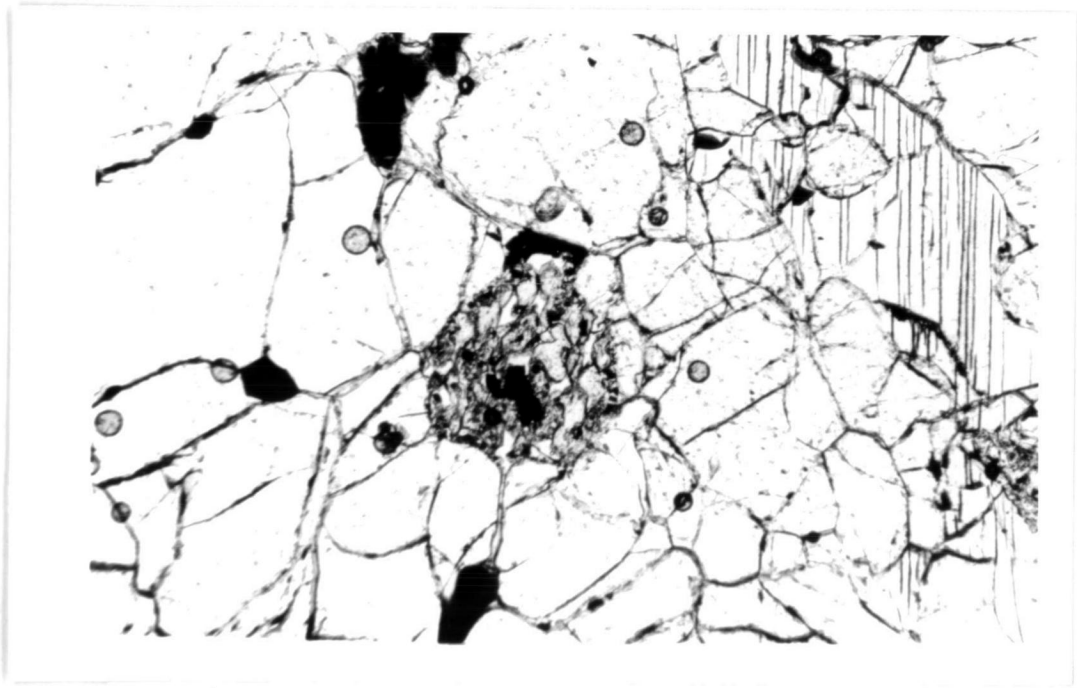

Figure 62: Patch of secondary assemblage after amphibole with some primary spinel in the centre of the assemblage. Sample BM-9, width of field approx. 4 mm.

Table 17

	BM-9					
	primary			secondary		
	cpx	sp	amph	cpx	sp	glass
Na_2O	2.31		3.45	0.87		6.79
MgO	15.24	13.14	17.04	16.50	17.89	2.01
Al_2O_3	3.34	16.75	10.22	3.48	26.21	22.43
SiO_2	54.84		42.12	52.47		59.69
K_2O			0.96			1.85
CaO	19.26		9.42	21.63		4.34
TiO_2			0.34		0.26	0.38
Cr_2O_3	2.95	52.57	3.19	3.04	42.83	
FeO*	2.07	16.88	2.95	1.94	13.44	2.44
Total	100.01	99.34	89.69	99.93	100.60	99.93
Mg*	92.86	58.11	91.12	93.80	73.2	59.48
Cr*	37.17	67.8	17.29	37.0	52.3	
Mg*(ol)	91.02			93.5		

	BM-154					
	primary			secondary		
	cpx	sp	amph	cpx	sp	glass
Na_2O	1.76		2.85	1.10		6.28
MgO	15.45	14.55	16.06	16.10	18.66	2.78
Al_2O_3	4.34	28.22	12.25	6.30	40.81	21.02
SiO_2	52.67		41.47	50.59		57.70
K_2O			1.23			2.88
CaO	20.03		10.32	19.94		5.06
TiO_2		0.29	1.25	0.95	0.64	1.33
Cr_2O_3	1.70	37.55	2.24	2.22	26.19	
FeO*	3.06	18.12	4.31	2.80	13.13	2.96
Total	100.01	98.73	91.98	100.00	99.43	100.01
Mg*	89.96	58.90	86.91	91.12	71.68	62.66
Cr*	20.85	47.17	10.95	19.16	30.10	
Mg*(ol)	87.12			90.47		

spinel in the secondary assemblage. A wider spread in mineral analyses (averages given) of secondary clinopyroxene indicates some zonation in respect to Cr and Al. These differences in chemistry are identical to those observed in other studies on amphibole breakdown in nodules from Victoria and elsewhere (Francis, 1976a; Frey & Green, 1974; Kleeman *et al.*, 1969; Stosch & Seck, 1980).

The analysed glass is in apparent disequilibrium with the highly magnesian phases of the secondary assemblage. For the given Mg-value of the glass (59-63) an olivine of about Fo_{86} would be in equilibrium (Irving, 1971). Attempts have been made to model the composition of a preserved amphibole with partial breakdown as a combination of the analysed phases of the secondary assemblage (amph = x% cpx + y% ol + z% sp + w% glass), but no good fit could be obtained. This is seen as further evidence for disequilibrium of the analysed glass with the secondary assemblage.

The compositions of the analysed glasses vary little within the individual assemblages, but Frey & Green (1974) reported considerable variation, especially close to mineral phases. This is in line with quenching behaviour of silicate melts in experiments (Green, 1973b) and may be present but was not sought in samples of this study. The presence of quench material is regarded as the cause of the apparent disequilibrium, the analysed glass is not representative of the original melt.

The presence of glass in all cases and of plagioclase in some examples indicates that dehydration/melting occurred at pressures and temperatures around 1 kb and T > 1000°C (cf. Holloway, 1973). The partial preservation of amphibole in many nodules argues for a process during which the thermal stability limit was not exceeded for prolonged times or by a large temperature margin.

Summarizing, the following conclusions have been drawn:

1. Due to decompression and heating from ambient temperatures to T > 1000°C amphibole of pargasitic character breaks down to a secondary assemblage of clinopyroxene, olivine, spinel and glass during the transport to the surface.
2. The thermal stability limit of pargasite in lherzolite was not greatly exceeded and/or was not exceeded for prolonged times.
3. Patches of the characteristic secondary assemblage without preservation of amphibole were derived from original amphibole and do not represent partial melting of the lherzolite assemblage (olivine, orthopyroxene, clinopyroxene, spinel) (Maaløe & Prinzlau, 1979).

Appendix 3

Averages of microprobe analyses of mineral phases in xenoliths

Abbrevations:

opx: orthopyroxene, cpx: clinopyroxene, sp: spinel, amph: amphibole, ol: olivine phlo: phlogopite, ilm: ilmenite, Mg': Mg/Mg+Fe, Ca': Ca/Ca+Mg+Fe, Cr': Cr/Cr+Al

Numbers in parenthesis indicate standard deviations from the average

Group A-1: anhydrous lherzolites

Sample BM - 54

Phases	opx		cpx		sp	
Na_2O	n.d.		0.70 (.16)	.049	n.d.	
MgO	33.08 (.08)	1.700	16.70 (.24)	.898	20.07 (.17)	.787
Al_2O_3	4.75 (.30)	.193	5.49 (.15)	.233	52.69 (.19)	1.633
SiO_2	55.02 (.28)	1.896	52.66 (.26)	1.900		
CaO	0.84 (.04)	.031	20.82 (.25)	.805		
Cr_2O_3	0.47 (.08)	.013	0.93 (.11)	.027	15.70 (.22)	.326
FeO	5.86 (.207	.169	2.70 (.12)	.082	10.41 (.01)	.229
Total	100.02	4.002	100.00	3.994	98.87	2.975
Mg'	90.96		91.63		77.46	
Ca'	1.63		45.10			
Cr'	6.31		10.38		16.64	
Mg'(ol)	90.58 (.06)					

Sample BM-69

Phases	opx		cpx		sp	
	wt.%	struc	wt.%	struc	wt.%	struc
Na_2O	n.d.		0.81 (.09)	.057		
MgO	33.21 (.17)	1.706	17.08 (.04)	.918	20.36 (.33)	.809
Al_2O_3	4.74 (.17)	.193	5.25 (.14)	.223	50.39 (.78)	1.583
SiO_2	54.97 (.36)	1.895	52.83 (.09)	1.904		
CaO	0.71 (.06)	.026	20.58 (.11)	.795		
Cr_2O_3	0.41 (.08)	.011	0.97 (.08)	.028	17.45 (.73)	.368
FeO	5.76 (.13)	.166	2.48 (.07)	.075	11.03 (.51)	.246
Total	99.80	3.997	100.00	4.000	99.23	3.006
Mg'	91.13		92.45		76.68	
Ca'	1.37		44.46			
Cr'	5.39		11.16		18.86	
Mg'(ol)	90.48 (.04)					

Sample BM - 99

Phases	opx		cpx		sp	
	wt.%	struc	wt.%	struc	wt.%	struc
Na_2O	n.d.		1.51 (.11)	.105		
MgO	33.33 (.10)	1.712	15.91 (.21)	.855	18.86 (.27)	.771
Al_2O_3	3.77 (.25)	.153	5.39 (.23)	.229	44.18 (.44)	1.427
SiO_2	55.71 (.28)	1.919	53.42 (.23)	1.925		
CaO	0.77 (.04)	.028	19.70 (.14)	.760		
Cr_2O_3	0.48 (.07)	.013	1.38 (.09)	.039	25.27 (.20)	.548
FeO	5.94 (.07)	.171	2.69 (.12)	.081	11.68 (.26)	.268
Total	99.97	3.996	100.00	3.994	99.99	3.014
Mg'	90.92		91.35		74.21	
Ca'	1.47		44.80			
Cr'	7.83		14.55		27.75	
Mg'(ol)	90.34 (.10)					

Sample BM - 160

Phases	opx		cpx		sp	
	wt.%	struc	wt.%	struc	wt.%	struc
Na_2O	n.d.		1.18 (.09)	.082		
MgO	32.99 (.11)	1.699	16.28 (.06)	.875	20.09 (.14)	.797
Al_2O_3	5.03 (.23)	.205	6.26 (.15)	.266	51.15 (.45)	1.604
SiO_2	54.49 (.36)	1.882	52.18 (.16)	1.883		
CaO	0.78 (.02)	.029	19.81 (.12)	.766		
Cr_2O_3	0.45 (.06)	.012	1.11 (.06)	.032	16.16 (.28)	.340
FeO	6.02 (.06)	.174	2.78 (.05)	.084	11.46 (.55)	.255
Total	99.76	4.001	100.01	3.999	99.17	3.002
Mg'	90.71		91.24		75.76	
Ca'	1.52		44.41			
Cr'	5.53		10.74		17.50	
Mg'(ol)	90.03 (.12)					

Sample LE - 00

Phases	opx		cpx		sp	
	wt.%	struc	wt.%	struc	wt.%	struc
Na_2O	n.d.		2.28 (.09)	.159		
MgO	33.85 (.12)	1.736	15.69 (.11)	.841	16.61 (.31)	.729
Al_2O_3	2.76 (.16)	.112	5.17 (.11)	.219	29.46 (1.3)	1.023
SiO_2	56.41 (.34)	1.941	53.86 (.26)	1.938		
CaO	0.75 (.03)	.028	18.03 (.1C)	.695		
Cr_2O_3	0.61 (.07)	.017	2.06 (.21)	.059	37.72 (1.3)	.879
TiO_2	n.d.		0.27 (.07)	.008	0.52 (.04)	.011
FeO	5.59 (.10)	.161	2.71 (.04)	.081	15.03 (.33)	.370
Total	99.97	3.995	100.07	4.000	99.34	3.012
Mg'	91.51		91.21		66.33	
Ca'	1.45		42.98			
Cr'	13.18		21.22		46.21	
Mg'(ol)	90.84 (.14)					

Sample LE - 50

Phases	opx		cpx		sp	
	wt.%	struc	wt.%	struc	wt.%	struc
Na_2O	n.d.		2.12 (.11)	.148		
MgO	32.75 (.21)	1.691	15.48 (.06)	.834	20.06 (.36)	.776
Al_2O_3	5.55 (.42)	.227	7.25 (.24)	.309	55.45 (.74)	1.696
SiO_2	53.79 (.35)	1.863	51.60 (.24)	1.866		
CaO	0.82 (.04)	.030	19.22 (.23)	.745		
TiO_2	n.d.		0.38 (.04)	.010	0.29 (.10)	.006
Cr_2O_3	0.41 (.06)	.011	0.97 (.09)	.028	11.97 (.27)	.246
FeO	6.23 (.12)	.180	2.99 (.09)	.090	11.05 (.13)	.240
Total	99.55	4.002	100.01	4.030	98.82	2.964
Mg'	90.38		90.26		76.38	
Ca'	1.58		44.64			
Cr'	4.62		8.31		12.67	
Mg'(ol)	90.03 (.10)					

Sample LE - 532

Phases	opx		cpx		sp	
	wt.%	struc	wt.%	struc	wt.%	struc
Na_2O	n.d.		1.24 (.04)	.087		
MgO	33.81 (.15)	1.735	16.21 (.21)	.872	16.90 (.19)	.727
Al_2O_3	3.03 (.06)	.123	4.67 (.15)	.198	34.87 (.22)	1.180
SiO_2	56.15 (.207	1.933	53.35 (.09)	1.926		
CaO	0.71 (.06)	.026	19.98 (.21)	.773		
Cr_2O_3	0.66 (.09)	.018	2.01 (.14)	.057	34.48 (.22)	.783
FeO	5.64 (.08)	.163	2.54 (.08)	.077	13.37 (.25)	.321
Total	100.00	3.998	100.00	3.990	99.62	3.011
Mg'	91.41		91.82		69.37	
Ca'	1.35		44.89			
Cr'	12.77		22.35		39.89	
Mg'(ol)	90.66 (.20)					

Sample LE - 539

Phases	OPX		CPX		SP	
	wt.%	struc	wt.%	struc	wt.%	struc
Na_2O	n.d.		1.69 (.12)	.118		
MgO	33.07 (.19)	1.703	15.70 (.10)	.843	20.66 (.20)	.814
Al_2O_3	4.40 (.22)	.179	6.28 (.17)	.267	52.67 (.30)	1.641
SiO_2	54.89 (.39)	1.897	52.70 (.20)	1.899		
CaO	0.63 (.06)	.023	19.39 (.09)	.749		
TiO_2	n.d.		0.38 (.05)	.010	n.d.	
Cr_2O_3	0.37 (.08)	.010	1.08 (.04)	.031	13.97 (.33)	.292
FeO	6.08 (.10)	.176	2.79 (.07)	.084	11.42 (.12)	.252
Total	99.44	3.988	100.01	4.001	98.72	2.999
Mg'	90.63		90.94		76.36	
Ca'	1.21		44.69			
Cr'	5.29		10.40		15.11	
Mg'(ol)	90.27 (.06)					

Sample LE - 2664

Phases	opx		cpx		sp	
	wt.%	struc	wt.%	struc	wt.%	struc
Na_2O	n.d.		0.92 (.07)	.065		
MgO	34.39 (.33)	1.762	16.26 (.17)	.875	19.39 (.12)	.786
Al_2O_3	3.03 (.19)	.123	4.19 (.17)	.178	45.68 (.36)	1.465
SiO_2	56.12 (.06)	1.929	53.49 (.14)	1.932		
CaO	0.32 (.05)	.012	21.97 (.11)	.850		
Cr_2O_3	0.34 (.01)	.009	1.23 (.14)	.035	22.96 (.43)	.494
FeO	5.49 (.07)	.158	1.91 (.05)	.058	11.05 (.11)	.251
Total	99.69	3.993	99.97	3.993	99.08	2.996
Mg'	91.18		93.78		75.80	
Ca'	0.62		47.67			
Cr'	6.82		16.43		25.22	
Mg'(ol)	90.94 (.15)					

Group A-2 : amphibole bearing lherzolites

Sample BM - 9

Phases	opx		cpx		sp		amph	
	wt.%	struc	wt.%	struc	wt.%	struc	wt.%	struc
Na_2O	n.d.		2.31 (.10)	.160			3.45 (.36)	1.035
MgO	35.57 (.12)	1.820	15.24 (.16)	.819	13.14 (.30)	.620	17.04 (.89)	3.931
Al_2O_3	0.86 (.09)	.035	3.34 (.05)	.142	16.75 (.56)	.625	10.22 (.47)	1.865
SiO_2	57.59 (.27)	1.976	54.84 (.08)	1.978			42.12 (1.5)	6.520
K_2O							0.96 (.09)	.190
CaO	0.26 (.05)	.010	19.26 (.12)	.744			9.42 (.18)	1.564
TiO_2							0.34 (.02)	.044
Cr_2O_3	0.25 (.05)	.007	2.95 (.19)	.084	52.57 (.66)	1.316	3.19 (.07)	.390
FeO	5.55 (.09)	.159	2.07 (.06)	.063	16.88 (.35)	.447	2.95 (.06)	.383
Total	100.08	4.007	100.01	3.990	99.34	3.008	89.69	15.922
Mg'	91.97		92.86		58.11		91.12	
Ca'	0.50		45.76					
Cr'	16.67		37.17		67.80		17.29	
Mg'(ol)	91.02 (.20)							

Sample BM - 15

Phases	opx wt.%	opx struc	cpx wt.%	cpx struc	sp wt.%	sp struc	amph wt.%	amph struc
Na_2O	n.d.		1.68 (.07)	.117			3.33 (.06)	.929
MgO	32.76 (.16)	1.688	15.08 (.08)	.811	20.24 (.18)	.780	17.07 (.30)	3.659
Al_2O_3	4.58 (.40)	.187	6.68 (.20)	.285	58.04 (.24)	1.770	15.20 (.30)	2.577
SiO_2	55.09 (.30)	1.904	52.59 (.28)	1.897			42.51 (.99)	6.122
K_2O							1.01 (.02)	.185
CaO	0.64 (.04)	.024	20.08 (.19)	.776			10.70 (.29)	1.649
TiO_2			0.41 (.14)	.011			1.86 (.13)	.201
Cr_2O_3	n.d.		0.51 (.08)	.014	10.44 (.33)	.214	0.78 (.07)	.088
FeO	6.93 (.10)	.200	2.97 (.11)	.090	11.28 (.26)	.244	4.09 (.27)	.491
Total	100.00	4.003	100.00	4.000	100.00	3.008	96.55	15.901
Mg'	89.41		90.01		76.17		88.17	
Ca'	1.26		46.27					
Cr'	0.00		4.70		10.79		3.30	
Mg'(ol)	88.64 (.13)							

Sample BM - 27

Phases	opx wt.%	opx struc	cpx wt.%	cpx struc	sp wt.%	sp struc	amph wt.%	amph struc
Na_2O	n.d.		1,71 (.11)	.120			3.26 (.08)	.911
MgO	33.69 (.14)	1.734	15.68 (.14)	.844	20.14 (.23)	.770	17.33 (.33)	3.724
Al_2O_3	4.25 (.33)	.173	5.94 (.13)	.253	58.57 (.50)	1.769	15.08 (.28)	2.562
SiO_2	54.97 (.37)	1.897	52.65 (.26)	1.901			43.42 (1.2)	6.260
K_2O							0.92 (.04)	.169
CaO	0.54 (.05)	.020	20.71 (.20)	.801			9.78 (.34)	1.510
TiO_2			0.24 (.03)	.007			1.63 (.11)	.176
Cr_2O_3	0.25 (.05)	.007	0.77 (.10)	.022	10.16 (.48)	.206	0.66 (.09)	.075
FeO	6.13 (.08)	.177	2.37 (.08)	.072	10.11 (.34)	.217	3.26 (.24)	.393
Total	99.83	4.008	100.07	4.020	98.98	2.962	95.34	15.784
Mg'	90.74		92.14		78.01		90.45	
Ca'	1.04		46.65					
Cr'	3.89		8.00		10.43		2.85	
Mg'(ol)	90.17 (.16)							

Sample BM - 58

Phases	opx wt.%	opx struc	cpx wt.%	cpx struc	sp wt.%	sp struc	amph wt.%	amph struc
Na_2O	n.d.		2.18 (.17)	.153			3.28 (.14)	.910
MgO	32.76 (.52)	1.696	14.93 (.39)	.805	19.77 (.30)	.776	17.22 (.207	3.676
Al_2O_3	4.64 (.16)	.190	7.19 (.26)	.307	51.93 (.68)	1.611	15.15 (.18)	2.556
SiO_2	54.72 (1.1)	1.900	52.66 (.76)	1.905			43.35 (.19)	6.206
K_2O							1.57 (.03)	.286
CaO	0.69 (.04)	.026	18.27 (.27)	.708			9.82 (.12)	1.507
TiO_2							1.20 (.06)	.130
Cr_2O_3	0.48 (.09)	.013	1.21 (.09)	.034	15.96 (.63)	.333	1.50 (.05)	.169
FeO	5.96 (.14)	.173	2.92 (.18)	.088	11.47 (.28)	.252	3.85 (.06)	.461
Total	99.25	3.998	99.36	4.000	99.13	2.972	96.94	15.901
Mg'	90.74		90.15		75.49		88.86	
Ca'	1.37		44.22					
Cr'	6.40		9.97		17.13		6.20	
Mg'(ol)	90.60 (.06)							

Sample BM - 62

Phases	opx wt.%	opx struc	cpx wt.%	cpx struc	sp wt.%	sp struc	amph wt.%	amph struc
Na_2O	n.d.		1.39 (.07)	.097			3.57 (.08)	1.014
MgO	34.02 (.15)	1.747	15.81 (.17)	.851	18.12 (.35)	.732	17.94 (.26)	3.920
Al_2O_3	2.60 (.07)	.106	4.73 (.15)	.202	47.95 (1.9)	1.531	14.05 (.46)	2.426
SiO_2	56.45 (.07)	1.945	53.56 (.14)	1.933			42.73 (1.1)	6.261
K_2O							n.d.	
CaO	0.38 (.02)	.014	21.07 (.12)	.815			10.43 (.25)	1.636
TiO_2							0.54 (.11)	.060
Cr_2O_3	0.28 (.02)	.008	1.07 (.04)	.031	20.74 (1.6)	.444	1.49 (.15)	.173
FeO	6.27 (.05)	.180	2.37 (.12)	.071	12.26 (.48)	.278	3.23 (.10)	.396
Total	100.00	4.000	100.00	4.000	99.07	2.985	93.98	15.886
Mg'	90.66		92.30		72.48		90.82	
Ca'	0.72		46.92					
Cr'	7.02		13.30		22.48		6.66	
Mg'(ol)	89.75 (.17)							

Sample BM - 74

Phases	opx wt.%	opx struc	cpx wt.%	cpx struc	sp wt.%	sp struc	amph wt.%	amph struc
Na_2O	n.d.		1.55 (.04)	.108			2.97 (.10)	.843
MgO	33.08 (.11)	1.704	15.96 (.28)	.858	18.82 (.19)	.761	16.91 (.51)	3.687
Al_2O_3	3.63 (.15)	.148	5.14 (.16)	.219	47.68 (.32)	1.525	14.28 (.23)	2.461
SiO_2	55.62 (.14)	1.922	53.46 (.14)	1.927			42.45 (.83)	6.210
K_2O							0.92 (.07)	.171
CaO	0.39 (.07)	.014	20.44 (.20)	.790			10.79 (.21)	1.691
TiO_2							1.14 (.05)	.125
Cr_2O_3	0.29 (.04)	.008	1.06 (!11)	.030	19.71 (.28)	.423	1.68 (.08)	.194
FeO	6.39 (.08)	.185	2.39 (.04)	.072	12.61 (.15)	.286	3.81 (.12)	.466
Total	99.95	3.981	100.95	4.004	98.82	2.995	94.95	15.848
Mg'	90.21		92.23		72.67		88.78	
Ca'	0.75		45.92					
Cr'	5.13		12.05		21.71		7.31	
Mg'(ol)	89.18 (.06)							

Sample BM - 134

Phases	opx wt.%	opx struc	cpx wt.%	cpx struc	sp wt.%	sp struc	amph wt.%	amph struc
Na_2O	n.d.		2.33 (.11)	.162			3.89 (.30)	1.145
MgO	34.47 (.11)	1.773	15.34 (.18)	.822	15.55 (.35)	.675	16.90 (.79)	3.826
Al_2O_3	1.80 (.39)	.074	4.28 (.06)	.182	33.04 (1.4)	1.137	12.45 (.46)	2.230
SiO_2	56.61 (.49)	1.953	54.69 (.14)	1.968			41.58 (1.3)	6.376
K_2O							0.32 (.04)	.062
CaO	0.24 (.06)	.008	19.62 (.09)	.757			9.44 (.33)	1.538
TiO_2							0.36 (.12)	.041
Cr_2O_3	0.28 (.06)	.008	1.54 (.14)	.044	35.24 (1.5)	.814	2.25 (.14)	.270
FeO	6.30 (.11)	.182	2.21 (.10)	.066	15.42 (.33)	.377	3.48 (.12)	.443
Total	99.70	3.998	100.01	4.001	99.25	3.003	90.67	15.931
Mg'	90.69		92.57		64.16		89.62	
Ca'	0.41		46.02					
Cr'	9.76		19.47		41.72		10.80	
Mg'(ol)	89.73 (.06)							

Sample BM - 139

Phases	opx		cpx		sp		amph	
	wt.%	struc	wt.%	struc	wt.%	struc	wt.%	struc
Na_2O	n.d.		1.87 (.18)	.131			3.50 (.32)	.986
MgO	33.01 (.11)	1.701	15.11 (.17)	.811	19.40 (.18)	.763	17.31 (.36)	3.742
Al_2O_3	3.60 (.29)	.147	6.35 (.15)	.266	53.64 (1.5)	1.668	14.70 (.17)	2.514
SiO_2	55.66 (.52)	1.924	53.32 (.12)	1.921			42.80 (1.1)	6.207
K_2O							1.22 (.06)	.226
CaO	0.62 (.02)	.023	19.75 (.24)	.763			10.45 (.23)	1.623
TiO_2							0.90 (.05)	.098
Cr_2O_3	0.22 (.01)	.006	0.79 (.12)	.022	15.02 (1.4)	.314	0.99 (.08)	.114
FeO	6.97 (.13)	.201	3.00 (.11)	.090	11.84 (.08)	.261	3.94 (.11)	.478
Total	100.08	4.001	100.09	4.004	99.86	3.006	95.81	15.988
Mg'	89.43		90.01		74.51		88.67	
Ca'	1.19		45.90					
Cr'	3.92		7.64		15.84		4.34	
Mg'(ol)	88.60 (.13)							

Sample BM - 147

Phases	opx		cpx		sp		amph	
	wt.%	struc	wt.%	struc	wt.%	struc	wt.%	struc
Na_2O	n.d.		2.67 (.07)	.187			4.02 (.08)	1.108
MgO	34.43 (.15)	1.776	15.34 (.03)	.827	13.63 (.08)	.613	18.44 (.07)	3.907
Al_2O_3	2.12 (.13)	.086	4.70 (.26)	.200	27.13 (.88)	.965	13.62 (.19)	2.284
SiO_2	55.93 (.22)	1.935	53.71 (.25)	1.941			44.69 (.22)	6.352
K_2O							0.57 (.03)	.104
CaO	0.38 (.01)	.014	19.61 (.11)	.759			10.16 (.05)	1.548
TiO_2							0.34 (.02)	.037
Cr_2O_3	0.31 (.01)	.009	1.47 (.15)	.042	41.74 (1.0)	.996	1.95 (.10)	.219
FeO	6.61 (.07)	.191	2.50 (.04)	.075	17.38 (.11)	.439	3.57 (.11)	.424
Total	99.78	4.011	100.00	4.031	99.88	3.013	97.33	15.980
Mg'	90.29		91.69		58.27		90.21	
Ca'	0.71		45.70					
Cr'	9.47		17.36		50.79		8.75	

Sample BM - 161

Phases	opx		cpx		sp		amph	
	wt.%	struc	wt.%	struc	wt.%	struc	wt.%	struc
Na_2O	n.d.		1.67 (.16)	.117			2.86 (.27)	.847
MgO	33.16 (.14)	1.705	15.62 (.19)	.839	19.71 (.42)	.780	16.00 (.79)	3.650
Al_2O_3	3.89 (.17)	.157	5.77 (.21)	.245	51.83 (1.4)	1.622	13.83 (.57)	2.496
SiO_2	55.62 (.24)	1.919	53.22 (.33)	1.918			40.51 (1.7)	6.202
K_2O							0.86 (.05)	.168
CaO	0.39 (.11)	.015	20.32 (.58)	.784			10.34 (.26)	1.702
TiO_2							1.27 (.12)	.147
Cr_2O_3	0.24 (.04)	.007	0.99 (.05)	.028	15.80 (1.4)	.332	1.36 (.06)	.165
FeO	6.18 (.08)	.178	2.42 (.13)	.073	11.37 (.41)	.253	3.53 (.11)	.453
total	99.48	3.981	100.01	4.004	98.71	2.987	90.56	15.830
Mg'	90.55		92.00		75.51		88.96	
Ca'	0.79		46.23					
Cr'	4.27		10.26		16.99		6.20	
Mg'(ol)	89.69 (.07)							

Sample BM - 166

Phases	opx		cpx		sp		amph	
	wt.%	struc	wt.%	struc	wt.%	struc	wt.%	struc
Na_2O	n.d.		1.01 (.11)	.071			3.49 (.12)	.983
MgO	34.31 (.22)	1.762	16.02 (.20)	.862	20.23 (.07)	.796	17.47 (1.1)	3.814
Al_2O_3	3.30 (.33)	.134	4.86 (.07)	.207	52.81 (.36)	1.642	14.65 (.65)	2.511
SiO_2	55.70 (.30)	1.919	53.11 (.07)	1.918			42.52 (3.0)	6.174
K_2O							0.20 (.01)	.037
CaO	0.28 (.05)	.010	21.72 (.17)	.841			10.99 (.80)	1.709
TiO_2			0.24 (.03)	.007			1.33 (.12)	.145
Cr_2O_3	0.27 (.06)	.007	1.00 (.08)	.029	15.42 (.32)	.322	1.19 (.02)	.137
FeO	5.94 (.09)	.171	2.09 (.07)	.063	10.54 (.09)	.233	3.03 (.24)	.368
Total	99.80	4.003	100.05	3.997	99.00	2.993	94.87	15.878
Mg'	91.15		93.19		77.36		91.20	
Ca'	0.51		47.62					
Cr'	4.96		12.29		16.40		5.17	
Mg'(ol)	90.53 (.11)							

Sample BM - 167

Phases	opx		cpx		sp		amph	
	wt.%	struc	wt.%	struc	wt.%	struc	wt.%	struc
Na_2O	n.d.		1.38 (.04)	.097			3.35 (.27)	.985
MgO	33.04 (.49)	1.703	15.47 (.22)	.831	20.32 (.24)	.790	16.68 (.31)	3.767
Al_2O_3	4.52 (.54)	.184	6.60 (.21)	.280	55.49 (.66)	1.707	14.59 (.37)	2.606
SiO_2	54.87 (.53)	1.897	52.54 (.23)	1.893			40.39 (.78)	6.121
K_2O							n.d.	
CaO	0.41 (.09)	.015	20.40 (.13)	.787			9.77 (.32)	1.587
TiO_2			0.36 (.01)	.010			1.62 (.12)	.185
Cr_2O_3	0.25 (.11)	.006	0.90 (.16)	.026	11.54 (.29)	.238	0.95 (.11)	.113
FeO	6.53 (.13)	.189	2.42 (.09)	.073	11.22 (.18)	.245	3.66 (.12)	.465
Total	99.62	3.994	100.07	3.997	98.57	2.979	91.01	15.829
Mg'	90.01		91.92		76.33		89.01	
Ca'	0.79		46.54					
Cr'	3.16		8.50		12.24		4.16	
Mg'(ol)	89.50 (.10)							

Sample LE - 2641

Phases	opx		cpx		sp		amph	
	wt.%	struc	wt.%	struc	wt.%	struc	wt.%	struc
Na_2O	n.d.		1.18 (.07)	.083			3.32 (.08)	.930
MgO	34.17 (.15)	1.750	15.95 (.24)	.857	20.50 (.06)	.806	18.16 (.40)	3.908
Al_2O_3	3.17 (.13)	.128	4.99 (.12)	.212	52.21 (2.4)	1.623	14.38 (.36)	2.446
SiO_2	56.36 (.33)	1.936	53.26 (.24)	1.921			43.02 (.84)	6.209
K_2O							n.d.	
CaO	0.28 (.04)	.010	21.57 (.04)	.833			10.99 (.20)	1.699
TiO_2			0.22 (.02)	.006			1.32 (.22)	.143
Cr_2O_3	0.22 (.07)	.006	0.92 (.17)	.026	16.52 (2.5)	.345	1.13 (.06)	.129
FeO	5.79 (.07)	.166	1.95 (.10)	.059	9.66 (.17)	.213	2.99 (.09)	.360
Total	99.99	3.996	100.04	3.997	98.89	2.987	95.31	15.824
Mg'	91.34		93.56		79.10		91.57	
Cr'	4.48		10.92		17.53		5.01	
Ca'	0.52		47.63					
Mg'(ol)	90.56 (.06)							

Group A - 3 : phlogopite bearing lherzolites

Sample LE - 67

Phases	opx		cpx		sp		phlo	
	wt.%	struc	wt.%	struc	wt.%	struc	wt.%	struc
Na_2O	n.d.		1.61 (.05)	.113			0.46 (.14)	.133
MgO	33.75 (.20)	1.729	16.15 (.17)	.867	19.28 (.11)	.778	21.10 (.71)	4.744
Al_2O_3	4.13 (.16)	.167	5.73 (.20)	.243	46.96 (.32)	1.498	17.26 (.53)	3.069
SiO_2	55.54 (.23)	1.909	53.18 (.14)	1.915			37.48 (1.4)	5.654
K_2O							9.61 (.31)	1.850
CaO	0.71 (.05)	.026	19.56 (.09)	.755				
TiO_2							2.65 (.11)	.300
Cr_2O_3	0.53 (.07)	.014	1.22 (.08)	.035	21.77 (.31)	.466	1.58 (.06)	.189
FeO	5.33 (.09)	.153	2.54 (.03)	.076	11.55 (.12)	.262	3.73 (.16)	.472
Total	99.99	3.998	99.99	4.004	99.56	3.004	93.87	16.411
Mg'	91.87		91.94		74.81		90.95	
Ca'	1.36		44.46					
Cr'	7.73		12.59		23.73		5.80	
Mg'(ol)	91.46 (.07)							

Sample LE - 68

Phases	opx		cpx		sp		phlo	
	wt.%	struc	et.%	struc	wt.%	struc	wt.%	struc
Na_2O	n.d.		1.72 (.07)	.120			0.74	.233
MgO	33.17 (.13)	1.701	15.68 (.16)	.842	20.46 (.23)	.800	19.69	4.746
Al_2O_3	4.66 (.10)	.189	6.53 (.15)	.277	54.22 (.51)	1.675	16.64	3.173
SiO_2	55.40 (.10)	1.906	52.86 (.19)	1.902			34.27	5.543
K_2O							8.67	1.788
CaO	0.71 (.02)	.026	19.51 (.11)	.752				
TiO_2							2.86	.348
Cr_2O_3	0.41 (.05)	.011	0.90 (.04)	.026	14.29 (.36)	.296	0.98	.125
FeO	5.66 (.06)	.163	2.68 (.08)	.081	1o.69 (.53)	.235	3.79	.513
Total	100.01	3,996	99.70	4.000	99.66	3.006	87.65	16.470
Mg'	91.26		91.22		77.29		90.25	
Ca'	1.38		44.90					
Cr'	5.50		8.58		15.02		3.79	
Mg'(ol)	90.92 (.05)							

Group A-4: lherzolites with sites of former hydrous phases, now only present as secondary assemblages

Sample BM - 48

Phases	opx		cpx		sp	
	wt.%	struc	wt.%	struc	wt.%	struc
Na_2O	n.d.		2.04 (.07)	.142		
MgO	34.56 (.27)	1.767	15.83 (.17)	.850	16.14 (.89)	.711
Al_2O_3	1.61 (.17)	.065	2.97 (.09)	.126	27.70 (.84)	.964
SiO_2	57.54 (.21)	1.973	55.33 (.35)	1.992		
CaO	0.34 (.07)	.013	20.24 (.55)	.781		
Cr_2O_3	0.34 (.07)	.009	1.44 (.04)	.041	40.60 (.85)	.948
FeO	5.64 (.10)	.157	2.16 (.19)	.065	14.01 (1.3)	.346
Total	99.85	3.984	100.01	3.997	98.45	2.969
Mg'	91.84		92.90		67.27	
Ca'	0.67		46.05			
Cr'	12.16		24.55		49.58	
Mg'(ol)	91.20 (.16)					

Sample BM - 144

Phases	opx		cpx		sp	
	wt.%	struc	wt.%	struc	wt.%	struc
Na_2O	n.d.		1.34 (.09)	.094		
MgO	33.37 (.16)	1.721	15.86 (.35)	.853	19.92 (.69)	.784
Al_2O_3	3.82 (.09)	.156	5.70 (.39)	.243	53.23 (.43)	1.658
SiO_2	55.17 (.26)	1.908	53.04 (.25)	1.913		
CaO	0.46 (.12)	.017	20.60 (.19)	.796		
Cr_2O_3	0.27 (.02)	.007	0.90 (.10)	.026	14.53 (.36)	.303
FeO	6.66 (.08)	.193	2.56 (.08)	.077	11.35 (.69)	.251
Total	99.75	4.002	100.00	4.002	99.08	2.996
Mg'	89.92		91.72		75.75	
Ca'	0.88		46.12			
Cr'	4.29		9.67		15.45	
Mg'(ol)	89.09 (.09)					

Sample BM - 162

Phases	opx		cpx		sp	
	wt.%	struc	wt.%	struc	wt.%	struc
Na_2O	n.d.		1.23 (.08)	.086		
MgO	33.41 (.17)	1.720	16.04 (.09)	.862	19.92 (.20)	.783
Al_2O_3	3.89 (.14)	.159	5.67 (.24)	.241	53.19 (.52)	1.653
SiO_2	55.41 (.42)	1.913	53.02 (.11)	1.911		
CaO	0.42 (.08)	.016	20.52 (.08)	.793		
Cr_2O_3	0.20 (.10)	.006	1.00 (.09)	.028	13.73 (.32)	.287
FeO	6.48 (.07)	.187	2.53 (.16)	.077	11.69 (.08)	.258
Total	99.81	4.001	100.01	3.998	98.53	2.981
Mg'	90.19		91.80		75.22	
Ca'	0.83		45.79			
Cr'	3.64		10.41		14.79	
Mg'(ol)	89.37 (.09)					

Sample LE - 4

Phases	opx		cpx		sp	
	wt.%	struc	wt.%	struc	wt.%	struc
Na_2O	n.d.		2.10 (.09)	.146		
MgO	32.39 (.23)	1.665	15.01 (.18)	.805	20.49 (.26)	.781
Al_2O_3	5.74 (.26)	.234	7.94 (.42)	.337	59.10 (.79)	1.781
SiO_2	54.19 (.28)	1.874	52.25 (.29)	1.879		
CaO	0.68 (.04)	.025	18.53 (.12)	.714		
TiO_2			0.44 (.06)	.012		
Cr_2O_3	0.32 (.06)	.009	0.67 (.09)	.019	7.93 (.07)	.160
FeO	6.39 (.15)	.185	3.07 (.06)	.092	10.49 (.05)	.224
Total	99.62	3.992	100.01	4.004	98.01	2.946
Mg'	90.00		89.74		77.71	
Ca'	1.33		44.32			
Cr'	3.70		5.34		8.24	
Mg'(ol)	89.53 (.23)					

Sample LE - 19

Phases	opx		cpx		sp	
	wt.%	struc	wt.%	struc	wt.%	struc
Na_2O	n.d.		1.92 (.37)	.134		
MgO	35.34 (.22)	1.809	16.69 (.80)	.898	14.63 (1.1)	.651
Al_2O_3	1.21 (.35)	.049	2.23 (.23)	.095	18.71 (.60)	.687
SiO_2	57.26 (.36)	1.967	54.64 (.88)	1.973		
CaO	0.35 (.05)	.012	19.14 (.84)	.741		
Cr_2O_3	0.26 (.03)	.007	3.49 (1.0)	.100	50.46 (.82)	1.243
FeO	5.58 (.07)	.160	1.92 (.02)	.058	15.81 (.65)	.412
Total	100.00	4.004	100.03	3.999	99.61	2.993
Mg'	91.87		93.93		61.24	
Ca'	0.61		43.67			
Cr'	12.50		51.28		64.40	
Mg'(ol)	90.91 (.02)					

Sample LE - 544

Phases	opx		cpx		sp	
	wt.%	struc	wt.%	struc	wt.%	struc
Na_2O	n.d.		1.03 (.12)	.072		
MgO	33.90 (.22)	1.745	16.07 (.22)	.867	20.47 (.14)	.806
Al_2O_3	3.42 (.15)	.139	4.76 (.16)	.203	52.80 (.40)	1.644
SiO_2	55.45 (.26)	1.915	52.71 (.18)	1.908		
CaO	0.33 (.03)	.012	21.84 (.18)	.847		
TiO_2			0.32 (.04)	.009		
Cr_2O_3	0.32 (.12)	.008	1.04 (.18)	.030	14.48 (.37)	.303
FeO	6.21 (.13)	.179	2.24 (.09)	.068	11.21 (.18)	.248
Total	99.63	3.998	100.01	4.004	98.96	3.001
Mg'	90.70		92.73		76.47	
Ca'	0.62		47.53			
Cr'	5.44		12.88		15.56	
Mg'(ol)	89.94 (.09)					

Sample LE - 2662

Phases	opx wt.%	opx struc	cpx wt.%	cpx struc	sp wt.%	sp struc
Na_2O	n.d.		1.42 (.02)	.099		
MgO	34.72 (.14)	1.777	16.84 (.08)	.903	18.26 (.21)	.777
Al_2O_3	2.26 (.11)	.092	3.53 (.07)	.149	34.61 (.78)	1.165
SiO_2	56.83 (.17)	1.950	54.52 (.06)	1.960		
CaO	0.33 (.07)	.012	20.39 (.16)	.786		
Cr_2O_3	0.30 (.05)	.008	1.43 (.09)	.041	34.76 (1.0)	.785
FeO	5.18 (.12)	.149	1.87 (.07)	.056	11.51 (.39)	.275
Total	99.62	3.988	100.00	3.994	99.14	3.002
Mg'	92.26		94.16		73.86	
Ca'	0.62		45.04			
Cr'	8.00		21.58		40.26	
Mg'(ol)	91.50 (.07)					

Group A - 5: amphibole and phlogopite bearing lherzolites

Sample BM - 143

ases	opx wt.%	opx struc	cpx wt.%	cpx struc	sp wt.%	sp struc	amph wt.%	amph struc	phlo wt.%	phlo struc
a_2O	n.d.		2.09(.12)	.146			3.01(.10)	.831	0.79(.04)	.223
gO	33.10(.11)	1.708	15.39(.21)	.829	19.71(.18)	.779	16.78(.37)	3.565	20.35(.19)	4.435
l_2O_3	4.91(.32)	.200	6.99(.21)	.298	51.22(.92)	1.600	14.76(.18)	2.480	17.13(.06)	2.951
iO_2	54.17(.40)	1.874	51.66(.25)	1.867			42.53(.81)	6.000	37.98(.22)	5.551
$_2O$							1.78(.04)	.324	9.17(.04)	1.709
aO	0.84(.04)	.031	18.94(.09)	.733			10.47(.18)	1.598		
iO_2	0.20(.05)	.005	0.78(.07)	.021	0.43(.10)	.008	3.59(.07)	.385	6.04(.11)	.664
r_2O_3	0.54(.05)	.015	1.26(.09)	.036	16.48(.91)	.345	1.35(.04)	.152	1.27(.03)	.146
eO	5.99(.13)	.173	2.89(.05)	.087	11.60(.23)	.257	3.75(.10)	.448	4.27(.15)	.522
otal	99.75	4.006	100.00	4.017	99.44	2.898	98.02	15.783	97.00	16.201
g'	90.80		90.50		75.19		88.84		89.47	
a'	1.62		44.45							
r'	6.98		10.78		17.74		5.78		4.71	
g'(ol)	90.39 (.18)									

Group A-6: Fe-rich lherzolites

Sample BM - 47

Phases	opx		cpx		amph	
	wt.%	struc	wt.%	struc	wt.%	struc
Na_2O	n.d.		1.41 (.20)	.099	3.29 (.14)	.917
MgO	33.13 (.20)	1.716	15.85 (.29)	.855	18.03 (.23)	3.859
Al_2O_3	1.96 (.35)	.080	3.47 (.46)	.148	13.47 (.28)	2.290
SiO_2	56.17 (.20)	1.952	54.20 (.20)	1.962	44.34 (1.1)	6.368
K_2O					1.13 (.03)	.208
CaO	0.51 (.06)	.019	20.85 (.44)	.809	10.53 (.36)	1.620
TiO_2					n.d.	
Cr_2O_3	0.26 (.04)	.007	1.11 (.10)	.032	1.72 (.05)	.195
FeO	7.97 (.09)	.232	3.08 (.16)	.093	4.29 (.27)	.515
Total	100.00	4.006	99.97	3.998	96.80	15.962
Mg'	88.09		90.19		88.23	
Ca'	0.97		46.04			
Cr'	8.05		17.78		7.88	

Mg'(ol) 86.85 (.12)

Sample BM - 154

Phases	opx		cpx		sp		amph	
	wt.%	struc	wt.%	struc	wt.%	struc	wt.%	struc
Na_2O	n.d.		1.76 (.06)	.124			2.85 (.14)	.840
MgO	32.67 (.10)	1.691	15.45 (.18)	.833	14.55 (1.0)	.652	16.06 (.74)	3.638
Al_2O_3	2.38 (.19)	.097	4.34 (.13)	.186	28.22 (1.2)	.999	12.25 (.43)	2.195
SiO_2	56.06 (.18)	1.947	53.67 (.23)	1.942			41.47 (1.6)	6.304
K_2O							1.23 (.02)	.239
CaO	0.39 (.05)	.014	20.03 (.21)	.777			10.32 (.06)	1.683
TiO_2					0.29 (.02)	.007	1.25 (.08)	.143
Cr_2O_3	0.30 (.06)	.009	1.70 (.09)	.049	37.55 (1.8)	.892	2.24 (.11)	.270
FeO	7.58 (.08)	.220	3.06 (.02)	.093	18.12 (1.4)	.455	4.31 (.13)	.548
Total	99.38	3.978	100.01	4.004	98.73	3.005	91.98	15.860
Mg'	88.49		89.96		58.90		86.91	
Ca'	0.73		45.63					
Cr'	8.49		20.85		47.17		10.95	

Mg'(ol) 87.12 (.03)

Group A-7: banded or layered lherzolites

Sample BM -137

Phases	opx		cpx		sp		amph	
	wt.%	struc	wt.%	struc	wt.%	struc	wt.%	struc
Na_2O	n.d.		0.60 (.15)	.042			2.66 (.37)	.786
MgO	33.99 (.36)	1.747	16.12 (.63)	.868	20.67 (.24)	.792	16.43 (1.3)	3.740
Al_2O_3	3.11 (.43)	.127	4.64 (.94)	.198	59.55 (1.1)	1.803	13.99 (.99)	2.518
SiO_2	56.00 (.38)	1.931	53.14 (.63)	1.920			39.94 (2.9)	6.100
K_2O							0.80 (.11)	.155
CaO	0.31 (.03)	.012	22.57 (.32)	.874			11.21 (.54)	1.836
TiO_2							1.54 (.17)	.177
Cr_2O_3			0.61 (.11)	.017	8.47 (.96)	.172	0.96 (.09)	.116
FeO	6.59 (.41)	.190	2.20 (.21)	.067	10.64 (.32)	.229	3.52 (.13)	.450
Total	100.00	4.007	99.88	3.986	99.33	2.996	91.05	15.878
Mg'	90.19		92.83		77.57		89.26	
Ca'	0.62		48.31					
Cr'	0		7.91		8.71		4.32	

Mg'(ol) 89.67 (.24)

Group B: wehrlites

Sample BM - 18

Phases	cpx		sp		amph		opx	
	wt.%	struc	wt.%	struc	wt.%	struc	wt.%	struc
Na_2O	1.81 (.42)	.1			4.09 (.15)	1.158	n.d.	
MgO	16.08 (.51)	.867	11.26 (.36)	.547	19.12 (.47)	4.140	35.14 (.15)	1.801
Al_2O_3	1.80 (.61)	.077	11.83 (.84)	.456	9.42 (.34)	1.614	n.d.	
SiO_2	55.22 (1.2)	1.998			45.98 (1.4)	6.679	58.28 (.17)	2.004
K_2O					n.d.			
CaO	21.35 (.60)	.828			10.03 (.24)	1.562	0.36 (.05)	.013
TiO_2			0.20 (.10)	.005	0.60 (.17)	.065		
Cr_2O_3	1.44 (.90)	.041	58.14 (1.1)	1.502	2.26 (.41)	.260	n.d.	
FeO	2.29 (.30)	.069	18.66 (.54)	.510	3.02 (.05)	.368	6.22 (.08)	.179
Total	100.00	4.007	100.09	3.020	95.08	15.950	100.00	3.997
Mg'	92.36		51.57		91.84		90.96	
Ca'	46.94						0.65	
Cr'	34.75		76.71		13.87		0	
Mg'(ol)	89.79 (.04)							

Sample BM - 51

Phases	cpx		sp		amph	
	wt.%	struc	wt.%	struc	wt.%	struc
Na_2O	2.36 (.28)	.166			4.48 (.16)	1.244
MgO	15.26 (.32)	.822	11.24 (.23)	.543	19.36 (.17)	4.135
Al_2O_3	2.88 (.37)	.123	13.89 (.68)	.530	9.86 (.16)	1.634
SiO_2	55.11 (.19)	1.992			46.96 (.26)	6.727
K_2O					0.66 (.02)	.121
CaO	20.36 (.40)	.789			9.97 (.10)	1.530
TiO_2					0.25 (.05)	.027
Cr_2O_3	1.42 (.20)	.041	56.07 (.89)	1.435	1.74 (.08)	.197
FeO	2.62 (.29)	.079	18.80 (.29)	.509	3.20 (.05)	.383
Total	100.01	4.012	100.00	3.017	96.48	15.998
Mg'	91.23		51.62		91.52	
Ca'	46.69					
Cr'	25.00		73.03		10.76	
Mg'(ol)	89.81 (.15)					

Sample BM - 135 BM -142

Phases	cpx		amph		cpx	
	wt.%	struc	wt.%	struc	wt.%	struc
Na_2O	1.63 (.18)	.115	4.10 (.10)	1.146	2.06 (.20)	.145
MgO	15.92 (.31)	.859	18.62 (.52)	4.004	15.59 (.17)	.846
Al_2O_3	2.22 (.23)	.094	10.13 (.17)	1.723	1.70 (.46)	.073
SiO_2	54.97 (.20)	1.990	45.94 (1.0)	6.637	54.60 (.13)	1.989
K_2O			0.83 (.02)	.153		
CaO	21.23 (.31)	.824	9.78 (.13)	1.513	20.38 (.48)	.795
TiO_2			0.89 (.07)	.096		
Cr_2O_3	1.20 (.28)	.034	1.87 (.11)	.213	2.11 (.08)	.061
FeO	2.84 (.09)	.086	3.83 (.06)	.462	3.57 (.03)	.109
Total	100.01	4.002	95.99	15.947	100.01	4.018
Mg'	90.90		89.66		88.59	
Ca'	46.58				45.43	
Cr'	26.56		11.00		45.52	
Mg'(ol)	87.92 (.20)				85.40 (.28)	

Sample	matrix			BM - 152			cumulate			
Phases	cpx			amph			cpx		opx	
	wt.%		struc	wt.%		struc	wt.%	struc	wt.%	struc
Na_2O	1.44	(.22)	.102	3.06	(.33)	.879	1.35 (.13)	.095	n.d.	
MgO	15.13	(.70)	.824	15.31	(.20)	3.777	14.67 (.22)	.798	30.72	1.613
Al_2O_3	6.69	(.71)	.289	14.24	(.12)	2.484	7.56 (.51)	.325	5.03	.209
SiO_2	50.63	(.69)	1.850	40.84	(.43)	6.044	50.33 (.54)	1.836	52.74	1.858
K_2O				1.23	(.11)	.232				
CaO	19.51	(.66)	.764	10.36	(.06)	1.643	19.79 (.28)	.774	0.92	.035
TiO_2	0.83	(.18)	.023	3.28	(.33)	.365	1.02 (.14)	.028	0.37	.010
Cr_2O_3	0.53	(.26)	.015	0.37	(.04)	.043	0.35 (.06)	.010	0.22	1006
FeO	5.25	(.19)	.160	6.63	(.10)	.820	4.94 (.16)	.151	10.01	.295
Total	100.01		4.027	95.32		15.878	100.01	4.017	100.01	4.025
Mg'	83.74			80.46			84.09		84.54	
Ca'	43.71						44.92			
Cr'	4.93			1.70			2.99		2.79	
Mg'(ol)	82.63	(.17)					83.39 (.22)			

Sample	LE - 27									
Phases	cpx			sp			phlo		opx	
	wt.%		struc	wt.%		struc	wt.%	struc	wt.%	struc
Na_2O	1.37	(.10)	.096				0.70 (.18)	.210	n.d.	
MgO	15.52	(.12)	.837	19.66	(.11)	.775	20.56 (.65)	4.749	33.09	1.704
Al_2O_3	6.05	(.09)	.258	52.99	(.01)	1.652	16.68 (.15)	3.046	4.27	.174
SiO_2	52.41	(.11)	1.895				36.99 (1.7)	5.728	55.12	1.904
K_2O							9.01 (.41)	1.780		
CaO	20.46	(.17)	.793				0.37 (.32)	.064	0.72	.027
TiO_2	0.43	(.01)	.012	0.21	(.02)	.004	4.72 (.13)	.551		
Cr_2O_3	0.80	(.09)	.023	15.15	(.19)	.317	0.97 (.07)	.119	0.40	.011
FeO	3.00	(.06)	.091	12.07	(.07)	.267	4.25 (.16)	.551	6.40	.185
Total	100.04		4.005	100.08		3.015	94.25	16.798	101.20	4.004
Mg'	90.19			74.38			89.60		90.21	
Ca'	46.08								1.41	
Cr'	8.19			16.10			3.76		5.95	
Mg'(ol)	89.75	(.11)								

Group C: harzburgites

Sample	BM -163							
Phases	opx			sp			amph	
	wt.%		struc	wt.%		struc	wt.%	struc
Na_2O	n.d.						4.61 (.27)	1.285
MgO	35.17	(.20)	1.801	12.46	(.37)	.593	19.14 (.50)	4.106
Al_2O_3	2.27	(.52)	.092	14.66	(.52)	.552	10.53 (.09)	1.787
SiO_2	56.57	(.47)	1.943				46.00 (1.8)	6.615
K_2O							0.62 (.11)	.114
CaO	0.32	(.06)	.012				9.28 (.49)	1.430
TiO_2							0.20 (.20)	.020
Cr_2O_3				56.07	(.59)	1.416	3.04 (.15)	.346
FeO	5.30	(.10)	.152	16.64	(.35)	.444	2.59 (.11)	.312
Total	99.63		4.000	99.83		3.005	96.01	16.015
Mg'	92.22			57.18			92.94	
Ca'	0.61							
Cr'	0			70.48			16.22	
Mg'(ol)	91.44	(.10)						

Group D: Hornblendites

Sample BM -117

Phases	amph		phlo		ilm		ttmg	
	wt.%	struc	wt.%	struc	wt.%	struc	wt.%	struc
Na_2O	2.85 (.10)	.818	0.99 (.11)	.285				
MgO	12.08 (.15)	2.665	14.40 (.18)	3.204	9.38 (.35)	.669	8.23 (1.9)	.431
Al_2O_3	14.96 (.26)	2.610	16.38 (.10)	2.882	1.09 (.12)	.046	8.68 (.88)	.359
SiO_2	40.21 (.64)	5.954	36.87 (.28)	5.492				
K_2O	1.76 (.05)	.333	9.14 (.11)	1.743				
CaO	9.87 (.14)	1.565						
TiO_2	5.06 (.10)	.563	8.90 (.09)	.999	52.16 (.55)	1.876	24.80 (1.5)	.655
FeO	10.07 (.09)	1.247	11.89 (.23)	1.484	37.00 (.70)	1.480	57.70 (2.4)	1.697
MnO					0.22 (.02)	.009		
Total	96.86	15.755	98.57	16.089	99.85	4.079	99.41	3.142
Mg'	68.12		68.34		31.13			
Mg'(ol)	72.69 (.35)							

Sample BM -156

Phases	amph		phlo		ilm	
	wt.%	struc	wt.%	struc	wt.%	struc
Na_2O	2.71 (.10)	.778	0.94 (.06)	.277		
MgO	12.48 (.54)	2.750	14.71 (.14)	3.339	8.67 (.37)	.619
Al_2O_3	14.87 (.32)	2.594	16.45 (.21)	2.953	0.82 (.08)	.046
SiO_2	39.97 (.48)	5.942	36.26 (.41)	5.523		
K_2O	1.78 (.03)	.338	8.93 (.07)	1.735		
CaO	10.06 (.14)	1.602				
TiO_2	4.42 (.17)	.495	7.21 (.12)	.826	52.51 (.35)	1.894
FeO	10.54 (.29)	1.310	12.01 (.21)	1.530	37.84 (.72)	1.518
MnO					0.22 (.02)	.009
Total	96.83	15.809	96.51	16.183	100.00	4.086
Mg'	67.73		68.58		28.97	

Sample BM - 156 (pyroxenitic pocket)

Phases	amph		opx		cpx	
	wt.%	struc	wt.%	struc	wt.%	struc
Na_2O	2.76 (.15)	.789	n.d.		1.13 (.05)	.081
MgO	13.83 (.26)	3.040	26.23 (.50)	1.410	13.56 (.46)	.744
Al_2O_3	14.45 (.23)	2.512	4.75 (.47)	.202	7.17 (.68)	.311
SiO_2	40.76 (.76)	6.011	52.30 (.34)	1.885	50.16 (.46)	1.846
K_2O	1.20 (.08)	.225				
CaO	10.39 (.14)	1.642	0.91 (.04)	.035	19.28 (.35)	.760
TiO_2	3.76 (.16)	.418	0.26 (.04)	.007	1.13 (.13)	.032
FeO	9.55 (.17)	1.178	15.60 (.42)	.471	7.52 (.39)	.232
Total	96.70	15.815	100.05	4.010	99.95	4.006
Mg'	72.10		74.96		76.23	
Ca'			1.83		43.78	
Mg'(ol)	73.41 (.28)					

Groups E and F: pyroxenites and composite xenoliths

Sample BM - 109 (primary phases)

Phases	opx		cpx		sp		amph	
	wt.%	struc	wt.%	struc	wt.%	struc	wt.%	struc
Na_2O	n.d.		1.69 (.06)	.118			3.38 (.12)	.951
MgO	33.59 (.37)	1.732	15.65 (.08)	.842	15.56 (.60)	.667	17.51 (.31)	3.791
Al_2O_3	2.64 (.10)	.108	4.50 (.11)	.192	36.44 (1.6)	1.235	13.80 (.28)	2.361
SiO_2	55.95 (.18)	1.935	53.94 (.18)	1.948			43.39 (1.0)	6.300
K_2O							0.79 (.05)	.146
CaO	0.57 (.05)	.021	19.50 (.23)	.755			10.06 (.27)	1.566
TiO_2							0.48 (.07)	.054
Cr_2O_3	0.46 (.04)	..013	1.40 (.17)	.040	31.01 (1.5)	.706	2.10 (.06)	.241
FeO	6.79 (.39)	.197	3.34 (.35)	.101	16.23 (1.1)	.391	4.01 (.12)	.487
Total	100.00	4.006	100.02	3.996	99.24	2.999	95.52	15.896
Mg'	89.79		89.29		63.04		88.62	
Ca'	1.08		44.46					
Cr'	10.74		17.24		36.37		9.26	
Mg'(ol)	88.94 (.25)							

Sample BM - 109 (vein)

Phases	amph		phlo		cpx		Trans-amph	
	wt.%	struc	wt.%	struc	wt.%	struc	wt.%	struc
Na_2O	3.39 (.11)	.927	1.17 (.09)	.328	1.90 (.16)	.133	3.31 (.12)	.929
MgO	16.79 (.20)	3.527	21.02 (.68)	4.527	15.23 (.28)	.822	17.02 (.28)	3.678
Al_2O_3	13.28 (.27)	2.206	16.62 (.37)	2.830	5.18 (.35)	.221	13.19 (.37)	2.254
SiO_2	45.01 (.43)	6.340	39.68 (1.0)	5.733	53.73 (.09)	1.944	43.10 (.62)	6.244
K_2O	1.31 (.03)	.235	9.06 (.21)	1.670			1.11 (.02)	.205
CaO	10.01 (.11)	1.511			18.93 (.18)	.734	10.12 (.08)	1.571
TiO_2	2.66 (.15)	.282	4.39 (.26)	.477	0.27 (.04)	.007	2.08 (.12)	.226
Cr_2O_3							1.80 (.14)	.206
FeO	7.02 (.25)	.828	6.69 (.70)	.808	4.77 (.35)	.144	4.58 (.12)	.554
Total	99.47	15.856	98.63	16.373	100.01	4.005	96.31	15.867
Mg'	80.99		84.85		85.09		86.91	
Ca'					43.18			
Cr'							8.37	

Sample BM - 114 gt-pyroxenite amph-clinopyroxenite

Phases	gt		cpx		opx		amph	
	wt.%	struc	wt.%	struc	wt.%	struc	wt.%	struc
Na_2O			1.50 (.12)	.105			3.19 (.25)	.894
MgO	19.98 (.10)	2.127	15.09 (.15)	.811	32.00 (.21)	1.653	17.15 (.84)	3.694
Al_2O_3	23.80 (.31)	2.003	7.23 (.26)	.307	5.45 (.07)	.223	17.16 (.52)	2.923
SiO_2	41.31 (.47)	2.949	52.57 (.20)	1.895	54.24 (.18)	1.882	42.14 (2.0)	6.088
K_2O							0.80 (.04)	.147
CaO	4.76 (.03)	.365	20.16 (.13)	.779	0.51 (.05)	.019	10.11 (.62)	1.588
TiO_2							0.54 (.09)	.058
Cr_2O_3			0.34 (.04)	.010				
FeO	9.42 (.19)	.562	3.17 (.06)	.096	7.53 (.05)	.219	4.24 (.19)	.513
MnO	0.36 (.07)	.022						
Total	99.63	8.028	100.06	4.003	99.73	3.996	95.33	15.905
Mg'	79.10		89.42		88.30		87.81	
Ca'	11.95		46.20		1.00			
Cr'			3.15					

Sample BM - 116 (lherzolite)

Phases	opx		cpx		sp		amph	
	wt.%	struc	wt.%	struc	wt.%	struc	wt.%	struc
Na_2O	n.d.		1.66 (.09)	.116			3.30 (.20)	.905
MgO	34.11 (.18)	1.751	16.00 (.11)	.859	18.93 (.53)	.777	17.95 (.64)	3.788
Al_2O_3	3.06 (.07)	.124	5.14 (.37)	.218	43.71 (.86)	1.417	15.26 (.87)	2.543
SiO_2	55.96 (.12)	1.928	53.59 (.22)	1.930			44.00 (2.0)	6.226
K_2O							0.98 (.04)	.176
CaO	0.47 (.07)	.017	20.12 (.05)	.777			10.48 (.44)	1.589
TiO_2							0.52 (.10)	.056
Cr_2O_3	0.35 (.02)	.010	1.24 (.07)	.036	24.29 (.83)	.528	1.80 (.12)	.202
FeO	5.70 (.12)	.164	2.26 (.03)	.068	12.16 (.26)	.280	3.42 (.11)	.405
Total	99.65	3.994	100.01	4.004	99.04	3.002	97.71	15.890
Mg'	91.44		92.66		73.51		90.34	
Ca'	0.88		45.60					
Cr'	7.46		14.17		27.15		7.36	
Mg'(ol)	90.07 (.07)							

Sample clinopyroxenite BM - 116 transition-zone

Phases	cpx		sp		cpx		sp	
	wt.%	struc	wt.%	struc	wt.%	struc	wt.%	struc
Na_2O	1.60 (.08)	.112			1.50 (.12)	.105		
MgO	15.46 (.35)	.831	20.06 (	.799	15.39 (.21)	.825	22.25 (.17)	.834
Al_2O_3	6.33 (.46)	.269	50.03	1.576	7.17 (.32)	.304	64.07 (.35)	1.898
SiO_2	52.78 (.31)	1.902)			52.71 (.32)	1.895		
CaO^2	20.43 (.16)	.789			20.26 (.15)	.781		
Cr_2O_3	1.01 (.08)	.029	17.82	.376	0.51 (.12)	.014	3.37 (.43)	.067
FeO	2.31 (.11)	.070	11.14	.249	2.45 (.10)	.074	9.51 (.14)	.200
Total	99.92	4.002	99.05	3.000	99.99	3.998	99.20	2.999
Mg'	92.23		76.24		91.77		80.66	
Ca'	46.69				46.49			
Cr'	9.43		19.26		4.40		3.41	

Sample transition zone BM - 116 gt-pyroxenite

Phases	amph		opx		gt		cpx		opx	
	wt.%	struc	wt.%	struc	wt.%	struc	wt.%	struc	wt.%	struc
Na_2O	2.85(.34)	.863					1.66(.16)	.116		
MgO	15.66(.80)	3.656	33.31(.07)	1.713	20.55(.07)	2.172	15.22(.16)	.815	32.41(.07)	1.670
Al_2O_3	14.66(.65)	2.736	4.92(.13)	.200	23.86(.23)	1.995	7.52(.19)	.318	5.84(.20)	.238
SiO_2	39.03(1.8)	6.116	54.97(.01)	1.890	41.89(.29)	2.970	52.74(.17)	1.895	54.19(.19)	1.874
K_2O	0.74(.05)	.149								
CaO	10.15(.28)	1.705	0.54(.04)	.020	4.64(.04)	.353	19.98(.19)	.769	0.49(.02)	.018
TiO_2	1.07(.11)	.125								
Cr_2O_3	0.57(.10)	.071			0.22(.20)	.012	0.31(.10)	.009		
FeO	3.69(.09)	.484	6.12(.11)	.176	8.25(.18)	.489	2.60(.11)	.078	6.42(.10)	.186
MnO					0.33(.08)	.020				
Total	88.42	15.905	99.68	3.999	99.52	7.999	100.03	4.000	99.35	3.986
Mg'	88.31		90.68		81.62		91.27		89.98	
Ca'			1.05		11.71		46.27		0.96	
Cr'	2.53		0		0.60		2.75		0	

Sample LE - 00 (vein, lherzolite phases see A-1)

Phase	phlo	
	wt.%	struc
Na_2O	0.92 (.11)	.288
MgO	20.97 (.42)	4.640
Al_2O_3	16.32 (.26)	2.856
SiO_2	38.11 (.24)	5.657
K_2O	9.30 (.11)	1.761
TiO_2	4.34 (.07)	.484
Cr_2O_3	1.74 (.11)	.204
FeO	3.84 (.10)	.476
Total	95.54	16.366
Mg'	90.70	
Cr'	6.67	

Group G: cumulate textured wehrlite

Sample BM- 168

Phases	cpx		amph		phlo		opx	
	wt.%	struc	wt.%	struc	wt.%	struc	wt.%	struc
Na_2O	2.22 (.08)	.156	3.25 (.10)	.912	0.76 (.08)	.222		
MgO	14.57 (.25)	.790	15.28 (.27)	3.293	18.58 (.36)	4.170	29.77	1.570
Al_2O_3	7.34 (.24)	.314	14.87 (.21)	2.535	17.29 (.43)	3.069	4.49	.187
SiO_2	51.66 (.13)	1.878	41.98 (.89)	6.069	37.37 (.79)	5.607	53.35	1.887
K_2O			1.65 (.05)	.304	8.87 (.32)	1.697		
CaO	18.00 (.25)	.701	9.89 (.19)	1.533			0.98	.037
TiO_2	0.56 (.07)	.015	3.40 (.20)	.370	4.79 (.21)	.543		
FeO	5.49 (.08)	.167	7.32 (.16)	.885	7.97 (.25)	1.004	11.20	.331
Total	99.84	4.021	97.64	15.901	95.63	16.312	99.86	4.012
Mg'	82.55		78.82		80.60		82.60	
Ca'	42.28						1.91	

Mg'(ol) 80.76 (.16)

APPENDIX 4

Comparison of bulk rock chemistry of lherzolites from Lake Bullenmerri with those from other localities.

Bulk rock chemistry data for spinel lherzolite xenoliths from other volcanic centres around the world are compared to the data from Lake Bullenmerri to infer whether the history deduced from Lake Bullenmerri lherzolites is a local case or may be seen as a more generally applicable process.

The comparison of the data from Lake Bullenmerri with chemical variation lines obtained by statistical methods from a large number of lherzolite nodules from different localities grouped together (Maaløe & Aoki, 1977) is not meaningful unless all can be shown to have a very similar history. Principally every single location may have its own history with different degrees of extraction of differing melts from differing sourc compositions.

Localities have been chosen for which a number of analyses were available, which come from geographically different areas, and which show a considerable spread in chemistry. The compared data were taken from Frey & Prinz (1978) (San Carlos, Arizona), Girod *et al.* (1981) (Hoggar, Algeria) Hutchinson *et al.* (1975) (France), Kuno & Aoki (1970) (Dreiser Weiher, Germany and Hawaii), Ottonello *et al.* (1978) (Assab, Ethiopia), and Sachtleben & Seck (1981) (Dreiser Weiher, Germany).

Plots of MgO vs. major oxides for these data are given in fig. 63a-g. The trend of the chemical variation of Lake Bullenmerri nodules is indicated in these plots except for Na_2O, where uncertainties prevented the deduction of a clearly defined trendline.

The data from Germany, France, Algeria and Hawaii are very similar to the data from this work for all elements. However, bias exists for TiO_2 and Cr_2O_3 from Dreiser Weiher. Although taken from the same locality the analyses presented by Kuno & Aoki (1970) show systematic displacement

Figure 63: a-g Plots of MgO vs oxides in wt.% for bulk rock compositions of spinel lherzolites from various localities. Data from Frey & Prinz (1978), Girod *et al.* (1981), Hutchinson (1975), Kuno & Aoki (1970), Ottonello *et al.* (1978), Sachtleben & Seck (1981), and this work.

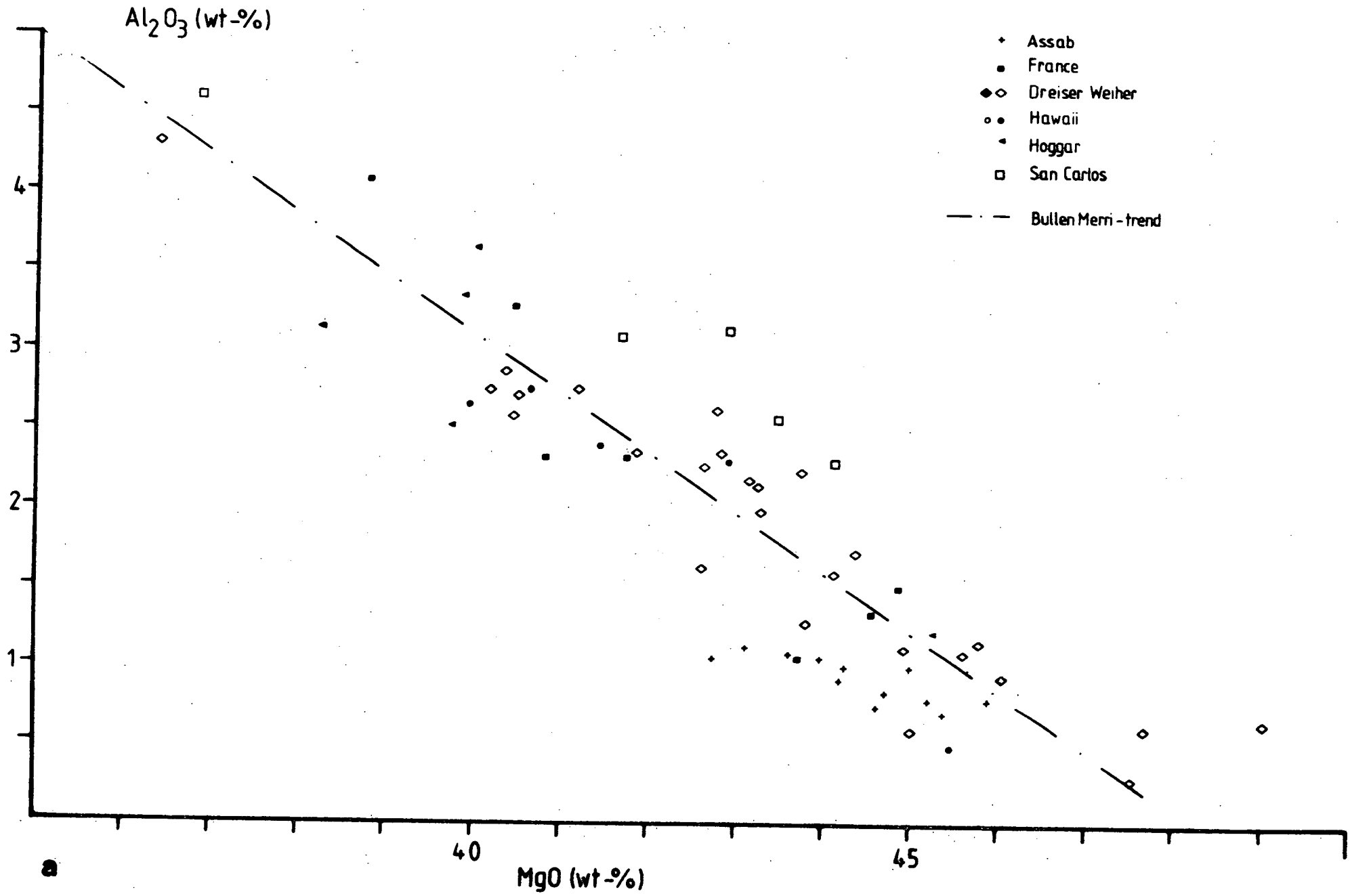
Al_2O_3 (wt-%)
4
3
2
1
40
45
MgO (wt-%)
a
Assab
France
Dreiser Weiher
Hawaii
Hoggar
San Carlos
Bullen Merri - trend

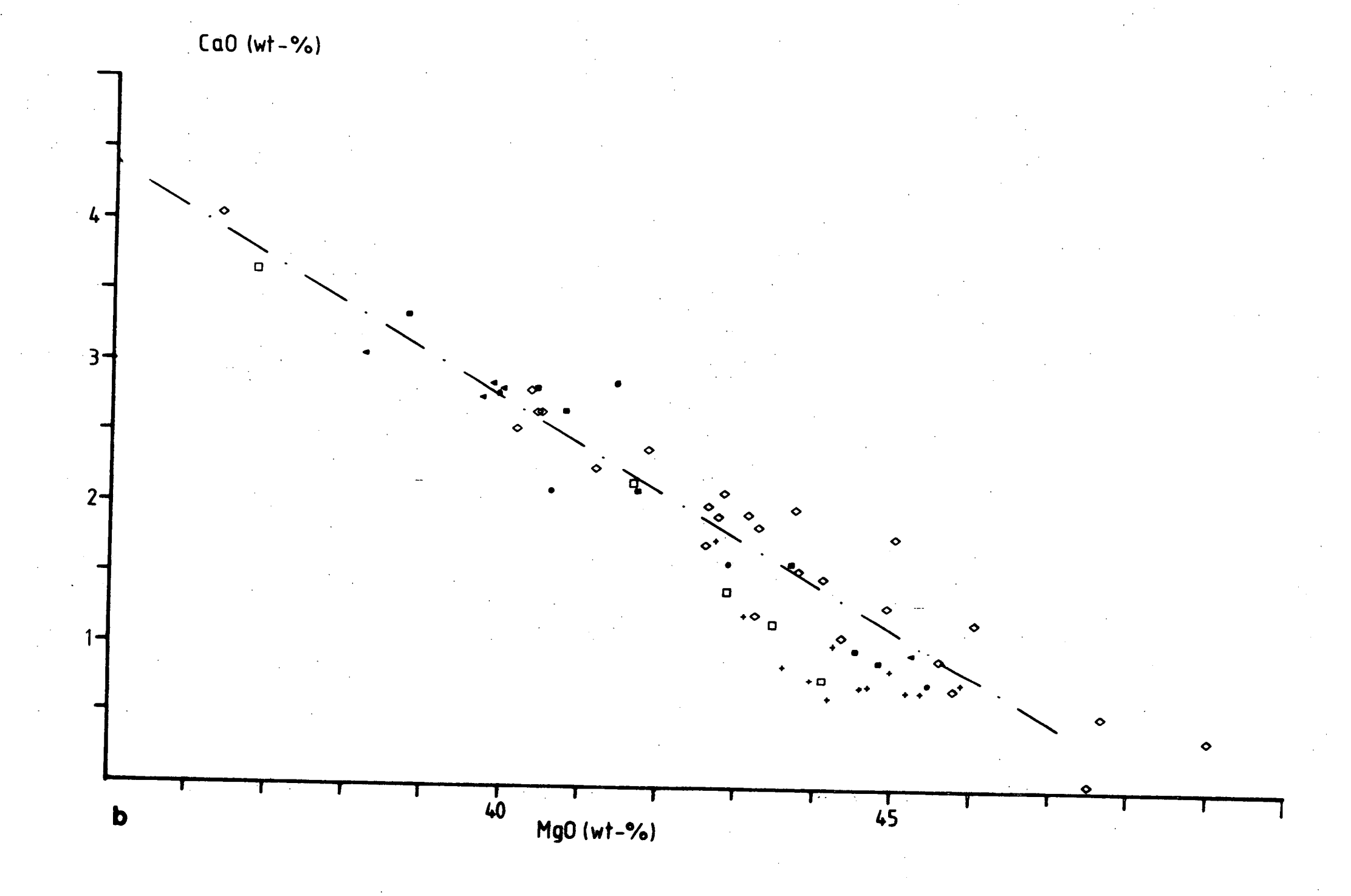
CaO (wt-%)
4
3
2
1
b
40
MgO (wt-%)
45

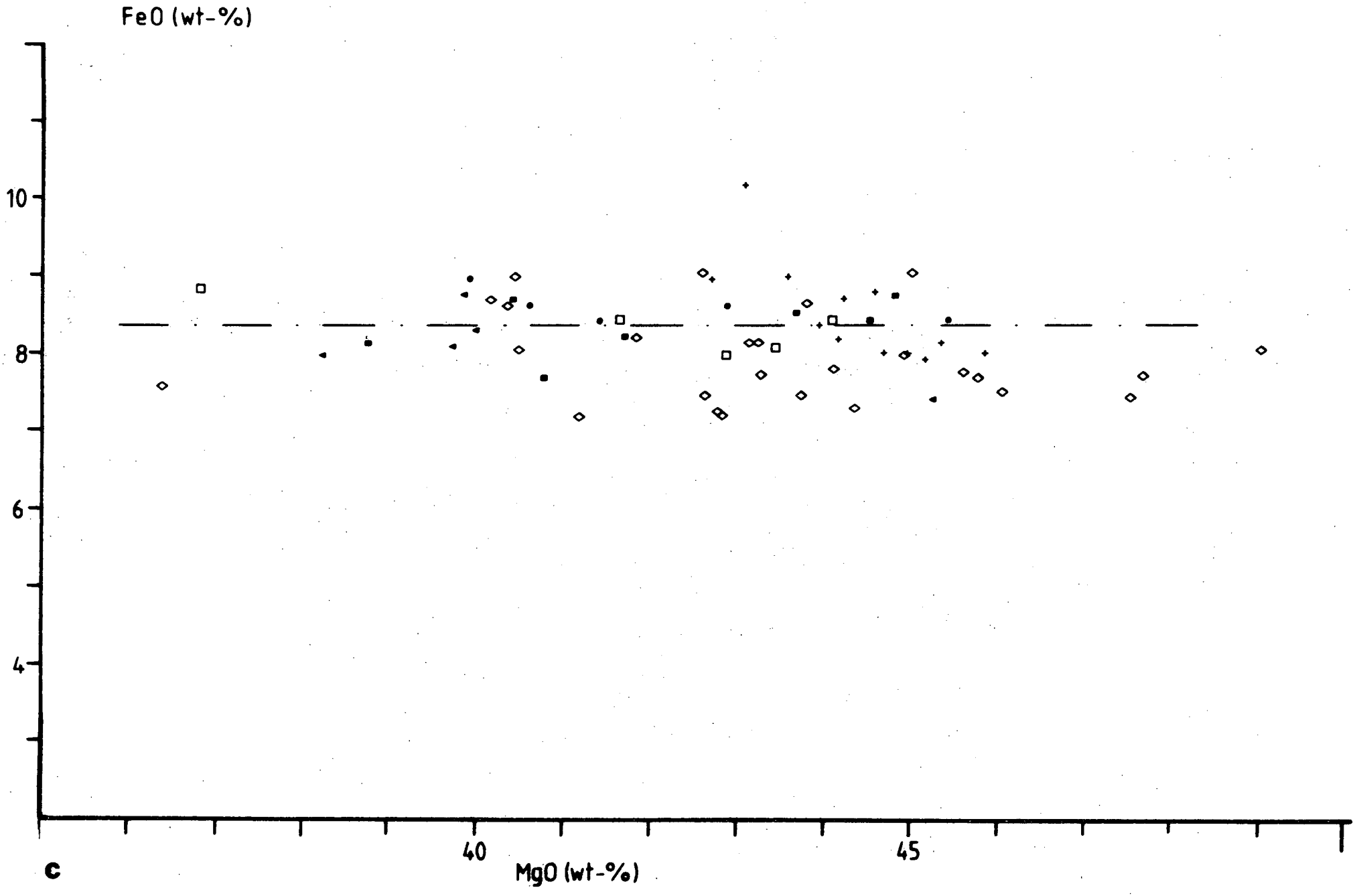

c

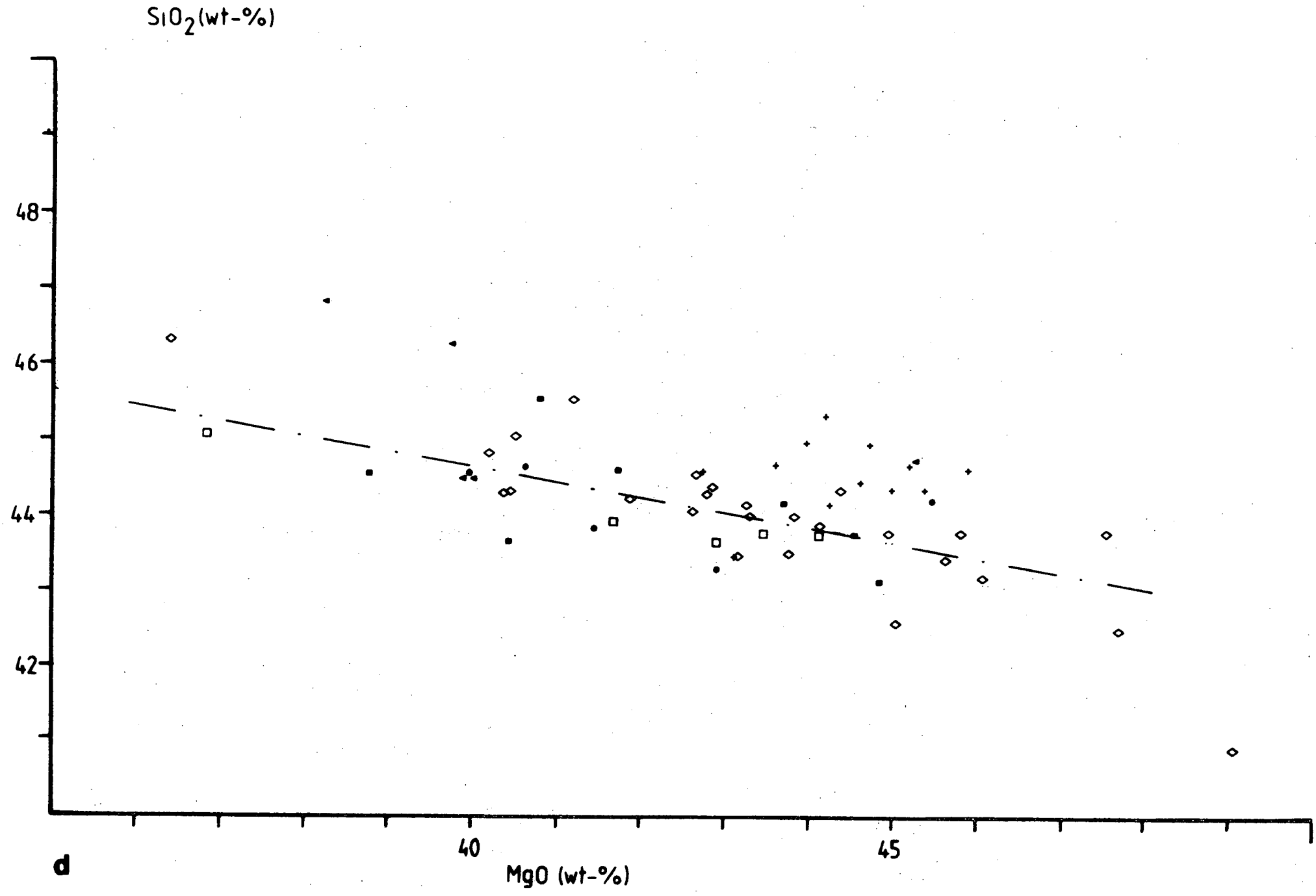
SiO2(wt-%)
48
46
44
42
40
45
MgO (wt-%)
d

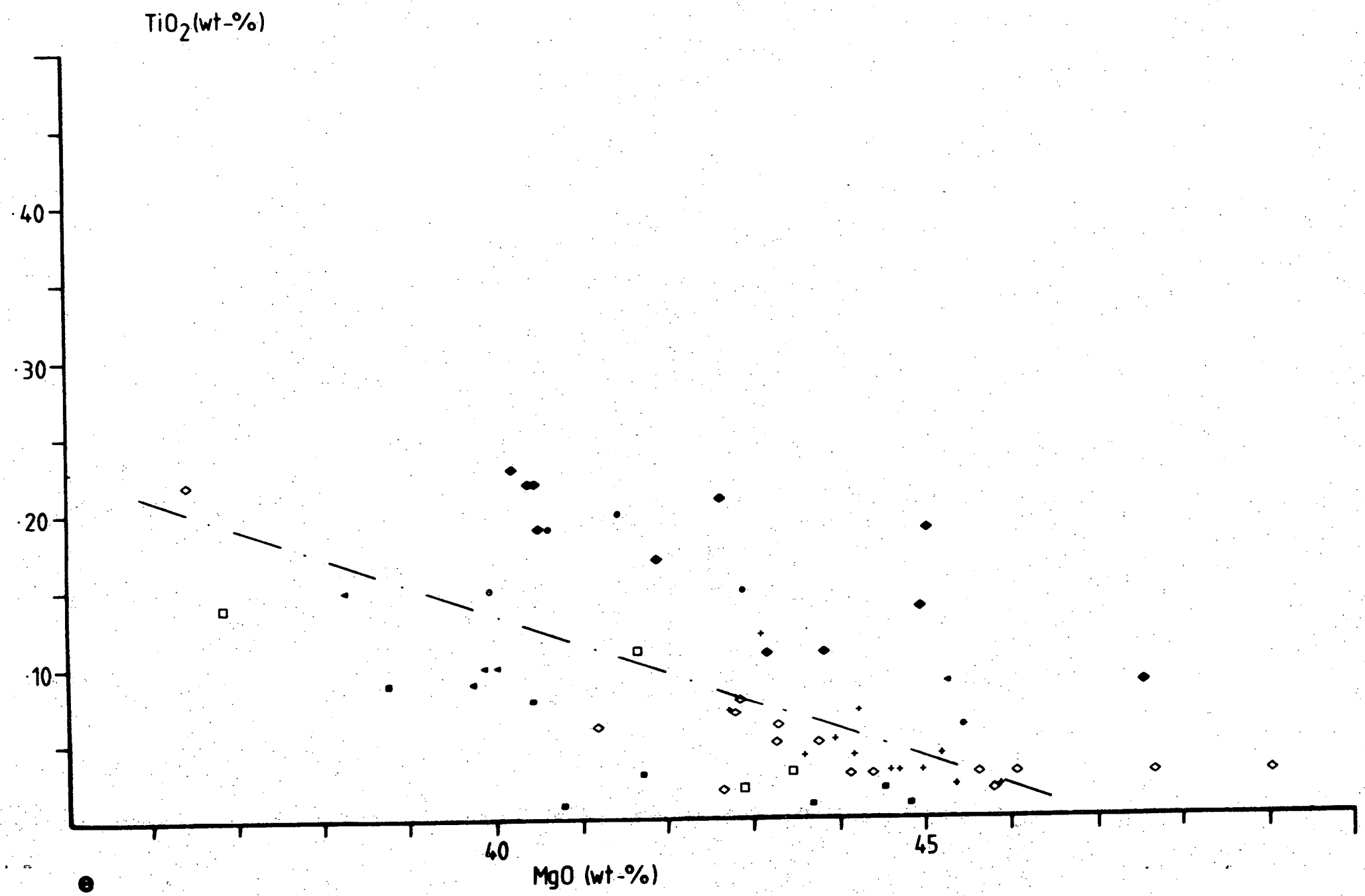
TiO2(wt-%)
40
30
20
10
40
45
MgO (wt-%)

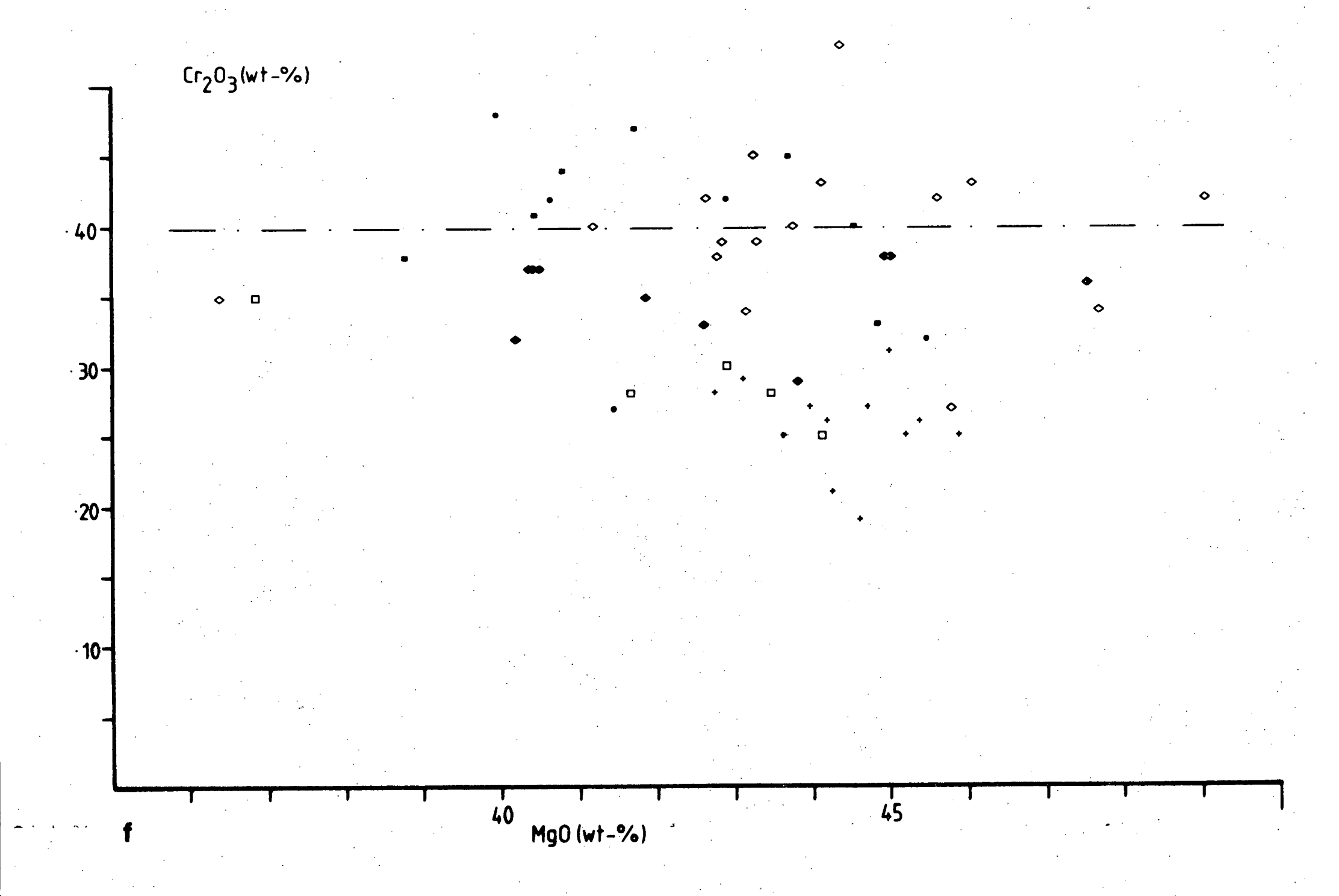

f

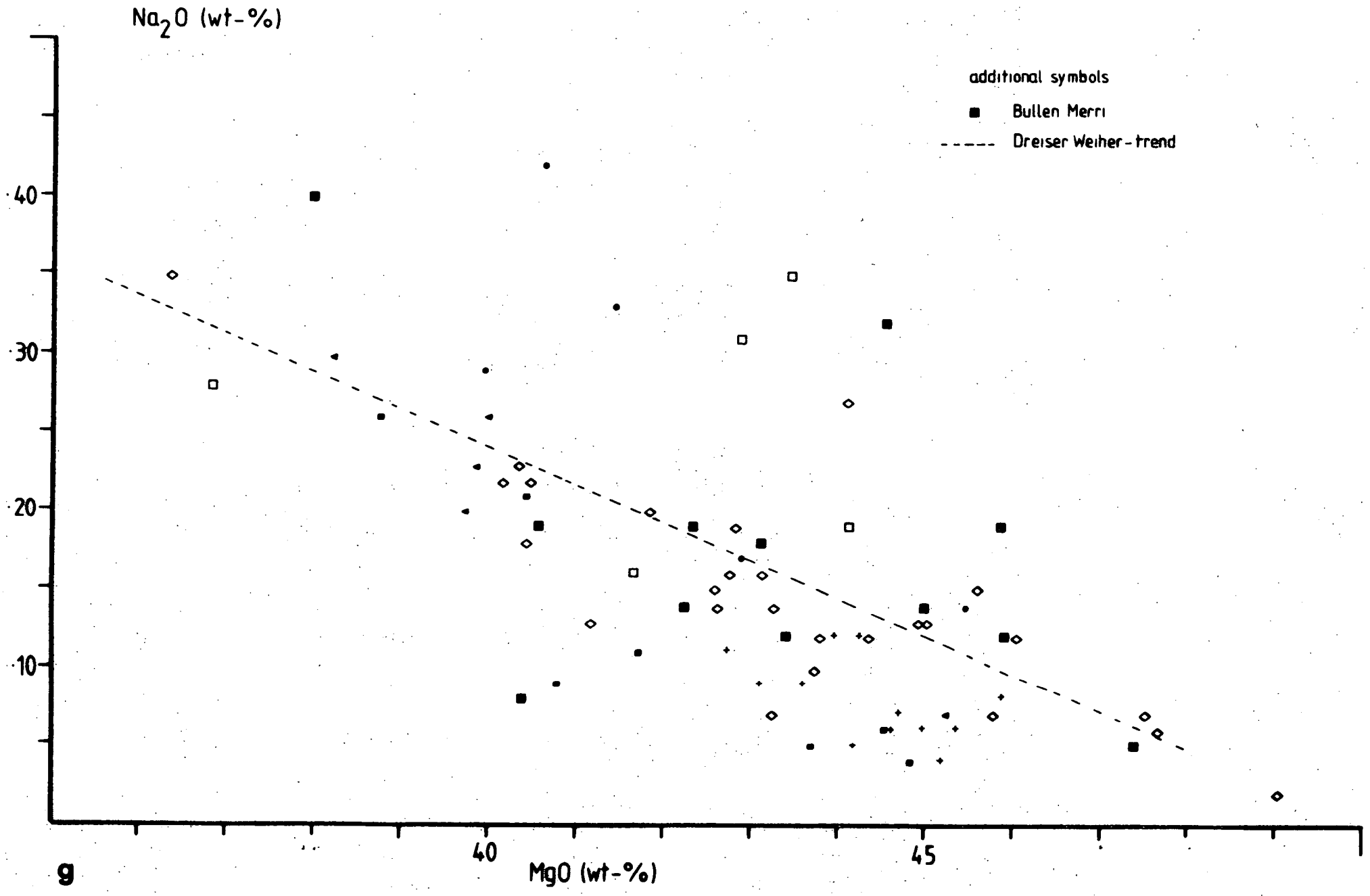
Na2O (wt-%)
additional symbols
Bullen Merri
Dreiser Weiher-trend
40
30
20
10
40
45
MgO (wt-%)
g

Figure 64: Plot of CaO vs. Al_2O_3 (wt.%) of bulk rock compositions from spinel lherzolites. Data sources as for fig. 63.

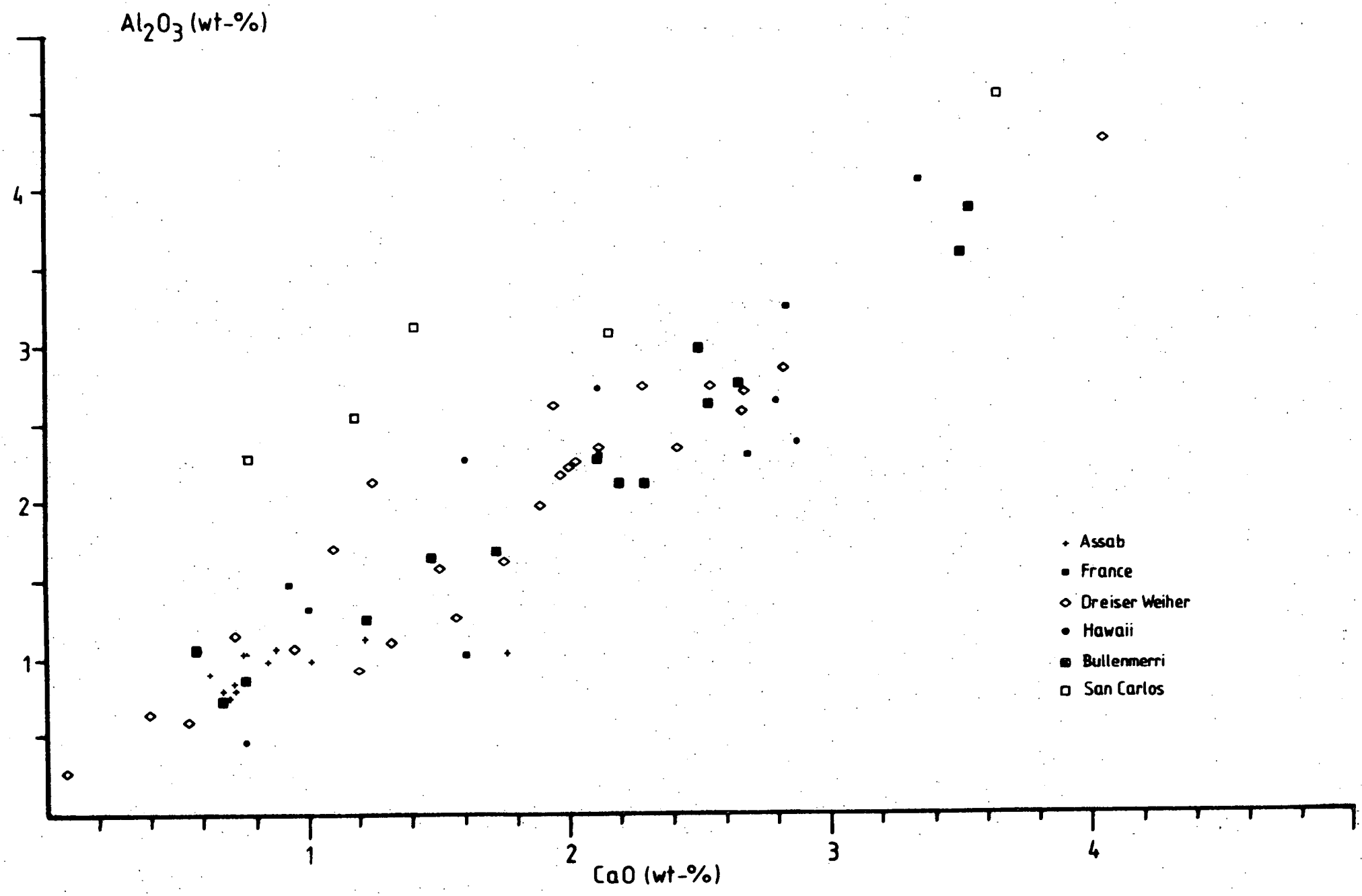
Al_2O_3 (wt-%)
4
3
2
1
1
2
3
4
CaO (wt-%)
Assab
France
Dreiser Weiher
Hawaii
Bullenmerri
San Carlos

towards higher TiO_2 values and lower Cr_2O_3 values when compared to the data of Sachtleben & Seck (1981). This is shown in figs. 63e and 63f, where the data of Kuno & Aoki (1970) are represented by filled symbols and the data of Sachtleben & Seck (1981) are open symbols. It is assumed that a systematic analytical error exists and the more recent data are preferred. The tendency of the Hawaiian data (Kuno & Aoki, 1970) to be somewhat higher in TiO_2 is therefore not taken as evidence for a real difference in the variations compared to Bullenmerri lherzolites.

In fig. 63g it is apparent that a good correlation exists between MgO and Na_2O, especially for the Dreiser Weiher lherzolites. Most samples from Lake Bullenmerri fit well to this trend. Sample BM-139 however is far removed from this trendline (off scale, not plotted). The unusual character of this nodule with respect to alkalis and some trace elements has been discussed before.

It should be noted that the Dreiser Weiher samples consist of two suites (anhydrous and hydrous), as do the samples of this work. Again it is apparent that there is no chemical difference in terms of major elements, including Na, between the two suites.

While the nodules from France, Germany, Algeria and Hawaii have trends extremely close to the variation of the Australian samples, and hence may be interpreted as having a very smilar history, nodules from some locations show systematic differences.

The suite of nodules from San Carlos shows systematically higher values of Al_2O_3 and lower Cr_2O_3 values for a given MgO content. The unusual character of the San Carlos population is demonstrated by CaO vs. Al_2O_3 (fig. 64), where all other suites show a similar behaviour.

The suite from Assab, Ethiopia, shows also some subtle differences in Al_2O_3, CaO and a markedly lower Cr_2O_3 content.

Despite the differences, the chemical variationswithin each of these suites are still defined by rectilinear trends, hence batch melting models may be applicable. The different trends may be seen as evidence

for primary (i.e. before extraction of melt) major element differences in the chemical compositions of the source regions. Whether these differences represent primordial major element heterogeneity of the uppermost mantle or are due to more complex multi-stage histories cannot be specified.

Summarizing, the similarity in chemical variations between Lake Bullenmerri lherzolites and those from a number of geographically widely distributed localities makes it likely that large parts of the uppermost mantle have undergone a history of oceanic-type partial melting with the extraction of picritic liquids to varying degrees. The source composition is inferred to be comparable to model mantle compositions ("pyrolite", Green *et al.*, 1979; Ringwood, 1966).

These is no evidence for major element chemical variations derived by a process other than melt extraction (e.g. metasomatism), even where mineralogical differences (hydrous, anhydrous) exist.

Some lherzolite suites however (San Carlos, possibly Assab) do not fit to the trend of the majority and require differences in source region compositions or in the character of the melt/residue equilibrium during partial melting.

The model and the conclusions derived may not be applied directly to garnet lherzolites and harzburgites from kimberlite inclusions. Plots of the type MgO vs. oxides (fig. 65a-c) show significant differences from those of spinel lherzolite suites.

The scatter of data points is much higher for garnet lherzolites (compare also figs. 1 and 4 of Maaløe & Aoki, 1977) and slopes of chemical variations are different for sheared and granular nodules. Garnet lherzolites are generally more refractory than spinel lherzolites (both in terms of Mg/Mg+Fe values and concentrations of incompatible elements).

The indicated slope for MgO vs. oxides, especially vs. SiO_2 and FeO (figs.65a,b) is in many cases parallel or subparallel to a mixing line

Figure 65a-c: Plots of MgO vs. oxides in wt.% for bulk rock compositions of garnet lherzolites from inclusions in kimberlite. Data from Carswell *et al.* (1979), Cox *et al.* (1973), Nixon & Boyd (1973a), Rhodes & Dawson (1975) and Sobolev (1977).

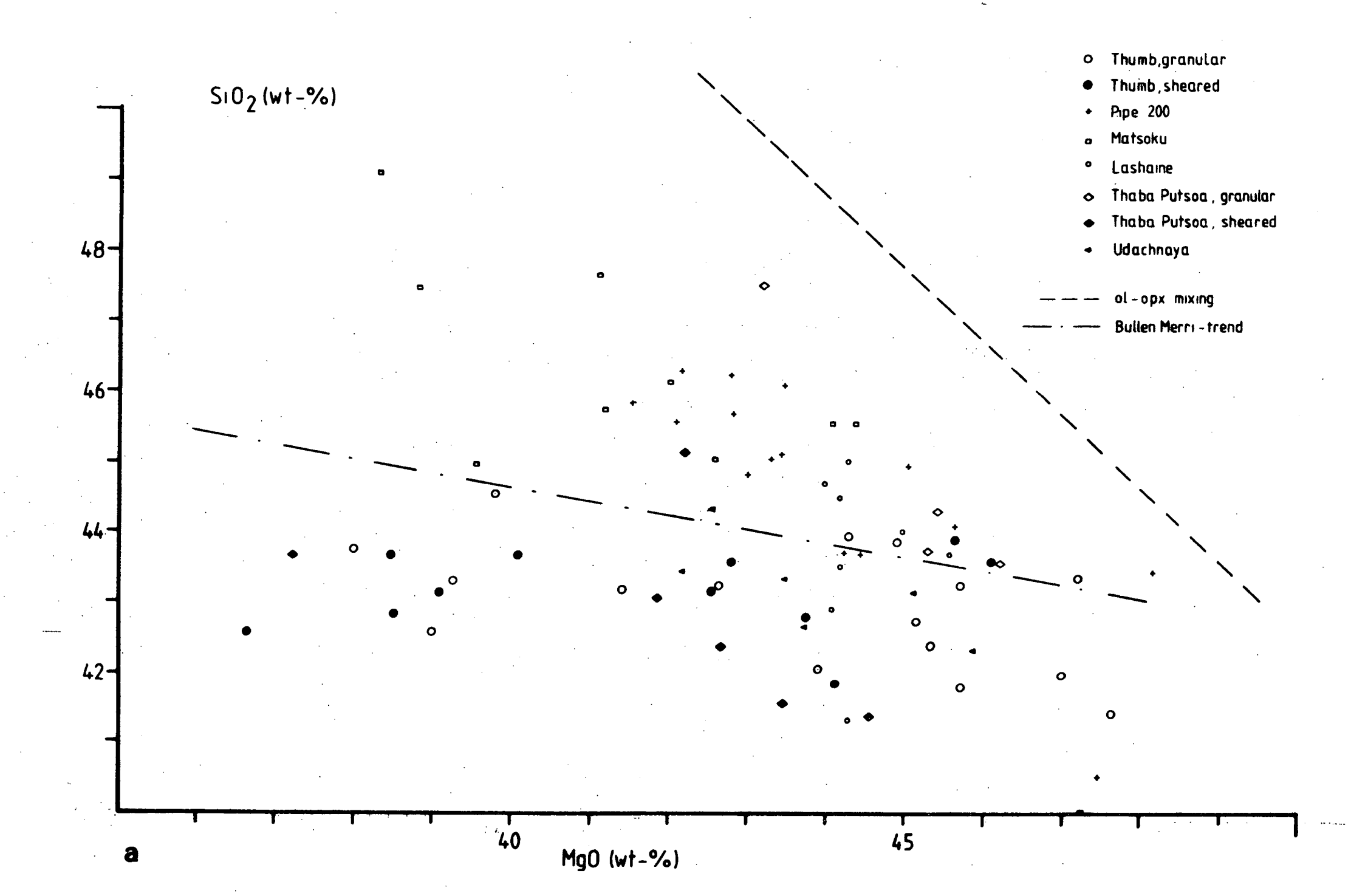
SiO2 (wt-%)
48
46
44
42
40
45
MgO (wt-%)
a
Thumb, granular
Thumb, sheared
Pipe 200
Matsoku
Lashaine
Thaba Putsoa, granular
Thaba Putsoa, sheared
Udachnaya
ol - opx mixing
Bullen Merri - trend

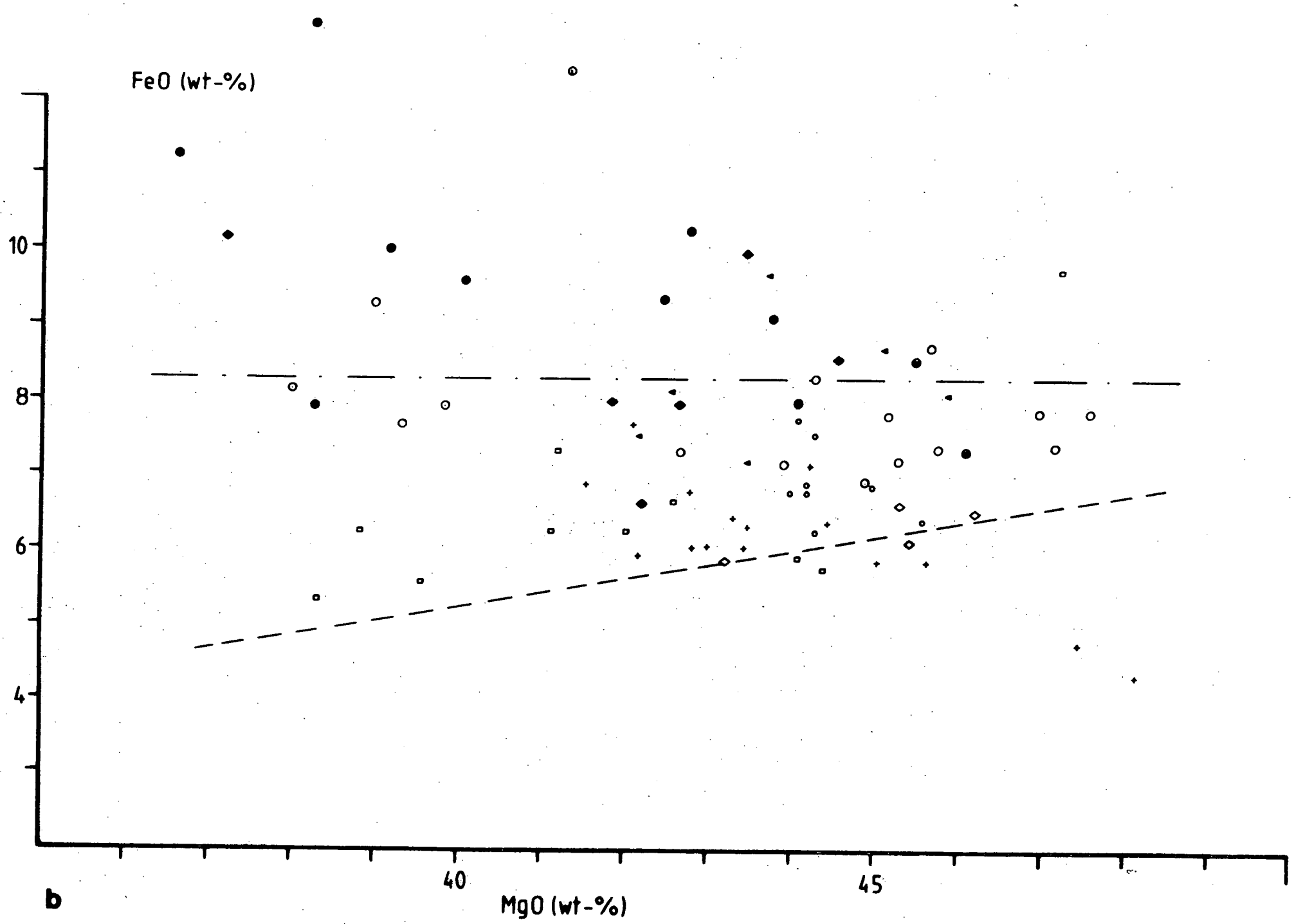
FeO (wt-%)
10
8
6
4
40
45
MgO (wt-%)
b

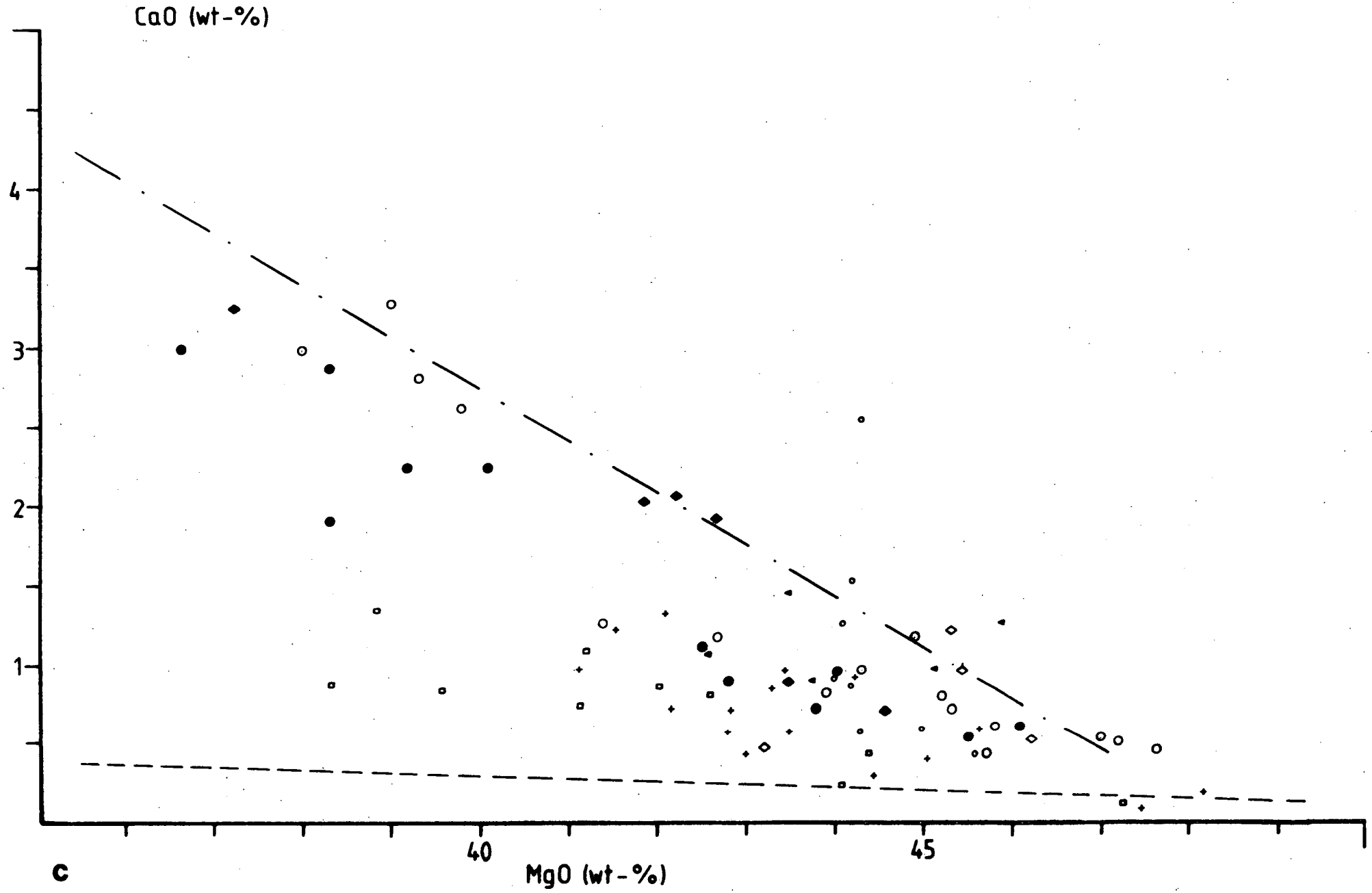
CaO (wt-%)
4
3
2
1
40
45
MgO (wt-%)
c

for olivine-orthopyroxene. The slope of the dashed line in fig. 65 is that of the mixing of an average orthopyroxene with an average olivine from Pipe 200 nodules. This places considerable doubt on the validity of the analyses in respect to them being representative samples. I interpret the chemical variations as real variations, but strongly overprinted by modal variations of olivine and orthopyroxene of the individual nodule. This seems likely, if both coarse grainsize and small size of analysed nodules are considered.

Furthermore, the greater depths of origin for garnet lherzolites enhances the probability of a more complex history. Experimental geochemical studies of Green (1971) showed that a variety of magmas can be generated and extracted from likely original mantle compositions and the variety of primitive basaltic magmas found on continents argues in the same direction. From this point of view individual nodule suites may record the individual magma generation and extraction process of a given part of the upper mantle. Multi-stage histories with more than one event of melt extraction are also envisaged.

Apart from possible metasomatic events which could further contribute to compositional changes in nodules, further complexities are indicated by the difference between granular and sheared nodules. The inferred high temperatures of equilibration and increased levels of incompatible elements in the sheared nodules may be interpreted as the result of magma-nodule (wall-rock) interaction.

For all these reasons it is concluded that a meaningful modelling of the origin of the chemical variation among garnet lherzolites is not possible at this stage. Models ignoring the likelihood of these complexities and the probable sampling errors of the analyses (O'Hara *et al.*, 1975) are subject to large errors and may be misleading.

A suite of garnet lherzolites in minette from the Navajo volcanic field (Ehrenberg, 1979, 1982) shows linear trends in plots of MgO vs. major elements (fig.65a-c). The trendlines are generally subparallel to the trend shown by Bullenmerri lherzolites. For this suite it is possible to model the composition of the nodules are residues of an incomplete magma extraction. The trendlines do not pass through a composition similar to "pyrolite" and the primary composition of the mantle beneath that region may have been different. Alternatively, different styles of magma generation and extraction (e.g. multiple fractional partial melting) may explain the variations. Ehrenberg records both granular and sheared types, which do not yield different P-T estimates from each other, but systematic differences in FeO and TiO_2 (fig. 65b). A complex history which may include magma-wallrock interaction is therefore envisaged.

APPENDIX 5

Mineral chemistry of phases generated in experimental runs in the SMACCR system.

RUN: T-656, SSO-HC, Pt capsule, Dry Assemblage
Conditions: 1400 C, 25 kb, 24 hrs.

Phases	opx		cpx		gt		sp
	wt.%	struc	wt.%	struc	wt.%	struc	wt.%
MgO	34.35(.26)	1.734	20.55(.36)	1.087	24.00(.23)	2.494	25.40(.27)
Al_2O_3	7.10(.33)	.283	7.40(.60)	.309	20.53(.31)	1.688	38.00(.67)
SiO_2	54.25(.50)	1.837	51.43(.51)	1.825	43.00(.07)	2.999	2.12(.73)
CaO	1.89(.08)	.068	17.58(.30)	.668	6.80(.01)	.508	0.38(.05)
Cr_2O_3	2.40(.16)	.064	3.03(.17)	.085	5.67(.04)	.313	34.07(.54)
Total		3.988		3.986		8.002	

RUN: T-778, SOGP-HC, Pt capsule, Dry Assemblage
Conditions: 1400 C, 25 kb, 24 hrs.

Phases	opx		cpx		gt		sp(min)
	wt.%	struc	wt.%	struc	wt.%	struc	wt.%
MgO	34.27(.32)	1.737	20.64(.29)	1.096	23.51(.19)	2.459	24.22
Al_2O_3	6.61(.27)	.264	6.60(.22)	.277	19.48(.21)	1.611	31.38
SiO_2	53.79(.31)	1.829	51.21(.22)	1.825	42.55(.19)	2.986	
CaO	2.20(.20)	.080	17.82(.33)	.680	6.96(.24)	.523	
Cr_2O_3	3.12(.29)	.083	3.72(.21)	.104	7.51(.24)	.416	44.41
Total		3.996		3.983		7.998	

RUN: T-1052, SSO-LC, Pt capsule, Dry Assemblage, Fo present
Conditions: 1400 C, 27 kb, 24 hrs.

Phases	opx		cpx		sp
	wt.%	struc	wt.%	struc	wt.%
MgO	35.00(.39)	1.760	20.94(.11)	1.104	27.43(.42)
Al_2O_3	7.50(.27)	.298	7.65(.20)	.319	55.88(.30)
SiO_2	54.65(.34)	1.843	51.99(.17)	1.839	4.85(.58)
CaO	1.97(.10)	.071	18.36(.15)	.696	0.84(.78)
Cr_2O_3	.88(.04)	.023	1.06(.06)	.030	10.98(.15)
Total		3.996		3.987	

RUN: T-1052, SOGP-LC, Pt capsule, Dry Assemblage, Fo present
Conditions: 1400 C, 27 kb, 24 hrs.

Phases	opx		cpx		sp(min)	
	wt.%	struc	wt.%	struc	wt.%	st
MgO	34.77(.08)	1.748	21.29(.16)	1.123	27.14	
Al_2O_3	7.13(.38)	.283	7.28(.15)	.304	56.90	
SiO_2	54.99(.33)	1.855	52.02(.12)	1.841	1.63	
CaO	2.12(.07)	.077	18.20(.20)	.690	0.82	
Cr_2O_3	.99(.03)	.026	1.21(.09)	.034	13.51	
Total		3.990		3.991		

RUN: T-1068, SOGP-MC2, Pt capsule, Dry Assemblage, Fo present
Conditions: 1400 C, 27 kb, 24 hrs.

Phases	opx		cpx		sp(min)
	wt.%	struc	wt.%	struc	wt.%
MgO	35.10(.16)	1.768	21.57(.72)	1.138	27.29
Al_2O_3	6.54(.23)	.260	6.32(.49)	.264	45.05
SiO_2	54.91(.40)	1.856	52.48(.49)	1.858	3.64
CaO	2.11(.15)	.076	18.15(.69)	.688	0.57
Cr_2O_3	1.34(.13)	.036	1.49(.14)	.042	23.46
Total		3.996		3.990	

RUN: T-795, SOGP-HC, Pt capsule, Dry Assemblage
Conditions: 1400 C, 22 kb, 24 hrs.

Phases	opx		cpx		sp(min)
	wt.%	struc	wt.%	struc	wt.%
MgO	33.13(.16)	1.676	20.49(.50)	1.084	24.78
Al_2O_3	8.24(.23)	.329	8.63(.30)	.361	34.16
SiO_2	53.35(.26)	1.811	50.47(.45)	1.792	0.55
CaO	2.08(.12)	.075	16.55(.53)	.629	0.26
Cr_2O_3	3.20(.10)	.085)	3.79(.25)	.106	40.25
Total		3.980		3.973	

RUN: T-1045, SSO-LC, Pt capsule, Dry Assemblage, Fo present
Conditions: 1400 C, 25 kb, 24 hrs.

Phases	opx		cpx		sp
	wt.%	struc	wt.%	struc	wt.%
MgO	34.57(.13)	1.737	21.10	1.111	27.47(.41)
Al_2O_3	7.69(.35)	.305	8.11	.336	57.57(1.1)
SiO_2	54.79(.32)	1.847	52.12	1.838	3.53(2.3)
CaO	2.07(.12)	.074	17.77	.671	1.48(1.0)
Cr_2O_3	0.89(.06)	.023	0.86	.024	9.94(0.9)
Total		3.988		3.981	

RUN: T-1045, SOGP-LC, Pt capsule, Dry Assemblage, Fo present
Conditions: 1400 C, 25 kb, 24 hrs.

Phases	opx		cpx		sp(min)
	wt.%	struc	wt.%	struc	wt.%
MgO	34.57(.22)	1.739	21.64(.86)	1.137	28.75
Al_2O_3	7.51(.28)	.298	7.60(.10)	.315	52.39
SiO_2	54.66(.29)	1.845	52.21(.33)	1.841	8.58
CaO	2.42(.11)	.087	17.50(1.0)	.661	0.23
Cr_2O_3	0.83(.05)	.022	1.05(.05)	.029	10.05
Total		3.993		3.985	

RUN: T-1058, SSO-MC, Pt capsule, Dry Assemblage, Fo present
Conditions: 1400 C, 25 kb, 24 hrs.

Phases	opx		cpx		sp
	wt.%	struc	wt.%	struc	wt.%
MgO	35.19(.25)	1.772	21.61(.33)	1.139	27.68(.71)
Al_2O_3	6.04(.53)	.240	6.18(.18)	.257	46.71(2.6)
SiO_2	55.29(.50)	1.868	52.65(.23)	1.862	3.62(3.5)
CaO	2.19(.18)	.079	18.04(.28)	.683	0.55(.68)
Cr_2O_3	1.29(.16)	.034	1.52(.16)	.042	21.41(1.5)
Total		3.994		3.986	

RUN: T-1058, SOGP-MC, Pt capsule, Dry Assemblage, Fo present
Conditions: 1400 C, 25 kb, 24 hrs

Phases	opx		cpx		sp(min)
	wt.%	struc	wt.%	struc	wt.%
MgO	35.17(.30)	1.770	21.90(.46)	1.152	26.47
Al_2O_3	6.27(.27)	.249	6.88(.59)	.286	46.76
SiO_2	55.25(.23)	1.865	52.40(.87)	1.850	3.63
CaO	2.17(.04)	.078	17.39(.38)	.657	0.75
Cr_2O_3	1.14(.14)	.030	1.43(.29)	.039	22.38
Total		3.994		3.986	

RUN: T- 1068, SSO-HC2, Pt capsule, Dry Assemblage, Fo present
Conditions: 1400 C, 27 kb, 24 hrs.

Phases	opx		cpx		sp	
	wt.%	struc	wt.%	struc	wt.%	struc
MgO	35.27(.26)	1.777	22.04(.75)	1.164	27.71(.95)	1.137
Al_2O_3	5.39(.36)	.215	4.55(.64)	.193	39.48(1.5)	1.281
SiO_2	55.60(.47)	1.880	53.49(.59)	1.895	3.71(1.6)	
CaO	2.12(.25)	.077	18.28(.63)	.694	0.27(.16)	
Cr_2O_3	1.61(.14)	.043	1.63(.24)	.046	28.81(.96)	.627
Total		3.991		3.988		3.045

RUN: T-850, SSO-HC, Pt capsule, Dry Assemblage
Conditions: 1400 C, 27.5 kb, 24 hrs.

Phases	opx		cpx		gt		sp
	wt.%	struc	wt.%	struc	wt.%	struc	wt.%
MgO	34.72(.40)	1.755	21.64(.50)	1.144	24.41	2.543	25.51(.18)
Al_2O_3	6.48(.22)	.259	6.37(.32)	.266	20.04	1.651	35.94(.23)
SiO_2	54.30(.30)	1.842	51.86(.31)	1.840	42.72	2.985	0.69(.48)
CaO	2.04(.30)	.072	17.09(.57)	.650	6.57	.492	0.00
Cr_2O_3	2.46(.16)	.066	3.05(.14)	.086	6.26	.346	37.84(.52)
Total		3.994		3.986		8.016	

RUN: T-1040, SSO-LC, Pt capsule, Dry Assemblage, Fo present
Conditions: 1400 C, 30 kb, 24 hrs.

Phases	opx		cpx		gt	
	wt.%	struc	wt.%	struc	wt.%	struc
MgO	35.19(.31)	1.766	21.84(.52)	1.150	25.17(.35)	2.584
Al_2O_3	5.49(.22)	.218	5.19(.20)	.216	22.36(1.1)	1.815
SiO_2	56.40(.18)	1.899	53.69(.22)	1.897	43.79(.78)	3.017
CaO	2.13(.17)	.077	18.25(.43)	.691	6.32(.67)	.466
Cr_2O_3	0.80(.07)	.021	0.98(.05)	.027	2.36(.17)	.129
Total		3.981		3.981		8.011

RUN: T-1057, SSO-MC, Pt capsule, Dry Assemblage, Fo present
Conditions: 1400 C, 30 kb, 26.5 hrs.

Phases	opx		cpx		gt		sp
	wt.%	struc	wt.%	struc	wt.%	struc	wt.%
MgO	35.38(.33)	1.783	21.96(.38)	1.158	24.17(.23)	2.499	27.58(1.7)
Al_2O_3	5.70(.55)	.227	5.51(.34)	.230	21.16(.18)	1.730	42.51(3.0)
SiO_2	55.34(.58)	1.871	53.08(.35)	1.877	43.66(.25)	3.028	2.66(2.7)
CaO	2.11(.13)	.076	17.91(.29)	.679	6.95(.19)	.516	0.32(.28)
Cr_2O_3	1.47(.31)	.039	1.54(.23)	.043	4.06(.30)	.223	26.90(1.5)
Total		3.996		3.986		7.996	

RUN: T-1057, SOGP-MC, Pt capsule, Dry Assemblage, Fo present
Conditions: 1400 C, 30 kb, 26.5 hrs.

Phases	opx		cpx		gt		sp(min)
	wt.%	struc	wt.%	struc	wt.%	struc	wt.%
MgO	35.05(.16)	1.766	22.19(.52)	1.171	24.59(.26)	2.536	26.52
Al_2O_3	5.70(.20)	.227	5.57(.22)	.232	21.37(.44)	1.742	43.84
SiO_2	55.54(.13)	1.877	52.78(.22)	1.868	43.84(.31)	3.033	2.45
CaO	2.29(.15)	.083	17.74(.52)	.673	6.37(.19)	.472	0.72
Cr_2O_3	1.42(.04)	.038	1.72(.05)	.048	3.82(.50)	.209	26.47
Total		3.991		3.992		7.992	

RUN: T- 921, SSO-HC, Pt capsule, Dry Assemblage
Conditions: 1400 C, 30 kb, 24 hrs.

Phases	opx		cpx		gt		sp
	wt.%	struc	wt.%	struc	wt.%	struc	wt.%
MgO	35.32(.35)	1.784	21.31(.44)	1.128	23.72(.25)	2.475	25.57(.40)
Al_2O_3	5.52(.38)	.220	5.36(.27)	.224	19.34(.25)	1.596	32.48(.92)
SiO_2	54.93(.48)	1.861	52.59(.23)	1.868	43.24(.50)	3.027	3.33(2.3)
CaO	1.86(.04)	.068	18.33(.42)	.698	7.36(.15)	.552	0.94(.22)
Cr_2O_3	2.38(.40)	.064	2.41(.16)	.067	6.33(.57)	.350	37.65(3.0)
Total		3.997		3.986		8.000	

RUN: T-808, SOGP-HC, Pt capsule, Dry Assemblage, melt present
Conditions: 1400 C, 30 kb, 24 hrs.

Phases	opx		cpx		gt		sp(min)
	wt.%	struc	wt.%	struc	wt.%	struc	wt.%
MgO	35.39(.14)	1.784	no cpx other		23.47(.52)	2.466	26.43
Al_2O_3	5.19(.09)	.206			18.27(.09)	1.519	25.46
SiO_2	55.39(.18)	1.874	then quench		42.33(.36)	2.987	1.41
CaO	1.37(.06)	.049	found		6.90(.41)	.521	0.40
Cr_2O_3	2.65(.10)	.070			9.03(.58)	.503	46.30
Total		3.986				8.000	

RUN: T-853, SSO-HC, Pt capsule, Dry Assemblage, Fo present
Conditions: 1400 C, 32.5 kb, 24 hrs.

Phases	opx		cpx		gt		sp
	wt.%	struc	wt.%	struc	wt.%	struc	wt.%
MgO	35.94(.29)	1.814	21.61(.28)	1.146	23.25(.18)	2.445	24.30(.55)
Al_2O_3	4.00(.45)	.159	3.85(.14)	.162	18.55(.33)	1.542	25.27(1.1)
SiO_2	55.89(.44)	1.893	53.27(.20)	1.895	42.33(.22)	2.986	0.54(.37)
CaO	2.08(.36)	.075	18.68(.32)	.712	7.57(.19)	.572	0.38(.37)
Cr_2O_3	2.08(.18)	.055	2.58(.14)	.073	8.29(.55)	.462	49.49(2.0)
Total		3.999		3.988		8.010	

RUN: T-854, SOGP-HC, Pt capsule, Dry Assemblage
Conditions: 1400 C, 32.5 kb, 24 hrs.

Phases	opx		cpx		gt		sp(min)
	wt.%	struc	wt.%	struc	wt.%	struc	wt.%
MgO	35.93(.20)	1.816	not found		23.88(.36)	2.510	24.63
Al_2O_3	4.11(.24)	.164			18.32(.39)	1.523	21.04
SiO_2	55.57(.34)	1.884			42.27(.13)	2.980	
CaO	1.80(.08)	.066			6.76(.29)	.510	
Cr_2O_3	2.58(.19)	.069			8.77(.50)	.488	54.33
Total		3.999				8.013	

RUN: T-855, SSO-HC, Pt capsule, Dry Assemblage, Fo present
Conditions: 1400 C, 35 kb, 24 hrs.

Phases	opx		cpx		gt		sp
	wt.%	struc	wt.%	struc	wt.%	struc	wt.%
MgO	36.37(.20)	1.834	22.27(.29)	1.176	23.89(.27)	2.512	24.76(.61)
Al_2O_3	3.38(.18)	.134	3.42(.16)	.142	18.28(.28)	1.520	25.46(1.2)
SiO_2	56.34(.35)	1.906	54.05(.24)	1.915	42.20(.16)	2.977	1.02(1.1)
CaO	1.97(.20)	.071	17.60(.35)	.668	7.00(.20)	.529	0.22(.19)
Cr_2O_3	1.94(.28)	.052	2.66(.17)	.074	8.63(.26)	.481	48.52(1.8)
Total		3.999		3.976		8.021	

RUN: T-794, SOGP-HC, Pt capsule, Dry Assemblage
Conditions: 1400 C, 35 kb, 24 hrs.

Phases	opx		cpx		gt		sp(min)
	wt.%	struc	wt.%	struc	wt.%	struc	wt.%
MgO	35.76(.40)	1.802	22.48(.15)	1.191	23.55(.42)	2.467	23.58
Al_2O_3	4.08(.52)	.162	3.37(.10)	.141	18.65(.55)	1.544	20.16
SiO_2	56.21(.49)	1.901	53.30(.25)	1.895	42.85(.32)	3.011	0.30
CaO	1.99(.09)	.072	18.35(.44)	.699	6.82(.27)	.513	0.30
Cr_2O_3	1.96(.09)	.052	2.49(.08)	.070	8.14(.88)	.452	55.66
Total		3.991		3.998		7.989	

RUN: T-905,SSO-HC, Pt capsule, Dry Assemblage
Conditions: 1400 C, 40 kb, 24 hrs

Phases	opx		cpx		gt		sp
	wt.%	struc	wt.%	struc	wt.%	struc	wt.%
MgO	36.40(.14)	1.835	21.61(.38)	1.144	23.29(.07)	2.438	24.18
Al_2O_3	3.98(.32)	.158	4.28(.32)	.179	19.51(.47)	1.614	27.09
SiO_2	56.02(.41)	1.894	53.22(.72)	1.891	42.66(.22)	2.996	3.16
CaO	1.72(.08)	.062	18.57(.52)	.707	7.78(.04)	.585	0.98
Cr_2O_3	1.86(.18)	.049	2.30(.32)	.064	6.75(.67)	.374	44.58
Total		4.000		3.986		8.009	

RUN: T-899, SOGP-HC, Pt capsule, Dry Assemblage
Conditions: 1400 C, 40 kb, 24 hrs.

Phases	opx		cpx		gt		sp(min)
	wt.%	struc	wt.%	struc	wt.%	struc	wt.%
MgO	36.03(.33)	1.819	22.97(.11)	1.212	23.62(.43)	2.479	24.59
Al_2O_3	3.66(.29)	.146	4.00(.13)	.166	18.20(.34)	1.510	25.09
SiO_2	56.11(.31)	1.909	53.36(.46)	1.889	42.80(.50)	3.014	0.81
CaO	2.06(.13)	.074	16.64(.53)	.631	7.00(.44)	.528	
Cr_2O_3	2.12(.19)	.056	3.03(.24)	.084	8.36(.52)	.465	49.52
Total		3.997		3.984		7.997	

RUN: T-912, SSO-HC, Pt capsule, Dry Assemblage
Conditions: 1400 C, 45 kb, 24 hrs.

Phases	opx		cpx		gt		sp
	wt.%	struc	wt.%	struc	wt.%	struc	wt.%
MgO	36.15(.16)	1.820	22.24(.54)	1.173	23.41(.30)	2.447	24.96(.28)
Al_2O_3	3.59(.26)	.142	3.83(.24)	.159	19.36(.81)	1.600	28.79(1.0)
SiO_2	56.62(.27)	1.913	54.02(.29)	1.911	42.89(.33)	3.008	3.58(.60)
CaO	1.92(.09)	.069	17.81(.47)	.675	7.51(.32)	.564	0.91(.14)
Cr_2O_3	1.72(.14)	.045	2.10(.15)	.058	6.84(.74)	.379	41.75(.02)
Total		3.992		3.978		8.001	

RUN: T-876, SSO-HC, Pt capsule, Dry Assemblage
Conditions: 1350 C, 30 kb, 27.5 hrs.

Phases	opx		cpx		gt		sp
	wt.%	struc	wt.%	struc	wt.%	struc	wt.%
MgO	36.05(.30)	1.831	20.57(.18)	1.090	22.83(.24)	2.387	23.97(.23)
Al_2O_3	4.38(.21)	.174	4.23(.17)	.177	19.24(.21)	1.591	28.34(.22)
SiO_2	56.30(.24)	1.900	53.71(.24)	1.909	43.17(.26)	3.029	0.95(.07)
CaO	1.48(.07)	.053	19.26(.30)	.733	7.36(.31)	.554	0.23(.02)
Cr_2O_3	1.76(.14)	.046	2.23(.11)	.063	7.40(.31)	.410	46.49(.24)
Total		3.988		3.972		7.971	

RUN: T-876, SOGP-HC, Pt capsule, Dry Assemblage
Conditions: 1350 C, 30 kb, 27.5 hrs.

Phases	opx		cpx		gt		sp(min)
	wt.%	struc	wt.%	struc	wt.%	struc	wt.%
MgO	35.92(.17)	1.811	20.77(.06)	1.100	23.18(.35)	2.424	26.86
Al_2O_3	4.07(.15)	.162	4.08(.10)	.171	19.00(.34)	1.572	21.05
SiO_2	56.12(.26)	1.898	53.43(.34)	1.905	43.11(.32)	3.025	2.63
CaO	1.88(.15)	.068	18.78(.28)	.715	7.02(.26)	.528	
Cr_2O_3	1.99(.11)	.053	2.77(.11)	.077	7.69(.46)	.427	49.46
Total		3.993		3.970		7.976	

RUN: T-630, SSO-HC, Pt capsule, Dry Assemblage
Conditions: 1300 C, 15 kb, 43 hrs.

Phases	opx		cpx		sp
	wt.%	struc	wt.%	struc	wt.%
MgO	34.62(.48)	1.752	20.17(.07)	1.071	24.53(.42)
Al_2O_3	6.35(.30)	.254	6.78(.26)	.284	36.76(2.8)
SiO_2	54.24(.37)	1.841	51.32(.14)	1.829	5.79(3.5)
CaO	2.34(.28)	.085	18.92(.14)	.722	1.84(1.0)
Cr_2O_3	2.44(.29)	.065	2.80(.09)	.078	31.07(1.4)
Total		3.998		3.988	

RUN: T-629, SSO-HC, Pt capsule, Dry Assemblage
Conditions: 1300 C, 20 kb, 43 hrs.

Phases	opx		cpx		sp
	wt.%	struc	wt.%	struc	wt.%
MgO	34.95(.40)	1.765	21.19(.50)	1.122	25.30(.45)
Al_2O_3	6.51(.53)	.259	6.68(.34)	.279	38.88(.72)
SiO_2	54.40(.30)	1.843	51.55(.17)	1.831	1.48(1.6)
CaO	1.86(.05)	.067	17.82(.35)	.678	0.40(.15)
Cr_2O_3	2.27(.16)	.060	2.75(.05)	.077	33.91(1.5)
Total		3.996		3.989	

RUN:T-811, SOGP-HC, Pt capsule, Dry Assemblage, some persisting pure pyropes
Conditions: 1300 C, 20 kb, 24 hrs.

Phases	opx		cpx		sp(min)
	wt.%	struc	wt.%	struc	wt.%
MgO	34.40(.49)	1.733	19.77(.77)	1.048	26.00
Al_2O_3	8.44(.65)	.336	7.32(.30)	.307	21.67
SiO_2	53.51(.73)	1.809	51.43(.15)	1.830	7.28
CaO	0.99(.28)	.035	18.61(.90)	.709	0.28
Cr_2O_3	2.66(.61)	.071	2.86(.07)	.080	44.73
Total		3.986		3.976	

RUN: T-909, SSO-HC, Pt capsule, Dry Assemblage
Conditions: 1300 C, 25 kb, 48 hrs.

Phases	opx		cpx		gt		sp
	wt.%	struc	wt.%	struc	wt.%	struc	wt.%
MgO	35.15(.32)	1.773	18.94(.07)	1.010	23.31(.17)	2.423	25.01(.31)
Al_2O_3	7.06(.14)	.281	6.50(.16)	.274	21.31(.19)	1.752	35.48(1.3)
SiO_2	54.04(.12)	1.829	51.43(.16)	1.840	42.68(.27)	2.977	2.38(1.1)
CaO	1.44(.30)	.052	20.39(.27)	.781	7.25(.22)	.541	0.17(.15)
Cr_2O_3	2.31(.11)	.061	2.74(.04)	.077	5.45(.25)	.300	36.93(.89)
Total		3.998		3.983		7.996	

RUN: T-918, SOGP-HC, Pt capsule, Dry Assemblage
Conditions: 1300 C, 25 kb, 46 hrs.

Phases	opx		cpx		sp(min)
	wt.%	struc	wt.%	struc	wt.%
MgO	34.67(.18)	1.749	19.42(.89)	1.032	25.64
Al_2O_3	7.04(.23)	.281	7.33(.35)	.308	31.41
SiO_2	54.34(.32)	1.838	51.20(.43)	1.826	8.35
CaO	1.61(.12)	.058	19.28(1.0)	.737	0.85
Cr_2O_3	2.33(.30)	.062	2.76(.20)	.078	33.75
Total		3.989		3.981	

RUN: T-877, SSO-HC, Pt capsule, Dry Assemblage
Conditions: 1300 C, 30 kb, 31 hrs.

Phases	opx		cpx		gt		sp
	wt.%	struc	wt.%	struc	wt.%	struc	wt.%
MgO	36.17(.31)	1.819	20.32(.31)	1.076	22.97(.29)	2.400	24.95(.80)
Al_2O_3	4.14(.17)	.164	4.21(.30)	.176	19.39(.30)	1.602	27.25(1.1)
SiO_2	56.47(.18)	1.905	53.83(.29)	1.912	43.22(.32)	3.029	2.60(.82)
CaO	1.48(.15)	.053	19.22(.28)	.731	7.29(.23)	.548	1.40(1.0)
Cr_2O_3	1.72(.17)	.045	2.42(.06)	.068	7.12(.29)	.394	43.78(2.4)
Total		3.989		3.964		7.973	

RUN: T-879, SOGP-HC, Pt capsule, Dry Assemblage
Conditions: 1300 C, 30 kb, 31 hrs.

Phases	opx		cpx		gt		sp(min)
	wt.%	struc	wt.%	struc	wt.%	struc	wt.%
MgO	35.87(.15)	1.807	20.37(.32)	1.081	23.30(.30)	2.438	24.69
Al_2O_3	4.36(.18)	.173	4.43(.13)	.186	19.29(.44)	1.596	24.59
SiO_2	56.11(.21)	1.896	53.30(.35)	1.898	42.87(.36)	3.006	1.56
CaO	1.65(.18)	.059	19.50(.59)	.744	7.38(.32)	.555	0.29
Cr_2O_3	1.99(.09)	.053	2.39(.06)	.068	7.16(.44)	.397	48.87
Total		3.990		3.977		7.992	

RUN: T-883, SSO-HC, Pt capsule, Dry Assemblage
Conditions: 1250 C, 30 kb, 46 hrs.

Phases	opx		cpx		gt		sp
	wt.%	struc	wt.%	struc	wt.%	struc	wt.%
MgO	36.72(.19)	1.847	19.95(.15)	1.060	23.55(.53)	2.449	25.27(.95)
Al_2O_3	4.00(.30)	.159	3.58(.29)	.150	19.87(.40)	1.634	26.64(2.4)
SiO_2	56.34(.56)	1.901	53.88(.06)	1.921	43.50(.36)	3.035	3.49(3.8)
CaO	1.04(.08)	.037	20.72(.15)	.791	7.11(.34)	.531	0.39(.01)
Cr_2O_3	1.90(.49)	.051	1.87(.05)	.052	5.98(.86)	.329	44.18(3.5)
Total		3.995		3.976		7.981	

RUN: T-889, SOGP-HC, Pt capsule, Dry Assemblage, melt present
Conditions: 1250 C, 30 kb, 47.5 hrs.

Phases	opx		cpx		gt		sp(min)
	wt.%	struc	wt.%	struc	wt.%	struc	wt.%
MgO	37.03(.27)	1.862	no good analyses obtained, but present		23.30(.25)	2.438	25.73
Al_2O_3	3.51(.28)	.139			19.51(.59)	1.614	20.89
SiO_2	56.55(.31)	1.908			42.65(.28)	2.994	0.53
CaO	1.18(.09)	.042			7.58(.25)	.570	
Cr_2O_3	1.71(.14)	.045			6.96(.69)	.386	52.85
Total		3.998				8.004	

RUN: T-623, SSO-HC, Pt capsule, Dry Assemblage, melt present
Conditions: 1200 C, 15 kb, 48 hrs.

Phases	opx		cpx		sp
	wt.%	struc	wt.%	struc	wt.%
MgO	33.98(.61)	1.725	18.13(.85)	.967	24.47(.40)
Al_2O_3	9.29(.97)	.372	7.79(.54)	.328	38.87(1.8)
SiO_2	51.54(1.2)	1.755	50.75(.58)	1.816	1.53(1.4)
CaO	1.29(.15)	.047	20.16(.92)	.773	0.43(.14)
Cr_2O_3	3.88(.77)	.104	3.13(.31)	.088	34.67(1.2)
Total		4.005		3.974	

RUN: T-622, SSO-HC, Pt capsule, Dry Assemblage
Conditions: 1200 C, 20 kb, 48 hrs.

Phases	opx		cpx		sp
	wt.%	struc	wt.%	struc	wt.%
MgO	33.28(.48)	1.676	18.73(1.2)	.997	24.71(.41)
Al_2O_3	8.51(.24)	.338	7.90(.37)	.332	38.58(2.2)
SiO_2	54.13(.14)	1.829	50.79(.25)	1.813	1.97(1.4)
CaO	1.74(.23)	.063	19.57(1.2)	.749	0.53(.27)
Cr_2O_3	2.32(.08)	.061	3.01(.22)	.085	34.18(1.3)
Total		3.970		3.977	

RUN: T-796, SOGP-HC, Pt capsule, Dry Assemblage
Conditions: 1200 C, 20 kb, 24 hrs.

Phases	opx		cpx		sp(min)
	wt.%	struc	wt.%	struc	wt.%
MgO	33.73(.28)	1.701	17.94(.44)	.956	25.90
Al_2O_3	9.00(.62)	.358	8.88(.66)	.374	32.88
SiO_2	53.29(.39)	1.803	50.10(.45)	1.792	2.78
CaO	1.57(.24)	.056	19.88(.63)	.761	
Cr_2O_3	2.39(.20)	.063	3.21(.23)	.090	38.44
Total		3.984		3.975	

RUN: T-655, SSO-HC, Pt capsule, Dry Assemblage
Conditions: 1200 C, 20 kb, 48 hrs.

Phases	opx		cpx		sp
	wt.%	struc	wt.%	struc	wt.%
MgO	34.42(.26)	1.738	17.58(.82)	.939	25.02(.29)
Al_2O_3	8.60(.36)	.343	8.60(.31)	.363	38.62(.907
SiO_2	52.92(.53)	1.793	50.05(.37)	1.794	0.78(.63)
CaO	1.06(.09)	.038	20.40(.77)	.783	0.36(.11)
Cr_2O_3	3.01(.24)	.080	3.36(.14)	.095	35.20(1.1)
Total		3.994		3.976	

RUN: T-1054, SSO-LC, Pt capsule, Dry Assemblage, Fo present
Conditions: 1200 C, 21kb, 72 hrs.

Phases	opx		cpx		sp
	wt.%	struc	wt.%	struc	wt.%
MgO	36.17(.14)	1.813	19.12(.37)	1.017	28.06(.72)
Al_2O_3	6.50(.40)	.258	6.25(.15)	.263	57.05(5.3)
SiO_2	55.52(.31)	1.867	52.27(.18)	1.865	5.32(5.2)
CaO	1.21(.07)	.044	21.49(.41)	.822	0.47(.37)
Cr_2O_3	0.61(.06)	.016	.87(.05)	.025	9.07(.74)
Total		3.997		3.991	

RUN: T-1054, SOGP-LC, Pt capsule, Dry Assemblage, Fo present
Conditions: 1200 C, 21 kb, 72 hrs.

Phases	opx		cpx		sp(min)
	wt.%	struc	wt.%	struc	wt.%
MgO	36.18(.28)	1.813	19.38(.35)	1.031	28.77
Al_2O_3	6.27(.74)	.248	6.21(.22)	.261	57.16
SiO_2	55.68(.49)	1.872	52.22(.16)	1.863	2.90
CaO	1.38(.15)	.050	21.43(.17)	.819	0.24
Cr_2O_3	0.51(.13)	.014	0.76(.09)	.021	10.93
Total		3.997		3.996	

RUN: T-895, SSO-HC, Pt capsule, Dry Assemblage
Conditions: 1200 C, 22.5 kb, 72 hrs.

Phases	opx		cpx		gt		sp
	wt.%	struc	wt.%	struc	wt.%	struc	wt.%
MgO	35.83(.32)	1.806	18.52(.48)	.988	23.79(.39)	2.466	25.05(.11)
Al_2O_3	6.44(.40)	.257	6.52(.35)	.275	21.35(.19)	1.750	36.05(2.7)
SiO_2	54.49(.38)	1.842	51.46(.44)	1.842	43.11(.25)	2.998	1.88(.88)
CaO	1.14(.16)	.042	20.80(.42)	.798	6.99(.36)	.521	0.23(.21)
Cr_2O_3	2.09(.21)	.056	2.70(.16)	.076	4.76(.22)	.262	36.77(2.1)
Total		4.003		3.979		7.997	

RUN: T-1062, SSO-LC, Pt capsule, Dry Assemblage, Fo present
Conditions: 1200 C, 23 kb, 96 hrs.

Phases	opx		cpx		sp
	wt.%	struc	wt.%	struc	wt.%
MgO	36.00(.11)	1.805	19.60(.39)	1.042	28.83(1.8)
Al_2O_3	7.13(.50)	.283	6.94(.32)	.292	53.41(1.2)
SiO_2	55.00(.44)	1.850	51.67(.19)	1.842	8.16(.37)
CaO	1.13(.08)	.041	20.85(.47)	.796	0.71(.37)
Cr_2O_3	0.74(.10)	.020	0.95(.09)	.027	8.86(.16)
Total		3.999		3.999	

RUN: T-1062, SOGP-LC, Pt capsule, Dry Assemblage, Fo present
Conditions: 1200 C, 23 kb, 96 hrs.

Phases	opx		cpx		sp(min)
	wt.%	struc	wt.%	struc	wt.%
MgO	36.26(.44)	1.817	19.42(.36)	1.030	29.23
Al_2O_3	6.01(.53)	.238	6.13(.24)	.257	50.63
SiO_2	55.89(.15)	1.879	52.66(.23)	1.875	11.74
CaO	1.20(.01)	.043	21.11(.32)	.805	0.32
Cr_2O_3	0.64(.03)	.017	0.69(.15)	.019	8.08
Total		3.994		3.987	

RUN: T-1047, SSO-LC, Pt capsule, Dry Assemblage, Fo present
Conditions: 1200 C, 25 kb, 96 hrs.

Phases	opx		cpx		gt		sp
	wt.%	struc	wt.%	struc	wt.%	struc	wt.%
MgO	36.51(.35)	1.830	19.84(.40)	1.055	24.95(.42)	2.557	27.17(1.2)
Al_2O_3	5.37(.32)	.213	5.13(.34)	.215	22.95(.48)	1.860	56.34(4.1)
SiO_2	56.13(.23)	1.888	52.71(.57)	1.881	43.88(.32)	3.017	3.64(3.2)
CaO	1.21(.10)	.044	21.29(.35)	.814	6.48(.09)	.477	0.88(1.2)
Cr_2O_3	0.78(.07)	.021	1.04(.18)	.029	1.73(.22)	.094	11.95(2.8)
Total		3.995		3.996		8.006	

RUN: T-1047, SOGP-LC, Pt capsule, Dry Assemblage, Fo present
Conditions: 1200 C, 25 kb, 96 hrs.

Phases	opx		cpx		gt		sp(min)
	wt.%	struc	wt.%	struc	wt.%	struc	wt.%
MgO	36.52(.39)	1.833	19.48(.32)	1.050	25.21(.44)	2.583	27.41
Al_2O_3	4.90(.33)	.194	4.63(.29)	.197	22.69(.30)	1.839	37.52
SiO_2	56.25(.18)	1.894	53.10(.21)	1.883	43.99(.11)	3.022	5.43
CaO	1.43(.15)	.052	21.56(.07)	.835	5.93(.13)	.437	0.64
Cr_2O_3	0.90(.07)	.024	1.22(.07)	.035	2.19(.10)	.119	29.00
Total		3.997		4.000		8.000	

RUN: T-1060, SSO-MC, Pt capsule, Dry Assemblage, Fo present, melt present,
Conditions: 1200 C, 25 kb, 96 hrs.

Phases	opx		cpx		sp
	wt.%	struc	wt.%	struc	wt.%
MgO	36.13(.26)	1.814	19.76(.27)	1.051	30.32(2.0)
Al_2O_3	5.40(.39)	.214	4.81(.24)	.202	43.41(6.7)
SiO_2	55.94(.50)	1.884	53.00(.13)	1.891	8.48(4.0)
CaO	1.43(.15)	.052	21.19(.36)	.810	1.03(1.3)
Cr_2O_3	1.11(.20)	.030	1.24(.02)	.035	16.75(.78)
Total		3.994		3.990	

RUN: T-1060, SOGP-MC, Pt capsule, Dry Assemblage, Fo present,gt zoned
Conditions: 1200 C, 25 kb, 96 hrs.

Phases	opx		cpx		gt(max)		sp(min)
	wt.%	struc	wt.%	struc	wt.%	struc	wt.%
MgO	35.71(.17)	1.795	19.96(.58)	1.061	25.34	2.599	26.06
Al_2O_3	5.05(.36)	.201	5.11(.29)	.214	21.69	1.759	43.33
SiO_2	56.20(.37)	1.895	52.81(.44)	1.883	44.48	3.060	5.33
CaO	2.20(.15)	.080	20.92(.55)	.780	6.31	.465	1.60
Cr_2O_3	0.83(.18)	.022	1.21(.10)	.034	2.18	.119	23.69
Total		3.993		3.992		8.001	

RUN: T-645, SSO-HC, Pt capsule, Dry Assemblage,
Conditions: 1200 C, 25 kb, 70 hrs.

Phases	opx		cpx		gt		sp
	wt.%	struc	wt.%	struc	wt.%	struc	wt.%
MgO	36.01(.47)	1.814	18.32(.42)	.980	23.99(.15)	2.493	26.59(.97)
Al_2O_3	5.50(.79)	.218	5.54(1.4)	.234	21.18(.27)	1.741	26.85(1.4)
SiO_2	55.17(.68)	1.865	51.86(.55)	1.861	42.63(.37)	2.972	5.65(4.1)
CaO	0.92(.05)	.033	21.34(1.2)	.821	6.94(.44)	.519	0.51(.46)
Cr_2O_3	2.40(.43)	.063	2.93(.24)	.083	5.27(.92)	.291	40.37(1.8)
Total		3.993		3.979		8.016	

RUN: T-812, SOGP-HC, Pt capsule, Dry Assemblage
Conditions: 1200 C, 25 kb, 48 hrs.

Phases	opx		cpx		gt		sp(min)
	wt.%	struc	wt.%	struc	wt.%	struc	wt.%
MgO	35.45(.40)	1.785	18.84(.37)	1.006	23.49(.29)	2.447	24.67
Al_2O_3	5.64(.24)	.225	5.18(.45)	.219	20.27(.26)	1.667	26.29
SiO_2	55.44(.19)	1.872	52.11(.62)	1.865	43.29(.30)	3.021	1.78
CaO	1.33(.25)	.048	20.79(1.0)	.798	7.41(.46)	.554	
Cr_2O_3	2.14(.12)	.057	3.08(.46)	.087	5.53(.38)	.305	47.26
Total		3.987		3.975		7.992	

RUN: T-1053, SSO-LC, Pt capsule, Dry Assemblage, Fo present
Conditions: 1200 C, 27 kb, 72 hrs.

Phase	opx		cpx		gt		sp	sp
	wt.%	struc	wt.%	struc	wt.%	struc	wt.%	
MgO	35.95(.33)	1.803	19.86(.18)	1.055	24.97(.61)	2.558		
Al_2O_3	5.55(.27)	.220	4.93(.12)	.207	22.24(1.2)	1.802		
SiO_2	56.11(.38)	1.888	53.12(.29)	1.893	44.37(.49)	3.050		not fou
CaO	1.41(.08)	.051	20.91(.54)	.798	6.28(.14)	.463		
Cr_2O_3	0.99(.17)	.026	1.18(.14)	.033	2.17(.07)	.118		
Total		3.989		3.987		7.990		

RUN: T-1053, SOGP-LC, Pt capsule, Dry Assemblage, Fo present, both pyrope and picotite unreacted
Conditions: 1200 C, 27 kb, 72 hrs.

Phases	opx		cpx	
	wt.%	struc	wt.%	struc
MgO	36.49(.26)	1.832	20.25(.70)	1.074
Al_2O_3	4.78(.51)	.190	4.61(.25)	.193
SiO_2	56.30(.36)	1.896	53.52(.23)	1.904
CaO	1.37(.13)	.049	20.65(.61)	.787
Cr_2O_3	1.07(.33)	.028	§.97(.30)	.027
Total		3.995		3.986

RUN: T-1068, SSO-MC, Pt capsule, Dry Assemblage, Fo present
Conditions: 1200 C, 27 kb, 72 hrs.

Phases	opx		cpx		gt		sp
	wt.%	struc	wt.%	struc	wt.%	struc	wt.%
MgO	36.70(.17)	1.840	19.56(.54)	1.043	24.76(.74)	2.542	29.33(2.1)
Al_2O_3	4.63(.19)	.184	4.01(.17)	.169	22.64(.76)	1.838	40.15(4.9)
SiO_2	56.57(.21)	1.903	53.27(.36)	1.905	43.73(.13)	3.012	8.69(5.0)
CaO	1.07(.10)	.039	21.93(.37)	.840	6.04(1.1)	.446	1.30(1.0)
Cr_2O_3	1.02(.11)	.027	1.24(.16)	.035	2.84(.56)	.155	20.51(2.6)
Total		3.992		3.993		7.992	

RUN: T-1068, SOGP-MC, Pt capsule, Dry Assemblage, Fo present
Conditions: 1200 C, 27 kb, 72 hrs.

Phases	opx		cpx		gt		sp(min)
	wt.%	struc	wt.%	struc	wt.%	struc	wt.%
MgO	36.40(.20)	1.825	19.90(.69)	1.059	24.89(.66)	2.551	24.72
Al_2O_3	4.66(.22)	.185	4.18(.29)	.176	22.94(.68)	1.859	31.18
SiO_2	56.64(.27)	1.905	53.28(.54)	1.903	43.88(.06)	3.017	12.98
CaO	1.29(.16)	.046	21.28(.64)	.814	6.07(.59)	.447	4.30
Cr_2O_3	1.01(.06)	.027	1.36(.12)	.038	2.22(.63)	.121	26.83
Total		3.989		3.990		7.994	

RUN: T-1048, SSO-LC, Pt capsule, Dry Assemblage, Fo present
Conditions: 1200 C, 30 kb, 96 hrs.

Phases	opx		cpx		gt	
	wt.%	struc	wt.%	struc	wt.%	struc
MgO	37.33(.26)	1.870	20.18(.36)	1.073	24.57(.08)	2.526
Al_2O_3	3.74(.32)	.148	3.60(.26)	.151	22.69(.27)	1.844
SiO_2	57.11(.28)	1.920	53.83(.09)	1.920	43.59(.07)	3.006
CaO	1.16(.10)	.042	21.32(.42)	.814	6.54(.17)	.483
Cr_2O_3	0.67(.06)	.018	1.07(.05)	.030	2.60(.23)	.142
Total		3.997		3.989		8.001

RUN: T-1048, SOGP-LC, Pt capsule, Dry Assemblage, Fo present
Conditions: 1200 C, 30 kb, 96 hrs.

Phases	opx		cpx		gt	
	wt.%	struc	wt.%	struc	wt.%	struc
MgO	36.89(.17)	1.852	19.91(.39)	1.060	24.17(.46)	2.490
Al_2O_3	3.93(.38)	.156	3.90(.28)	.164	22.22(.98)	1.810
SiO_2	56.70(.27)	1.910	53.39(.40)	1.907	43.68(.11)	3.018
CaO	1.40(.13)	.050	21.24(.37)	.813	6.92(.48)	.512
Cr_2O_3	1.09(.07)	.029	1.57(.07)	.044	3.01(.95)	.164
Total		3.998		3.989		7.994

RUN: T-1059, SSO-MC, Pt capsule, Dry Assemblage, Fo present
Conditions: 1200 C, 30 kb, 96 hrs.

Phases	opx		cpx		gt		sp
	wt.%	struc	wt.%	struc	wt.%	struc	wt.%
MgO	36.94(.19)	1.853	20.35(.51)	1.082	23.77(.29)	2.461	26.23(.05)
Al_2O_3	3.76(.38)	.149	3.63(.17)	.153	20.96(1.0)	1.716	37.32(.88)
SiO_2	57.02(.37)	1.919	53.66(.29)	1.914	43.76(.24)	3.039	3.35(2.0)
CaO	1.14(.22)	.041	20.95(.56)	.801	7.45(.55)	.554	1.29(.60)
Cr_2O_3	1.13(.14)	.030	1.41(.07)	.040	4.05(.63)	.222	31.80(1.9)
Total		3.992		3.989		7.992	

RUN: t-1059, SOGP-MC, Pt capsule, Dry Assemblage, Fo present
Conditions: 1200 C, 30 kb, 96 hrs.

Phases	opx		cpx		gt		sp(min)
	wt.%	struc	wt.%	struc	wt.%	struc	wt.%
MgO	36.76(.18)	1.844	20.23(.52)	1.075	23.96(.23)	2.469	26.17
Al_2O_3	3.66(.19)	.145	3.50(.15)	.147	22.03(.50)	1.795	33.16
SiO_2	57.10(.20)	1.922	53.89(.17)	1.922	43.78(.25)	3.027	4.13
CaO	1.42(.26)	.051	21.03(.68)	.803	6.80(.29)	.504	0.80
Cr_2O_3	1.06(.07)	.028	1.35(.05)	.038	3.44(.51)	.188	35.74
Total		3.991		3.986		7.982	

RUN: T-1072, SOGP-MC2, Pt capsule, Dry Assemblage, Fo present
Conditions: 1200 C, 30 kb, 72 hrs.

Phases	opx		cpx		gt		sp(min)
	wt.%	struc	wt.%	struc	wt.%	struc	wt.%
MgO	36.77(.10)	1.845	20.29(.39)	1.079	24.33(.18)	2.507	25.63
Al_2O_3	4.06(.11)	.161	3.91(.11)	.164	21.70(.40)	1.768	35.39
SiO_2	56.75(.08)	1.911	53.46(.36)	1.907	43.83(.24)	3.030	2.19
CaO	1.28(.13)	.046	20.81(.36)	.795	6.66(.06)	.493	1.30
Cr_2O_3	1.14(.03)	.030	1.53(.15)	.043	3.49(.19)	.191	35.50
Total		3.994		3.989		7.990	

RUN: T-1079, SOGP-MC2, Dry Assemblage, Pt capsule, Fo present
Conditions: 1200 C, 30 kb, 73 hrs.

Phases	opx		cpx		gt		sp(min)
	wt.%	struc	wt.%	struc	wt.%	struc	wt.%
MgO	36.94(.22)	1.854	19.81(.64)	1.056	24.31(.25)	2.505	25.84
Al_2O_3	4.02(.17)	.160	4.00(.26)	.169	22.12(.43)	1.803	37.36
SiO_2	56.68(.23)	1.909	53.11(.37)	1.900	43.52(.14)	3.009	4.41
CaO	1.23(.23)	.044	21.56(.61)	.826	6.61(.24)	.490	0.85
Cr_2O_3	1.13(.06)	.030	1.53(.19)	.043	3.45(.40)	.189	31.54
Total		3.997		3.994		7.995	

RUN: T-1072, SSO-HC2, Pt caspule, Dry Assemblage,Fo present
Conditions: 1200 C, 30 kb, 72 hrs.

Phases	opx		cpx		sp
	wt.%	struc	wt.%	struc	wt.%
MgO	36.61(.17)	1.839	19.73(.27)	1.051	27.53(1.1)
Al_2O_3	4.76(.35)	.189	4.30(.25)	.181	38.76(2.4)
SiO_2	56.04(.57)	1.889	53.06(.34)	1.897	3.09(2.9)
CaO	1.24(.12)	.045	21.50(.17)	.823	0.16(.22)
Cr_2O_3	1.36(.23)	.036	1.42(.12)	.040	30.43(2.3)
Total		3.998		3.993	

RUN: T- 1079, SSO-HC2, Pt capsule, Dry Assemblage, Fo present
Conditions: 1200 C, 30 kb, 73 hrs.

Phases	opx		cpx		gt		sp
	wt.%	struc	wt.%	struc	wt.%	struc	wt.%
MgO	36.55(.28)	1.835	19.62(.47)	1.046	23.96(.37)	2.477	26.51(.40)
Al_2O_3	4.60(.13)	.183	3.76(.18)	.158	21.45(.38)	1.753	38.39(1.4)
SiO_2	56.33(.25)	1.897	53.48(.27)	1.912	43.61(.35)	3.024	3.03(2.1)
CaO	1.34(.17)	.048	21.70(.57)	.831	7.22(.27)	.536	0.40(.30)
Cr_2O_3	1.19(.16)	.032	1.44(.07)	.041	3.75(.19)	.206	31.64(2.2)
Total		3.995		3.988		7.996	

RUN: T-644, SSO-HC, Pt capsule, Dry Assemblage
Conditions: 1200 C, 30 kb, 70 hrs.

Phases	opx		cpx		gt		sp
	wt.%	struc	wt.%	struc	wt.%	struc	wt.%
MgO	36.89(.16)	1.857	20.43(.82)	1.087	23.83	2.478	25.84(1.2)
Al_2O_3	3.77(.47)	.150	3.21(.56)	.135	20.52	1.687	24.19(1.6)
SiO_2	56.30(.41)	1.901	53.61(.55)	1.915	42.98	2.998	4.10(2.5)
CaO	1.15(.14)	.041	20.22(.88)	.774	6.72	.502	0.46(.11)
Cr_2O_3	1.90(.34)	.051	2.54(.11)	.072	5.96	.329	45.39(2.4)
Total		4.000		3.983		7.994	

RUN: T-813, SOGP-HC, Pt capsule, Dry Assemblage, gt zoned
Conditions: 1200 C, 30 kb, 48 hrs.

Phases	opx		cpx		gt(max)		sp(min)
	wt.%	struc	wt.%	struc	wt.%	struc	wt.%
MgO	36.46(.39)	1.835	20.30(.78)	1.079	24.10	2.503	23.64
Al_2O_3	3.44(.25)	.136	3.41(.13)	.143	20.48	1.682	16.31
SiO_2	56.70(.28)	1.914	53.61(.32)	1.912	43.15	3.006	1.38
CaO	1.53(.30)	.055	19.69(.86)	.752	6.47	.483	0.28
Cr_2O_3	1.85(.20)	.049	3.00(.34)	.084	5.80	.319	58.39
Total		3.991		3.973		7.993	

RUN: T-1073, SSO-MC, Pt capsule, Dry Assemblage, Fo present
Conditions: 1200 C, 35 kb, 72 hrs.

Phases	opx		cpx		gt		sp
	wt.%	struc	wt.%	struc	wt.%	struc	wt.%
MgO	37.54(.30)	1.883	20.05(.29)	1.068	23.88(.06)	2.483	present , but
Al_2O_3	2.49(.34)	.099	2.34(.35)	.099	20.24(.38)	1.664	
SiO_2	57.69(.47)	1.941	54.41(.27)	1.945	43.21(.28)	3.014	no good analyses
CaO	1.09(.16)	.039	21.83(.27)	.836	7.16(.11)	.535	
Cr_2O_3	1.19(.37)	.032	1.36(.09)	.039	5.52(.08)	.304	obtained
Total		3.994		3.986		8.001	

RUN: T-1073, SOGP-MC, Pt capsule, Dry Assemblage, Fo present
Conditions: 1200 C, 35 kb, 72 hrs.

Phases	opx		cpx		gt		sp(min)
	wt.%	struc	wt.%	struc	wt.%	struc	wt.%
MgO	37.39(.24)	1.876	20.24(.26)	1.078	23.26(.55)	2.424	25.24
Al_2O_3	2.76(.24)	.109	2.38(.35)	.100	19.79(.53)	1.631	20.32
SiO_2	57.52(.14)	1.936	54.40(.42)	1.943	43.40(.32)	3.034	6.12
CaO	1.28(.17)	.046	21.49(.40)	.822	7.83(.57)	.587	1.24
Cr_2O_3	1.03(.12)	.027	1.49(.13)	.042	5.72(.79)	.316	47.08
Total		3.995		3.986		7.992	

RUN: T-1061, SSO-HC , Pt capsule, Dry Assemblage
Conditions: 1200 C, 35 kb, 96 hrs.

Phases	opx		cpx		gt		sp
	wt.%	struc	wt.%	struc	wt.%	struc	wt.%
MgO	37.50(.08)	1.880	19.47(.18)	1.037	23.46(.24)	2.450	27.01(1.3)
Al_2O_3	2.57(.22)	.102	2.35(.11)	.099	18.88(.72)	1.559	22.41(3.0)
SiO_2	57.71(.58)	1.941	54.79(.08)	1.957	43.49(.12)	3.047	3.24(4.2)
CaO	1.02(.03)	.037	21.77(.31)	.833	7.59(.21)	.570	0.23(.20)
Cr_2O_3	1.19(.14)	.032	1.61(.13)	.046	6.59(.45)	.365	47.09(6.1)
Total		3.992		3.971		3.991	

RUN: T-1061, SOGP-HC2, Pt capsule, Dry Assemblage
Conditions: 1200 C, 35 kb, 96 hrs.

Phases	opx		cpx		gt		sp(min)
	wt.%	struc	wt.%	struc	wt.%	struc	wt.%
MgO	37.16(.24)	1.866	19.63(.29)	1.046	22.98(.11)	2.407	25.16
Al_2O_3	2.74(.22)	.109	2.55(.14)	.107	18.72(.21)	1.550	21.45
SiO_2	57.40(.20)	1.934	54.36(.24)	1.943	43.21(.13)	3.037	1.18
CaO	1.23(.08)	.044	21.42(.38)	.820	7.90(.07)	.595	
Cr_2O_3	1.47(.17)	.039	2.04(.18)	.058	7.19(.38)	.399	52.20
Total		3.992		3.974		7.988	

RUN: T-923, SSO-HC, Pt capsule, Dry Assemblage
Conditions: 1150 C, 25 kb, 118 hrs.

Phases	opx		cpx		gt		sp
	wt.%	struc	wt.%	struc	wt.%	struc	wt.%
MgO	36.21(.21)	1.820	18.41(.23)	.983	23.74(.33)	2.462	26.22(.60)
Al_2O_3	5.39(.17)	.214	4.90(.15)	.207	21.20(.91)	1.738	32.60(.24)
SiO_2	55.61(.28)	1.875	52.69(.15)	1.888	43.17(.50)	3.003	4.95(1.7)
CaO	0.96(.12)	.035	21.90(.45)	.841	7.35(.67)	.548	0.67(.40)
Cr_2O_3	1.83(.20)	.049	2.10(.06)	.059	4.56(1.1)	.251	35.55(.69)
Total		3.993		3.979		8.002	

RUN: T-891, SSO-HC, Pt capsule, Dry Assemblage
Conditions: 1150 C, 30 kb, 118 hrs.

Phases	opx		cpx		gt		sp
	wt.%	struc	wt.%	struc	wt.%	struc	wt.%
MgO	38.00(.21)	1.904	19.33(.58)	1.048	23.40(.57)	2.439	24.82(.80)
Al_2O_3	2.84(.22)	.112	2.48(.52)	.104	19.83(.52)	1.634	21.65(1.2)
SiO_2	57.33(.20)	1.928	54.12(.42)	1.937	43.21(.11)	3.022	3.74(1.8)
CaO	0.68(.06)	.024	21.83(.70)	.837	7.66(.27)	.574	0.99(1.1)
Cr_2O_3	1.14(.09)	.030	1.92(.37)	.054	5.88(.75)	.325	48.78(3.0)
Total		4.000		3.982		7.997	

RUN: T-888, SOGP-HC, Pt capsule, Dry Assemblage
Conditions: 1150 C, 30 kb, 72 hrs.

Phases	opx		cpx		gt		sp(min)
	wt.%	struc	wt.%	struc	wt.%	struc	wt.%
MgO	37.24(.40)	1.871	19.33(.41)	1.032	23.28(.24)	2.431	24.89
Al_2O_3	3.60(.44)	.143	3.03(.20)	.128	19.76(.27)	1.632	23.48
SiO_2	56.61(.60)	1.908	53.74(.13)	1.925	42.94(.19)	3.009	1.90
CaO	1.06(.35)	.039	21.96(.72)	.843	7.55(.23)	.567	
Cr_2O_3	1.49(.21)	.040	1.93(.07)	.055	6.47(.27)	.358	49.82
Total		4.001		3.983		7.997	

RUN: T-640, SSO-HC, Pt capsule, Dry Assemblage, opx possibly zoned
Conditions: 1100 C, 15 kb, 87 hrs.

Phases	opx		cpx		sp
	wt.%	struc	wt.%	struc	wt.%
MgO	34.49(.31)	1.743	18.79(1.2)	1.002	24.77(.32)
Al_2O_3	7.79(.79)	.311	7.31(.73)	.308	39.76(2.2)
SiO_2	53.38(1.5)	1.810	50.82(1.0)	1.819	3.64(1.1)
CaO	1.28(.12)	.046	19.88(1.6)	.762	0.59(.17)
Cr_2O_3	3.06(.97)	.082	3.17(.66)	.089	31.21(2.2)
Total		3.993		3.981	

RUN: T-627, SSO-HC, Pt capsule, Dry Assemblage, opx possibly zoned
Conditions: 1100 C, 20 kb, 72 hrs.

Phases	opx		cpx		sp
	wt.%	struc	wt.%	struc	wt.%
MgO	34.11(.93)	1.728	17.29(1.4)	.923	24.68(.02)
Al_2O_3	8.61(1.3)	.345	7.74(.25)	.327	37.03(.27)
SiO_2	52.32(1.7)	1.779	50.92(.44)	1.825	0.33(.33)
CaO	0.99(.18)	.036	20.91(1.5)	.803	0.27(.01)
Cr_2O_3	3.95(1.3)	.106	3.10(.13)	.087	37.66(.65)
Total		3.995		3.967	

RUN: T-639, SSO-HC, Pt capsule, Dry Assemblage
Conditions: 1100 C, 25 kb, 87 hrs.

Phases	opx		cpx		gt		sp
	wt.%	struc	wt.%	struc	wt.%	struc	wt.%
MgO	36.61(.12)	1.844	18.99(.71)	1.015	24.27(.37)	2.508	27.05(.25)
Al_2O_3	4.72(.34)	.188	5.48(.56)	.231	21.82(.67)	1.783	32.77(1.4)
SiO_2	55.46(.83)	1.874	51.73(.69)	1.855	43.21(.42)	2.996	5.45(.92)
CaO	0.94(.25)	.034	20.67(.49)	.794	6.61(.47)	.491	0.46(.13)
Cr_2O_3	2.25(.71)	.060	3.14(.70)	.088	4.06(.16)	.222	34.24(.72)
Total		4.001		3.984		8.001	

RUN: T-628, SSO-HC, Pt capsule, Dry Assemblage, Fo present, melt present
Conditions: 1100 C, 30 kb, 72 hrs.

Phases	opx		cpx		gt		sp
	wt.%	struc	wt.%	struc	wt.%	struc	wt.%
MgO	37.15(.20)	1.870	19.29(1.1)	1.026)	23.12(.48)	2.598	25.02(.16)
Al_2O_3	3.52(.08)	.140	3.23(.56)	.135	20.39(1.3)	1.668	23.02(2.1)
SiO_2	56.27(.31)	1.900	54.10(.63)	1.931	43.57(1.1)	3.024	4.73(1.2)
CaO	0.82(.10)	.029	20.58(1.2)	.787	6.08(.27)	.452	0.61(.07)
Cr_2O_3	2.24(.47)	.060	2.81(.55)	.079	4.84(.07)	.265	46.60(1.6)
Total		3.999		3.960		8.008	

RUN: T-676, SSO-HC, $Ag_{50}Pd_{50}$ capsule, Wet Assemblage, water added
Conditions: 1050 C, 20 kb, 24 hrs.

Phases	opx		cpx		sp
	wt.%	struc	wt.%	struc	wt.%
MgO	37.27(.38)	1.870	19.04(.65)	1.018	24.51(.80)
Al_2O_3	4.43(.56)	.175	3.43(.35)	.145	38.53(1.5)
SiO_2	56.20(.73)	1.892	53.25(.45)	1.911	4.71(2.4)
CaO	0.64(.06)	.023	22.69(.58)	.872	0.89(.49)
Cr_2O_3	1.44(.56)	.038	1.57(.22)	.044	31.33(.99)
Total		4.000		3.993	

RUN: T-682, SSO-HC, $Ag_{50}Pd_{50}$ capsule, Wet Assemblage, water added
Conditions: 1050 C, 30 kb, 72 hrs.

Phases	opx		cpx		gt		sp
	wt.%	struc	wt.%	struc	wt.%	struc	wt.%
MgO	38.07(.53)	1.908	19.59(.28)	1.050	23.12(.40)	2.417	25.27(1.1)
Al_2O_3	1.85(.52)	.073	2.08(.19)	.088	19.78(.72)	1.635	19.25(.58)
SiO_2	58.11(.55)	1.953	53.67(.38)	1.930	42.84(.12)	3.004	5.46(2.1)
CaO	0.63(.16)	.023	22.67(.22)	.873	7.94(.57)	.597	0.76(.50)
Cr_2O_3	1.35(.28)	.036	2.00(.23)	.057	6.33(.97)	.351	49.24(1.2)
Total		3.993		3.998		8.004	

RUN: T-712, SSO-HCF, $Ag_{50}Pd_{50}$ capsule, Wet Assemblage, water added, Fo present
Conditions: 1000 C, 20 kb, 72 hrs.

Phases	opx		cpx		sp
	wt.%	struc	wt.%	struc	wt.%
MgO	37.85(.26)	1.897	18.81(.05)	1.008	27.86(1.7)
Al_2O_3	3.64(.42)	.144	2.68(.30)	.113	40.17(1.8)
SiO_2	56.75(.36)	1.909	53.59(.26)	1.907	4.17(.60)
CaO	0.58(.12)	.020	23.55(.46)	.907	0.21(.42)
Cr_2O_3	1.16(.12)	.030	1.3 (.12)	.038	27.56(1.3)
Total		4.003		3.996	

RUN: T-722, SGL-HCF, $Ag_{50}Pd_{50}$ capsule, Wet Assemblage, water added
Conditions: 1000 C, 20 kb, 72 hrs.

Phases	opx		cpx		sp
	wt.%	struc	wt.%	struc	wt.%
MgO	37.06(.40)	1.854	18.88(.82)	1.011	27.82(.42)
Al_2O_3	4.27(.92)	.169	3.46(.46)	.146	35.67(3.1)
SiO_2	57.05(.75)	1.914	53.03(.89)	1.906	5.60(3.2)
CaO	0.58(.09)	.020	23.29(.95)	.897	1.11(1.5)
Cr_2O_3	1.04(.24)	.027	1.34(.29)	.038	29.77(7.7)
Total		3.986		4.000	

RUN: T-742, SSO-HC, $Ag_{50}Pd_{50}$ capsule, Wet Assemblage, water added, Fo present
Conditions: 1000 C, 30 kb, 335 hrs.

Phases	opx		cpx		gt		sp
	wt.%	struc	wt.%	struc	wt.%	struc	wt.%
MgO	38.54(.28)	1.930	20.01(.36)	1.069	23.70(.19)	2.474	22.56(1.2)
Al_2O_3	1.81(.28)	.072	1.73(.33)	.073	20.43(.63)	1.686	21.61(2.3)
SiO_2	58.02(.35)	1.950	54.20(.34)	1.943	42.41(.54)	2.969	1.86(1.4)
CaO	0.45(.15)	.016	22.48(.63)	.864	7.26(.31)	.544	0.32(.64)
Cr_2O_3	1.17(.24)	.031	1.58(.30)	.045	6.20(.86)	.343	53.62(4.4)
Total		3.999		3.994		8.016	

RUN: T-729, SGL-HC, $Ag_{50}Pd_{50}$ capsule, Wet Assemblage, water added, Fo present
Conditions: 1000 C, 30 kb, 48 hrs.

Phases	opx		cpx		gt		sp
	wt.%	struc	wt.%	struc	wt.%	struc	wt.%
MgO	38.15(.34)	1.910	19.17(.14)	1.027	23.13(.99)	2.416	present, but no good analyses obtained
Al_2O_3	1.87(.37)	.074	1.85(.23)	.078	20.03(1.2)	1.654	
SiO_2	58.23(.32)	1.956	53.93(.38)	1.940	42.72(.34)	2.994	
CaO	0.47(.06)	.016	23.06(.12)	.888	7.65(1.2)	.574	
Cr_2O_3	1.25(.18)	.033	1.99(.30)	.056	6.47(1.4)	.358	
Total		3.990		3.992		7.998	

RUN: T-683, SSO-HC, $Ag_{50}Pd_{50}$ capsule, Wet Assemblage, water added
Conditions: 1000 C, 30 kb, 72 hrs.

Phases	opx		cpx		gt		sp(min)
	wt.%	struc	wt.%	struc	wt.%	struc	wt.%
MgO	38.07(.27)	1.911	19.62(.26)	1.050	22.53	2.356	23.87(.03)
Al_2O_3	2.23(.25)	.088	1.77(.49)	.074	19.92	1.647	22.32(.24)
SiO_2	57.35(.45)	1.931	54.13(.51)	1.944	42.80	3.004	4.59(2.2)
CaO	0.49(.09)	.017	22.99(.37)	.884	8.12	.610	0.97(.49)
Cr_2O_3	1.85(.40)	.049	1.47(.24)	.041	6.64	.368	48.23(2.6)
Total		3.999		3.996		7.987	

RUN: T-693, SSO-HC, $Ag_{50}Pd_{50}$ capsule, Wt Assemblage, water added
Conditions: 950 C, 20 kb, 120 hrs.

Phases	opx		cpx		gt		sp
	wt.%	struc	wt.%	struc	wt.%	struc	wt.%
MgO	36.59(.76)	1.833	18.99(.35)	1.015	23.86(.84)	2.472	26.00(.52)
Al_2O_3	4.98(.56)	.197	3.10(.49)	.131	21.39(.24)	1.752	36.00(.82)
SiO_2	56.42(.68)	1.896	53.77(.17)	1.927	43.29(.14)	3.009	2.64(3.1)
CaO	0.43(.02)	.015	22.43(.78)	.862	7.73(.82)	.575	0.13(.16)
Cr_2O_3	1.56(.21)	.041	1.72(.16)	.049	3.71(.40)	.203	35.21(3.6)
Total		3.984		3.984		8.012	

RUN: T-688, SSO-HC, $Ag_{50}Pd_{50}$ capsule, Wet Assemblage, water added, Fo presen
Conditions: 950 C, 30 kb, 96 hrs.

Phases	opx		cpx		gt		sp
	wt.%	struc	wt.%	struc	wt.%	struc	wt.%
MgO	38.24(.22)	1.918	19.60(.91)	1.049	22.95(.49)	2.388	probably present, not found
Al_2O_3	2.19(.22)	.086	1.47(1.3)	.062	21.20(.23)	1.744	
SiO_2	57.47(.43)	1.934	54.33(.55)	1.952	42.96(.99)	2.999	
CaO	0.42(.05)	.015	23.24(2.0)	.894	8.78(.70)	.656	
Cr_2O_3	1.65(.48)	.043	1.35(.45)	.038	4.09(1.5)	.225	
Total		3.999		3.997		8.015	

RUN: T-937, SSO-HC, $Ag_{75}Pd_{25}$ capsule, Wet Assembalge, water added
Conditions: 900 C, 25 kb, 168 hrs.

Phases	opx		cpx		gt		sp
	wt.%	struc	wt.%	struc	wt.%	struc	wt.%
MgO	37.36(.32)	1.874	18.90(.66)	1.012	24.18(.81)	2.512	25.47
Al_2O_3	4.10(.29)	.162	3.09(.39)	.130	20.16(.36)	1.656	31.86
SiO_2	56.50(.10)	1.901	53.37(.23)	1.918	43.45(.75)	3.028	6.48
CaO	0.35(.05)	.012	22.85(.82)	.879	7.70(.76)	.575	1.17
Cr_2O_3	1.67(.06)	.044	1.76(.15)	.050	4.50(.67)	.247	35.02
Total		3.995		3.991		8.019	

RUN: T-948, SOGP-HC, $Ag_{75}Pd_{25}$ capsule, Wet Assemblage, water added, gt zoned
Conditions: 900 C, 25 kb, 168 hrs.

Phases	opx		cpx		gt(max)		sp(min)
	wt.%	struc	wt.%	struc	wt.%	struc	wt.%
MgO	36.37(.19)	1.819	19.01(.48)	1.016	25.80	2.645	19.96
Al_2O_3	4.43(.12)	.175	2.66(.68)	.112	20.77	1.683	26.91
SiO_2	57.26(.20)	1.921	53.91(.53)	1.934	44.83	3.083	10.51
CaO	0.56(.09)	.020	22.48(.40)	.864	5.14	.378	1.39
Cr_2O_3	1.36(.36)	.036	1.92(.53)	.054	3.46	.188	41.22
Total		3.972		3.982		7.980	

RUN: T-930, SSO-HC, $Ag_{75}Pd_{25}$ capsule, Wet Assemblage, water added
Conditions: 900 C, 30 kb, 168 hrs.

Phases	opx		cpx		gt		sp
	wt.%	struc	wt.%	struc	wt.%	struc	wt.%
MgO	38.46(.32)	1.922	18.63(.12)	1.001	23.52(.40)	2.441	26.27(.88)
Al_2O_3	2.21(.26)	.087	0.11(.19)	.005	20.13(.15)	1.652	27.02(1.4)
SiO_2	58.18(.19)	1.951	55.34(.15)	1.995	44.05(.32)	3.067	5.21(3.1)
CaO	0.22(.15)	.008	25.40(.21)	.981	8.47(.20)	.632	0.45(.77)
Cr_2O_3	0.93(.19)	.025	0.52(.05)	.015	3.83(.41)	.211	41.04(1.9)
Total		3.993		3.996		8.001	

RUN: T-932, SOGP-HC, $Ag_{75}Pd_{25}$ capsule, Wet Assemblage, water added, gt zoned
Conditions: 900 C, 30 kb, 168 hrs.

Phases	opx		cpx		gt(max)		sp(min)
	wt.%	struc	wt.%	struc	wt.%	struc	wt.%
MgO	38.55(.31)	1.927	19.00(.17)	1.020	24.10	2.502	25.02
Al_2O_3	1.81(.30)	.072	1.13(.12)	.048	20.42	1.676	17.00
SiO_2	58.43(.22)	1.960	54.46(.10)	1.961	43.41	3.024	0.60
CaO	0.46(.07)	.017	24.09(.14)	.929	7.68	.573	
Cr_2O_3	0.75(.08)	.020	1.34(.05)	.038	4.39	.242	57.38
Total		3.995		3.996		8.017	

APPENDIX 6

Analyses of run products of experiments in multicomponent ("natural") systems.

RUN: T-1148, TP-40, $Ag_{75}Pd_{25}$ capsule, Wet Assemblage
Conditions: 1000 C, 35 kb, 96 hrs.

Phases	opx		cpx		gt(max)	
	wt.%	struc	wt.%	struc	wt.%	struc
Na_2O			1.45(.12)	.101		
MgO	33.72(.39)	1.733	17.09(.41)	.919	19.04	2.033
Al_2O_3	1.42(.20)	.057	2.67(.08)	.113	21.61	1.824
SiO_2	57.26(.14)	1.974	54.68(.12)	1.974	42.21	3.024
CaO	0.75(.26)	.027	19.77(.44)	.764	5.59	.429
TiO_2					0.21	.011
Cr_2O_3	0.35(.05)	.009	1.19(.08)	.033	2.06(	.116
FeO	6.50(.07)	.187	3.12(.11)	.094	9.04	.541
MnO					0.25	.015
Total		3.991		4.002		7.995

RUN: T-1148, TP-40C, $Ag_{75}Pd_{25}$ capsule, Wet Assemblage
Conditions: 1000 C, 35 kb, 96 hrs.

Phases	opx		cpx		gt(max)		sp	
	wt.%	struc	wt.%	struc	wt.%	struc	wt.%	struc
Na_2O			1.46(.08)	.102				
MgO	34.00(.31)	1.748	17.31(.47)	.933	19.33	2.083	12.25(.37)	.601
Al_2O_3	1.38(.18)	.056	2.26(.10)	.096	19.43	1.655	12.09(.13)	.469
SiO_2	57.04(.39)	1.967	54.46(.17)	1.969	41.93	3.030		
CaO	0.57(.07)	.021	19.65(.44)	.761	6.17	.478		
TiO_2							1.60(.09)	.039
Cr_2O_3	0.72(.25)	.019	1.87(.15)	.053	4.01	.229	49.91(.33)	1.299
FeO	6.27(.08)	.180	2.97(.17)	.089	8.77	.530	23.76(.36)	.654
MnO					0.35	.022	0.40(.10)	.011
Total		3.994		4.006		8.027		3.075

RUN: T-1121, TP-40, $Ag_{50}Pd_{50}$ capsule, Wet Assemblage
Conditions: 1100 C, 35 kb, 168 hrs.

Phases	opx		cpx		gt(max)	
	wt.%	struc	wt.%	struc	wt.%	struc
Na_2O			0.92(.05)	.064		
MgO	33.59(.26)	1.726	17.92(.24)	.965	19.34	2.063
Al_2O_3	1.30(.13)	.073	2.43(.23)	.103	21.37	1.803
SiO_2	56.97(.28)	1.964	54.40(.32)	1.965	42.14	3.016
CaO	1.04(.19)	.038	20.02(.12)	.775	6.11	.469
TiO_2					0.26	.014
Cr_2O_3	0.42(.06)	.011	0.95(.04)	.027	2.28	.129
FeO	6.17(.21)	.177	3.33(.07)	.100	8.19	.490
MnO					0.33	.020
Total		3.992		4.001		8.004

RUN: T-1121, TP-40C, $Ag_{50}Pd_{50}$ capsule, Wet Assemblage
Conditions: 1100 C, 35 kb, 168 hrs.

Phases	opx		cpx		gt(max)		sp	
	wt.%	struc	wt.%	struc	wt.%	struc	wt.%	struc
Na_2O			1.07(.07)	.074				
MgO	33.69(.16)	1.732	18.07(.56)	.972	18.90	2.034	17.32	.815
Al_2O_3	1.70(.05)	.069	2.33(.25)	.099	19.31	1.643	15.18	.563
SiO_2	56.88(.15)	1.962	54.36(.32)	1.963	41.86	3.022		
CaO	0.93(.16)	.034	19.13(.55)	.740	6.97	.539		
TiO_2					0.34	.019	1.26	.029
Cr_2O_3	0.79(.08)	.021	1.81(.13)	.051	4.75	.271	47.77	1.193
FeO	5.99(.14)	.172	3.22(.15)	.097	7.52	.454	18.12	.478
MnO					0.34	.021	0.40	.010
Total		3.992		3.998		8.002		3.091

RUN: T-1131, TP-40, $Ag_{50}Pd_{50}$ capsule, Wet Assemblage
Conditions: 1200 C, 35 kb, 72 hrs.

Phases	opx		cpx		gt(max)	
	wt.%	struc	wt.%	struc	wt.%	struc
Na_2O	0.16(.13)	.010	1.18(.06)	.082		
MgO	33.80(.64)	1.732	18.96(.14)	1.073	20.87	2.212
Al_2O_3	2.70(.27)	.109	3.63(.17)	.153	21.58	1.809
SiO_2	56.45(.32)	1.941	54.35(.12)	1.949	42.23	3.002
CaO	1.58(.09)	.058	17.62(.18)	.677	5.89	.449
TiO_2					0.38	.020
Cr_2O_3	0.46(.02)	.012	1.00(.02)	.028	1.70	.095
FeO	4.82(.48)	.138	3.22(.25)	.096	7.13	.424
MnO					0.23	.014
Total		4.003		4.000		8.025

RUN: T-1131, TP-40C, $Ag_{50}Pd_{50}$ capsule, Wet Assemblage
Conditions: 1200 C, 35 kb, 72 hrs.

Phases	opx		cpx		gt(max)		sp	
	wt.%	struc	wt.%	struc	wt.%	struc	wt.%	struc
Na_2O	0.23(.20)	.015	1.44(.07)	.100				
MgO	32.71(.37)	1.685	18.74(.39)	1.003	20.25	2.165	24.50(4.4)	1.095
Al_2O_3	2.58(.19)	.105	3.39(.16)	.143	19.56	1.653	18.53(.51)	.655
SiO_2	56.09(.34)	1.939	54.13(.18)	1.944	42.32	3.034		
CaO	1.63(.12)	.060	16.86(.38)	.649	6.30	.484		
TiO_2					0.22	.012	0.84(.21)	.019
Cr_2O_3	1.18(.10)	.032	2.36(.21)	.067	3.95	.224	45.36(1.9)	1.075
FeO	5.56(.55)	.160	3.05(.32)	.091	7.17	.430	10.27(2.5)	.257
MnO					0.22	.014	0.50(.19)	.012
Total		3.999		4.000		8.015		3.115

RUN: T-1142, TP-40, Graphite-Pt- capsule, Buffer Assemblage
Conditions: 1300 C, 35 kb, 24 hrs.

Phases	opx		cpx		gt(max)	
	wt.%	struc	wt.%	struc	wt.%	struc
Na_2O			1.00(.12)	.069		
MgO	31.82(.28)	1.643	20.80(.66)	1.107	20.43	2.166
Al_2O_3	3.13(.09)	.127	4.01(.24)	.168	22.04	1.847
SiO_2	56.05(.26)	1.941	54.22(.24)	1.937	42.02	2.988
CaO	1.88(.19)	.069	14.27(.65)	.546	5.62	.428
TiO_2			0.11(.12)	.002	0.33	.018
Cr_2O_3	0.50(.04)	.013	0.85(.06)	.024	2.15	.121
FeO	6.61(.10)	.191	4.67(.18)	.139	7.17	.427
MnO			0.03(.08)	.000	0.23	.014
Total		3.987		3.997		8.010

RUN: T-1142, TP-40C, Graphite-Pt-capsule, Buffer Assemblage
Conditions: 1300 C, 35 kb, 24 hrs.

Phases	opx		cpx		gt(max)		sp	
	wt.%	struc	wt.%	struc	wt.%	struc	wt.%	struc
Na_2O	0.12(.11)	.008	1.26(.08)	.087				
MgO	31.92(.16)	1.649	19.54(.28)	1.046	19.31	2.064	15.77(.74)	.725
Al_2O_3	2.98(.09)	.121	3.80(.50)	.160	20.40	1.725	20.43(.57)	.742
SiO_2	55.81(.24)	1.934	53.78(.36)	1.931	42.02	3.014		
CaO	1.65(.09)	.061	15.32(.58)	.589	6.29	.484		
TiO_2			0.10(.13)	.002	0.34	.018	1.22(.09)	.028
Cr_2O_3	1.17(.04)	.032	2.00(.10)	.056	4.05	.230	45.23(1.8)	1.103
FeO	6.34(.12)	.183	4.17(.16)	.125	7.34	.440	17.04(.44)	.439
MnO					0.24	.015	0.33(.21)	.008
Total		3.992		4.000		7.990		3.048

RUN: T-1141, TP-40, Graphite-Pt-capsule, Buffer Assemblage
Conditions: 1400 C, 35 kb, 8 hrs.

Phases	opx		cpx		gt(max)	
	wt.%	struc	wt.%	struc	wt.%	struc
Na_2O	0.16(.13)	.010	0.77(.10)	.052		
MgO	30.77(.69)	1.592	23.24(.48)	1.229	20.49	2.166
Al_2O_3	4.29(.14)	.175	5.06(.36)	.211	22.37	1.870
SiO_2	55.14(.35)	1.915	53.82(.23)	1.909	42.15	2.989
CaO	2.52(.39)	.093	10.67(.59)	.405	5.51	.419
TiO_2			0.09(.12)	.002	0.36	.019
Cr_2O_3	0.63(.01)	.017	0.80(.04)	.022	2.09	.117
FeO	6.48(.20)	.180	5.48(.12)	.162	6.73	.399
MnO			0.04(.09)	.001	0.30	.018
Total		3.993		3.997		7.998

UN: T-1141, T-40C, Graphite-Pt-capsule, Buffer Assemblage
onditions: 1400 C, 35 kb, 8 hrs.

Phases	opx		cpx		gt(max)		sp	
	wt.%	struc	wt.%	struc	wt.%	struc	wt.%	struc
Na_2O	0.19(.16)	.012	0.97(.15)	.067				
MgO	30.67(.36)	1.592	22.44(.77)	1.192	20.16	**2.155**	18.28(.53)	.811
Al_2O_3	3.79(.49)	.155	4.07(.11)	.171	20.29	1.715	26.17(.83)	.918
SiO_2	54.89(.61)	1.912	53.78(.18)	1.917	41.73	2.992		
CaO	2.62(.33)	.097	11.61(.35)	.443	6.29	.483		
TiO_2			0.17(.09)	.004	0.41	.022	1.02(.09)	.022
Cr_2O_3	1.42(.30)	.039	1.77(.11)	.049	3.85	.218	38.99(1.4)	.918
FeO	6.42(.10)	.187	5.11(.25)	.152	6.96	.418	15.13(.33)	.376
MnO			0.08(.11)	.002	0.31	.019	0.41(.01)	.010
Total		3.997		4.000		8.020		3.058

APPENDIX 7

Computer program for calculating pressure and temperature.

```
0001   "PT": CLEAR: USING
0002   INPUT "SAMPLE ?"; V$                    key in sample no/description
-------------------------------------------------------------------------
0003   INPUT "Na2O opx=";N1
0004   INPUT "MgO  opx=";M1
0005   INPUT "Al2O3 opx=";A1
0006   INPUT "CaO  opx=";C1                    key in orthopyroxene data from
0007   INPUT "TiO2 opx=";T1                    structural formula
0008   INPUT "Cr2O3 opx=";CO
0009   INPUT "FeO  opx=";F1
0010   INPUT "MnO  opx=";MO
-------------------------------------------------------------------------
0011   INPUT "Na2O cpx=";N2
0012   INPUT "MgO  cpx=";M2
0013   INPUT "Al2O3 cpx=";A2
0014   INPUT "CaO  cpx=";C2                    key in clinopyroxene data from
0015   INPUT "TiO2  cpx=";T2                   structural formula
0016   INPUT "Cr2O3 cpx=";CC
0017   INPUT "FeO  cpx=";F2
0018   INPUT "MnO  cpx=";MC
-------------------------------------------------------------------------
0019   INPUT "MgO  gt=";M3
0020   INPUT "Al2O3  gt=";A3
0021   INPUT "CaO   gt=";C3                    key in garnet data from
0022   INPUT "Cr2O3 gt=";CG                    structural formula
0023   INPUT "FeO  gt=";F3
0024   INPUT "MnO  gt=";MG
-------------------------------------------------------------------------
0025   FO = F1/(F1+M1)                         calculates Fe/(Fe+Mg)
0026   AO = (A1-CO-2xT1+N1)/2                    opx      Al in M1
0027   MA = 1-AO-CO-T1                                    (Mg,Fe,Mn) in M1
0028   M4 = MA x (M1/(M1+F1+MO))                          Mg in M1
0029   MB = 1-C1-N1                                       (Mg,Fe,Mn) in M2
0030   M5 = MB x (M1/(M1+F1+MO))                          Mg in M2
0031   F4 = MA x (F1/(M1+F1+MO))                          Fe in M1
-------------------------------------------------------------------------
0032   AC = (A2-CC-2xT2+N2)/2                  calculates Al in M1
0033   MD = 1-AC-CC-T2                           cpx      (Mg,Fe,Mn) in M1
0034   M6 = MD x (M2/(M2+F2+MC))                          Mg in M1
0035   ME = 1-C2-N2                                       (Mg,Fe,Mn) in M2
0036   M7 = ME x (M2/(M2+F2+MC))                          Mg in M2
-------------------------------------------------------------------------
0037   M8 = M3/(M3+F3+MG)                      calculates Mg/(Mg+Fe+Mn)
0038   X1 = M3/(M3+F3+C3+MG)                     gt       X Mg gt
0039   X2 = C3/(M3+F3+C3+MG)                              X Ca gt
0040   X3 = F3/(M3+F3+C3+MG)                              X Fe gt
0041   X4 = A3/(A3+CG)                                    X Al gt
0042   X5 = CG/(A3+CG)                                    X Cr gt
-------------------------------------------------------------------------
```

```
0043   K1 = M6 x M7/(M4 x M5)                          KD for therometry
0044   L1 = LN K1                                      ln KD
0045   TW = 7341/(3.355+2.44 x FO-L1)                  T (Wells, 1977) in °K
0046   TC = TW-273                                     in °C
-------------------------------------------------------------------------
0047   K2 = ((1-X2)*3) x (X4*2)/(MAx(MB*2) x AO)       KD Al-barometry
0048   L2 = LN K2                                      ln KD
0049   R2 = 1.987 x L2 x TW                            RT ln KD
0050   V1 = -(183.3 + 178.98 x AO x (1-AO))            dVr
0051   W1 = 9000 x (X2*2)                              3 W(CaMg) X Ca gt squared
0052   W2 = 7590 x X2 x X3                             3 W(CaMg-FeCa) XFe XCa(gt)
0053   W3 = 90853 - 52.1 x TW                          dG rec
0054   W4 = W3 x X2 x X5                               XCa XCr dGrec
0055   W5 = 3400 x (2 x (X5*2)-(M4 x CO))              W(CrAl) 2XCr gt sq.-MgM1 Cr
0056   W6 = 5157 x (M4 x F4)                           W(FeAl) MgM1 FeM1
0057   G1 = 3.23 x TW - 6047                           dH-TdS
0058   G2 = R2+W1+W2+W4+W5-W6+G1                       RT ln KD+nonideal terms+dH-
0059   P1 = -G2/V1                                     P(kb) Al-barometer
-------------------------------------------------------------------------
0060   K3 = ((1-X2*3) x X4 x X5)/(MA x (MB*2)x CO)
0061   K3 = K3*2                                       KD Cr-barometry
0062   L3 = LN K3                                      ln KD
0063   R3 = 1.987 x L3 x TW                            RT ln KD
0064   V2 = -392.1 + 1346 x CO x (1-CO)                dVr
0065   W1 = W1 x 2                                     6W*CaMg) XCa(gt) sq.
0066   W2 = W2 x 2                                     6W(CaMg-FeCa)XFe XCa(gt)sq.
0067   W4 = W3 x X2                                    XCA(gt) dGrec
0068   W5 = 6800 x ((X4*2)+(X5*2)-(M4 x AO))           2W(CrAl)(XAl XCr(gt)sq.-MgM1
0069   W6 = W6 x 2                                     2W(FeAl) MgM1 FeM1
0070   G3 = 10.51 x TW - 17716                         dH - TdS
0071   G4 = R3+W1+W2+W4+W5-W6+G3                       RT ln KD+nonideal+dH-TdS
0072   P2 = -G4/V2                                     P(kb) Cr-barometer
-------------------------------------------------------------------------
0073   LPRINT " Estimates for"
0074   LPRINT V$
0075   IF TC>850 GOTO 0077
0076   LPRINT "        WARNING: T-estimate below calibrated range"
0077   LF 1
0078   USING "&&&&&&&&&&&"
0079   USING "#######.##"
0080   LPRINT "        ";"     T(C)";"   P(KB)"
0081   LPRINT "Al-Barom";TC;P1
0082   LPRINT "Cr-Barom";TC;P2
0083   PM=(P1+P2)/2
0084   IF AO<0.01 AND CO<0.005 GOTO 91
0085   IF AO<0.01 THEN LET PM=P2
0086   IF CO<0.005 THEN LET PM=P1
0087   LF 1
0088   LPRINT "Estimate";TC;PM
0089   LF 2
0090   END
0091   LPRINT "Sorry"
0092   USING
0093   LPRINT "Al and Cr too low"
0094   LPRINT "Unreliable estimate"
0095   LPRINT "Numerical values"
0096   LPRINT TC,PM
0097   END
```

APPENDIX 8

Conversion table of sample numbers used in the text to Tasmania University collection numbers.

Sample number in text	Tas.Uni. collection number.
BM-54	64100
BM-69	64101
BM-99	64102
BM-160	64103
BM-9	64104
BM-15	64105
BM-27	64106
BM-58	64107
BM-62	64108
BM-74	64109
BM-134	64110
BM-139	64111
BM-147	64112
BM-161	64113
BM-166	64114
BM-167	64115
BM-48	64116
BM-144	64117
BM-162	64118
BM-143	64119
BM-47	64120
BM-154	64121
BM-137	64122
BM-18	64123
BM-51	64124
BM-135	64125
BM-142	64126
BM-152	64127
BM-163	64128
BM-117	64129
BM-156	64130
BM-109	64131
BM-114	64132
BM-116	64133
BM-168	64134
BMH-9	64142

Sample number in text	Tas.Uni. collection number
LE-00	64135
LE-50	64136
LE-532	47532
LE-539	47539
LE-2664	47611
LE-2641	47609
LE-67	64137
LE-68	64138
LE-4	64139
LE-19	64140
LE-544	47544
LE-2662	47614
LE-27	64141

REFERENCES

ADAMS, G.E. and BISHOP, F.C. (1982): Experimental investigation of Ca-Mg exchange between olivine, orthopyroxene, and clinopyroxene: potential for geobarometry.- Earth Planet. Sci. Lett. 57: 241-250.

AKELLA, J. (1976): Garnet pyroxene equilibria in the system $CaSiO_3$-$MgSiO_3$-Al_2O_3 and in a natural mineral mixture.- Am. Min. 61: 589-598.

AKELLA, J. and BOYD, F.R. (1973): Effect of pressure on the composition of coexisting pyroxenes and garnets in the system $CaSiO_3$-$MgSiO_3$-$FeSiO_3$-$CaAlTi_2O_6$.- Carn. Inst. Wash. Yb. 72: 523-527.

AKELLA, J. and BOYD, F.R. (1974): Petrogenetic grid for garnet peridotites.- Carn. Inst. Wash. Yb. 73: 269-273.

ARIMA, M. and ONUMA, K. (1977): The solubility of alumina in enstatite and the phase equilibria in the join $MgSiO_3$-$MgAl_2SiO_6$ at 10-25 kb.- Contr. Min. Petr. 61: 251-265.

BASALTIC VOLCANISM STUDY PROJECT (1981): Basaltic volcanism on the terrestrial planets. Pergamon Press, New York, 1286 pp.

BASU, A.R. (1980): Reply (to Wolff, J.A.).- Nature 288: 104.

BEST, M.G. (1975): Amphibole bearing cumulate inclusions, Grand Canyon, Arizona, and their bearing on silica-undersaturated hydrous magmas in the upper mantle.- J. Petr. 16: 212-236.

BOETTCHER, A.L. and O'NEIL , J.R. (1980): Stable isotopes, chemical, and petrographic studies of high-pressure amphiboles and micas: evidence for metasomatism in the mantle source regions of alkali basalts and kimberlites.- Am. J. Sci. 280-A: 594-621.

BOYD, F.R. (1973): A pyroxene geotherm.- Geoch. Cosm. Acta 37: 2533-2546.

BOYD, F.R. (1974): Ultramafic nodules from the Frank Smith kimberlite pipe, South Africa.- Carn. Inst. Wash. Yb. 73: 285-294 .

BOYD, F.R. and ENGLAND, J.L. (1964): The system enstatite-pyrope.- Carn. Inst. Wash. Yb. 63: 157-161.

BOYD, F.R., FUJII, T. and DANCHIN, R.V. (1976): A noninflected geotherm for the Udachnaya kimberlite pipe, USSR.- Carn. Inst. Wash. Yb. 75: 523-531.

BOYD, F.R. and NIXON, P.H. (1975): Origins of the ultramafic nodules from some kimberlites of Northern Lesotho and the Monastery mine, South Africa.- Phys. Chem. Earth 9: 431-454.

BOYD, F.R. and NIXON, P.H. (1978): Ultramafic nodules from the Kimberley pipes, South Africa.- Geoch. Cosm. Acta 42: 1367-1382 and appendix.

BOYD, F.R. and SCHAIRER, J.F. (1964): The system $MgSiO_3$-$CaMgSi_2O_6$.- J. Petr. 5: 275-309.

BREY, G. (1982): Enstatite-diopside solvus to 60 kb.- Terra cognita 2 (3): 217.

BREY, G. and GREEN, D.H. (1975): The role of CO_2 in the genesis of olivine melilitites.- Contr. Min. Petr. 49: 93-103.

BREY, G. and GREEN, D.H. (1976): Solubility of CO_2 in olivine melilitite at high pressures and the role of CO_2 in the earth's upper mantle.- Contr. Min. Petr. 55: 217-230.

BREY, G. and GREEN, D.H. (1977): Systematic study of liquidus phase relations in olivine melilitite+H_2O+CO at high pressures and petrogenesis of an olivine melilitite magma.- Contr. Min. Petr. 61: 141-162.

BROWN, G.M., PINSENT, R.H. and COISY, P. (1980): The petrology of spinel-peridotite xenoliths from the Massif Central, France.- Am. J. Sci. 280-A: 471-498.

BUNDY, F.P., BOVENKERK, H.P., STRONG, H.M. and WENTORF, R.H. Jr. (1961): Diamond-graphite equilibrium line from the growth and graphitization of diamond.- J. Chem. Phys. 35: 383-391.

BURNS, R.G. (1970): Mineralogical applications of crystal field theory.- Cambridge University Press.

BURNS, R.G. (1975): Crystal-field effects in chromium and its partitioning in the mantle.- Geoch. Cosm. Acta 39: 857-864.

BURNS, V.M. and BURNS, R.G. (1975): Mineralogy of chromium.- Geoch. Cosm. Acta 39: 303-310.

CARSWELL, D.A. (1975): Primary and secondary phlogopites and clinopyroxenes in garnet lherzolite xenoliths.- Phys. Chem. Earth 9: 417-429.

CARSWELL, D.A., CLARKE, D.B. and MITCHELL, R.H. (1979): The petrology of ultramafic nodules from pipe 200, Northern Lesotho.- Proc. 2nd Int. Kimb. Conf. 2: 127-144.

CARSWELL, D.A. and GIBB, F.G.F. (1980): Geothermometry of garnet lherzolite nodules with special reference to those from kimberlites of Northern Lesotho.- Contr. Min. Petr. 74: 403-416.

CARTER-HEARN, B and BOYD, F.R. (1975): Garnet peridotite xenoliths in a Montana, U.S.A., kimberlite.- Phys. Chem. Earth 9: 247-255.

CHATTERJEE, N.D., LEISTNER, H., TERHART, L., ABRAHAM, K. and KLASKA, R. (1982): Thermodynamic mixing properties of corundum-eskolaite, alpha-$(Al,Cr^{3+})_2O_3$, crystalline solutions at high temperatures and pressures.- Am. Min. 67: 725-735.

CHATTERJEE, N.D. and SCHREYER, W. (1972): The reaction enstatite+sillimanite= sapphirine+quartz.- Contr. Min. Petr. 36: 49-62.

CLARK, S.P. Jr and RINGWOOD, A.E. (1964): Density distribution and constitution of the mantle.- Rev. Geophys. 2: 35-88.

CONDIE, K.C. (1976): Plate tectonics and crustal evolution.- Pergamon Press, New York, 288 pp,

COOPER, J.A. and GREEN, D.H. (1969): Lead isotope measurements on lherzolite inclusions and host basanites from Western Victoria, Australia.- Earth Plan. Sci. Lett. 6: 69-76.

COX, K.G., GURNEY, J.J. and HARTE, B. (1973): Xenoliths from the Matsoku pipe.- In: Nixon, P. (ed.): Lesotho kimberlites.- pp.76-100, Lesotho National Devel. Corp., Maseru.

CRAWFORD, A.J. (1983): Tectonic development of the Lachlan foldbelt and construction of the continental crust of southeastern Australia.- Abstr. 6th Aust. Geol. Conv., pp.30-32, Canberra.

CRAWFORD, A.J. and KEAYS, R.R. (1978): Cambrian greenstone belts in Victoria: marginal sea-crust slices in the Lachlan fold belt of southeastern Australia.- Earth Plan. Sci. Lett. 41: 197-208.

DAHL, P.S. (1980): The thermal-compositional dependence of Fe^{2+}-Mg distributions between coexisting garnet and pyroxene: applications to geothermometry.- Am. Min. 65: 854-866.

DANCHIN, R.V. and BOYD, F.R. (1976): Ultramafic nodules from the Premier kimberlite pipe, South Africa.- Carn. Inst. Wash. Yb. 75: 531-538.

DANCKWERTH, P.A. and NEWTON, R.C. (1978): Experimental determination of the spinel peridotite to garnet peridotite reaction in the system $MgO-Al_2O_3-SiO_2$ in the range 900-1100°C and Al_2O_3-isopleths of enstatite in the spinel field.- Contr. Min. Petr. 66: 189-201.

DASCH, E.J. and GREEN, D.H. (1975): Strontium isotope geochemistry of lherzolite inclusions and host basaltic rocks, Victoria, Australia.- Am. J. Sci. 275: 461-469.

DAVIS, B.T.C. and BOYD, F.R. (1966): The join $Mg_2Si_2O_6-CaMgSi_2O_6$ at 30 kb pressure and its application to pyroxenes from kimberlites.- J. Geophys. Res. 71: 3567-3576.

DAWSON, J.B. (1980): Kimberlites and their xenoliths.- Minerals and Rocks, vol.15. Springer-Verlag, Berlin, 252 pp.

DAWSON, J.B., POWELL, D.G. and REID, A.M. (1970): Ultrabasic xenoliths and lava from the Lashaine volcano, northern Tanzania.- J. Petr. 11: 519-548.

DAWSON, J.B. and SMITH, J.V. (1975): Occurrence of diamond in a mica-garnet lherzolite xenolith from kimberlite.- Nature 254: 580-581.

DAWSON, J.B. and SMITH, J.V. (1982): Coarse and veined peridotites from northern Tanzanian tuff cones.- Terra cognita 2: 230.

DICK, H.J.B. and SINTON, J.M. (1979): Compositional layering in alpine peridotites: evidence for pressure solution creep in the mantle.- J. Geol. 87: 403-416.

DICKEY, J.S. Jr and YODER, H.S. Jr (1970): Partitioning of chromium and aluminium between clinopyroxene and spinel.- Carn. Inst. Wash. Yb. 71: 384-392.

DICKEY, J.S., YODER, H.S. and SCHAIRER, J.F. (1971): Chromium in silicate-oxide systems.- Carn. Inst. Wash. Yb. 70: 118-122.

EGGLER, D.H. and McCALLUM, M.E. (1976): A geotherm from megacrysts in the Sloan kimberlite pipes, Colorado.- Carn. Inst. Wash. Yb. 75: 538-541.

EGGLER, D.H., McCALLUM, M.E. and SMITH, S.B. (1979): Megacryst assemblages in kimberlites from northern Colorado and southern Wyoming: Petrology, geothermometry-barometry, and areal distribution.- Proc. 2nd Int. Kimb. Conf. 2: 213-226.

EGGLER, D.H. and WENDLANDT, R.F. (1979): Experimental studies on the relationship between kimberlite magmas and partial melting of perioditite.- Proc. 2nd Int. Kimb. Conf. 1: 330-338.

EHRENBERG, S.N. (1979): Garnetiferous ultramafic inclusions in minette from the Navajo Volcanic Field.- Proc. 2nd Int. Kimb. Conf. 2: 330-344.

EHRENBERG, S.N. (1982): Petrogenesis of garnet lherzolite and mega-crystalline nodules from the Thumb, Navajo Volcanic Field.- J. Petr. 23: 507-547.

ELLIS, D.J. (1976): High-pressure cognate inclusions in the Newer Volcanics of Victoria.- Contr. Min. Petr. 58: 149-180.

ELLIS, D.J. and GREEN, D.H. (1979): An experimental study of the effect of Ca upon garnet-clinopyroxene Fe-Mg exchange equilibria.- Contr. Min. Petr. 71: 13-22.

EMBEY-ITSZTIN, A. (1976): Amphibolite/lherzolite composite xenoliths from Szigliget, north of the Lake Balaton, Hungary.- Earth Plan. Sci. Lett. 31: 297-304.

ENGI, M. and EVANS, B.W. (1980): A re-evaluation of the olivine-spinel geothermometer: discussion.- Contr. Min. Petr. 73: 201-203.

ERLANK, A.J., ALLSOPP, H.L., HAWKESWORTH, C.J. and MENZIES, M.A. (1982): Chemical and isotopic characterisation of upper mantle metasomatism in peridotite nodules from the Bultfontein kimberlite.- Terra cognita 2: 261-263.

EVANS, B.W. and FROST, B.R. (1975): Chrome-spinel in progressive meta-morphism - a preliminary analysis.- Geoch. Cosm. Acta 39: 952-972.

EVANS, B.W. and TROMMSDORFF, V. (1978): Petrogenesis of garnet lherzolite, Cima di Gagnone, Lepontine Alps.- Earth Plan. Sci. Lett. 40: 333-348.

FERGUSON, J., ELLIS, D.J. and ENGLAND, R.N. (1977): Unique spinel-garnet lherzolite inclusions in kimberlite from Australia.- Geology 5: 278-280.

FERGUSON, J. and SHERATON, J.W. (1979): Petrogenesis of kimberlitic rocks and associated xenoliths of southeastern Australia.- Proc. 2nd Int. Kimb. Conf. 1: 140-160.

FESQ, H.W., BIBBY, D.M., ERASMUS, C.S., KABLE, E.J.D. and SELLSCHOP, J.P.F. (1975): A comparative trace element study of diamonds from Premier, Finsch and Jagersfontein mines, South Africa.- Phys. Chem. Earth 9: 817-836.

FLEET, M.E. (1974): Partitioning of major and minor elements and equilibration in coexisting pyroxenes.- Contr. Min. Petr. 44: 259-274.

FRANCIS, D.M. (1976a): Amphibole pyroxenite xenoliths: cumulate or replacement phenomena from the upper mantle, Nunivak Island, Alaska.- Contr. Min. Petr. 58: 51-61.

FRANCIS, D.M. (1976b): The origin of amphibole in lherzolite: xenoliths from Nunivak Island, Alaska.- J. Petr. 17: 357-378.

FREY, F.A. and GREEN, D.H. (1974): The mineralogy, geochemistry and origin of lherzolite inclusions in Victorian basanites.- Geoch. Cosm Acta 38: 1023-1059.

FREY, F.A., GREEN, D.H. and ROY, S.D. (1978): Integrated models of basalt petrogenesis: A study of quartz tholeiite to olivine melilitite from south eastern Australia utilizing geochemical and experimental petrological data.- J. Petr. 19: 463-513.

FREY, F.A. and PRINZ, M. (1978): Ultramafic inclusions from San Carlos, Arizona: petrologic and geochemical data bearing on their petrogenesis.- Earth Plan. Sci. Lett. 38: 129-176.

FYFE, W.S., TURNER, F.J. and VERHOOGEN, J. (1958): Metamorphic reactions and metamorphic facies.- Geol. Soc. Am. Mem. 73.

GANGULY, J. and GHOSE, S. (1979): Aluminous orthopyroxene: order-disorder, thermodynamic properties, and petrologic implications.- Contr. Min. Petr. 69: 375-385.

GANGULY, J. and KENNEDY, G.C. (1974): The energetics of natural garnet solid solution - I. Mixing of the alumino-silicate endmembers.- Contr. Min. Petr. 48: 137-14

GARRISON, J.R. Jr. and TAYLOR, L.A. (1980): Megacrysts and xenoliths in kimberlite, Elliot county, Kentucky: A mantle sample from beneath the Permian Appalachian Plateau.- Contr. Min. Petr. 75: 27-42.

GIROD, M., DAUTRIA, J.M. and GIOVANNI, R. de (1981): A first insight into the constitution of the upper mantle under the Hoggar area (southern Algeria): the lherzolite xenoliths in the alkali basalts.- Contr. Min. Petr. 77: 66-73.

GLASSER, F.P. and OSBORN, E.F. (1958): Phase equilibria studies in the system $CaO-Cr_2O_3-SiO_2$.- J. Am. Ceram. Soc. 41: 358-367.

GRAYSON, H.J. and MAHONY, D.J. (1910): The geology of the Camperdown and Mt. Elephant districts.- Mem. Geol. Sirv. Vict. 9.

GRIFFIN, B.J. (1979): Energy dispersive analysis system calibration and operation with TAS-SUEDS, an advanced interactive data reduction package.- Univ. of Tasmania, Geol. Dept pub. no. 343.

GREEN, D.H. (1970): The origin of basaltic and nephelinitic magmas.- Trans. Leicester Lit. Phil. Soc. 64: 28-54.

GREEN, D.H. (1971): Composition of basaltic magmas as indicators of conditions of origin: application to oceanic volcanism.- Phil. Trans. Roy. Soc. Lond. A-268: 707-725.

GREEN, D.H. (1973a): Conditions of melting of basanite magma from garnet peridotite.- Earth Planet. Sci. Lett. 17: 456-465.

GREEN, D.H. (1973b): Experimental melting studies on model upper mantle compositions at high pressures under both water-saturated and water-undersaturated conditions.- Earth Planet. Sci. Lett. 19: 37-53.

GREEN, D.H., HIBBERSON, W.O. and JAQUES, A.L. (1979): Petrogenesis of Mid-Ocean Ridge basalts.- In: McElhinny (ED.): The Earth: Its Origin, Structure and Evolution.- Academic Press, London.

GREEN, D.H. and RINGWOOD, A.E. (1967): The stability fields of aluminous pyroxene peridotite and garnet peridotite and their relevance in upper mantle structure.- Earth Planet. Sci. Lett. 3: 151-160.

GREEN, D.H. and RINGWOOD, A.E. (1967b): The genesis of basaltic magmas.- Contr. Min. Petr. 15: 103-190.

GREEN, D.H. and RINGWOOD, A.E. (1970): Mineralogy of peridotitic compositions under upper mantle conditions.- Phys. Earth Plan. Int. 3: 359-371.

GREEN, T.H., RINGWOOD, A.E. and MAJOR, A. (1966): Friction effects and pressure calibration in a piston-cylinder apparatus at high pressure and temperature.- J. Geophys. Res. 71: 3589-3595.

GURNEY, J.J. and HARRIS, J.W.(1982): Some observations relevant to the formation of natural diamonds.- Terra cognita 2: 199.

GURNEY, J.J., HARRIS, J.W. and RICKARDS, R.S. (1979b): Silicate and oxide inclusions in diamonds from the Finsch kimerlite pipe.- Proc. 2nd Int. Kimb. Conf. 2: 1-15.

GURNEY, J.J. and HARTE, B. (1980): Chemical variations in upper mantle nodules from South African kimberlites.- Phil. Trans. Roy. Soc. Lond. A-297: 273-293.

GURNEY, J.J., HARTE, B. and COX, K.G. (1975): Mantle xenoliths in the Matsoku kimberlite pipe.- Phys. Chem. Earth 9: 507-524.

GURNEY, J.J., JAKOB, W.R.O. and DAWSON, J.B. (1979a): Megacrysts from the Monastery kimberlite pipe, South Africa.- Proc. 2nd Int. Kimb. Conf. 2: 227-243.

HAGGERTY, S.E. (1979): Spinels in high-pressure regimes.- Proc. 2nd Int. Kimb. Conf. 2: 183-196.

HAGGERTY, S.E., BOYD, F.R., BELL, P.M., FINGER, L.W. and BRYAN, W.B. (1970): Opaque minerals and olivine in lavas and breccias from Mare Tranquillitatis.- Proc. apollo 11 Lun. Sci. Conf., Geoch. Cosm. Acta suppl.1, 1: 513-538.

HALES, A.L. (1981): The upper mantle velocity distribution.- Phys. Earth Plan. Int. 25: 1-11.

HARLEY, S.L. (1981): Garnet-orthopyroxene assemblages as pressure-temperature indicators.- Unpub. Ph.D. thesis, Univ. of Tasmania.

HARLEY, S.L. and GREEN, D.H. (1982): Garnet-orthopyroxene barometry for granulites and peridotites.- Nature 300: 697-701.

HARTE, B. (1977): Rock nomenclature with particular relation to deformation and recrystallization textures in olivine bearing xenoliths.- J. Geol. 85: 279-288.

HARTE, B. (1978): Kimberlite nodules, upper mantle petrology and geotherms.- Phil. Trans. Roy. Soc. Lond. A-288: 487-500.

HARTE, B., GURNEY, J.J. and HARRIS, J.W. (1980): The formation of peridotitic suite inclusions in diamonds.- Contr. Min. Petr. 72: 181-190.

HATTON, C.J. and GURNEY, J.J. (1979): A diamond-graphite eclogite from the Roberts Victor mine.- Proc. 2nd Int. Kimb. Conf. 2: 29-36.

HENSEN, B.J. (1973): Pyroxenes and garnets as geothermometers and barometers.- Carn. Inst. Wash. Yb. 72: 527-535.

HENSEN, B.J. and ESSENE, E.J. (1971): The stability of pyrope-quartz in the system MgO-Al_2O_3-SiO_2.- Contr. Min. Petr. 30: 72-83.

HERVIG, R.L., SMITH, J.V., STEELE, I.M., GURNEY, J.J., MEYER, H.O.A. and HARRIS, J.W. (1980): Diamonds: Minor elements in silicate inclusions: pressure-temperature implications.- J. Geophys. Res. 85: 6919-6929.

HERZBERG, C.T. (1978a): The bearing of phase equilibria in simple and complex systems and the origin and evolution of some well-documented garnet websterites.- Contr. Min. Petr. 66: 375-382.

HERZBERG, C.T. (1978b): Pyroxene geothermometry and geobarometry: experimental and thermodynamic evaluation of some subsolidus phase relations involving pyroxenes in the system $CaO-MgO-Al_2O_3-SiO_2$.- Geoch. Cosm. Acta 42: 945-957.

HOLDAWAY, M.J. (1976): Mutual compatibility relations of the Fe^{2+}-Mg-Al silicates at 800°C and 3 kb.- Am. J. Sci. 276: 285-309.

HOLLIS, J.D. (1981): Ultramafic and gabbroic nodules from the Bullenmerri and Gnotuk maars, Camperdown, Victoria.- Roy. Soc. Vict. Proc. 91: 155-167.

HOLLOWAY, J.R. (1973): The system pargasite-H_2O-CO_2: a model for melting of a hydrous mineral with a mixed-volatile fluid. - I. epxerimental results to 8 kb.- Geoch. Cosm. Acta 37: 651-666.

HOWELLS, S. and O'HARA, M.J. (1975): Paleogeotherms and the enstatite-diopside solvus.- Nature 254: 406-408.

HOWELLS, S. and O'HARA, M.J. (1978): Low solubility of alumina in enstatite and uncertainties in estimated paleogeotherms.- Phil. Trans. Roy. Soc. Lond. 288-A: 471-486.

HSU, L.C. and BURNHAM, C.W. (1969): Phase relationships in the system $Fe_3Al_2Si_3O_{12}$-$Mg_3Al_2Si_3O_{12}$-H_2O at 2.0 kilobars.- Geol. Soc. Am. Bull. 80: 2393-2408.

HUTCHINSON, R.B., CHAMBERS, A.L., PAUL, D.K. and HARRIS, P.G. (1975): Chemical variation among French ultramafic xenoliths evidence for a heterogeneous upper mantle.- Min. Mag. 40: 153.

IKEDA, K. and OHASHI, H. (1974): Crystal field spectra of diopside-kosmochlor solid solutions formed at 15 kb pressure.- J. Jap. Ass. Min. Pet. Econ. Geol. 69: 103-106.

IKEDA, K. and YAGI, K. (1972): Synthesis of kosmochlor and phase equilibria in the join $CaMgSi_2O_6$-$NaCrSi_2O_6$.- Contr. Min. Petr. 36: 63-72.

IKEDA, K. and YAGI, K. (1977): Experimental study on the phase equilibria in the join $CaMgSi_2O_6$-$CaCrCrSiO_2$ with special reference to the blue diopside.- Contr. Min. Petr. 61: 91-106.

IKEDA, K. and YAGI, K. (1978): Reply to H.D. Schreiber.- Contr. Min. Petr. 66: 343-344.

IKEDA, K. and YAGI, K. (1982): Crystal-field spectra for blue and green diopsides synthesized in the join $CaMgSi_2O_6$-$CaCrAlSiO_6$.- Contr. Min. Petr. 81: 113-118.

IRFUNE, T., OHTANI, E. and KUMUZAWA, M. (1982): Stability field of knorringite $Mg_3Cr_2Si_3O_{12}$ at high pressures and its implications to the occurrence of Cr-rich pyrope in the upper mantle.- Phys. Earth Plan. Int. 27: 263-272.

IRVING, A.J. (1971): Geochemical and high-pressure experimental studies of xenoliths, megacrysts and basalts from southeastern Australia.- Ph.D. thesis, A.N.U., Canberra.

IRVING, A.J. (1974a): Megacrysts from the Newer Basalts and other basaltic rocks of southeastern Australia.- Geol. Soc. Am. Bull. 85: 1503-1514.

IRVING, A.J. (1974b): Pyroxene-rich ultramafic xenoliths in the Newer Basalts of Victoria, Australia.- N. Jb. Min. Abh. 120: 147-167.

IRVING, A.J. (1976): On the validity of paleogeotherms determined from xenolith suites in basalts and kimberlites.- Am. Min. 61: 638-642.

IRVING, A.J. (1980): Petrology and geochemistry of composite ultramafic xenoliths in alkalic basalts and implications for magmatic processes within the mantle.- Am. J. Sci. 280-A: 389-426.

IRVING, A.J. and GREEN, D.H. (1976): Geochemistry and petrogenesis of the Newer Basalts of Victoria and South Australia.- J. Geol. Soc. Aust. 23: 45-66.

JACOBY, W.R. and SCHMELING, H. (1982): On the effects of the lithosphere on mantle convection and evolution.- Phys. Earth Plan. Int. 29: 305-319.

JAGOUTZ, E., PALME, H., BADDENHAUSEN, H., BLUM, K., CENDALES, M., DREIBUS, G., SPETTEL, B., LORENZ, V. and WÄNKE, H. (1979): The abundance of major, minor and trace elements in the earth's mantle as derived from primitive ultramafic nodules.- Proc. Lun. Planet. Sci. Conf. 10: 2031-2050.

JAQUES, A.L. and GREEN, D.H. (1979): Determination of liquid compositions in high-pressure melting of peridotite.- Am. Min. 64: 1312-1321.

JAQUES, A.L. and GREEN, D.H. (1980): Anhydrous melting of peridotite at 0-15 kb pressure and the genesis of tholeiitic basalts.- Contr. Min. Petr. 73: 287-310.

JARVIS, G.T. and PELTIER, W.R. (1982): Mantle convection as a boundary layer phenomenon.- Geophys. J. Roy. Astr. Soc. 68: 385-424.

JENKINS, D.M. and NEWTON, R.C. (1979): Experimental determination of the spinel peridotite to garnet peridotite inversion at 900 and 1000°C in the system $CaO-MgO-Al_2O_3-SiO_2$, and at 900°C with natural garnet and olivine.- Contr. Min. Petr. 68: 407-419.

JOHANNES, W., BELL, P.M., MAO, H.K., BOETTCHER, A.L., CHIPMAN, D.W., HAYS, J.F., NEWTON, R.C. and SEIFERT, F. (1971): An inter-laboratory comparison of piston-cylinder pressure calibration using the albite-breakdown reaction.- Contr. Min. Petr. 32: 24-38.

KENNEDY, C.S. and KENNEDY, G.C. (1976): The equilibrium boundary between graphite and diamond.- J. Geophys. Res. 81: 2467-2470.

KESSON, S. and PRICE, R.C. (1972): The major and trace element chemistry of kaersutite and its bearing on the petrogenesis of alkaline rocks.- Contr. Min. Petr. 35: 119-124.

KLEEMAN, J.D., GREEN, D.H. and LOVERING, J.F. (1969): Uranium distribution in ultramafic inclusions from Victorian basalts.- Earth Plan. Sci. Lett. 5: 449-458.

KUNO, H. (1969): Mafic and ultramafic nodules in basaltic rocks of Hawaii.- Geol. Soc. Am. Mem. 115: 189-234.

KUNO, H. and AOKI, K. (1970): Chemistry of ultramafic nodules and their bearing on the origin of basaltic magmas.- Phys. Earth Plan. Int. 3: 273-301.

KRETZ, R. (1982): Transfer and exchange equilibria in a portion of the pyroxene quadrilateral as deduced from natural and experimental data.- Geoch. Cosm. Acta 46: 411-421.

LAMBERT, I.B. and WYLLIE, P.J. (1968): Stability of hornblende and a model of the low velocity zone.- Nature 219: 1240-1241.

LANE, D.L. and GANGULY, J. (1980): Al_2O_3 solubility in orthopyroxene in the system $MgO-Al_2O_3-SiO_2$: a re-evaluation, and a mantle geotherm.- J. Geophys. Res. 85: 6963-6972.

LENSCH, G. (1976): Ariegite und Websterite im Lherzolith von Balmuccia (Val Sesia, Zone von Ivrea).- N. Jb. Miner. Abh. 128: 189-208.

LINDSLEY, D.H. and DIXON, S.A. (1976): Diopside-enstatite equilibria at 850 to 1400°C, 5 to 35 kb.- Am. J. Sci. 276: 1285-1301.

LINDSLEY, D.H., GROVER, J.E. and DAVIDSON, P.M. (1981): The thermodynamics of the $Mg_2Si_2O_6$-$CaMgSi_2O_6$ join: a review and an improved model.- In: Newton, R.C., Navrotsky, A. and Wood, B.J. (1981): Thermodynamics of minerals and melts.- (Advances in Physical Geochemistry), 1: 149-175. Springer, New York.

LLOYD, F.E. and BAILEY, D.K. (1975): Light element metasomatism of the continental mantle: the evidence and the consequences.- Phys. Chem. Earth 9: 389-416.

MAALØE, S. and AOKI, K. (1977): The major element composition of the upper mantle estimated from the composition of lherzolites.- Contr. Min. Petr. 63: 161-17 .

MAALØE, S. and PRINTZLAU, I. (1979): Natural partial melting of spinel lherzolite.- J. Petr. 20: 727-741.

MacGREGOR, I.D. (1970): The effect of CaO, Cr_2O_3, Fe_2O_3 and Al_2O_3 on the stability of spinel and garnet peridotites.- Phys. Earth Plan. Int. 3: 372-377.

MacGREGOR, I.D. (1974): The system $MgO-Al_2O_3-SiO_2$: Solubility of Al_2O_3 in enstatite for spinel and garnet peridotite compositions.- Am. Min. 59: 110-119.

MacGREGOR, I.D. (1982): Geothermometers and geobarometers for spinel-bearing ultramafic rocks.- Terra cognita 2 (3): 217.

McCALLUM, M.E. and EGGLER, D.H. (1976): Diamonds in an upper mantle peridotite nodule from kimberlite in Southern Wyoming.- Science 192: 253-256.

MEDARIS, L.G. Jr (1980): Petrogenesis of the Lien peridotite and associated eclogites, Almklovdalen, western Norway.- Lithos 13: 339-353.

MENGEL, K., WEDEPOHL, K.H. and OEHM, J. (1982): Depleted mantle rocks and metasomatically altered peridotite inclusions in Tertiary basalts from the Hessian depression (N.W. Germany).- Terra cognita 2: 230.

MENZIES, M. and MURTHY, V.R. (1980): Mantle metasomatism as a precursor to the genesis of alkaline magmas - isotopic evidence.- Am. J. Sci. 280-A: 622-638.

MENZIES, M. and MURTHY, V.R. (1980b): Enriched mantle: Nd and Sr isotopes in diopside from kimberlite nodules.- Nature 283: 634-636.

MERCIER, J.C. and NICOLAS, A. (1975): Textures and fabrics of upper mantle peridotites as illustrated by xenoliths from basalts.- J. Petr. 16: 454-487.

MEYER, H.O.A. (1975): Chromium and the genesis of diamond.- Geoch. Cosm. Acta 39: 929-936.

MEYER, H.O.A. and BOYD, F.R. (1972): Composition and origin of crystalline inclusions in natural diamonds.- Geoch. Cosm. Acta 36: 1255-1273.

MIRWALD, P.W., GETTING, I.C. and KENNEDY, G.C. (1975): Low friction cell for piston-cylinder high-pressure apparatus.- J. Geophys. Res. 80: 1519-1525.

MITCHELL, R.H. (1978): Garnet lherzolites from Somerset Island, Canada and aspects of the nature of perturbed geotherms.- Contr. Min. Petr. 67: 341-347.

MITCHELL, R.H., CARSWELL, D.A. and CLARKE, D.B. (1980): Geological implications and validity of calculated equilibration conditions for ultramafic xenoliths from the pipe 200 kimberlite, northern Lesotho.- Contr. Min. Petr. 72: 205-207.

MORI, T. (1976): Pyroxene equilibria in ultramafic rocks.- Ph.D. thesis, A.N.U., Canberra.

MORI, T. and GREEN, D.H. (1975): Pyroxenes in the system $Mg_2Si_2O_6$-$CaMgSi_2O_6$ at high pressures.- Earth Plan. Sci. Lett. 26: 277-286.

MORI, T. and GREEN, D.H. (1976): Subsolidus equilibria between pyroxenes in the CaO-MgO-SiO_2 system at high pressures and temperatures.- Am. Min. 61: 616-625.

MORI, T. and GREEN, D.H. (1978): Laboratory duplication of phase equilibria observed in natural garnet lherzolites.- J. Geol. 86: 83-97.

MUAN, A. (1975): Phase relations in chromium oxide containing systems at elevated temperatures.- Geoch. Cosm. Acta 39: 781-802.

MYSEN, B.O. (1976): Experimental determination of some geochemical parameters relating to conditions of equilibration of peridotite in the upper mantle.- Am. Min. 61: 677-683.

NEHRU, C.E. and WYLLIE, P.J. (1974): Electron microprobe measurements of pyroxenes coexisting with H_2O undersaturated liquids on the join $CaMgSi_2O_6$-$Mg_2Si_2O_6$-H_2O at 30 kbars with applications to geothermometry.- Contr. Min. Petr. 48: 221-228.

NIXON, P.H. and BOYD, F.R. (1973a): Petrogenesis of the granular and sheared ultrabasic nodule suite in kimberlites.- In: Nixon, P.H. (Ed.): Lesotho Kimberlites, pp.48-56. Lesotho Nat. Dev. Corp., Cape Town.

NIXON, P.H. and BOYD, F.R. (1973b): The discrete nodule (megacryst) association in kimberlites from Northern Lesotho.- In Nixon, P.H. (Ed.): Lesotho Kimberlites, pp. 67-75. Lesotho Nat. Dev. Corp., Cape Town.

NIXON, P.H. and BOYD, F.R. (1979): Garnet bearing lherzolites and discrete nodule suites from the Malaita Alnoite, Solomon Islands, S.W. Pacific, and their bearing on oceanic mantle composition and geotherm.- Proc. 2nd Int. Kimb. Conf. 2: 400-423.

OBATA, M. (1976): The solubility of Al_2O_3 in orthopyroxene in spinel and plagioclase peridotites and spinel pyroxenites.- Am. Min. 61: 804-816.

OBATA, M. (1980): The Ronda peridotite: garnet-, spinel-, and plagioclase lherzolite facies and the P-T trajectories of a high-temperature mantle intrusion.- J. Petr. 21: 533-572.

O'HARA, M.J., RICHARDSON, S.W. and WILSON, G. (1971): Garnet-peridotite stability and occurrence in crust and mantle.- Contr. Min. Petr. 32: 48-68.

O'HARA, M.J., SAUNDERS, M.J. and MERCY, E.L.P. (1975): Garnet-peridotite, primary ultrabasic magma and eclogite: interpretation of upper mentle processes in kimberlite.- Phys. Chem. Earth 9: 571-604.

OKA, Y. (1977): A thermodynamic treatment of chemical reactions in orthopyroxenes.- Geoch. J. 11: 101-106.

OKA, Y. (1978): Experimental study on the partitioning of Fe and Mg between garnet and olivine and its application to kimberlites.- Jour. Fac. Sci. Hokkaido Univ. Ser. IV, 18 (3): 351-376.

O'NEILL, H.St.C. (1981): The transition between spinel lherzolite and garnet lherzolite, and its use as a geobarometer.- Contr. Min. Petr. 77: 185-194.

ONUMA, K. and TOHARA, T. (1981): Clinopyroxenes and spinels in the system $CaMgSi_2O_6$-$CaAl_2SiO_6$-$CaCrAlSiO_6$: a preliminary report.- J. Fac. Sci. Hokkaido Univ. Ser. IV, 19 (4): 495-503.

OTTONELLO, G., PICCARDO, G.B., JORON, J.L. and TREUIL, M. (1978): Evolution of the upper mantle under the Assab Region (Ethiopia): suggestions from petrology and geochemistry of tectonitic ultramafic xenoliths and host basaltic lavas.- Geol. Rdsch. 67 (2): 547-576.

PARKER, R.L. and OLDENBURG, D.W. (1973): Thermal model of ocean ridges.- Nature 242: 137-139.

PELTIER, W.R. (1980): Mantle convection and viscosity.- Proc. Enrico Fermi Int. Sch. Phys. (LXXVIII), New York.

PELTIER, W.R. (1981): Surface plates and thermal plumes: separate scales of mantle convection circulation.- In: O'Connel, R. and Fyfe, W. (Eds): Evolution of the Earth, pp.134-143. A.G.U., Washington.

PELTIER, W.R. and JARVIS, G.T. (1982): Whole mantle convection and the thermal evolution of the earth.- Phys. Earth Plan. Int. 29: 281-304.

PERKINS, D., HOLLAND, T.J.B. and NEWTON, R.C. (1981): The Al_2O_3 contents of enstatite in equilibrium with garnet in the system MgO-Al_2O_3-SiO_2 at 15 to 40 kb and 900 to 1600°C.- Contr. Min. Petr. 78: 99-109.

PERKINS, D. and NEWTON, R.C. (1980): The compositions of coexisting pyroxenes and garnet in the system CaO-MgO-Al_2O_3-SiO_2 at 900-1100°C and high pressures.- Contr. Min. Petr. 75: 291-300.

PIKE, J.E.N., MEYER, C.E. and WILSHIRE, H.G. (1980): Petrography and chemical composition of a suite of ultramafic xenoliths from Lashaine, Tanzania.- J. Geol. 88: 343-352.

POKHILENKO, N.P., SOBOLEV, N.V., SOBOLEV, S. and LAVRENT'YEV, Y.G. (1976): Xenoliths of diamond-bearing ilmenite-pyrope lherzolite from the Udachnaya kimberlite pipe, Yakutia.- Doklady Akad. Nauk SSSR, 231: 149-151.

PRESNALL, D.C., BRENNER, N.L. and O'DONELL, T.H. (1973): Drift of Pt/Pt 10 Rh and We 3 Re/W 25 Re thermocouples in a single stage piston-cylinder apparatus.- Am. Min. 58: 771-777.

RAESIDE, R.P. and HELMSTAEDT, H. (1982): The Ile Bizard intrusion, Montreal, Quebec - kimberlite or lamprophyre.- Can. J. Earth Sci. 19: 1996-2011 + appendix.

REID, A.M., DONALDSON, C.H., BROWN, R.W., RIDLEY, W.I. and DAWSON, J.B. (1975): Mineral chemistry of peridotite xenoliths from the Lashaine Volcano, Tanzania.- Phys. Chem. Earth 9: 525-544.

RICE, A. (1982): Soret convection and rheology (viscous dissipation); arguments for whole-mantle convection.- Phys. Earth Plan. Int. 29: 330-343.

RICHARDSON, S.H., ERLANK, A.J. and SHIMIZU, N. (1982): Nd isotopic disequilibrium in garnet peridotites from the Bultfontein kimberlite and implications for mantle metasomatic component addition.- Terra cognita 2: 231-232.

RINGWOOD, A.E. (1966): The chemical composition and origin of the earth. In: Hurley, P.M. (Ed): Advances in Earth Science, pp.287-356. M.I.T. Press, Cambridge, Mass.

RINGWOOD, A.E. (1977): Synthesis of pyrope-knorringite solid solution series.- Earth Plan. Sci. Lett. 36: 443-448.

ROBIE, R.A., HEMINGWAY, B.S. and FISHER, J.R. (1978): Thermodynamic properties of minerals and related substances at 298.15 K and 1 bar (10^5 pascals) pressure and at higher temperatures.- U.S. Geol. Surv. Bull. 1452

RODEN, M.F., FRANCIS, D.M. and FREY, F.A. (1982): Mantle heterogeneity: isotopic and trace element evidence from Nunivak Island, Alaska.- Terra cognita 2: 231.

ROEDER, P.L., CAMPBELL, I.H. and JAMIESON, H.E. (1979): A re-evaluation of the olivine-spinel geothermometer.- Contr. Min. Petr. 68: 325-334.

ROSS, C.S., FOSTER, M.D. and MYERS, A.T. (1954): Origin of dunites and of olivine-rich inclusions in basaltic rocks.- Am. Min. 39: 693-737.

ROVETTA, M.R. (1981): Melt and vapor migration in the upper mantle: ultramafic nodule permeability estimated from fluid/melt inclusions.- EOS 62: 1062.

SACHTLEBEN, T. and SECK, H.A. (1981): Chemical control of Al-solubility in orthopyroxene and its implications on pyroxene geothermometry.- Contr. Min. Petr. 78: 157-165.

SACK, R.O. (1980): Some constraints on the thermodynamic mixing properties of Fe-Mg orthopyroxenes and olivines.- Contr. Min. Petr. 71: 257-269.

SAXENA, S.K. (1981): Fictive component model of pyroxenes and multicomponent phase equilibria.- Contr. Min. Petr. 78: 345-351.

SCHREIBER, H.D. (1977): On the nature of synthetic blue diopside crystal: the stabilization of tetravalent chromium.- Am. Min. 62: 522-527.

SCHREYER, W. (1967): A reconnaissance study of the system $MgO-Al_2O_3-SiO_2-H_2O$ at pressures between 10 and 25 kb.- Carn. Inst. Wash. Yb 66: 380-385.

SHANNON, R.D. and PREWITT, C.T. (1969): Effective ionic radii in oxides and fluorides.- Acta Cryst. B 25: 925-946.

SHEE, S.R., GURNEY, J.J. and ROBINSON, D.N. (1982): Two diamond-bearing peridotite xenoliths from the Finsch kimberlite, South Africa.- Contr. Min. Petr. 81: 79-87.

SINGLETON, O.P. and JOYCE, E.B. (1969): Cainozoic volcanicity in Victoria.- Geol. Soc. Aust. Spec. Pub. 2: 145-154.

SKINNER, B.J. and BOYD, F.R. (1964): Aluminous enstatites.- Carn. Inst. Wash. Yb. 63: 163-165.

SOBOLEV, N.V. (1977): Deep-seated inclusions in kimberlites and the problem of the composition of the upper mantle.- A.G.U., Washington.

SPARKS, R.J.S., PINKERTON, H. and MacDONALD, R. (1977): The transport of xenoliths in magmas.- Earth Plan. Sci. Lett. 35: 234-238.

STOSCH, H.-G. and SECK, H.A. (1980): Geochemistry and mineralogy of two spinel peridotite suites from Dreiser Weiher, West Germany.- Geoch. Cosm. Acta 44: 457-470.

STUBICAN, V.S. and GRESKOVICH, C. (1975): Trivalent and divalent chromium ions in spinels.- Geoch. Cosm. Acta 39: 875-881.

SUTHERLAND, F.L. and HOLLIS, J.D. (1982): Mantle-lower crust petrology from inclusions in basaltic rocks in eastern Australia - an outline.- J. Volc. Geoth. Res. 14: 1-29.

THOMPSON, A.B. and HARLEY, S.L. (1982): Mantle mineral assemblages and palaeogeotherms.- Terra cognita 2: 225-226.

TOXOPEUS, J.M.A.B. (1977): The development of microtextures and dislocation substructures in naturally deformed olivines from various geological environments.- Leid. Geol. Med. 51: 49-55.

TSAI, H., MEYER, H.O.A., MOREAU, J. and MILLEDGE, H.J. (1979): Mineral inclusions in diamond: Premier, Jagersfontein and Finsch kimberlites, South Africa.- Proc. 2nd Int. Kimb. Conf. 1: 16-26.

VARNE, R. (1970): Hornblende lherzolite and the upper mantle.- Contr. Min. Petr. 27: 45-51.

VREDEVOOGD, J.J. and FORBES, W.C. (1975): The system diopside-ureyite at 20 kb.- Contr. Min. Petr. 52: 147-156.

WAGNER, P.A. (1928): The evidence of the kimberlite pipes on the constitution of the outer part of the earth.- S. Afr. J. Sci. 25: 127-148.

WASS, S.Y. (1980): Geochemistry and origin of xenolith-bearing and related alkali basaltic rocks from the Southern Highlands, New South Wales, Australia.- Am. J. Sci. 280-A: 639-666.

WASS, S.Y., HENDERSON, P. and ELLIOT, C.J. (1980): Chemical heterogeneity and metasomatism in the upper mantle: evidence from rare earth and other elements in apatite-rich xenoliths in basaltic rocks from eastern Australia.- Phil. Trans. Roy. Soc. Lond. A 297: 333-346.

WASS, S.Y. and IRVING, A.J. (Eds) (1976): XENMEG - A catalogue of occurrences of xenoliths and megacrysts in volcanic rocks of eastern Australia.- The Australian Museum, Sydney.

WASS, S.Y. and ROGERS, N.W. (1980): Mantle metasomatism - precursor to continental alkaline volcanism.- Geoch. Cosm. Acta 44: 1811-1823.

WARSHAW, I. and KEITH, M.L. (1954): Solid solution and chromium oxide loss in part of the system MgO-Al_2O_3-Cr_2O_3-SiO_2.- J. Am. Ceram. Soc. 37: 161-168.

WELLS, P.R.A. (1977): Pyroxene thermometry in simple and complex systems.- Contr. Min. Petr. 62: 129-139.

WHITE, R.W. (1966): Ultramafic inclusions in basaltic rocks from Hawaii.- Contr. Min. Petr. 12: 245-314.

WHITE, W.B. and ROY, R. (1975): The system chromium-oxygen at high oxygen pressures.- Geoch. Cosm. Acta 39: 803-817.

WILSHIRE, H.G., NEILSON PIKE, J.E., MEYER, C.E. and SCHWARZMANN, E.C. (1980): Amphibole-rich veins in lherzolite xenoliths, Dish Hill, and Deadman Lake, California.- Am. J. Sci. 280-A: 576-593.

WILSHIRE, H.G. and TRASK, N.J. (1971): Structural and rextural relationships of amphibole and phlogopite in peridotite inclusions, Dish Hill, California.- Am. Min. 56: 240-255.

WOOD, B.J. (1974): The solubility of alumina in orthopyroxene coexisting with garnet.- Contr. Min. Petr. 46: 1-15.

WOOD, B.J. and BANNO, S. (1973): Garnet-orthopyroxene and orthopyroxene-clinopyroxene relationships in simple and complex systems.- Contr. Min. Petr. 42: 109-124.

WOOD, B.J. and FRASER, D.G. (1978): Elementary thermodynamics for geologists.- Oxford Univ. Press, Oxford. 303 pp.

WOOD, B.J. and NICHOLLS, J. (1978): The thermodynamic properties of reciprocal solid solutions.- Contr. Min. Petr. 66: 389-400.

WOLFF, J.A. (1980): Peridotite xenoliths in basalts and mantle dynamics.- Nature 288: 104.

WYLLIE, P.J. (1979): Kimberlite magmas from the system peridotite-CO_2-H_2O.- Proc. 2nd Int. Kimb. Conf. 1: 319-329.

YODER, H.S. Jr (1955): Almandite garnet stability range.- Am. Min. 40: 342.

YODER, H.S. Jr and KULLERUD, G. (1971): Kosmochlor and the chromite-plagioclase association.- Carn. Inst. Wash. Yb. 69: 155-157.

YUEN, D.A., PELTIER, W.R. and SCHUBERT, G. (1981): On the existence of a second scale of convection in the upper mantle.- Geophys. J. Roy. Astr. Soc. 65: 171-190.

SUPPLEMENT TO REFERENCES

ERNST, W.G. (1978): Petrochemical study of some lherzolite rocks from the Western Alps.- J. Petr. 19: 341-392.

FURSENKO, B.A. (1981): Synthesis of new high pressure garnets: $MnCr_2Si_3O_{12}$ and $Fe_3Cr_2Si_3O_{12}$.- Bull. Mineral. 104: 418-422.

KUSHIRO, I., SYONO, Y. and AKIMOTO, S. (1968): Melting of a peridotite nodule at high pressures and high water pressures.- J. Geophys. Res. 73: 6023-6029.

RHODES, J.M. and DAWSON, J.B. (1975): Major and trace element chemistry of peridotite inclusions from the Lashaine Volcano, Tanzania.- Phys. Chem. Earth 9: 545-558.